REPORT DOCUMENTATION PAGE

Form Approved OMB No. 0704-0188

1. REPORT DATE *(DD-MM-YYYY)*	2. REPORT TYPE	3. DATES COVERED *(From – To)*
02-04-2004	Final Report	01-Nov-00 - 01-May-04

4. TITLE AND SUBTITLE

Investigation of Structure, Properties and Deformation Mechanisms of Elevated Temperature Al Alloys with High Specific Properties

5a. CONTRACT NUMBER
STCU Registration No: P-061

5b. GRANT NUMBER

5c. PROGRAM ELEMENT NUMBER

6. AUTHOR(S)

Professor Yuly V. Milman

5d. PROJECT NUMBER

5d. TASK NUMBER

5e. WORK UNIT NUMBER

7. PERFORMING ORGANIZATION NAME(S) AND ADDRESS(ES)

Frantsevich Institute For Problems of Materials Science
3, Krzhizhanovsky Str.
Kyiv 03142
Ukraine

8. PERFORMING ORGANIZATION REPORT NUMBER

N/A

9. SPONSORING/MONITORING AGENCY NAME(S) AND ADDRESS(ES)

EOARD
PSC 802 BOX 14
FPO 09499-0014

10. SPONSOR/MONITOR'S ACRONYM(S)

11. SPONSOR/MONITOR'S REPORT NUMBER(S)
STCU 00-8005

12. DISTRIBUTION/AVAILABILITY STATEMENT

Approved for public release; distribution is unlimited.

13. SUPPLEMENTARY NOTES

14. ABSTRACT

The present project was devoted to the investigation of structure and mechanical properties of high-strength aluminum alloys, especially alloys for elevated temperatures. High-strength aluminum alloys can have strengths approximately 50 times higher than the strength of unalloyed aluminum. Such a strong increase of the alloy strength is a unique case in the science of metallic materials and is a consequence of a tremendous number of theoretical and experimental works. For this reason a further increase of the level of mechanical properties of aluminum alloys is possible using new ideas and technologies. Just this approach was used for all six tasks of the present project. Investigation of mechanical properties was carried out by tension and bending test in various temperature ranges. Structural investigation were performed by X-ray diffraction technique, TEM, SEM, OM, DSC analysis and by local X-ray spectral analysis. Correlation of processing, chemical composition, structure and mechanical properties was investigated for obtained high-strength aluminum alloys. The mechanisms of alloy deformation and fracture in most strong condition were revealed.

15. SUBJECT TERMS
EOARD, Materials, Metallurgy & Metallography, aluminum, scandium, high-temperature, alloy

16. SECURITY CLASSIFICATION OF:			17. LIMITATION OF ABSTRACT	18, NUMBER OF PAGES	19a. NAME OF RESPONSIBLE PERSON
a. REPORT	b. ABSTRACT	c. THIS PAGE			CHARLES H. WARD, Lt Col, USAF
UNCLAS	UNCLAS	UNCLAS	UL	107	19b. TELEPHONE NUMBER *(Include area code)* +44 (0)20 7514 3154

Structure and Properties of Elevated Temperature Al Alloys

Project manager: Yuly V.Milman, Professor, Dr of Science (Physics and Mathematics), Corresponding Member of Ukrainian Academy of Sciences, Head of Department of the Institute for Problems of Material Science of NAS of Ukraine
Phone: (044)424-30-61, **Fax:** (044)424-30-61,
E-mail: milman@materials.kiev.ua
Institutions:
1. Frantsevych Institute for Problems of Material Science of the NAS of Ukraine (IPMS)
2. Paton Welding Institute of the NAS of Ukraine (PWI)
3. Kurdyumov Institute for Metal Physics of the NAS of Ukraine (IPM)
Financing parties: EOARD, USA
Operative commencement date: 01.11.2000
Project duration: 3 years
Date of submission: 31.01.2004

Abstract

It is difficult to overestimate the significance of aluminum alloys for modern industry. These alloys are widely used in aircraft building, space construction, motor car construction, shipbuilding, railway and other types of transport for production of sports inventories, in house-building and other branches of industry.

The quantity of the produced aluminum per one person is a very important indicator of the industrial development of the country.

The present project was devoted to investigation of structure and mechanical properties of high-strength aluminum alloys, especially alloys for elevated temperatures.

High-strength aluminum alloys had the strength approximately 50 times higher than the strength of unalloyed aluminum to the moment of this project beginning. Such strong increasing of the alloy strength is a unique case in material science of metallic materials and is a consequence of a tremendous number of theoretical and experimental works.

For this reason a further increase of the level of mechanical properties of aluminum alloys is possible with using new ideas and technologies only. Just this approach was used for all 6 tasks of the present project.

In Task 1 we used the so-called “Sc effect” to improve mechanical properties with the increase of strength and the preservation of a good ductility of the strongest aluminum alloys of Al-Zn-Mg-Cu system using additional alloying by Sc in combination with other transition or rare-earth metals (TM and REM).

It was shown that alloying of high-strength Al-Zn-Mg-Cu alloys with scandium permits to increase the concentration of the main alloying element Zn to 9-12 wt. % and the content of Cu to 2.3 wt. %, and alloys with a record level of strength YS = 700-740 MPa, UTS = 770-820 MPa at a rather good plasticity of EL = 9-14 % in T6 wrought semi-products can be produced.

In Task 2 the technology for producing sheet semi-finished products from ingots of Sc-containing alloys (developed in frames of Task 1) is elaborated. Investigation of the weldability of new alloys showed that they may be considered in the category of commercially weldable materials. A conclusion was made on the rationality of applying the developed alloys and their welding technologies for product manufacturing in most diverse industrial sectors, primaryly in aerospace engineering and transportation. The main advantage of their application is the fact that the structure weight can be reduced by 8-12 %, which will ensure significant saving of power resources.

08/04/04

In charge *Date* *Signature*

POf *Sliusarenko S., PhD*

DED

In Task 3 the first developed method for production of powders from high-alloyed aluminum alloys by high-pressure water atomization was used. Powder consolidation technique by severe plastic deformation without sintering was elaborated.

PM alloys with a record level of mechanical properties that approaches to the properties of the best alloys produced by casting were produced.

In addition, T6 treated rods of PM alloys not containing expensive alloying elements like Sc, Hf etc. possess the strength properties much higher than rods of the same alloys produced by casting. It was shown that an increased concentration of Fe (to 1 wt. %) and Si (to 0.5 wt. %) in PM alloys did not affect a high level of mechanical properties. It enables to use the recycled aluminum, which may contain a rather high amount of Si and Fe, for production of these alloys.

In Task 4 as a result of the researches carried out in the ternary Al-Ti-Cr system a large compositional region has been established, in which a univariant eutectic transformation $L \leftrightarrow L1_2+\beta$ is realized. Eutectic alloys containing two cubic phases $L1_2$ and β were elaborated. These light-weight, high-modulus cast alloys have a unique complex of mechanical properties. It is very important that a high level of mechanical properties is preserved up to 750 ^oC.

In Task 5 we used a heat resistant aluminum alloy reinforced by quasicrystalline nanosize particles, which was elaborated in frames of Task 3 and 6, as the matrix of a composite.

As a result elevated temperature mechanical properties of the elaborated composites are essentially higher in comparison with the properties of Al-alloy based composites known from the literature.

Task 6 has been devoted to the investigation of non-equilibrium states in aluminum alloys manufactured by rapid solidification (RS) techniques, and of the possibility to obtain high-strength and elevated temperature materials by this way.

A number of new results were obtained in this task that had a searching character. For example, it was shown that in the Al-Ce-Sc system a formation of a composite that consists of an amorphous matrix with embedded nanosize (5-10 nm) α-Al particles and has a high hardness HV = 3.5 GPa is possible. It was first shown that in RS aluminum alloys with a high concentration of Sc (of about 15 at. %) an icosahedral quasicrystalline phase in the form of nanosize (60-140 nm) particles is formed.

Elevated temperature PM aluminum alloys reinforced with nanosize quasicrystalline particles were produced with using the water-atomization technique and studied.

The best alloys of this group are based on the Al-Fe-Cr system. The PM rod semi-products of the best compositions of Al-Fe-Cr-Ti and Al-Fe-Cr-Ti-Zr had tensile strength at 300 °C on the level of 300 MPa and higher together with the residual elongation at ambient temperature of about 8 % and Young modulus close to 89 GPa.

It is seen that high-strength Al alloys were produced in this project by different technologies.

The investigation of mechanical properties was carried out by tension and bending test in various temperature ranges.

Structural investigation were performed by X-ray diffraction technique, TEM, SEM, OM, DSC analysis and by local X-ray spectral analysis.

Correlation of processing, chemical composition, structure and mechanical properties was investigated for obtained high-strength aluminum alloys. The mechanisms of alloy deformation and fracture in most strong condition were revealed.

Content of final report

Task 6. Investigation of structure, phase transitions and mechanical properties of high-strength rapidly solidificated Al alloys with amorphous and quasicrystalline phases and with micro- and nanocrystalline structure

6.1. Alloys with amorphous structure

6.1.1. Studying the effect of Sc alloying on properties of Al-based amorphous alloys

The data presented in the literature [1] show that the formation of Al-based amorphous alloys is possible in a few alloy systems, namely Al-R, Al-R-LM and Al-EM-LM, where R = rare-earth metals or Y, LM = late transition metal (Fe, Co, Ni, Cu), EM = early transition metal (Ti, Zr, Hf, V etc.). Sc electron structure is similar to one of Y and rare-earth metals, so that Sc is a promising element for alloys of Al-R and Al-R-LM group. Taking into account a positive effect of Sc on usual Al alloys [2], it is interesting to study the influence of Sc additions on the behavior of amorphous alloys on Al base while crystallization. At the same time, no data was found in the literature on the effect of Sc alloying on properties of Al-based amorphous alloy. Therefore in the framework of this project structure and properties of rapidly solidified Al alloys containing Sc were studied.

6.1.1.1. Binary Al-Sc alloys

A series of rapidly solidified $Al_{100-x}Sc_x$ (x = 1, 3, 5, 7, 9, 10, 11, 13.5, 14.9 at. %) alloys was manufactured by melt spinning technique, and structure and hardness of the alloys were studied. At rare earth element concentration of 9-10 at. % an amorphous phase was obtained for all Al-R alloys described in work [1]. Therefore Sc concentration range of 9-11 at. % was studied in more details. It was found that no amorphous phase was formed in the alloys obtained, and accordingly to the results of X-ray study (Fig. 6.1) the material consisted of Al solid solution at Sc content up to 3 at. %, Al solid solution + Al_3Sc intermetallic at Sc content of 3-13.5 at. %, Al solid solution + Al_3Sc intermetallic + icosahedral quasicrystalline phase at Sc content of about 14.9 at. %. In the ribbon of the last composition (checked by chemical analysis) some peaces consisted of three phases, and some other peaces contained small (of 60-140 nm in size) quasicrystalline particles embedded into α-Al matrix (Fig. 6.2). X-ray peaks of the icosahedral phase in the XRDP of such a peace (Fig. 6.1, b) are marked with Cahn indices N/M [3]. Noteworthy that among these peaks a rather strong intensity is observed for the peak 15/23 with odd N that is an evidence of a partly face-centered character of the 6-dimensional lattice of the quasicrystalline icosahedral phase [3,4]. The appearance of this peak together with a redistribution of intensities of peaks with even N (strong lowering the intensity of the peak 20/32 with the increase of the intensity of the peak 14/21) were observed in Al-Mn-Ce ribbons [4] and explained by increasing the degree of quasicrystalline lattice ordering under the influence of alloying with REM. Thus, in this influence Sc is quite similar to REM.

The formation of a quasicrystalline phase in a rapidly solidified Al-Sc alloy was first revealed in this investigation. At least in the alloy Al – 14.9 at. % Sc this phase was non-stable at room temperature and disappeared in 90 days.

The effect of Sc concentration on the hardness of Al-Sc alloys is presented in Fig. 6.3. An increase of Sc content up to 7 at. % in the ribbons led to a monotonous growth of hardness, that is evidently connected with the increase of the amount of Al_3Sc phase in the material. Lowering the rate of hardness growth with further increase of Sc content can be explained by the fact that the amount of the intermetallic in the alloy becomes higher than the amount of the α-Al phase, and ribbon hardness comes close to the hardness of Al_3Sc itself. Hardness of the alloy α-Al + nanosize quasicrystalline particles was practically on the same level.

6.1.1.2. Ternary Al-Ce-Sc alloys

Rapidly solidified $Al_{91}Ce_{9-x}Sc_x$ alloys containing x = 0, 1, 3, 7, 9 at. % of Sc were manufactured in the form of melt spun ribbons. X-ray diffraction spectra for these alloys are shown in Fig. 6.4. The alloy containing 1 at. % Sc had a completely amorphous structure. But a further increase of Sc content led to decreasing the alloy glass forming ability. As a result, a mixed amorphous-crystalline structure was obtained in $Al_{91}Ce_6Sc_3$ alloy (a small amount of α-Al phase was revealed by X-ray analysis). Alloys containing 5 and 7 at. % of Sc had a completely crystalline structure formed by α-Al together with Al_4Ce and Al_3Sc intermetallics. Fine structure of ribbons from alloys with 3 at. % Sc and 5 at. % Sc are shown in Fig. 6.5.

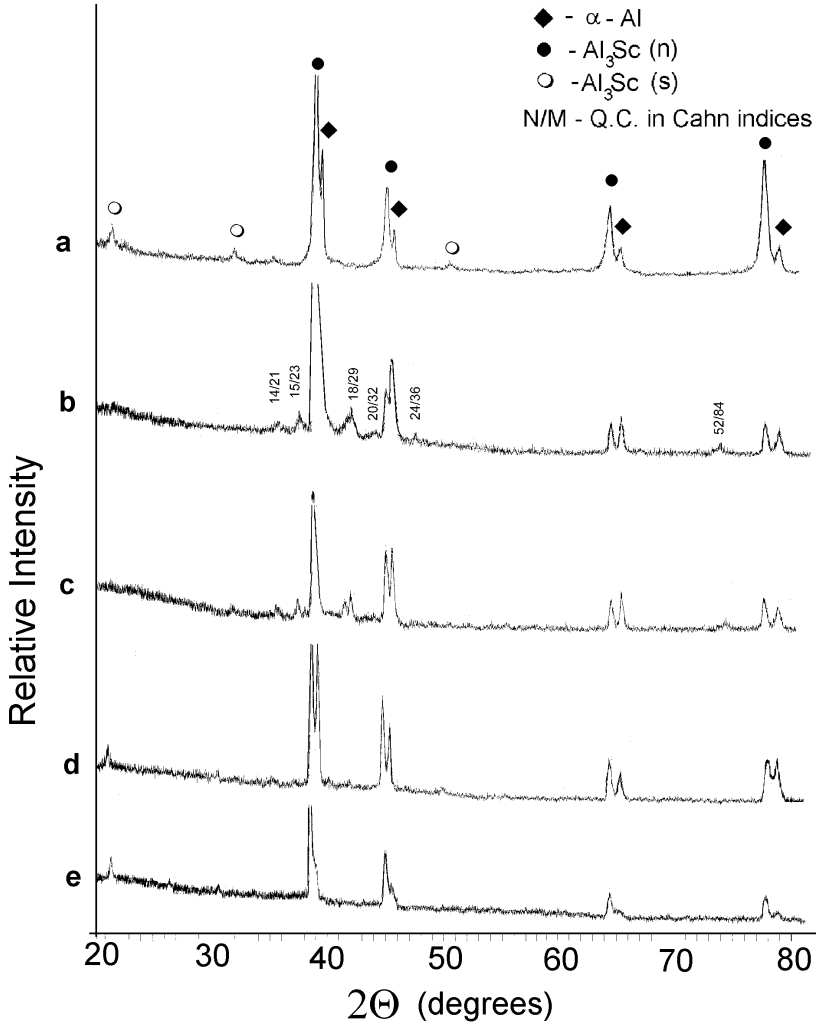

Figure 6.1. Fragments of XRD patterns of Al-14.9 Sc alloy:
a – initial cast ingot; b – ribbon of 30 μm in thickness, 1 day after manufacture; c – the same ribbon, 45 days after manufacture; d – the same ribbon, 90 days after manufacture; e – the same ribbon, 300 days after manufacture;
n – normal lines, s – superstructural lines of Al_3Sc

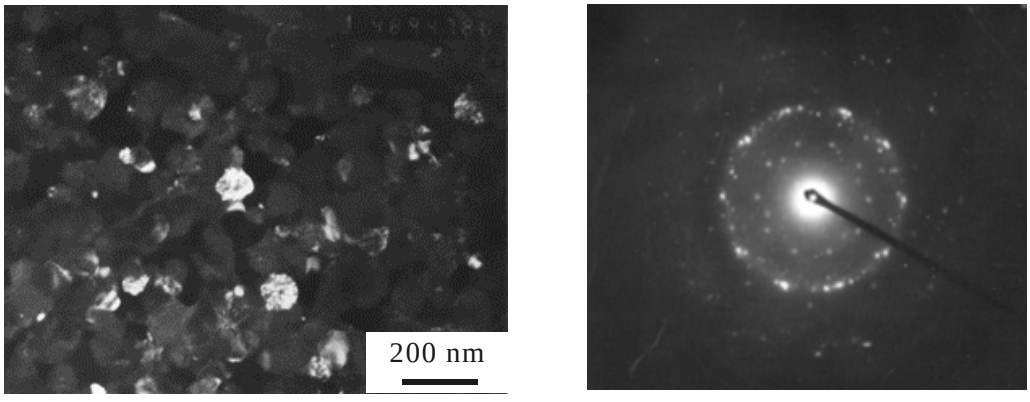

a b

Figure 6.2. Quasicrystalline particles in the ribbon Al-14.9Sc of 70 μm in thickness, 20 days after manufacture: a – dark field image with using a part of intense rings of i-phase in the electron diffraction pattern formed by the area (a); b - electron diffraction pattern formed of a quasicrystalline particle at the edge of the foil in the area (a)

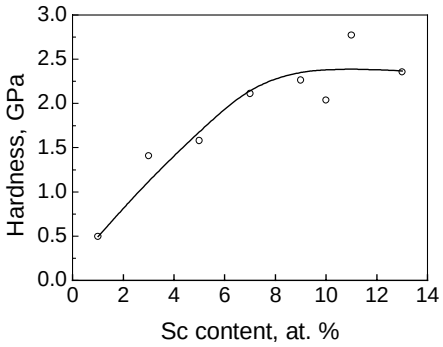

Figure 6.3. Effect of scandium concentration
on hardness of RS ribbons of binary Al-Sc alloys

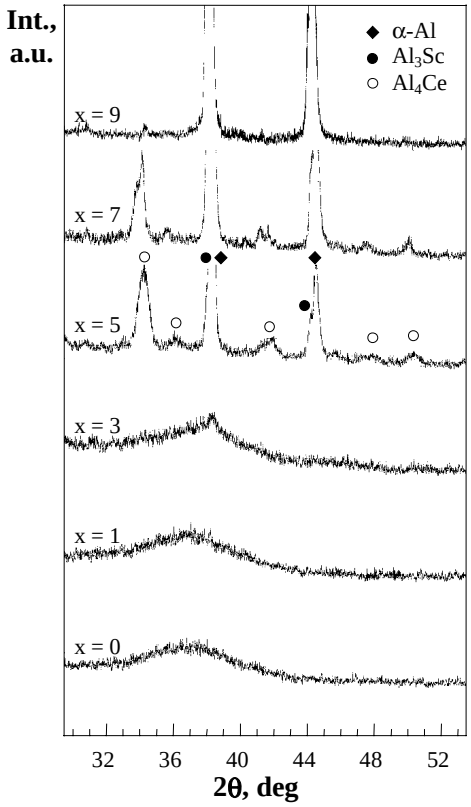

Figure 6.4. X-ray diffraction patterns of rapidly solidified $Al_{91}Ce_{9-x}Sc_x$ alloys

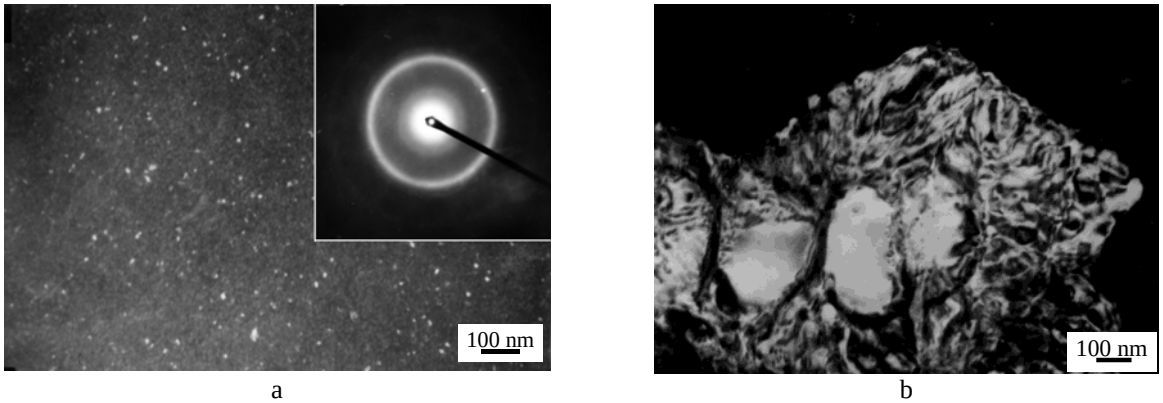

a b

Figure 6.5. Precipitates of α-Al in amorphous matrix of the ribbon $Al_{91}Ce_6Sc_3$, TEM dark field image using a part of (220) α-Al ring (a); Structure of the ribbon $Al_{91}Ce_4Sc_5$ consisting of α-Al, Al_4Ce and Al_3Sc particles, dark field image using a (002) Al reflection

Ribbons with amorphous structure of the ternary alloy have the lowest level of hardness of about 2 GPa (Fig. 6.6). Increasing of Sc content to 3 at. % leads to the formation of α-Al precipitates of 5-10 nm in size in the amorphous matrix (Fig. 6.5, a). As a result, a nanocomposite consisting of amorphous matrix and α-Al nano-inclusions was obtained that led to a sharp increase of hardness to 3.5 GPa, which corresponds to about 1 GPa strength (along with the material density below 3 g/cm^3). A further growth of Sc content leads to the formation of a fine hypoeutectic structure (Fig.6.5, b). It this alloy hardness remains on almost the same level (Fig. 6.6). Increasing Sc content above 5 at. % results in a growth of the intermetallic grains, and hardness decreases.

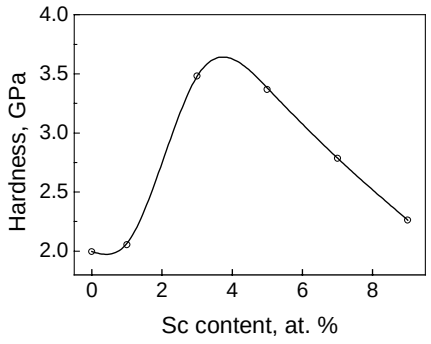

Figure 6.6. Effect of scandium concentration on the hardness of $Al_{91}Ce_{9-x}Sc_x$ alloys

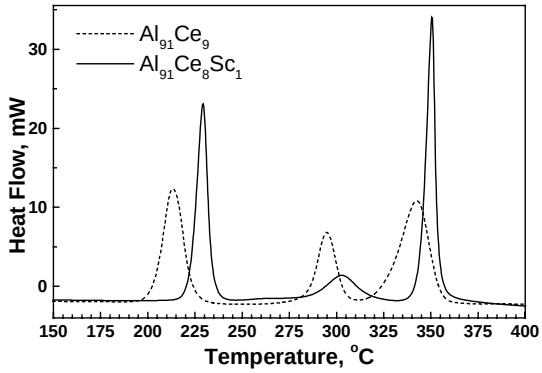

Figure 6.7. DSC traces for $Al_{91}Ce_9$ and $Al_{91}Ce_8Sc_1$ ribbons (heating rate 20 °C/min)

Substitution of 1 at. % Sc for Ce appreciably increased the thermal stability of the amorphous structure, i.e. increased the temperature of beginning the crystallization processes (Fig. 6.7). It may be attributed to a known deceleration of diffusion processes in Al under the influence of Sc [2].

6.1.1.3. Quarternary Al-Ni-Ce-Sc alloys

Effect of Sc additions on the structure and hardness of $Al_{85}Ni_{10}Ce_{5-x}Sc_x$ (x = 0, 1, 2, 3, 4, 5 at. %) alloys was investigated. It was found that a replacement of Ce with Sc does not drastically change the alloy glass forming ability, and an amorphous state can be obtained in all range of the alloy concentrations under investigation (Fig. 6.8). At the same time for $Al_{85}Ni_{10}Sc_5$ alloy a critical thickness of the ribbon, for which pure amorphous structure can be obtained, is lower than 50 μm that is smaller than the critical thickness of 80-100 μm announced in the literature for $Al_{85}Ni_{10}Ce_5$ alloy. Therefore we can conclude that Sc in this alloy decreases its glass forming ability. Hardness of the ribbons obtained was found to keep at an almost constant (but quite high) level of 3.7 GPa (Fig. 6.9).

On the base of the investigations carried out it is possible to conclude that although the electronic structure of Sc is similar to that of yttrium and rare-earth metals, a partial substituting of Sc for rare-earth metal (Ce) strongly lowers alloy glass forming ability, and in melt-spun binary Al-Sc alloys the attainment of amorphous state is impossible. Maybe, such effect of Sc is connected with its smaller atomic radius (0.164 nm) in comparison to rare-earth metals (0.18 nm and higher). In the case of Al-Ni-Sc alloy scandium plays a role of rather an early transition metal than of a rare-earth metal. As a result when replacing Ce by Sc we make the transition from the Al-TM-RE amorphous alloy system to the Al-EM-LM system. Since both of these systems allow the formation of amorphous state [1], we have obtained amorphous Al-Ni-Ce-Sc ribbons. For this reason the hardness of the alloys under consideration in amorphous state weakly depended on the content of Sc (Fig. 6.9).

6.1.2. Manufacturing and consolidation of Al-based amorphous alloy powders

For the first time water atomized powders of $Al_{85}Ni_{10}Ce_5$ and $Al_{87}Ni_9Ce_3Fe_1$ at. % alloys were produced, and its structure was studied. In order to reveal the phase composition of powders depending on powder size fraction, X-ray diffraction study of the powder samples was carried out. The results of the study presented in Fig. 6.10 (alloy $Al_{85}Ni_{10}Ce_5$) and Fig. 6.11 (alloy $Al_{87}Ni_9Ce_3Fe_1$) have shown that all powders consist of an amorphous phase (which forms a halo in the 2θ range of 40-60°) and intermetallic compounds. In OM investigation of sections of powder particles etched under the selected conditions these phases were colored in various colors (Fig. 6.12): the amorphous phase looked brown, crystalline phases looked white and blue.

For both alloys the content of the amorphous phase increases with decreasing of the average particle size that is connected with higher cooling rate of smaller particles in atomization process.

Since it is difficult to determine the content of the amorphous phase in the material from the X-ray data, a DSC study of powders and rapidly solidified ribbons (being completely amorphous) was performed. DSC scans for

powders and ribbons of $Al_{85}Ni_{10}Ce_5$ and $Al_{87}Ni_9Ce_3Fe_1$ alloys are shown in Figs 6.13 and 6.14, respectively. Basing on the DSC results, the content of the amorphous phase in the powders was determined, and the results of calculations are presented in Tables 6.1 and 6.2.

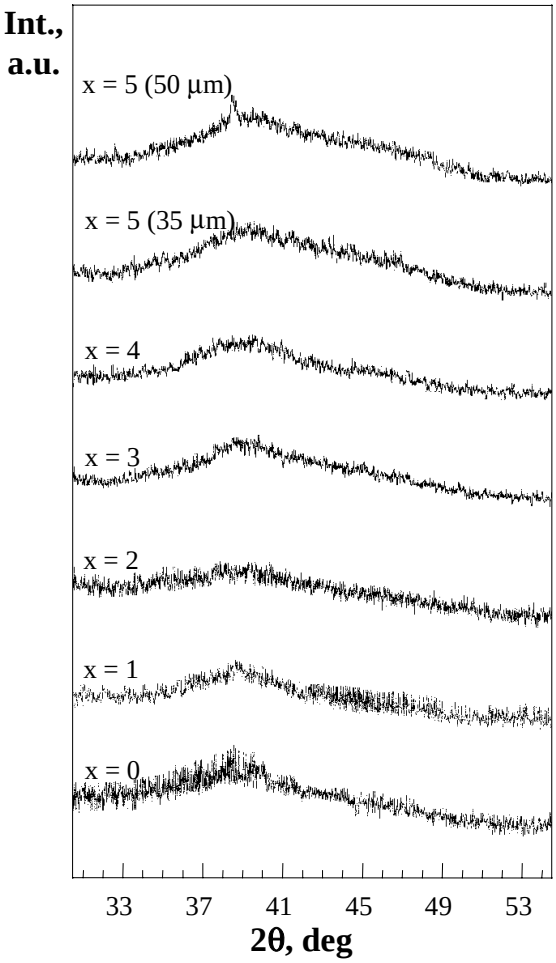

Figure 6.8. X-ray diffraction patterns of rapidly solidified $Al_{85}Ni_{10}Ce_{5-x}Sc_x$ alloys. The thickness of ribbons with x = 0÷4 was of about 35 μm

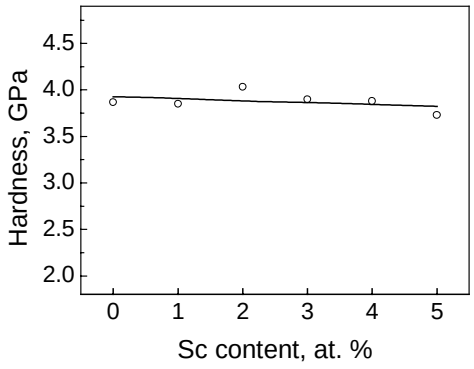

Figure 6.9. Effect of scandium concentration on the hardness of melt-spun ribbons of about 35 μm thick of $Al_{85}Ni_{10}Ce_{5-x}Sc_x$ alloys

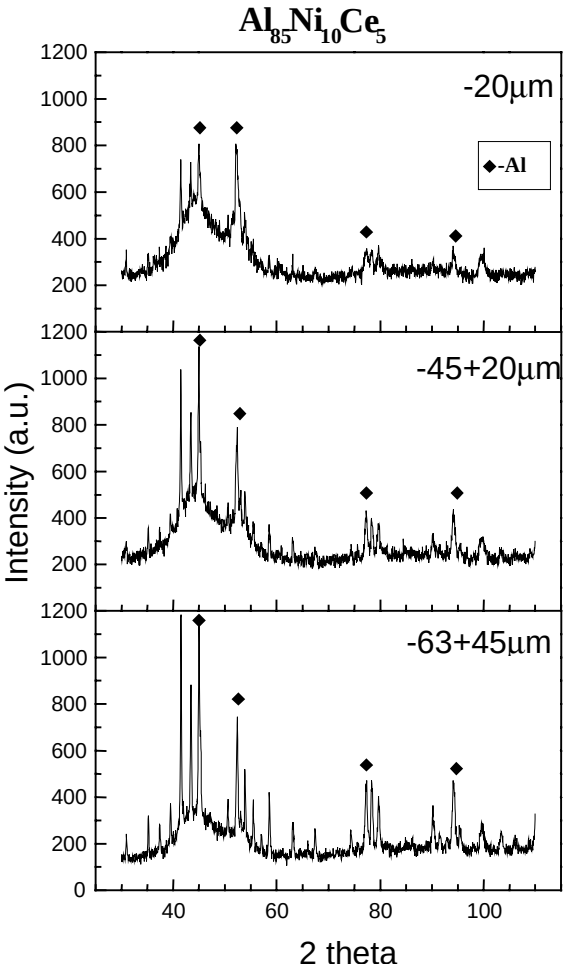

Figure 6.10. X-ray diffraction patterns of various size fractions of $Al_{85}Ni_{10}Ce_5$ powders

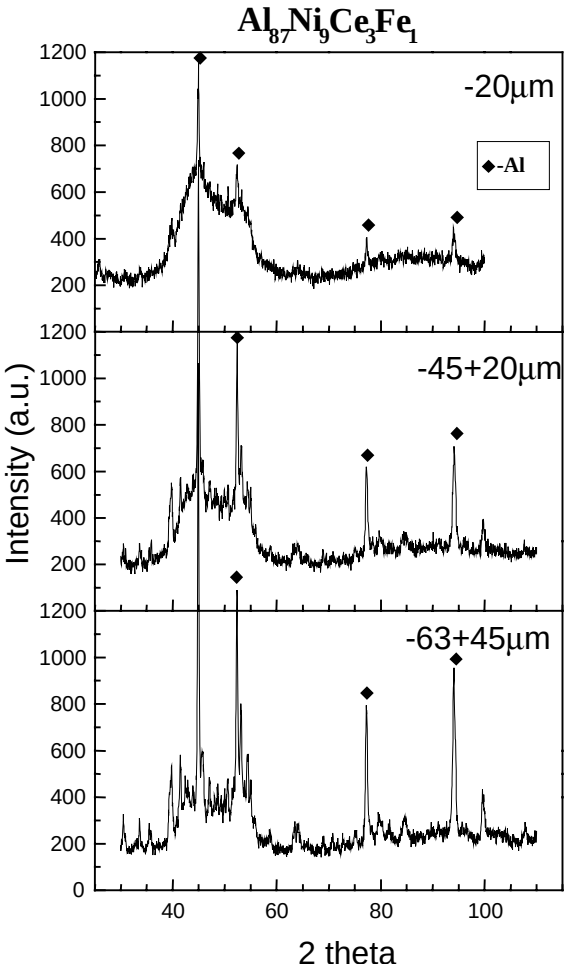

Figure 6.11. X-ray diffraction patterns of various size fractions of $Al_{87}Ni_9Ce_3Fe_1$ powders

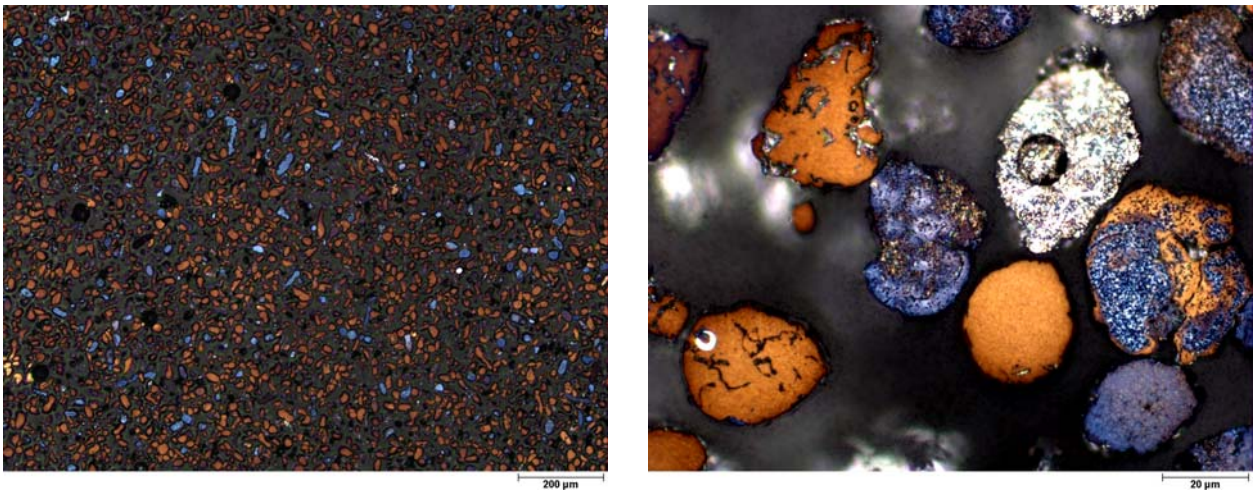

a b

Figure 6.12. Etched sections of particles of water-atomized $Al_{87}Ni_9Ce_3Fe_1$ powder: a – size fraction of (0-20) µm, b – size fraction of (20-45) µm.
Brown areas are the amorphous phase, white and blue areas are crystalline phases

Table 6.1.

Crystallization enthalpies for water atomized powders and melt spin ribbon of $Al_{85}Ni_{10}Ce_5$ alloy

Powder size fraction, μm	Enthalpy of crystallization (first exothermal peak) ΔH, J/g	**Amorphous phase content, wt. %**
ribbon	54.5	**100**
-20	28.7	**53**
-45+20	27.7	**51**
-63+45	22.1	**41**
-125+63	15.1	**28**
-250+125	10.8	**20**

Table 6.2.

Crystallization enthalpies for water atomized powders and melt spin ribbon of $Al_{87}Ni_9Ce_3Fe_1$ alloy

Powder size fraction, μm	Enthalpy of crystallization ΔH, J/g		Amorphous phase content, wt. %		
	First peak	Second peak	From first peak	From second peak	Average
ribbon	55.2	96.3	100	100	**100**
-20	25.3	74.6	46	77	**61**
-45+20	15.2	47.9	28	50	**39**
-63+45	8.6	27.8	16	29	**22**
-125+63	3.2	11.1	6	12	**9**
-250+125	0.7	3.63	1	4	**2**

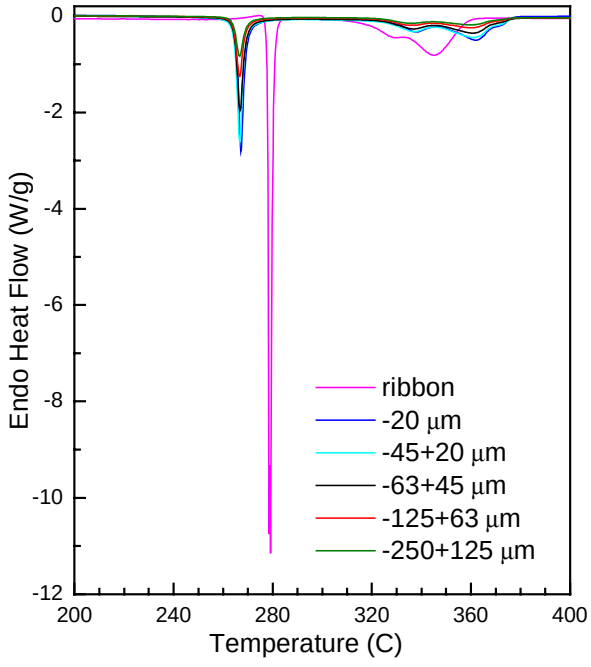

Figure 6.13. DSC scans for water atomized powders and melt spin ribbon of $Al_{85}Ni_{10}Ce_5$ alloy (heating rate of 20 K/min).

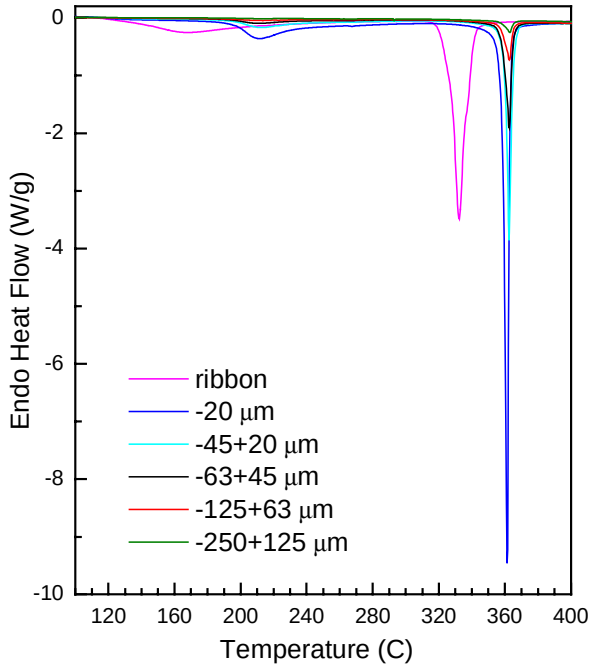

Figure 6.14. DSC scans for water atomized powders and melt spin ribbon of $Al_{87}Ni_9Ce_3Fe_1$ alloy (heating rate of 20 K/min)

In frames of this project an attempt was made to consolidate the finest (0-20 μm) powder size fraction of $Al_{87}Ni_9Ce_3Fe_1$ water atomized alloy into a bulk sample using hot extrusion as a consolidation technique. The lowest temperature, at which it was possible to consolidate the powder, was 350 ^{0}C that is close to the crystallization temperature of this alloy. As a result, no amorphous phase remained in the material after extrusion that was confirmed by XRD studies.

Task 5. Investigation of structure and mechanical properties of high-strength Al based composites

5.1. Optimizing the composite production technology

Composite production technology used in this study included the next stages: mixing of the matrix and the reinforcement powders, cold pressing of the powder mixture into billets, hot vacuum forging of the billets, hot extrusion of the forged billets.

Mixing of the matrix and the reinforcement powders

The most uniform reinforcement distribution in the composites was realized upon two stage mixing: short time (1 hour) wet mixing (in ethyl alcohol), drying, and long-time (30 hours) dry mixing. To improve particle redistribution mixing bodies (20 % of total batch weight) were added to the powder blend. Two types of the bodies were tested: light steel "stars" and heavy WC balls. Better composite structure was obtained with the "stars", because rather milling than mixing took place on WC ball usage, and the composite matrix was contaminated with small fragments of SiC particles and the drum material (Fig. 5.1).

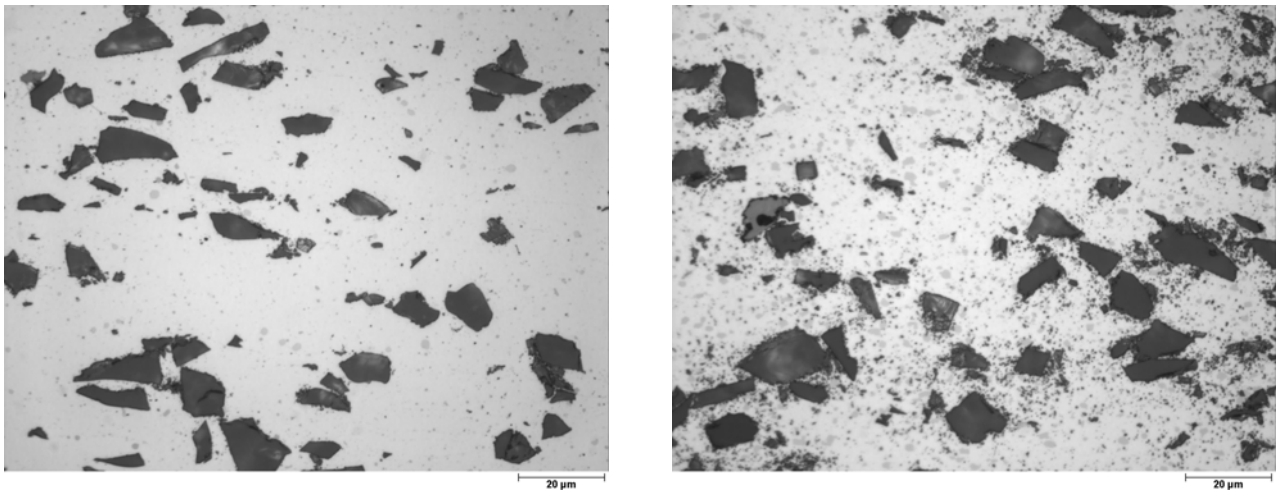

a b

Figure 5.1. Structure of Al-6Cu-0.4Mn + 15 vol. % SiC (14 µm mean particle size) composite produced using steel "stars" (a) and WC balls (b) as the mixing bodies

Cold pressing of the powder mixture into billets

Cold pressing of the powder mixtures was necessary for the composite production technique used in order to form billets for subsequent hot vacuum forging. In case of the unreinforced alloys (produced in the framework of Task 3 and 5) density of the cold pressed billets was of about 70 %. Billets of such density had high porosity promoting intense degassing on subsequent treatment. In case of the powders reinforced with SiC particles 70 % density was insufficient to get reasonable strength of the billet (due to lower adhesion of SiC particles to each other and to the matrix alloy particles). Therefore density of the cold pressed billets was increased up to 80 %.

Hot vacuum forging of the billets

Taking into consideration the temperature of quasicrystal-to-intermetallic transformation for Al-Cr-Fe-(Ti) rapidly solidified alloys, temperature of vacuum forging (as well as all subsequent thermal treatments) should not exceed 400 ^{0}C. At the same time lower forging temperature did not provide effective powder degassing and consolidation. Therefore namely this temperature was selected as an optimal one.

Hot extrusion of the forged billets

As it was previously mentioned, extrusion of the composites should be performed at the temperature not exceeding 400 ^{0}C. At the same time, matrix alloys used in this study had high yield stress even at elevated temperatures and therefore big press force was necessary to extrude them. Addition of the reinforcement to the matrix alloy resulted in still higher extrusion force necessary, which often exceeded the equipment capabilities. The possible way to resolve this problem was increasing of extrusion temperature or decreasing extrusion ratio. The last approach leads to worse reinforcement distribution in the extruded samples and results in lower critical reinforcement concentration when reinforcement clusters are not formed yet (see Fig. 5.2). Therefore extrusion temperature was increased up to 450 ^{0}C for

Al-Cr-Fe \ SiC composite. Decreasing of the extrusion ratio from 17.36 down to 12.76 was additionally used to extrude Al-Cr-Fe-Ti \SiC composites.

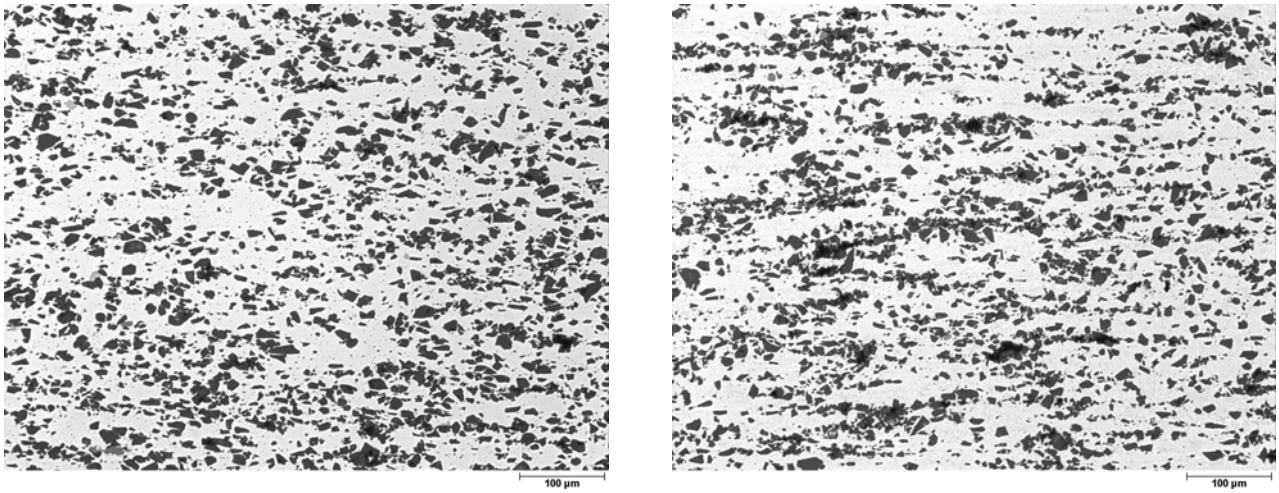

a b

Figure 5.2. Effect of extrusion ratio on the reinforcement distribution in SiC particle reinforced Al-based composites:
a – Al-6Cu-0.4Mn (40 µm) + 15 vol.% SiC (14 µm). Extrusion ratio of 17.36;
b – Al-4Cr-4Fe-2Ti (40 µm) + 15 vol.% SiC (14 µm). Extrusion ratio 12.76

5.2. Selection of the optimal reinforcement particle size

To select proper reinforcement particle size, Al-6Cu-0.4Mn (wt. %) matrix alloy composites reinforced with 3 and 14 µm (mean particle size) were made. Reinforcement content varied in the range of 0 – 20 % (Fig. 5.9). It was found that for the composite manufacturing technology used critical concentration of 3 µm reinforcement was about 5 vol. %, and critical concentration of 14 µm reinforcement was about 15 vol. %. When the critical concentration of the reinforcement in the material was exceeded, the reinforcement clustering was observed and composite property deterioration took place. Thus, increasing of the reinforcement particle size allows higher reinforcement concentration in powder metallurgy processed composites if the matrix alloy powder size fraction remains the same.

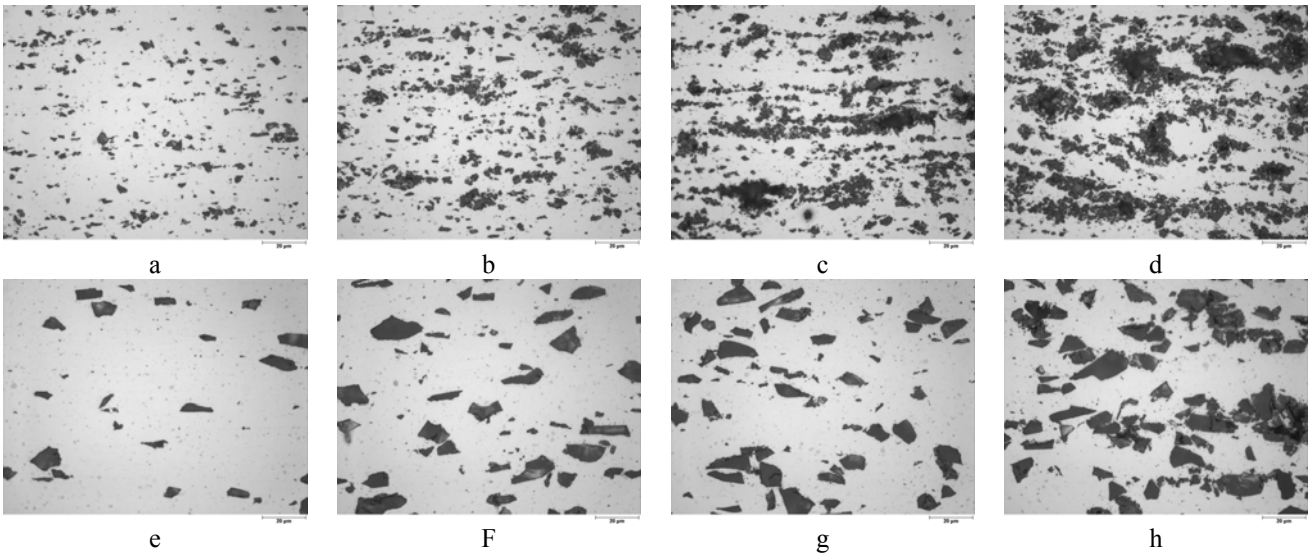

a b c d

e F g h

Figure 5.3. Effect of the reinforcement content and mean particle size on the Al-Cu-Mn \ SiC composite structure:
a-d – 3 µm SiC; e-h – 14 µm SiC;
a, e – 5 vol. %; b, f – 10 vol. %; c, g – 15 vol. %; d, h – 20 vol. %

At the same time, composites containing the same amount of 3 µm reinforcement had higher yield stress, tensile strength and lower Young's modulus in comparison with the composites reinforced with 14 µm SiC particles (Fig. 5.4).

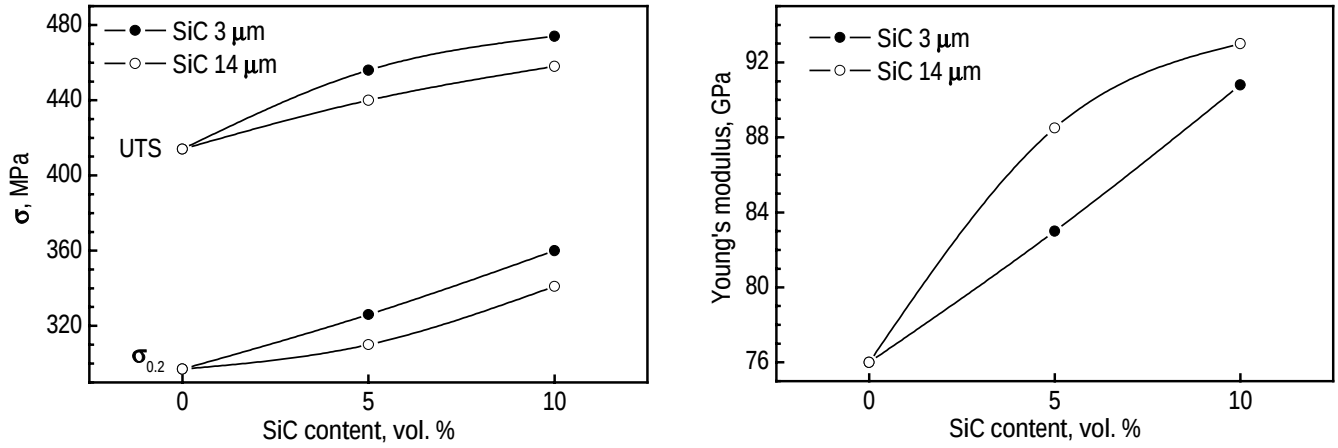

Figure 5.4. Effect of the reinforcement content and mean particle size on mechanical properties of Al-Cu-Mn \ SiC composites:
a – yield stress and ultimate tensile strength, b – Young's modulus

5.3. Studying the effect of matrix to reinforcement particle size ratio on the reinforcement distribution and the material properties

In order to study the effect of reinforcement clustering on the composite mechanical properties, composite samples reinforced with 15 vol. % SiC 14 μm and based on Al-Cu-Mn alloy (40, 80, 130 and 180 μm mean particle size fractions) were manufactured and studied. Increasing of the matrix alloy mean particle size lead to worse reinforcement distribution and clusters of SiC particles were form in the samples with high matrix to reinforcement particle size ratio (Fig. 5.5).

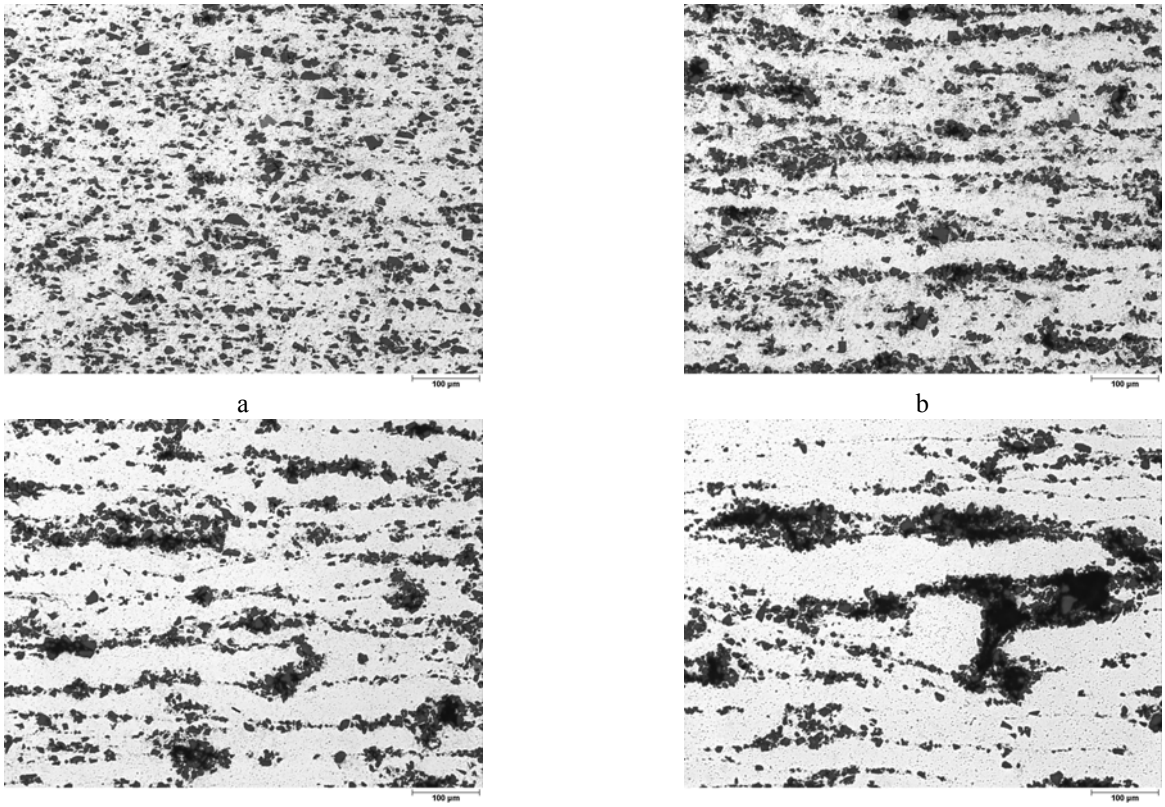

Figure 5.5. Structure of Al-6Cu-0.4Mn (wt. %) + 15 vol. % SiC (average particle size of 14 μm): mean matrix alloy particle size of 40 (a), 80 (b), 130 (c) and 180 μm (d)

Decreasing of the composite Young's modulus value due to reinforcement clustering is shown in Fig. 5.6. It was found that clustered composites contain pores located in SiC clusters. Decreasing of Young's modulus due to the material porosity was described in the framework of mean-field micromechanical model (dashed line in Fig. 5.6) and was found to be insufficient to explain experimentally observed results. A modified model was elaborated to describe the results on Young's modulus decreasing due to the reinforcement clustering which took into account contiguous SiC particles in the composite. This model operates with matrix to reinforcement particle size ratio to calculate the volume fraction of contiguous SiC particles (depending on reinforcement content and extrusion ratio applied upon the composite production) and well describe experimentally observed results (solid line in Fig. 5.6).

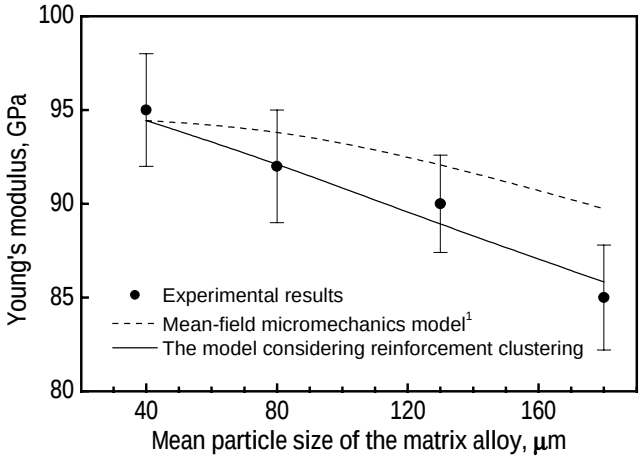

Figure 5.6. Dependence of Young's modulus of AlCuMn\15%SiC composites on the matrix alloy particle size

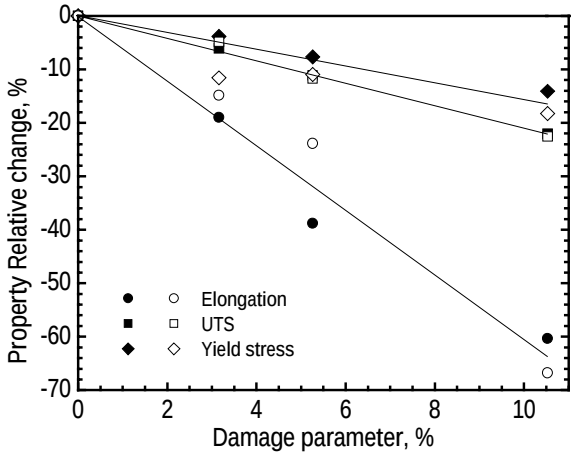

Figure 5.7. Relative property change for AlCuMn\15%SiC composites as function on the damage parameter

It was found that linear dependence exists between tensile property change and the damage parameter $D = 1 - \frac{E}{E_0}$, where E is Young's modulus of the clustered composite and E_0 is Young's modulus of the composite without reinforcement clusters (Fig. 5.7). Analysis of the dependences obtained shows that effect of the reinforcement clusters on relative change of the material properties does not depend on matrix alloy ductility because the similar results were obtained for solution heat treated (open symbols) and age hardened (solid symbols) composites. Plasticity was found to be a characteristic the most sensitive to the reinforcement clustering, and yield stress was the least sensitive one.

5.4. Manufacturing the composites based on high-strength elevated temperature Al alloys and studying their structure mechanical properties

Composite manufactured and studied in the framework of this project were based on Al-6Cu-0.4Mn (wt. %) aged alloy and on Al-Cr-Fe-Ti system quasicrystal reinforced alloys. The first Al-Cu-Mn alloy was selected because it has relatively high aging temperature (180 ^{0}C in comparison with 120 ^{0}C for Al-Zn-Mg-Cu alloy system) and therefore higher thermal stability, high elongation to fracture (up to 35% for the solution heat treated state) that is important for obtaining a ductile material after reinforcing with SiC particles and allows considerable variation of the matrix alloy properties by means of additional thermal treatment (YS = 154 – 308 MPa, UTS = 314 – 430 MPa, δ = 20 – 35 %). Alloys of Al-Cr-Fe-Ti system (Al-8Cr-1.5Fe, Al-5Cr-5Fe and Al-4Cr-4Fe-2Ti (wt. %)) have high thermal stability and high elevated-temperature mechanical properties because they are strengthened with fine and uniformly distributed Cr- and Fe-containing quasicrystalline or crystalline intermetallic particles [1]. These particles are stable to recrystallization and growth due to low Fe and Cr diffusivity in Al. In addition, in the frame of the present project Al-Cr-Fe-Ti elevated temperature alloy was obtained for the first time by water atomization technique in the form of powder, which was the ideal base for manufacturing particle-reinforced metal matrix composites by P/M route.

Mechanical properties of the composites studied in this project are shown in Table 5.1. The highest mechanical properties for the heat resistant Al alloy composites made (Al-Cr-Fe-Ti alloy system) at room temperature are: YS = 510 MPa, UTS = 530 MPa, δ = 1.5%; E = 106 GPa; at 300 ^{0}C the best properties are YS = 274 MPa, UTS = 293 MPa, δ = 2.3 %.

Table 5.1.

Mechanical properties of the composites

Composition of the matrix alloy, Reinforcement size and content (vol.%)	20 ˚C				190 ˚C			300 ˚C		
	YS, MPa	UTS, MPa	δ, %	E, GPa	YS, MPa	UTS, MPa	δ, %	YS, MPa	UTS, MPa	δ, %
Al-6Cu-0.4Mn SiC M3										
0	297	414	17.9	76	273	294	18.1			
5	326	456	12	83	295	336	11.6			
10	360	474	6.6	90.8	294	333	5			
15	359	446	2.6	92.2	276	308	2.6			
20	327	386	0.7	91.4	273	305	1.6			
SiC M14										
5	310	440	13	88.5						
10	341	458	9	93						
15	366	468	4.7	92.8	312	355	3.5			
20	385	468	2.7	110.4						
Al-8Cr-1.5Fe SiC M14										
0	358	437	5.56	88.1	252	302	10.47	163	202	11.73
5	373	444	4.1	91.2	278	312	7.67	172	207	5.67
10	392	464	2.87	100	295	328	5.33	189	219	4.74
15	428	476	1.07	106	309	344	3.5	190	228	3
20	438	489	0.97	109	305	354	2.57	197	229	1.93
Al-5Cr-5Fe SiC M14										
0	420	482	4.3	87.8	322	353	6	231	250	5.67
5	389	436	4.87	96.2	301	343	1.87	229	241	2.67
10	389	445	3.93	105	331	332	0.74	221	247	1.84
15	377	453	1.27	112	334	365	0.93	253	271	2.57
Al-4Cr-4Fe-2Ti SiC M14										
0	444	486	8.2	90	356	388	7.2	259	285	7.0
5	461	505	4.4	100.4	388	411	3.8	271	287	3.4
10	488	521	2.6	105.8	383	416	2.0	274	293	2.3
15	510	530	1.5	-	388	414	1.1	220	255	2.2
20	481	509	0.7	-	-	-	-	-	-	-

CONCLUSIONS

1. Technology for production of particle reinforced composites based on heat resistant Al alloys was elaborated. In elaboration process the conditions of powder mixing, the optimum reinforcement size, forging and extrusion temperatures were determined.

2. Effect of the matrix to reinforcement particle size ratio on the structure and the mechanical properties of the composites was studied. The model was elaborated, which describes well the decrease of the material Young's modulus due to the reinforcement clustering. It was found that a linear dependence exists between the tensile property change and the damage parameter $D = 1 - \frac{E}{E_0}$, where E is Young's modulus of the clustered composite and E_0 is Young's modulus of the composite without reinforcement clusters.

3. It was shown that the effect of the reinforcement clusters on the relative change of material properties does not depend on the matrix alloy ductility. The plasticity was found to be a characteristic the most sensitive to the reinforcement clustering, and the yield stress was the least sensitive one.

4. Composites based on the matrix of a heat resistant Al alloy reinforced by quasicrystalline particles (elaborated in frames of Tasks 3 and 6) and reinforced additionally with SiC particles were first manufactured, and their mechanical properties at room and elevated temperatures were studied. The highest mechanical properties were realized in Al-4Cr-4Fe-2Ti (wt. %) matrix alloy composites. The composite Al-Cr-Fe-Ti + 10 % SiC was found to have a high strength at 300 ^{0}C (UTS = 293 MPa) combined with a satisfactory (2 %) elongation to fracture at room temperature (2 %), increased Young's modulus (E = 106 GPa), increased wear resistance and decreased friction force. The composite Al-Cr-Fe-Ti + 5 % SiC also had good mechanical characteristics. It had approximately the same strength at 300 ^{0}C (287 MPa), but higher room-temperature ductility (4.4 %) and Young's modulus of 100 GPa. Thus, elevated temperature mechanical properties of the elaborated composites are essentially higher in comparison with the properties of Al-alloy based composites known from the literature.

References

1. Yu.V. Milman, D.V. Lotsko, O.D.Neikov et al., Materials Science Forum, **396-402** (2002) 723.

Task 4. Development of the physical fundamentals for creation of Al elevated temperature eutectic cast alloys with optimum combination of strength and ductility characteristics on the base of intermetallic phases

4.1. Introduction

A great attention has been recently paid to studying the structure and properties of alloys on the base of titanium trialuminide with the $L1_2$ structure [1-16] and to improving the methods of their production.

Such an interest is stipulated, in the first turn, by the complex of unique properties characteristic of these materials: high melting temperature and elasticity modulus, low density, and excellent stability in oxidizing media. However, low plastic characteristics of intermetallic alloys at room temperature are a stumbling-block in their practical use.

The analysis of the modern literature shows that a lot of researches is devoted to the development of concepts of the mechanisms of deformation and the nature of brittleness of their materials. At that, main efforts are directed to the development of physical and technological methods of improvement of their low-temperature plasticity and fracture toughness [8, 17, 18].

Among the whole variety of methods aimed at the improvement of these characteristics, one of the most efficient ones is the optimization of a microstructure. We can separate three main ways in this direction:

- change in the grain sizes from submicronic ones to macrosizes coinciding with the sizes of monocrystals or directionally solidified alloys;
- transformation of a crystal structure;
- creation of polyphase structures.

It is considered that the brittleness of titanium intermetallic Al_3Ti is caused by the insufficient number of sliding systems and is characteristic of a complicated crystal structure (DO_{22}). As known [19, 27], this drawback can be removed by the transformation of the DO_{22} structure to the ordered cubic one $L1_2$ which possesses a greater number of sliding systems (as compared to the initial DO_{22} structure). This transition occurs upon alloying of titanium intermetallic Al_3Ti with such elements as Ni, Cr, Fe, Mn, Cu, Ag, Zn, Pd and is accompanied by some enhancement of plasticity of intermetallic Al_3Ti under compression. Nevertheless, even in this case, plasticity of intermetallidic alloys is insufficient [21, 28].

One of the efficient ways in the construction of materials with prescribed properties is the creation of structures with the number of phases to be at least two. A significant role in the improvement of properties of such materials is played by the availability of a high density of interfaces (like in eutectoid-pearlite-steels and martensitically transformed and fine-grained structures).

It is known that a considerable improvement of plastic properties and impact toughness of the TiAl-based alloys was achieved upon the creation of a periodic lamellar two-phase structure [29]. The formation of such a structure is also possible under eutectic crystallization, when the periodic two-phase structure and phase composition of alloys are formed directly upon the transformation of the melt into two solid phases [30-32]. In this case, the phase components of an alloy are close to thermodynamically equilibrium ones and have low interphase energy and high thermal stability, which allows one to preserve a level of the mechanical properties of alloys up to high temperatures. Eutectic alloys have also other advantages: they have melting temperatures which are lower than those of single-phase intermetallics, and a narrow temperature interval of melting which leads to high casting properties, and a low porosity.

In view of the above-presented, the authors of the present project were faced with the problem of the establishment of physical foundations of the development of a high-modulus intermetallic $L1_2$ ($Al_3Ti_{1-x}Me_x$) matrix composite with optimum combination of strength and plastic characteristics.

The solution of this complicated problem has become possible due to the successive realization of a number of subsequent stages:

- determination of both the composition of the matrix of a developed eutectic composite and the chemical nature of phases participating in its formation;
- search for phase diagrams of the eutectic type and determination of peculiarities of the crystallization of alloys;
- determination of a balanced alloying system which preserves the eutectic structure and ensures the necessary level of mechanical properties of the alloys.

4.2. Experimental procedure

The investigation was carried out with as-cast alloys by metallographic, thermal and X-ray analysis. The mechanical properties were determined by hardness measurements at room and elevated temperatures and in compression and bending tests.

The alloys were prepared by arc melting in gettered argon atmosphere with a nonconsumable tungsten electrode on a water-cooled copper hearth with turning and remelting at least ten times to ensure homogeneity. The

high purity metals (Al, Ti, Cr, V, Mn, Re, Nb, B, Zr,) were used for smelting. Alloys composition was controlled by weighting method (the loss of weight didn't excess 0.1 %).

Differential thermal analysis (DTA) and thermal analysis (TA) were employed to establish the phase transformation temperatures. The TA method is based on recording the phase transformation temperatures at a constant thermal flux from the heater to the specimen, and the magnitudes of the starting and final temperatures of the phase transformation can be determined with an accuracy of ±5 °C. DTA and TA were performed on samples cut from the as-cast ingots which were contained in high purity aluminum crucibles in ultra high purity helium. DTA runs were performed at a heating/cooling rate of 20 °C/min (TA – at 2.5 °C/min) starting from room temperature.

An MIM-9 type light microscope was used for microstructural observation. Phase identification was done using CuK_α-radiation in a DRON-UM1 diffractometer. A graphite monocrystal was used as a monochromator. The program complex CSD was used for the phase identification. High temperature diffractometer investigations were performed in helium atmosphere, using UVD-2000 add-on device. Temperature control to within ±2K was made by using of Pt-10RhPt thermocouple. Pure silicon powder, either mixed to the grinded specimen or deposited as thin layer on the cast alloy, was used as internal standard in high temperature investigations. The diffractograms were registered by step scanning in the angle range 2ϑ: 10 – 130 ^{0}. Scanning step was 2θ=0.05 ^{0}, and exposure time was varied from 5 to 20 s. The improvement of calculations of the phases lattice spacing was made by least-squares method with taking into account all diffractional profiles registered. CSD software system was used for the calculations. The full-profile analysis of diffraction patterns was made by using of DBWS-9411 software.

The hardness was measured using a Vickers indenter at load 98N; Young's modulus was determined in four point bending tests (nominal specimen dimensions of 3.5x5x50 mm^3) at a cross-head speed of 0.2 mm/min. The equipment permits control of the strain before fracture in the deformation range of 10^{-5}-10^{-2} with the sensitivity not lower than $2x10^{-5}$.Compression tests (nominal specimen dimensions of 3x3x5 mm^3) were carried out with a strain rate of 10^{-3} s^{-1}; and yield strength σ_y (the stress under 0.2 % deformation), ultimate strength σ_f, ε_f (strain measured at the moment of macroscopic fracture) has been determined. The determination of the mechanical properties in the temperature interval of 20-850 °C were carried out into the air and above 850 °C – in vacuum.

4.3. Choice of the matrix composition for an eutectic $L1_2$ intermetallic matrix composite

The task of this stage consisted in the determination of a composition of alloyed intermetallic $Al_3Ti_{1-x}Me_x$ with the $L1_2$ structure ($L1_2$ in what follows) that became the base of the creation of casting high-modulus eutectic composites. Criteria of a choice were the simplicity of a phase composition, technological efficiency, values of the elasticity modulus, and characteristics of microplasticity.

We note that it was rather difficult to construct the full pattern of the phase regions, where $L1_2$ intermetallics exist, by using the literature data for various alloying systems, because the intermetallics were obtained by different methods (arc melting, arc melting + hot isostatic pressing, mechanical alloying, etc.). In addition, the results obtained by metallographic, thermal, and X-ray phase analyses did not agree with one another, information about the interconnection of the composition of alloys and their structure and physicomechanical properties was scanty, and information about the character of formation of the $L1_2$ phase was practically absent.

Therefore, at the first stage, we carried out the comparative studies of $L1_2$ intermetallics alloyed with Cr, Mn, Ni, and Fe. As a result, we defined more exactly the compositions of the alloys with maximum content of $L1_2$ intermetallic in the appropriate ternary systems Al-Ti-Me (Me = Cr, Ni, Mn, Fe). We established that they correspond to compositions $Al_{62}Ti_{28}Cr_{10}$, $Al_{67}Ti_{25}Ni_8$, $Al_{67}Ti_{25}Mn_8$, and $Al_{66}Ti_{66}Fe_8$. By thermal analysis, we determined the liquidus temperatures of these intermetallidic alloys (1370, 1350, 1372, and 1285 °C, respectively) and the dependence of the hardness of intermetallics $Al_3Ti_{1-x}Me_x$ (Me = Cr, Mn) on temperature in the interval 20 - 900 °C (Fig. 4.1). By the method of indentation with the use of a series of pyramidal indenters with various sharpening angles, we constructed the strain curves for both Al_3Ti and alloyed intermetallics $Al_3Ti_{1-x}Me_x$ (Fig. 4.2). In the coordinates "stress - strain," we showed that the characteristic of plasticity δ_H increases from ~0.68 for Al_3Ti to ~0.85 for $Al_{61}Ti_{27}Cr_{12}$ and $Al_{66}Ti_{23}Mn_{11}$, and the flow stress decreases in the row $Al_3Ti \rightarrow Al_{61}Ti_{27}Cr_{12} \rightarrow Al_{66}Ti_{23}Mn_{11}$ (Tabl. 4.1) [14]. The analysis of the curves obtained testified to the dislocation character of deformation of the alloyed intermetallics. In the mechanical tests in bending, we determined the elasticity moduli of the alloyed intermetallics which were 180 GPa for $Al_{61}Ti_{27}Cr_{12}$ and 118 GPa for $Al_{66}Ti_{23}Mn_{11}$. It was determined that plasticity in compression tests for of alloyed $L1_2$ intermetallics was 5-6%, whereas Al_3Ti revealed no plasticity in mechanical tests of all kinds.

Among the variety of $L1_2$ intermetallics on the base of Al_3Ti, a particular attention is attracted by alloys doped with Cr. They possess the best resistance to oxidation [3, 6], minimum hardness [33], and satisfactory plasticity in compression [4, 34]. All this defined the promises of their use as a basis for the development of new light-weight high-modulus heat-resistant materials.

To comprehend the processes running upon the derivation and thermal processing of these alloys, it was necessary to minutely know the phase equilibria in the existence region of $L1_2$ intermetallic. The literature contains the evidence for the existence, in the solid state, of two- and three-phase equilibria between $L1_2$ and other intermetallics, as well as between $L1_2$ and β (where β is the solid solution of Ti and Al in Cr) [4, 10]. However, the available data were contradictory. Using them, it was impossible both to form the ideas of the structure of alloys

belonging to different phase regions and of the types of phase equilibria and to establish the interconnection between a structure and properties of alloys.

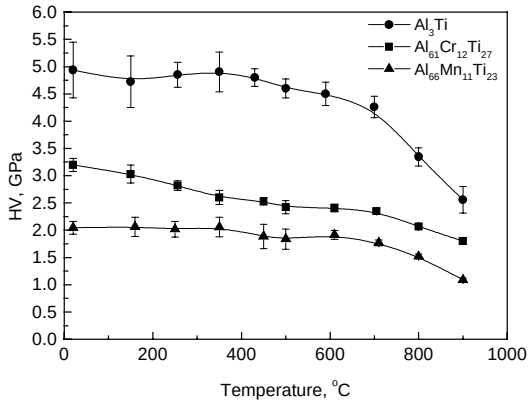

Figure 4.1. The temperature dependence of hardness.

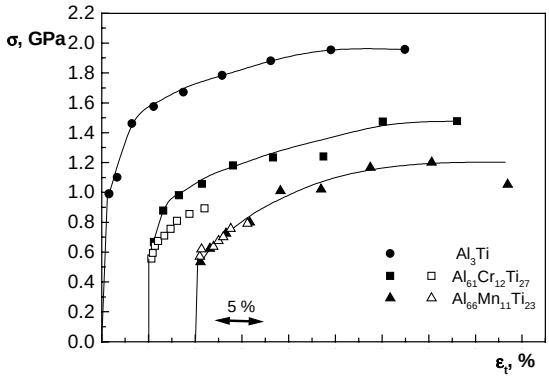

Figure 4.2. The stress-strain curves. Full marks – indentation technique, opened marks – compression tests.

Table 4.1.

Chemical and phase composition, mechanical properties and thermal characteristics of alloys

Materials		Al_3Ti	$Al_{61}Cr_{12}Ti_{27}$	$Al_{66}Mn_{11}Ti_{23}$
Phase composition	the basic phase	Tetragonal DO_{22}	Cubic $L1_2$	Cubic $L1_2$
	lattice parameters, Å	a=3.863(1), c=8.587(2)	a=3.965 (1)	a=3.959 (3)
	the second phase	Al, traces	non-identified, 7 %	Al_3Ti, 3 %
Young's modulus E, GPa	obtained in bending test	156	178	168
Fracture stress, MPa	in bending σ_{fb}	162	215	225
	in compression σ_{fc}	354	892	790
Mechanical characteristic, obtained by indentation method	yield stress σ_o, MPa	980	630	520
	plasticity characteristic δ_H	0.68	0.81	0.87
	strain hardening parameters:			
	N, GPa	2.4	1.58	1.66
	n	0.47	0.4	0.58
Thermal characteristics, ^{0}C	liquidus temperature T_l (TA)	1420	1370	1285
	solidus temperature T_s(DTA)	1395	1261	1248

Our own experimental studies of the structure and phase composition of alloys positioned immediately at the Al-rich corner of the Al-Ti-Cr phase diagram have shown that all they have peritectic character. Moreover, the analysis of phase equilibria in the boundary binary systems Al-Cr, Al-Ti, and Cr-Ti [35, 36], where there are large regions of solid solutions on the base of transition metals, allowed us to expect the existence of eutectic equilibrium between melt (L) and two solid phases $L1_2$ and β ($L \leftrightarrow L1_2+\beta$) in the ternary Al-Ti-Cr system.

The next stage of the work is devoted to the search for the conditions of existence of the eutectic $L \leftrightarrow L1_2+\beta$ transformation in the Al-Ti-Cr system, study of peculiarities of the structure formation of alloys, and comparative analysis of the mechanical properties of alloys depending on the relations of phases participating in the eutectic transformation.

4.4. Regularities of the formation of the eutectic structure in an $L1_2$ intermetallic matrix composite of the ternary Al-Ti-Cr system

As a result of the performed studies, we found that the melting diagram of the ternary system Al-Ti-Cr has eutectic character between the region of existence of the $L1_2$ phase and the Cr-rich corner and determined the regions of compositions of the alloys whose crystallization is accompanied by the formation of eutectic-type structures. We established that such structures are formed as a result of the running of two univariant eutectic reactions with participation of $L1_2$ intermetallic: $L \leftrightarrow L1_2+Al_{17}Cr_9$ and $L \leftrightarrow L1_2+\beta$ (Tabl. 4.2). We note that intermetallic $Al_{17}Cr_9$ does

not exist in the binary system Al-Cr, but its diffraction pattern most fully are described intermetallic Al_8Cr_5 alloyed with Ti [13]. The univariant eutectic equilibrium $L \leftrightarrow L1_2+Al_8Cr_5$ is observed in the temperature interval 1225-1260 °C, and the eutectic ($L1_2+Al_8Cr_5$) has fibrous structure (Fig. 4.3).

Table 4.2.

Characteristics of phases registered in as-cast alloys of the ternary Al-Ti-Cr system by X-ray diffraction analysis

Phase	Structure	Prototype	Symmetry	Space group
$Al_3Ti_{1-x}Cr_x$	$L1_2$	Cu_3Au	cubic	Pm3m
TiAlCr	C14	$MgZn_2$	hexagonal	$P6_3/mmc$
β	A2	W	cubic	Im3m
$AlCr_2$	$C11_b$	$MoSi_2$	tetragonal	I4/mmm
Al_8Cr_5	$D8_{10}$	Al_8Cr_5	trigonal	R3m

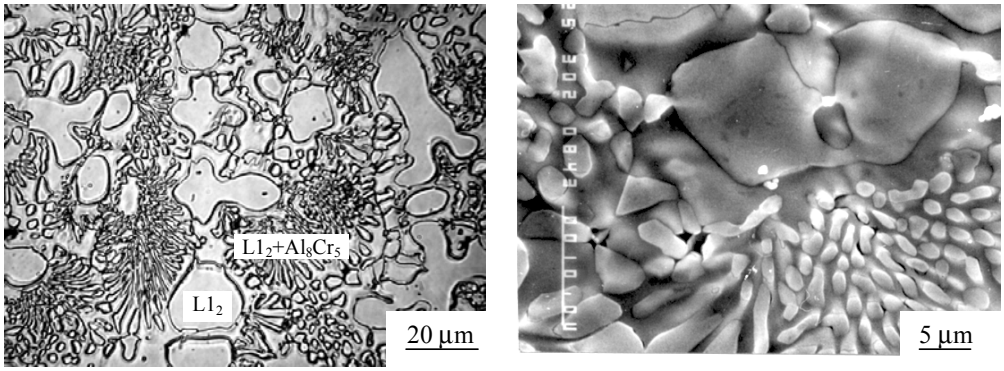

a b

Figure 4.3. Structure of the hypoeutectic ($L1_2+Al_8Cr_5$) alloy: (a) optical microscopy; (b) scanning electronic microscopy (selective etching).

The comparison of mechanical properties of the alloys of both systems showed that a higher level of plastic properties the ($L1_2$+β) eutectic alloys predetermines the promises of their use as a base of new alloys. Therefore, the most attention was given further to the study of regularities of the formation of the eutectic structure in ($L1_2$+β) alloys and to the investigation of their mechanical properties.

To solve the posed problem, namely the determination of the concentration-temperature conditions of existence of the eutectic transformation $L \leftrightarrow L1_2+\beta$ in the ternary system Al-Ti-Cr, we smelted the alloys, whose compositions are presented on the concentration triangle of the system Al-Ti-Cr (Fig. 4.4, Table 4.3). The comparison of results of the complex study of the structure, phase composition, melting temperature, and temperature interval of melting of the alloys allowed us to construct a projection of the line of univariant eutectic transformation $L \leftrightarrow L1_2+\beta$ (LUET) on the concentration triangle of the system Al-Ti-Cr.

The coordinates of this line were determined by the absence of primary dendrites of both phases ($L1_2$ or β) in the structure of alloys and by the absence of additional effects related to their melting on the thermal curves. We determined that this transformation is realized in a wide region of concentrations of Ti and Cr. The projection of LUET $L \leftrightarrow L1_2+\beta$ on the concentration triangle of the ternary system Al-Ti-Cr is represented by the line *ee´* which has the form of a smooth curve convex to the side of the β-phase and is described by the equation (at. %): $C_{Cr} = 21.18 + 2.44 \cdot \ln(27.67 - C_{Ti})$. A decrease in the Ti content in alloys from 25 to 20.5 at. % leads to a decrease of the final temperature of the eutectic ($L1_2$+β) transformation from 1285 to 1255 °C. The temperature interval of melting of the eutectic along LUET does not exceed 10 °C, which defines high casting properties of alloys. The data obtained testify to the existence of a wide region of two-phase ($L1_2$+β) alloys in the studied concentration region at high temperatures.

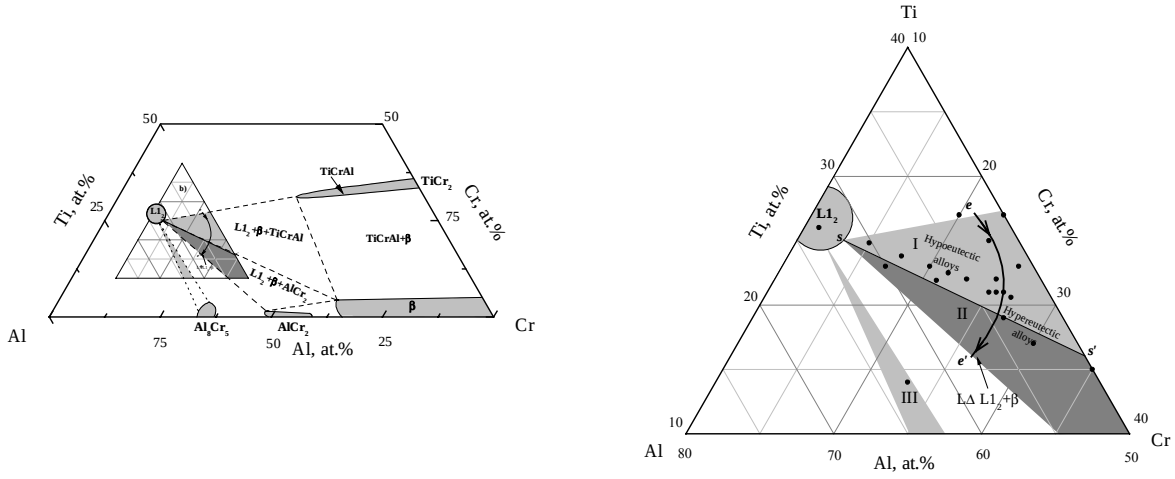

a b

Figure 4.4. Scheme of phase equilibrium in the ternary system Al-Ti-Cr (a) and portion of the liquidus surface at the Al-rich corner of the Al-Ti-Cr ternary system (b). Dots correspond to the compositions of investigated alloys; *ee´* is the line of the univariant eutectic transformation $L \leftrightarrow L1_2+\beta$; *ss´* is the line separating the regions of as-cast alloys in which the β-solid solution decomposes with the formation of aluminide TiAlCr (region I) or $AlCr_2$ (region II). III is the region of ($L1_2+Al_8Cr_5$) phases; the single phase regions [4, 6, 10] are designated by shading.

Table 4.3.

Chemical and phase composition, hardness and Young's modulus of some as-cast alloys

Alloy	Region (Fig.4.4)	Chemical composition, at. %			Phase content		Type of eutectic structure	HV, GPa	E, GPa
		Al	Ti	Cr	Composition	Ratio, %			
1	I	52.0	25.0	23.0	$L1_2$:ß: TiAlCr	65:35:trice	eutectic	3.36	189
2	II	54.0	19.0	27.0	$L1_2$: ß:$AlCr_2$	60:30:10	hyper	3.33	192
3	I	56.0	22.5	21.5	-	-	hypo	2.85	188
4	I	51.0	23.0	26.0	-	-	hyper	4.01	-
5	I	53.0	21.0	26.0	-	-	eutectic	-	-
6	III	63.0	14.0	23.0	$L1_2$: Al_8Cr_5	55:45	hypo	4.17	-
7	$L1_2$	63.0	26.0	11.0	$L1_2$:$AlCr_2$	99:1	-	2.25	182
8	II	60.0	23.0	17.0	$L1_2$:$AlCr_2$	90:10	hypo	2.17	181
9	I	55.0	22.0	23.0	$L1_2$:ß	70:30	hypo	2.66	182
10	I	53.0	22.0	25.0	$L1_2$:ß	50:50	hypo	3.02	-
11	I	53.0	27.0	20.0	$L1_2$: ß: TiAlCr	80:15:5	hypo	3.36	192
12	I	50.0	27.0	23.0	$L1_2$: ß: TiAlCr	70:15:15	hyper	3.76	184
13	I	58.5	23.8	17.7	-	-	hypo	2.47	-
14	I	53.5	21.0	25.5	-	-	hypo	3.14	-
15	I	52.7	20.6	26.7	-	-	hyper	3.45	-
16	I	57	23	20	$L1_2$:ß	85:15	hypo	2.43	175
17	I	54	21	25	$L1_2$:ß	65:35	hypo	2.85	-
18	II	53	17	30	$L1_2$:$AlCr_2$:ß	-	hyper	3.6	-
19	II	50	15	35	$L1_2$:$AlCr_2$:ß	40:50:10	hyper	4.29	-
20	I	60.2	24.8	15.0	$L1_2$:ß	93:7	hypo	2.42	181
21	I	57.1	21.9	21	$L1_2$:$AlCr_2$:ß	85:10:5	hypo	2.85	190

The eutectic structure of alloys positioned on LUET is formed by alternating fibres and plates of the $L1_2$ and β phases. The portion of fibres in the eutectic depends on the composition of alloys and increases with decrease in the content of Ti in them. The structure of two-phase eutectic ($L1_2$+β) alloys is analogous to eutectic structures of the ($Al+AlCu_2$) binary system described in [37] (Fig. 4.5). The last fact allows us to conclude that the crystallization of these eutectics occurs by a same mechanism. The base (generating the eutectic colony) phase is $L1_2$, whose primary

crystals are growing, preserving the edged form up to definite sizes depending on the conditions of crystallization. Then the β phase begins to crystallize on the surface of edged crystals, by forming a border around a primary crystal. Further, we observe the appearance of branches entering into a melt on the defect sections of this rim which initiate the development of a two-phase eutectic colony proper. From this moment of crystallization, the melt passes to the stage of common growth of two phases: $L1_2$ and β.

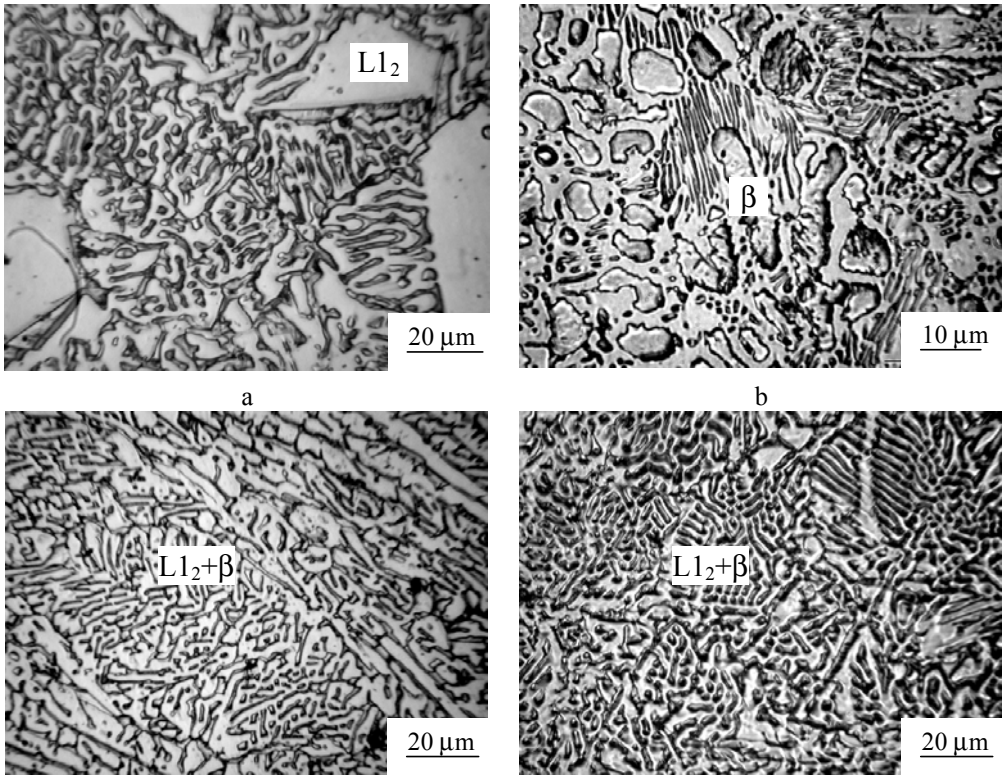

Figure 4.5. Characteristic microstructures of as-cast alloys: (a) hypoeutectic alloy 3, (b) hypereutectic alloy 4, (c) alloy 1 and (d) alloy 5 are situated near the line of univariant eutectic transformation.

4.5. Phase transformations in the solid state of eutectic ($L1_2$+β) alloys

On the next stage of the work, for a realized choice of base compositions and the creation of high alloyed alloys on their base, it was necessary to understand the processes running on their heating and crystallization and to make analysis of the influence of a structure on the mechanical properties of alloys. With this purpose, we studied phase transformations in the solid state.

The experimental studies showed that one of the phases, $L1_2$, of eutectic ($L1_2$+β) alloys is stable, and the second, a β-solid solution on the base of Cr, decays in the process of their cooling with the formation of various intermetallics (Tabl. 4.2, Fig. 4.4). Thermal stability of this phase and the nature of formed phases are defined by the initial composition of an alloy and can vary in wide limits. Using the method of X-ray *in situ* high-temperature analysis, we established the following. As a result of transformations in the solid state occurring under the cooling of alloys, AlTiCr or $AlCr_2$ is precipitated from the β-solid solution (Fig. 4.6). This leads to the formation of the two-phase ($L1_2$+β) state or three-phase ($L1_2$+β+$AlCr_2$) or ($L1_2$+β+TiAlCr) state after the cooling of alloys depending on their composition. In this case, the third phase in alloys enriched or depleted with Ti is, respectively, TiAlCr or $AlCr_2$. We note that the simultaneous precipitation of these two intermetallics from the β-phase was not observed under all conditions. We determined the position of the boundary, on which the change of precipitating phases occurs. According to the results obtained, we draw the line ss′ dividing the region of ($L1_2$+β) alloys which are two-phase under crystallization into two regions (I and II), respectively, ($L1_2$+β+TiAlCr) and ($L1_2$+β+$AlCr_2$) on the concentration triangle of the ternary system (Fig. 4.4 b). Near the boundary ss′, there exist cast alloys that preserve the two-phase ($L1_2$+β) state after the cooling to room temperature (Tabl. 4.3). We emphasize once more that the alloys in I and II regions have the same phase composition, ($L1_2$+β), at high temperatures.

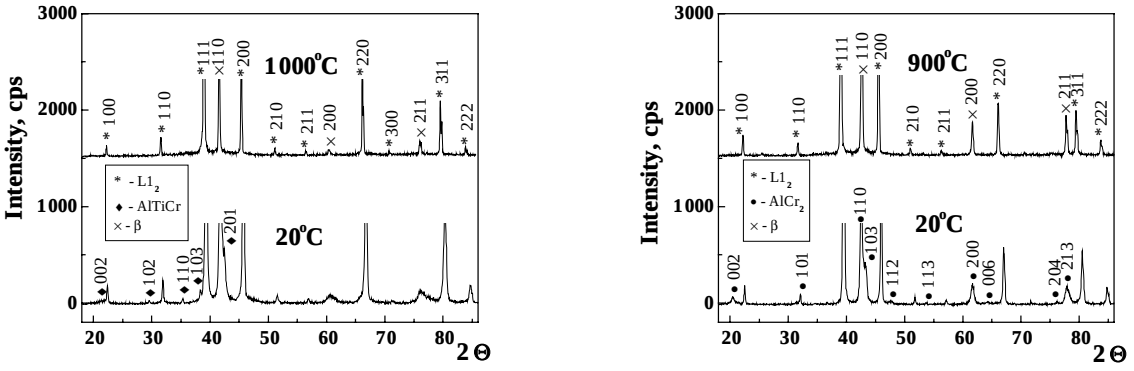

a b

Figure 4.6. Portion of the *in situ* diffraction paterns of as-cast alloys: a) region I and b) region II in fig. 4.4b. Cu K_α -radiation

Further, we studied the possibility to preserve the two-phase ($L1_2$+β) state by means of the stabilization of a β-solid solution and to extend the region of its existence upon a doping of alloys. This turns out to be possible due to a purposeful choice of the alloying system.

4.6. Influence of alloying on the concentration-temperature parameters of the L↔$L1_2$+β eutectic equilibrium

As known, alloying can significantly influence on the concentration-temperature limits of existence of two-phase eutectic alloys and the stability of solid solutions of the phases coexistent in equilibrium and can promote a change in the dispersion and morphology of structural components of the eutectic alloys.

By metallographic, differential thermal, X-ray diffraction and X-ray *in situ* analyses, we studied the influence of the separate elements alloying with elements of I - VIII groups of the Periodic table (Ag, Y, Sc, B, Sn, Zr, Hf, V, Nb, Mo, Mn, Re, and Ni) and with their combinations on the phase composition, melting temperature, morphology of structural components, and mechanical properties of the eutectic ($L1_2$+β) alloys. In this case, we determined the amount of each alloying element and their complexes which would not cause both a change in the phase composition of alloys and the appearance of additional phases.

On the choice of alloying elements, we considered the peculiarities of their interaction both with Cr and intermetallic $L1_2$. For example, V and Mo form the continuous series of solid solutions, and Re and Ni forms the extended regions of solid solutions with Cr [35]. Hence, the introduction of these elements must favour a considerable extension of the region of existence of a β-solid solution and suppress transformations in the solid state.

As a baseline alloy for alloying, we chose the hypoeutectic alloy containing (in at. %) 55Al-22Ti-23Cr, whose properties are given in Table 4.4.

Table 4.4.

Properties of 55Al-22Ti-23Cr baseline alloy

Phase ratio,%	DTA,°C heating	Mechanical properties									Density ρ, $g \cdot sm^{-3}$
		HV, MPa	compression			bending			modules		Poisson's ratio η	
			σ_y, MPa	σ_f, MPa	ε, %	σ_y, MPa	σ_f, MPa	δ, %	E, GPa	G, GPa		
$L1_2$+β, 70:30	736 1249	2660	598	1666	22	375	605	0.04	185 183*	74*	0.237*	3.9

* the result is obtained by ultrasonic method

As a result of the performed studies, we established that the introduction of doping elements can lead to a change in the phase ratio in the eutectic, to a displacement of its composition to the Al-rich corner of the ternary phase diagram (V, Re, and Mo) or in the opposite direction (Zr, Ni, Sn, Ag, Mn, and Nb), and to a change in the eutectic morphology from a lamellar to fibrous one (V and Mo) (Fig. 4.7).

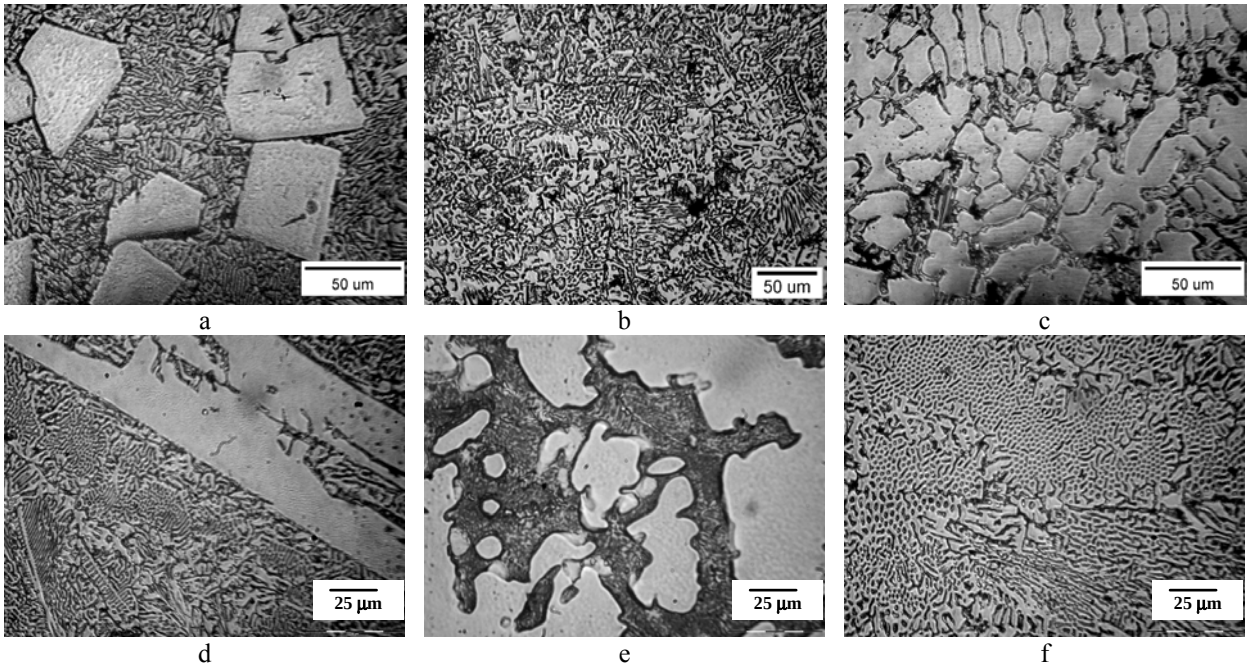

Figure 4.7. Effect of alloying of the baseline alloy on eutectic content in alloys and microstructure: a) without alloying; b) 1.5 at. % Mo; c) 2 at. % Ag; d) 1 at. % Sc; e) 10 at. % Ni; f) 6 at. % V

Table 4.5.

The influence of alloying on structure, phase composition, thermal and mechanical characteristics in compression of the baseline ($L1_2$+β) alloys

Alloying element, at. %		Phase ratio $L1_2$:β, %	Structure	DTA, °C heating		HV, MPa	Mechanical properties		
							σ_{ys}, MPa	σ_f, MPa	ε, %
Beseline alloy		70:30	hypo-	736	1249	2660	598	1666	20.3
Ag	2.0		hypo-	716	1234	2740			
Y	1.5		noneut.			3510			
Sc	1.0	70:30	hypo-			2850	593	1000	10.0
	0.02		hypo-	716	1251	2760			
B	0.15		hypo-			2720			
	0.3		hypo-			2760			
Sn	0.2		hypo-	710	1251	2700			
V	6.0	85:15	eutectic	-	1286	2870	670	2147	19.5
Nb	1.0	91:9	hypo-	716	1256	2740			
Mo	1.5		hyper-	704	1269	3110			
	2.0		hypo-	732	1245	2660	557	1596	16.7
	4.0		hypo-	765	1234	2560			
Mn	5.0	91:9	hypo-	726	1234	2490	533	1850	20.9
	6.0	-	hypo-	771	1220	2490	495	1563	17.8
	8.0	95:5	hypo-	737	1210	2850	485	1734	20.0
Re	1.0	89:11	hypo-	-	1256	2620			

On the basis of the results obtained, we separated a group of elements (V, Re, Mn, Nb, and Zr) for the creation of complex-doped eutectic ($L1_2$+β) alloys. These are elements that have an essential influence on the morphology and dispersion of the eutectic and primary crystals and on transformations in the solid state, but induced no changes in the phase composition of the baseline alloy in the limits of the concentrations under study. We showed that the simultaneous introduction of complexes VMnRe, VMnReNb, and VMnReNbZr leads to suppression of the solid-phase transformation of β→$AlCr_2$ for a definite ratio of the elements (Tabl. 4.6). This is testified by the absence of any additional peaks on the diffractograms of alloys upon their study by X-ray *in situ* analysis (Fig. 4.8) and on the curves derived by differential thermal analysis (Fig. 4.9).

Table 4.6.

Chemical composition, hardness, results of X-ray and DTA analysis of the complex-alloyed ($L1_2$+β) alloys

Chemical composition, at. %												Phase ratio, %	DTA, °C heating		Structure	HV, MPa
Al	Ti	Cr	V	Re	Mn	Nb	Zr	Hf	Ni	B	Sc					
54. 8	21.9	23	-	-	-	-	0.1		-	-	0.2	-	721	1251	hypo-	2790
54.9	21.1	23	-	-	-	-	0.9		-	0.1		-	716	1251	hypo-	3040
55	21	23	-	-	-	-	0.5	0.5	-	-	-	($L1_2$+β) (88:12)	721	1245	hypo-	2830
55	22	17	-	1	5	-	-		-	-		-	771	1227	hypo-	2540
55	22	17	2	-	4	-	-		-	-		($L1_2$+β) (88:12)	-	-	hypo-	2540
55	22	17	4	-	2	-	-		-	-		($L1_2$+β) (93:7)	636	1245	hypo-	2680
55	22	17	-	1	5	-	-		-	-	-	-	771	1272	hypo-	2540
57	23	9	10	1								-	-	1259	hypo-	2900
57	23	7	10	1	-	-	-		2	-	-	-	-	1186	3 phase	3330
55	22	16	4	1	2	-	-		-	-	-	($L1_2$+β) (89:11)	-	1269	hypo-	2540
55	21.2	16	4	1	2	0.8	-	-	-	-	-	($L1_2$+β) (90:10)	-	1269	hypo-	2700
55	20.7	16	4	1	2	0.8	0.5	-	-	-	-	($L1_2$+β) (91:9)	-	1269	hypo-	2900
55	22	19.2	-	1	-	0.8	-	-	2	-	-	-	-	-	none ut.	3020
55	22	15.2	4	1	-	0.8	-	-	2	-	-	($L1_2$+β+ß″) (88:11:1)	-	-	none ut.	3220
55	22	15.2	-	1	4	0.8	-	-	2	-	-	($L1_2$+β) (93:7)	-	-	none ut.	2920

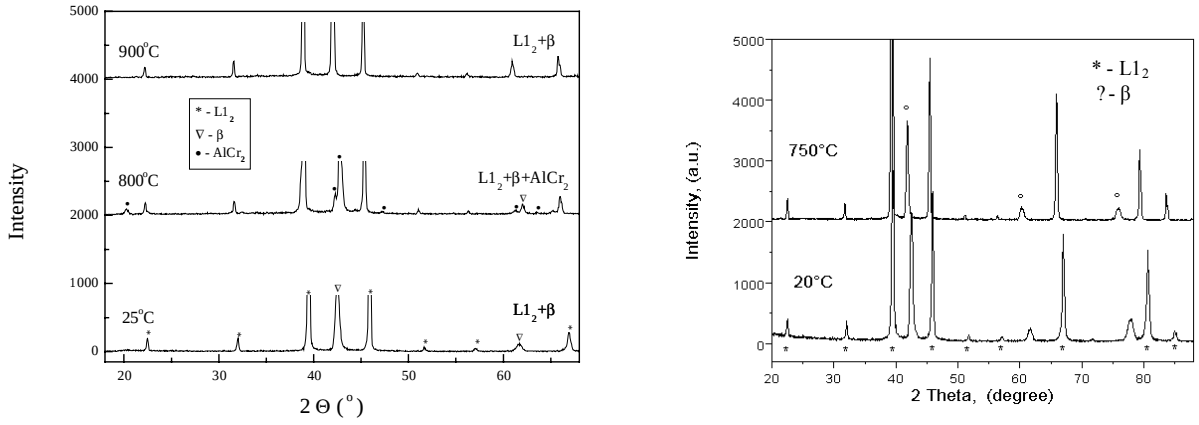

a b

Figure 4.8. Fragments of *in situ* difractograms of as-cast alloys: (a) baseline alloy without alloying, (b) alloyed with V (4 at.%), Mn (2 at.%) and Re (1 at. %) (while heating); CuK_α-radiation.

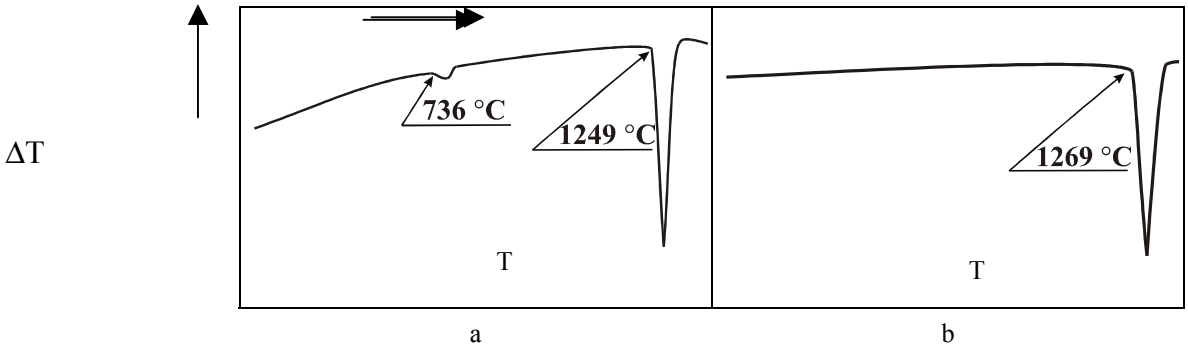

Figure 4.9. Thermograms (DTA) of as-cast ($L1_2$+β) alloys: (a) baseline alloy without alloying, (b) alloyed with V (4 at.%), Mn (2 at.%) and Re (1 at. %)

4.7. Influence of annealing temperature on the phase composition and mechanical properties of eutectic ($L1_2$+β) alloys

With the purpose to determine the effect of thermal treatment on the composition and mechanical properties of the alloys, we carried out thermal treatment in two regimes:

- annealing of cast alloys for 2 hours in the temperature interval 400-1100 °C,
- preliminary homogenization of cast alloys for 20 hours at 1150 °C in vacuum with a cooling in a furnace to room temperature and subsequent annealing for 2 hours in the temperature interval 400-1100 °C.

The results of tests showed that the homogenizing treatment or annealing of cast alloys with the base composition leads to a considerable deterioration of their plastic characteristics (Fig 4.10). The comparison of the results of thermal analysis, X-ray *in situ* analysis, and the tests of mechanical properties allows us to conclude that such a decreasing of mechanical properties of the alloys is caused, in the first turn, by the processes running in the β-solid solution and by the change of the phase composition due to the formation of new intermetallic phases.

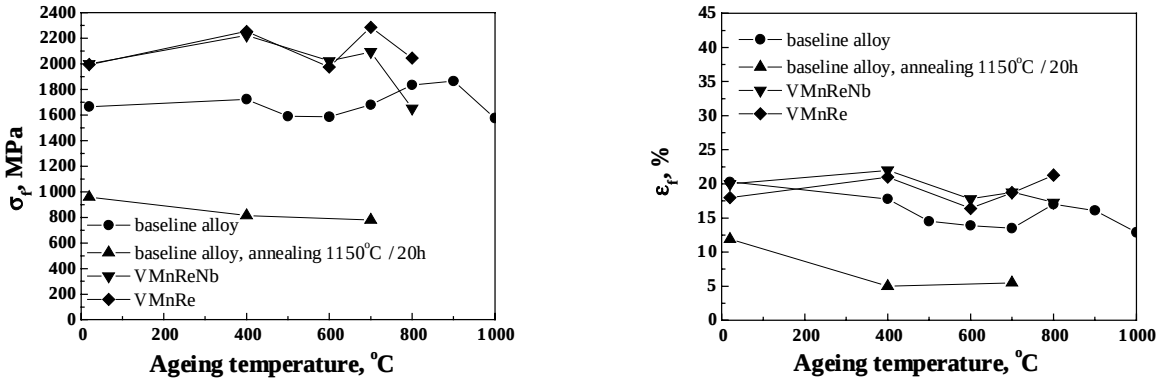

Figure 4.10. Influence of annealing on the mechanical properties of eutectic ($L1_2$+β) alloys.

Mechanical properties of the annealed alloys doped by complexes VMnRe and VMnReNb, in which these transformations are absent, are better as compared to those of undoped alloys (Fig. 4.10).

The analysis of the obtained results allowed us to conclude that it is necessary to perform additional studies of the fine structure of alloys by using electron microscopy for the deeper comprehension of all the processes occurring during a thermal treatment, the determination of optimum conditions for its execution, and the establishment of its interconnection with mechanical properties of the alloys.

4.8. Mechanical properties of eutectic ($L1_2$+β) alloys

We also needed to analyze the effect of a structure on the mechanical properties of alloys. We determined the durometrical characteristics of alloys and studied their behaviour under loading in mechanical tests.

By the results of durometrical measurements in the region of existence of the eutectic transformation L↔$L1_2$+β, we constructed the map of hardness (HV) of alloys (Fig. 4.11).

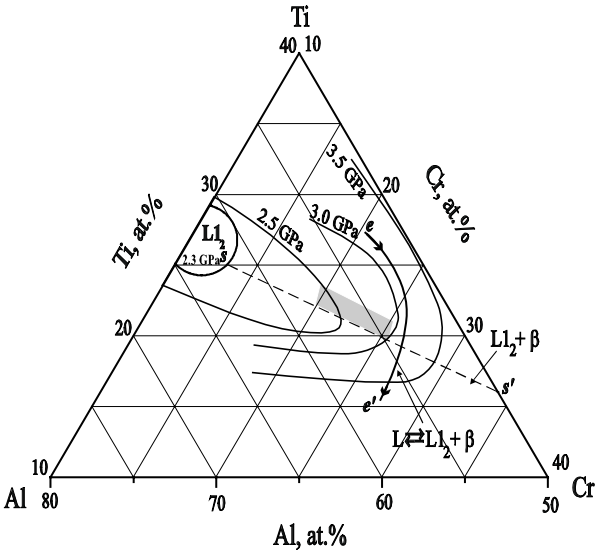

Figure 4.11. Distribution of hardness values in the Al-rich corner of the Al-Ti-Cr system. *ee′* is the line of the univariant eutectic transformation $L \leftrightarrow L1_2+\beta$; *ss′* is the line separating the regions of as-cast alloys with different phase compositions; the grey area is the region of alloys with optimum combination of strength and plasticity.

1.

The comparison of the results of this investigation with those of mechanical tests in compression showed that the formation of the cubic $L1_2$ phase leads to the essential decrease in hardness and the yield limit and to the enhancement of plasticity as compared to less symmetric structures of undoped intermetallics (e.g., DO_{22} for Al_3Ti). The appearance of the eutectic component in alloys and an increase in its volume part leads to the enhancement of hardness and to the improvement of strength and plastic characteristics (Fig. 4.12). In the best way, these properties are combined by two-phase ($L1_2+\beta$) alloys that are positioned near the line ss′ and formed by two cubic phases ($L1_2$ and β). These alloys are better adapted to plastic deformation than three-phase alloys, whose composition includes aluminides TiAlCr or $AlCr_2$.

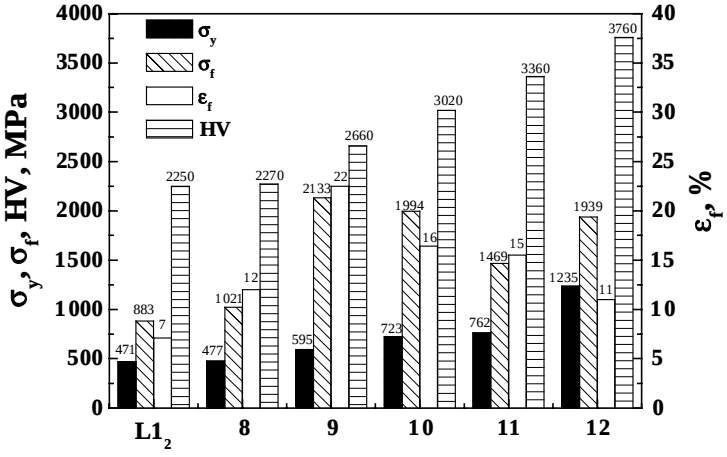

Figure 4.12. Mechanical properties (yield strength at 0.2 % deformation σ_y, ultimate stress σ_f, deformation to fracture ε_f) in compression tests and hardness HV of as-cast alloys. The alloy numbers are given in Table 4.3.

The evolution of the structure of alloys (Fig. 4.13) along the line ss′ (from one-phase to hypereutectic ones) also significantly influences their mechanical characteristics. As seen from Fig. 4.14, in compression tests, the strength σ_f and deformation ε_f which are determined at the moment of macroscopic fracture increase as we recede from the one-phase $L1_2$ region, reach the maximum values for hypoeutectic alloys positioned near the eutectic point, and then decrease. In the hypereutectic region, σ_f again somewhat increases because of a considerable increase in the yield limit.

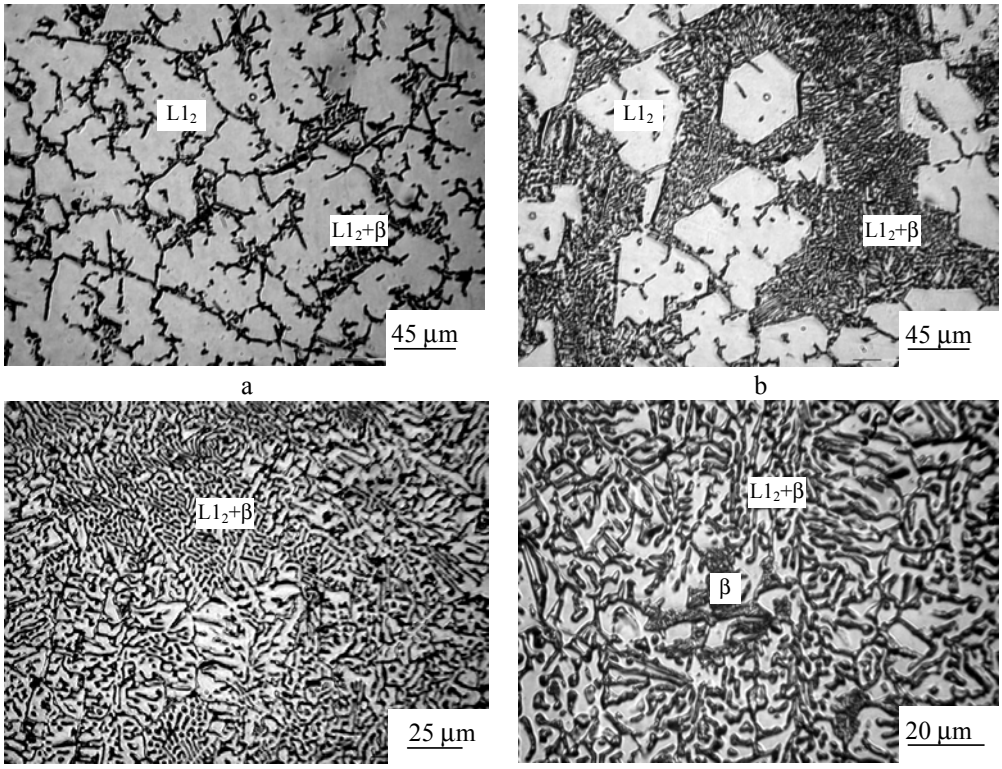

Figure 4.13. Microstructures of as-cast alloys along the line *ss*′: (a, b) hypoeutectic alloys 13 and 3, (c) alloy 14 positioned near eutectic composition and (d) hypereutectic alloy 15

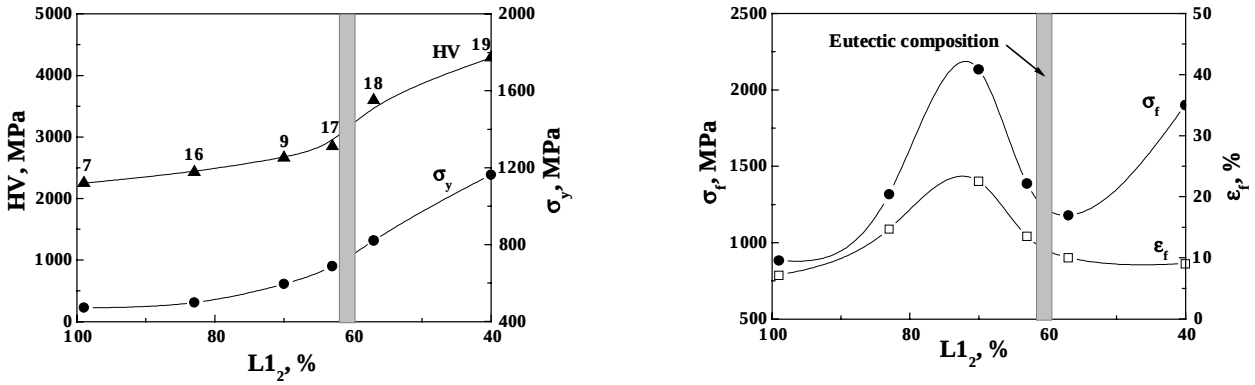

Figure 4.14. Mechanical properties of as-cast alloys along the line *ss*′: a) hardness (HV) and compressive yield stress (σ_y); b) deformation to fracture (ε_f) and ultimate compressive stress (σ_f). The alloys numbers are given in Table 4.3

This evidences about the important role of the eutectic in the formation of a mechanism of plastic deformation for the studied class of alloys. It is natural that the improvement of mechanical characteristics along the line ss′ is caused not only by a change in the structural components ratio, but also by an increase in their dispersion and in the homogeneity of the structure of alloys.

Apparently, plasticity of two-phase ($L1_2$+β) alloys is defined by plastic deformation prior to the fracture of the "softer" $L1_2$ phase. In hypoeutectic alloys with small volume part of the eutectic, a crack appears in the $L1_2$ phase after a deformation of 7-12% and rapidly propagates in this phase, by meeting no obstacles in the form of a disperse eutectic. An increase in its content induces the delay of cracks originating in $L1_2$ dendrites by the eutectic colonies surrounding these dendrites. In connection with this, the deformation ε_f prior to the macroscopic fracture increases and reaches the maximum value in hypoeutectic alloys positioned near the eutectic composition. The studies of the lateral surface of deformed specimens showed that microcracks in these alloys appear at deformations of 7-12 %, but they do not induce the macrofracture of a specimen if deformations are less than 20-22 %. Upon a deformation of alloys of the eutectic composition, where large dendrites of the more plastic $L1_2$ phase are absent, the value of ε_f again decreases to ≈ 10%.

From the viewpoint of mechanical properties, the optimum hypoeutectic character of a structure in

compression tests is also optimum for the tougher scheme of tests, the 4-point bending. The results of tests in bending of some alloys positioned along the line ss′ are given in Fig. 4.15, a. As seen, the cast alloy with hypoeutectic structure demonstrates a maximum strength of 604 MPa and microplasticity ε = 0.04%. The characteristic curves of microplastic deformation of the studied alloys are presented in Fig. 4.15, b. The analysis of these curves confirms the conclusion on that most perspective from the viewpoint of an increase in plasticity are the hypoeutectic alloys positioned near the eutectic composition. Further, such an alloy, (at. %) 55Al-22Ti-23Cr, with the best combination of strength and plastic properties was chosen as the base one for a subsequent alloying (Tabl. 4.4).

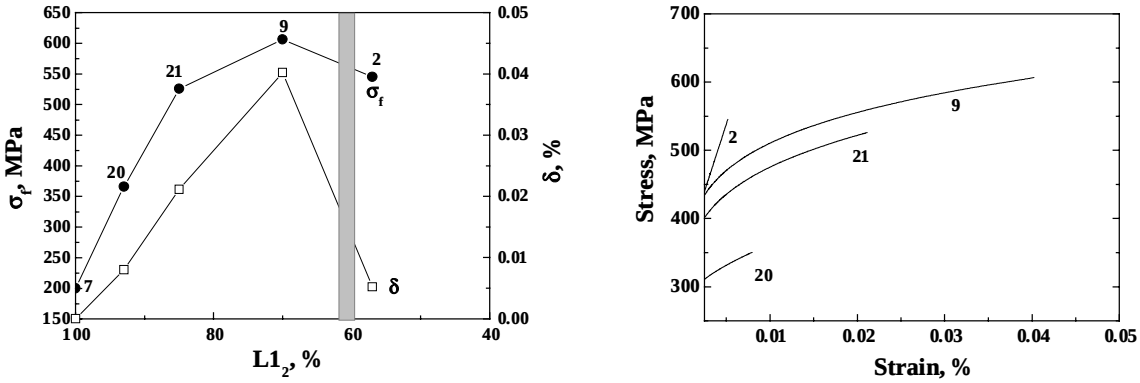

a b

Figure 4.15. Mechanical properties of cast alloys along the line *ss′*: (a) deformation to fracture (δ) and ultimate strength (σ_f) in bending tests; (b) "stress-strain" curves in bending tests of the as-cast alloys. The alloys numbers are given in Table 4.3.

We note that the alloys studied by us possess high values of the elasticity modulus (Tabl. 4.4).

The high melting temperature of the ($L1_2$+β) eutectic (up to 1270 °C) predetermined enhanced high-temperature properties of the alloys. For example, the baseline undoped alloy possesses high heat resistance (above 250 MPa at a temperature of 800 °C) and, at the same time, preserves the ability to hot deformation at temperatures above 1000 °C (0.8 T_{melt}) (Fig. 4.17).

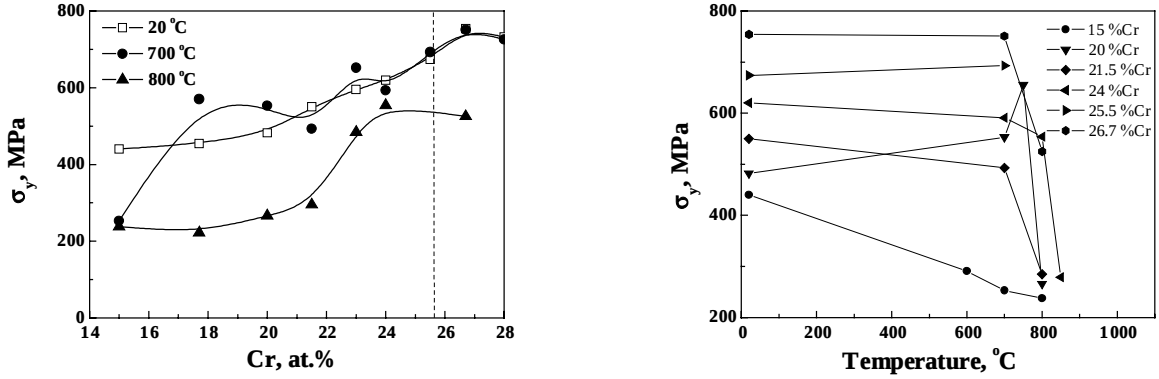

a b

Figure 4.16. Compressive yield strength σ_y (a) and the temperature dependences of σ_y (b) of as-cast alloys located along the line ss′. Dash line corresponds to the eutectic composition

In this case, we see the tendency to the increase in heat resistance as the volume part of the eutectic component in a structure grows: at 700 °C, the yield limit changes from 250 MPa for an alloy positioned near the one-phase region $L1_2$ to 750 MPa for hypereutectic alloy 8 (Fig. 4.16 a). The temperature of the beginning of softening of hypoeutectic ($L1_2$+β) alloys increases with the amount of the eutectic and is equal to 800 °C near the eutectic composition (Fig. 4.16 b).

As a result of alloying the baseline alloy with the complexes VMnRe, VMnReNb, and ReZrB, the yield strenth increases (approximately to 700-750 MPa) at temperatures of 600-700 °C (Fig. 4.17). However, in this case, the temperature of the transition into a softened state decreases, which can be caused by an increase in the amount of

the fibrous eutectic with lesser heat resistance or by a decrease in the volume part share of the eutectic component in doped alloys. The increase in the volume part of the eutectic in complex-doped alloys allows one to widen the temperature interval of their stability and to improve the strength properties of eutectic alloys.

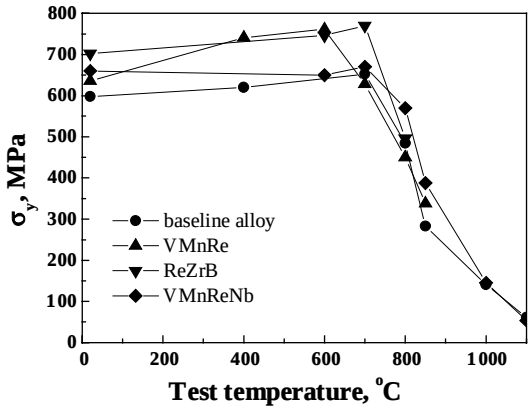

Figure 4.17. The temperature dependence of compressive yield strength σ_y of the baseline and complex alloyed eutectic ($L1_2$+β) alloys

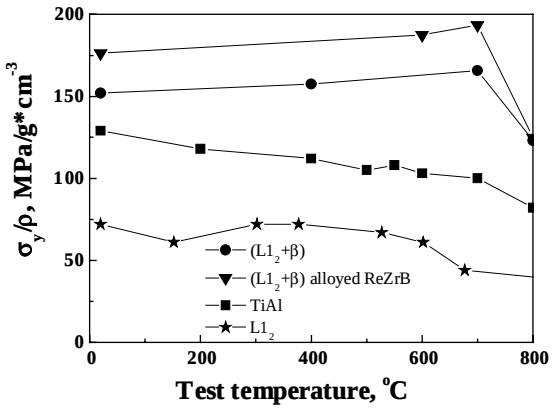

Figure 4.18. The temperature dependence of the specific characteristic (σ_y/ρ) of the eutectic ($L1_2$+β) alloys in comparison with modern alloys on the base of titanium aluminide [38] or powder materials on the base of $L1_2$ intermetallics [39]

Summing up the performed studies, we state the following. On the basis of the approach proposed in the present work that is based on the ideology of the creation of a two-phase eutectic composite with participation of the two cubic phases - $L1_2$ intermetallic and β-phase, the light-weight high-modulus cast alloys with the following complex of unique properties were elaborated:

- hardness in the interval 2000-3500 MPa,
- compressive and bending fracture strengths up to 2000 and 600 MPa, respectively,
- compressive yield strength up to 1200 MPa,
- plasticity up to 22% in compression and up to 0.04 % in bending,
- high and stable level of mechanical properties (compressive yield strength is 650-800 MPa up to 750 °C and is about 145 MPa at 1000 °C (0.8 T_{melt}),
- high values of the elasticity modulus (up to 190 GPa),
- small temperature interval of melting (about 10 °C), which stipulates good casting properties.

A significant content of Cr in alloys predetermines the enhanced corrosion resistance at high temperatures for a long time, and the availability of the eutectic leads to a good creep resistance. The specific characteristics of these materials are close to or better than those of modern alloys on the base of titanium aluminide or powder materials on the base of $L1_2$ intermetallics (Fig. 4.18).

The further improvement of the structure and properties of these alloys is possible at the expense of an increase in their dispersion under additional macro- or microalloying, by means of their manufacturing in the nano-size state, and also under thermomechanical treatment.

CONCLUSIONS

1. In the ternary Al-Ti-Cr system a large compositional region has been established, in which the eutectic transformation of the melt into two solid phases is realized: $L \leftrightarrow L1_2+\beta$. It was shown that this transformation is univariant and occurs in a narrow temperature interval. A decrease of the Ti content in these alloys decreases the temperature, at which the eutectic transformation $L \leftrightarrow L1_2+\beta$ begins, from 1275 °C to 1250 °C, and the temperature interval of this transformation does not exceed 10 °C.

2. The periodic structure of eutectic ($L1_2+\beta$) alloys is formed by alternate lamellae and/or fibers of two phases: $L1_2$ and β. Primary dendrites of these phases have different forms: in hypoeutectic alloys, primary dendrites of the phase $L1_2$ are crystallized in the faceted form, but dendrites of the β-phase are unfaceted in hypereutectic alloys.

3. In cooling of eutectic ($L1_2+\beta$) alloys, the intermetallic compounds $AlCr_2$ or TiAlCr can precipitate from the β solid solution as a result of the phase transformations in the solid state. The position of the boundary (ss′) between the compositions of alloys was determined, at which a change of precipitating phases occurs. It was found that the two-phase ($L1_2+\beta$) structure is partially preserved near this line.

4. In compression tests cast alloys containing the ($L1_2+\beta$) eutectic are characterized by a significant deformation before fracture, exceeding that of single-phase $L1_2$ alloys and of alloys, in which there is a dissolution of β-phases with the precipitation of less symmetric $AlCr_2$ or TiAlCr intermetallics. The hypoeutectic alloys formed by cubic $L1_2$ and β-phases with the compositions located near the intersection of the line *ss′* with the projection of the line of the univariant eutectic transformation $L \leftrightarrow L1_2+\beta$, have the optimum combination of strength and deformation to fracture: Young's modulus up to 190 GPa, compressive and bending strength up to 2000 MPa and 600 MPa, respectively, deformation to fracture up to 22 % in compression and up to 0.04 % in bending.

5. It was shown that the purposeful alloying allows to eliminate the solid state phase transformations and enhance the mechanical properties of alloys after annealing in the temperature interval of 400-800 °C. The compositions of the new system-alloyed alloys (at. %) 55Al22Ti16Cr4V2Mn1Re, 55Al21.2Ti16Cr4V2Mn1Re0.8Nb and 55Al20.7Ti16Cr4V2Mn1Re0.5Zr0.8Nb, in which the solid state phase transformations are absent, were determined. It is shown that the alloying system with the participation of V, Mn, Re, Nb and Zr let the phase composition ($Ll_2+\beta$) and the hypoeutectic structure of the baseline alloy to be retained as well as its melting temperature to be increased from 1249 to 1269 °C, while its hardness increasing is minor.

6. It was shown that the transition from the single-phase $L1_2$ alloys to the two-phase eutectic alloys is accompanied by an increase of the strength properties and plasticity in a wide temperature interval and an increase of the softening temperature. At that, high values of the elasticity modulus are obtained, a microplastic deformation in bending tests appears, and the eutectic character of alloys ensures their high casting properties. So, at 700 °C the compressive yield strength changes from 200 MPa for the single-phase $L1_2$ alloy to 700 MPa for the two-phase ($L1_2+\beta$) eutectic alloy. The softening temperature for the two-phase alloy is equal to 800 °C.

7. Complex (VMnRe, VMnReNb and ReZrB) alloyed eutectic ($L1_2+\beta$) alloys are characterized by extremely high and stable strength properties up to 750 °C: compressive yield strength in the temperature interval of 20-750 °C is of 650-800 MPa and of 145 MPa at 1000 °C (0.8 T_{melt}).

CONCLUSIONS BY THE PUBLISHED PAPERS:

Mechanical behaviour of Al_3Ti intermetallic and $L1_2$ phases on its base. *Intermetallics*, 2001, No.9, P. 839-845.

1. The temperature dependence of hardness HV of the trialuminide intermetallic Al_3Ti (tetragonal $D0_{22}$ structure) and of Al_3Ti alloyed with Cr and Mn to produce the cubic $L1_2$ structure was investigated. The transition of the crystalline structure from tetragonal to cubic $L1_2$ was shown to be accompanied by a decrease of hardness over the full range of temperatures investigated, to 900°C.
2. The stress-strain curves of Al_3Ti and of Cr- and Mn doped $Al_{61}Cr_{12}Ti_{27}$, $Al_{66}Mn_{11}Ti_{23}$ intermetallics were obtained by an indentation method using pyramidal indenters with various angles of sharpening. The data obtained from the indentation tests were analyzed to distinguish the characteristics of dislocation motion in these alloys. The flow behavior was characterized by high values of strain hardening, and by a strain hardening index that represents dislocation motion. A mean free path for dislocation motion was estimated to be much smaller than the grain size, consistent with the high strain hardening and the low plasticity of these materials. The yield stress of these alloys decreases in the sequence $Al_3Ti \rightarrow Al_{61}Cr_{12}Ti_{27} \rightarrow Al_{66}Mn_{11}Ti_{23}$.
3. The plasticity characteristics δ_H of these intermetallics were determined by the indentation technique as well. δ_H is found to increase from ~0.68 for Al_3Ti to ~0.8 for the $L1_2$ phase $Al_{61}Cr_{12}Ti_{27}$ and 0.87 for the $L1_2$ phase

$Al_{66}Mn_{11}Ti_{23}$, but δ_H was always lower than the critical value $\delta_H \approx 0.9$, which is generally required for bulk ductility during tension and bending tests. δ_H of the investigated intermetallics is higher in the athermal region than for covalent crystals, but it increases very slowly with increasing temperature. δ_H values of the $L1_2$ phases close to the critical value $\delta_H \approx 0.9$ gives some hope for the discovery of $L1_2$ phases based on Al_3Ti which may posses room temperature ductility.

The influence of Zr alloying on the structure and properties of Al_3Ti. *Intermetallics*, 2003, No.11, P. 241-249

1. Phases present in the $Al_3(T_{1-X}Zr_X)$ alloy system were studied using X-ray diffraction analysis. It is found that with an increase in the concentration of Zr the $D0_{22}$ structure typical to Al_3Ti transforms to the $D0_{23}$ structure. The volume fraction of the $D0_{23}$ phase increases rapidly to ~90 % when X increases to 0.24, and alloys with $X \geq 0.5$ are single phase $D0_{23}$. The melting temperature of the alloys increases continuously from 1408 ºC to 1607 ºC when the atomic fraction of Zr increases from X = 0 to 1. Hardness of the alloys at X = 0 is HV = 3.6 GPa, it rapidly decreases to about 2.8 GPa at X = 0.08, remains almost unchanged in the range of X = 0.08-0.32 and then continuously increases to ~3.7 GPa at X = 1. An indentation plasticity characteristic shows an opposite behavior indicating that alloys with the atomic fractions of Zr, X = 0.08-0.32 are less brittle than binary Al_3Ti and Al_3Zr intermetallics. Alloying of the Al_3Ti with Zr and Al_3Zr with Ti decreases hardness HV and increases plasticity characteristic δ_H, which was suggested to be a result of a decrease in the degree of the order of the DO_{22} and DO_{23} phases if they contain both Zr and Ti atoms.
2. The lattice parameters of the $D0_{22}$ phase increase with an increase in the amount of Zr. The increase is rapid in the range of X = 0 – 0.08. At higher atomic fractions of Zr, the lattice parameters remained practically unchanging. The lattice parameters of the $D0_{23}$ phase increase almost linearly with an increase in the amount of Zr in the alloy approaching the values typical to the Al_3Zr alloy at X = 1.
3. Study of the effect of temperature on phases in the $Al_3(Ti_{0.84}Zr_{0.16})$ intermetallic shows reversibility of the $D0_{22} \rightarrow D0_{23}$ transformation. The volume fraction of $D0_{23}$ phase increases from 50 % to 95 % when the temperature increases from 20 ºC to 700 ºC. However, at 1100 ºC, the amount of $D0_{23}$ phase decreases to ~50 %. During slow cooling from 1100 ºC to 650 ºC, the volume fraction of $D0_{23}$ increases again to 90 %. However, fast quenching to room temperature retains the high temperature structure indicating that the $D0_{23}$ ς $D0_{22}$ transitions are also diffusion controlled.
4. Since the atomic configurations in the $L1_2$ structure are closer to the $D0_{23}$ structure than to $D0_{22}$ structure, it is expected that addition of zirconium to Al_3Ti should facilitate formation of the $L1_2$ structure in the intermetallic after additional alloying with other transition elements.
5. It is shown with in-situ X-ray investigation that the low temperature $Al_{24}Ti_8$ phase exists in Al_3Ti in the temperature range below 650 ^oC. The phase transition $Al_{24}Ti_8 \rightarrow D0_{22}$ occurs above this temperature. The $Al_{24}Ti_8$ phase is found to form inside the surface layer of specimens as a result of grinding.
6. The positional parameters of the $D0_{23}$ atomic structure in the alloy $Al_3(Ti_{0.68}Zr_{0.32})$ were determined using a full-profile XRD analysis. It was found that zirconium atoms substitute titanium atoms in the fourfold positions. These positions in the $D0_{23}$ structure are statistically filled by Zr and Ti atoms in the proportion of 1 to 2 respectively.

References

1. Yang Y.E., Goo E., *Met. Mater. Trans. A.*, **26A** (1995) 1029.
2. Mabuchi H., Kito, A., Nakamoto, M., Tsuda H., Nakayama Y., *Intermetallics*, **4** (1996) 193.
3. Lee D.B., Kim S.H., Niinobe K., Yang C.W., Nakamura M., *Mater. Sci. and Eng*., **A290** (2000) 1.
4. Lee J.K., Park J.Y., Oh M.H., Wee D.M., *Intermetallics*, **8** (2000) 407.
5. Lee J.K., Lee H.N., Lee H.K., Oh M.H., Wee D.M., *Surface and Coatings Technology*, **155** (2002) 59.
6. Mabuchi H., Tsuda H., Kawakami T., Morii K., *Journal of the Japan Society of Powder and Powder Metallurgy*, Vol. 45, 3 (1998) 225.
7. Tian W.H., Nemoto M., *Intermetallics*, **8** (2000) 835.
8. Kumar K.S., Brown S.A., *Intermetallics*, **4** (1996) 231.
9. Shao G., Tsakiropoulos P., *Intermetallics*, **7** (1999) 579.
10. Jewett T.J., Ahrens B., Dahms M., *Intermetallics*, 4 (1996) 543.
11. Fu Y., Shi R., Zhang J., Sun J., Hu G., *Intermetallics*, **8** (2000) 1251.
12. Nic J.P., Klansky J.L., Mikkola D.E., *Mat. Sci. and Eng*., **A152 (**1992) 132.
13. Klansky J.L., Nic J.P., Mikkola D.E., *J. Mater. Res*., Vol.9**, 2** (1994) 255.
14. Milman Yu.V., Miracle D.B., Chugunova S.I. et al., *Intermetallics*, **9** (2001) 839.
15. Varin R.A., Zbroniec L., Wang Z.G., *Intermetallics*, **9** (2001) 195.
16. Lee J.K., Oh M.W., Oh M.H., Wee D.M., *Intermetallics*, 11 (2003) 857.
17. Fujiwara T., Nakamura A., Hosomi M., Nishitani S.R., Shirai Y., Yamaguchi M., *Philosophical Magazine*, Vol. 61, **4** (1990) 591.
18. Beaven P.A., Appel F., Dogan B., Wagner R., in *Ordered Intermetallics – Physical Metallurgy and Mechanical Behaviour*, ed. C.T. Liu R.W. Cahn & G. Sauthoff, Kluwer Academic Publisher, Netherlands, 1992, 413.
19. Durlu N., Inal O.T., J. Mater. Sci., **27** (1992) 1225.

20. Mabuchi H., Hirukava K., Tsuda H., Nakayama Y., Scr. Met. et Mater**.,** **24** (1990) 505.
21. Durlu N., Inal O.T., Mat. Sci. Eng., A152 (1992) 67.
22. Mazdiyasni S., Miracle D.B., Dimiduc D.M., Scr. Met., **23** (1989) 327.
23. Zhang S., Nic J.P., Mikkola D.E., Scr. Met. et Mater., **24** (1990) 57.
24. Durlu N., Inal O.T., J. Mater. Sci., **27** (1992) 1175.
25. Yang T.Y., Goo E., Metallurgical and Mater. Trans.A. **26A** (1995) 1029.
26. Mabuchi H., Hirukawa K., Katayama K., Tsuda H., Nakayama Y., Scr. Met. et Mater., **24** (1990) 1553.
27. Kumar K.S., Brown S.A., Intermetallics, **4,** N3 (1996) 231.
28. Milman Yu.V., Galanov B.A., Chugunova S.I., Acta Metal. Mater. **41,** N9 (1993) 2523**.**
29. Kim Y.W., *Journal of Metals*, **41** (1989) 24.
30. Elliott R., *Eutectic Solidification Processing*, Butterword and Co (Publishers) Ltd., 1983.
31. Barabash O.M., Sulgenko O.V., Legkaya T.N., Korzhova N.P., *Journal of Phase Equilibria*, Vol. 22, **1** (2001) 5.
32. Barabash O.M., Milman Yu.V., Korzhova N.P , Legkaya T.N., Podrezov Y.N., *Materials Science Forum*, Vol.396-402 (2002) 729.
33. Nic J.P., Zhang S. Mikkola D.E., *Scripta. Mater*., **24** (1990) 1099.
34. Zhang S., Nic J.P., Mikkola D.E., *Scripta Metall. Mater*., **24** (1990) 57.
35. Barabash O.M., Koval Yu.N, *The crystal structure of metals and alloys,* Kiev, Naukova Dumka (1986).
36. Braun J., Ellner M., *Metallurgical and Materials Transactions*, **32A** (2001) 1037.
37. Taran Yu.N., Mazur V.I., in *Structure of eutectic alloys*, Moscow, Metallurgiya, 1978, p.162.
38. Structural Intermetallics, Ed. by Darolia R., Lewandowski J.J. et al., MMS, (1993) p. 221.
39. Zhang S., Nic J.P., Milligan W.W., Mikkola D.E., *Scripta Metall. Mater*., **24** (1990) 1441.

Task 3. Elaboration of high-strength and elevated temperature Al alloys produced by PM methods

3.1. Basic principles for manufacture of water atomized powders of rapid solidified alloys

Although many processes are capable of preparation of RS Al particles, the most common are the planar flow casting with various modifications, centrifugal and gas atomization [1]. However, the existing RS technologies have serious specific limitations. In particular, methods based on the centrifugal atomization of melts onto a water surface usually develop cooling rates of $< 10^4$ K/s and produce rather coarse powders (~0.1 mm) and/or granules (~1 mm). The gas atomization appears more suitable for production of high-performance powders for powder metallurgy (PM) applications. In this case, the powder size can range from 0.01 to 0.2 mm and the cooling rate increases up to 10^5 K/s. Nevertheless, gas atomization technology is characterized as a highly explosive procedure, necessitating special safety measures, which increase the price of products.

The well-known water atomization (WA) process allows one to increase the cooling rate. This technology is widely used for the production of ferrous metals and some non-ferrous ones (e.g. copper). However, this process has not been found application to aluminum alloys because of two main reasons: 1) explosion danger of the atomization process due to rapid hydrogen emission, and 2) high reactivity of aluminum that can cause heavy oxidation of the surface of atomized powders.

The problems of safe operation in the course Al alloy powder production and powder quality were solved by the use of water solutions of inhibitors, by the control of suspension temperature and hydrogen ion exponent (pH), by the hydraulic classification of atomized products, and by the optimization of dehydration procedure.

Figure 3.1 represents the schematic diagram of the pilot plant for production of aluminum alloy powder. The technological process consists of the following steps. The charge, which is prepared with the use of master, alloys containing all alloying elements, is melted in the induction furnace. The ready melt is fed in a tundish, whence it flows out through a calibrated pipe in the bottom. The melt stream is atomized by jets of the cooled high-pressure water through the nozzle in the atomizing chamber. Inhibitor is introduced into the cooled water reservoir.

Water suspension of the atomized metal powder forms at the bottom of the chamber and then it is poured out into the suspension reservoir. The suspension is continuously pumped out from the reservoir by the pumps and is supplied to the hydraulic classifier. The suspended powder is classified there into various size fractions. The suspension with coarse fractions is returned into the suspension reservoir and is subjected to the mechanical dehydration by filtering under vacuum. The filtering with a high-performance porous filter dehydrates the suspension with fine fractions, or the suspension is dehydrated in. All classified powders are dried in vacuum. The automatic control system of the pilot plant controls the hydrogen ion exponent (pH) and the temperature of water and suspension.

In terms of the summarizing and analysis of investigation results that have been obtained within the framework of present project the methods of the process for water atomized powder producing WA-N of high-strength aluminum alloys (Al-Zn-Mg-Cu system) and elevated temperature aluminum alloys (Al-Fe-Cr, Al-Fe-Cr-Ti, and Al-Fe-Cr-Zr systems) were optimized.

The outcomes of the following investigations were analyzed and summarized:

− high-pressure water atomization of melts process, dependences of powder properties on the parameters of the process (melt temperature, water pressure, suspension temperature);

− the microstructure and surface chemistry of the atomized powders;

− the dependences of the particle surface chemistry on the interaction powder with water conditions;

− the kinetics of gas emission as a result of the interaction of moist powders with the water, depending on the temperature of the atomizing water, water hydrogen index pH and on the concentration of special substances – inhibitors that prevent the surface of powder particles against intense oxidation;

− combustibility and explosibility of the powders;

− the results of studying of the kinetics of dehydration in a vacuum filter and wet powders drying;

− processes of powders consolidation by vacuum forging (HDVC) and by the method including the stage of preliminary degassing of a powder in hermetic capsules with subsequent extrusion (CD).

− the dependences of the mechanical properties of the PM semi-products on the characteristics of the water atomized powders.

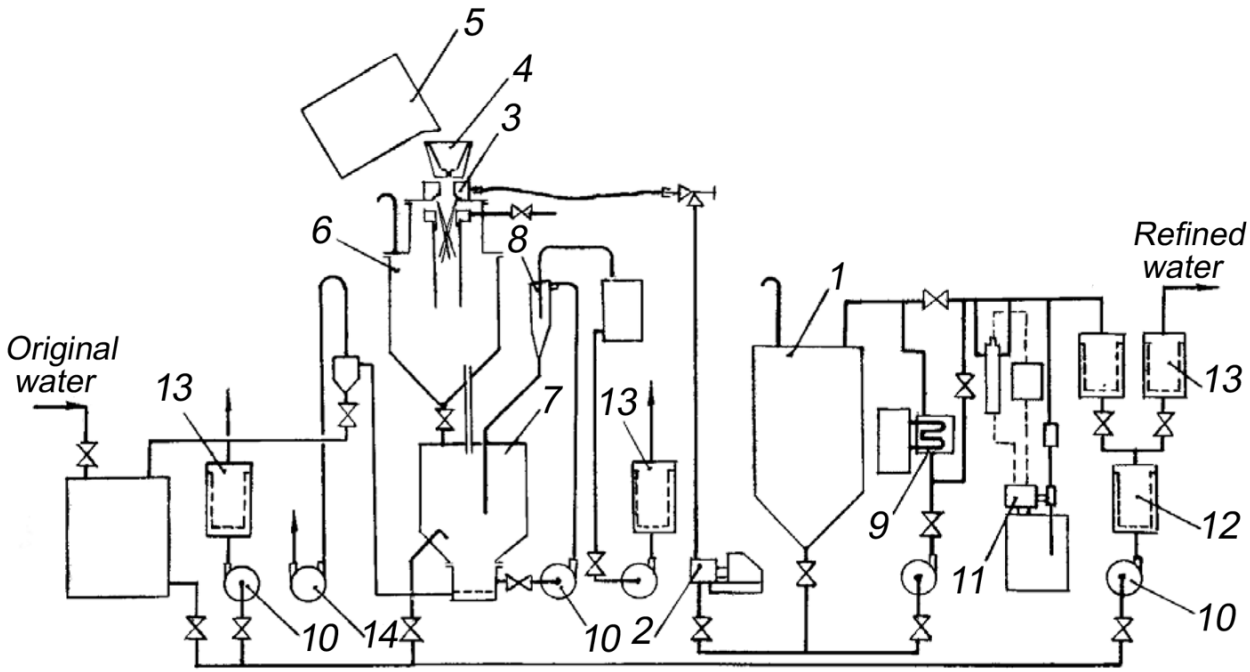

Figure 3.1. Functional diagram of the pilot plant to produce WA-N Al-base alloy powders:
1 – cooled water reservoir; 2 – high-pressure water pump; 3 – atomizing system; 4 – tundish; 5 – induction furnace; 6 – atomizing chamber; 7 – suspension reservoir with vacuum filter; 8 – hydraulic classifier; 9 – refrigeration unit; 10 – centrifugal pump; 11 – hydrogen index controller; 12, 13 – first and second stage water filters, respectively; 14 – vacuum pump

3.1.1. Improvements of the WA-N process

A new method of the PM semi-products obtaining based on the water atomization of the melt – WA-N process was used [2]. For elaboration of high-strength and elevated temperature aluminum alloys produced by PM methods it has been needed to improve and to optimize WA-N process, the main goal of which was the rise of the powder quality and providing the explosion security of the powder manufacture. These improvements of the WAN-process bring to following.

3.1.2. In area of purity of the melt

On the base of the SEM investigations the presence of the added impurities and evaluation of its sourses were studied. Increase of the purity of the melt was realized by means of fine cleaning of the initial water pollution used for melt atomization, use the special pastes for heat-proof, and non-stick coatings of the graphitic crusibles and tundish surface contiguous with melt for prevention of the melt by graphitic particles, and use of the multifunctional fluxes for removal the slages.

The fine water cleaning is accomplished in three-stage filter unit includes as the first stage the porous filter from material with size pores amount 5 μm, as the second filter – the activated charcoal filter for cleaning water from iron oxide, and third stage – the porous filter from material with size pores amount 1 μm.

Aluminum-oxide-coating AW, and Zirconium-coating ZR-M are used for coating of crusibles and tundish surface. These coatings are chemical stability up to 1800 ^{0}C at air as well as under vacuum and inert gas and provide the protect of the melt from graphite contamination during being its in crucible and tundish.

The compound ARSAL was chosen for removal of the slages during melt preparation in furnace.

3.1.3. In the area of the increasing of the fine particles yield

The increasing of the fine particles yield is arrived by means of the overheating the melt by pouring out above melting temperature amounts to 150 – 200 ^{0}C for the high-strength wrought aluminum alloys and 180 – 220 ^{0}C for the elevated temperature alloys. Along with this the flux MIKROSAL AL T 100 based on Ti-B for grain comminution and increasing the melt fluidity. Both of them contribute to decreasing the melt viscosity that increases of the fine particles yield. The content of powder fraction minus 50 μm increases on the amount 20 – 30 %.

3.1.4. In the area of the suspension dehydration

The enhanced vacuum filter for suspension filtration provides the decreasing of the powder losses by means of the powder invariable layer formation on the filter diaphragm and layer wisely removal of the powder sediment. The optimization of the suspension filtration process allowed the decreasing of residial moisture content from 28 – 30 to 12 – 16 wt %.

3.2. The high-strength RS supersaturated Al alloys of systems Al-Zn-Mg-Cu

Modem high-strength and elevated temperature Al alloys are multicomponent system containing 5 and more elements. Alloying by larger amounts of transition metals with the formation of strongly supersaturated solid solutions, which is possible only by various techniques of rapid solidification (RS) with producing granules, flakes or powders has been used also for increasing the content of main alloying components in the alloy.

The present task of project focuses on the effect of Sc, Zr and other TM (transition metal alloying additions on the structure and mechanical properties of Al-Zn-Mg-Cu and Al-Fe-C alloys manufactured by the new WA-N process based on the melt atomization of aluminum alloys with high pressure water provides the cooling rate of a melt up to 10 K/s and over. Special structural states has been obtained by a combination of special chemical composition and high cooling rate while solidification (to 10^6 K/s).

Modernization of the technology to produce powders of these alloys by spraying of melt with highly pressurized water (process WA-N) was targeted to reduce the amount of oxides ii powders (flux melting, definition of optimum hydrogen index of spraying water pH and it temperature, optimization of dehydration and drying of powders) and to increase fine-size fractions of powder lower than 100μm. It was shown that to obtain a required plasticity of powder semiproducts (rods) requires, while producing melt, to employ ceramic or graphite crucible with alundun coating.

Basing on the theoretical concepts, literary data and the experience of project authors there was chosen chemical compositions of powders alloys of two groups:

a) high-strength alloys based on Al – Zn – Mg – Cu system with additional alloying by Sc, Zr and a number of other transition metals;

b) elevated temperature alloys based on Al – Fe – Cr system with additional alloying by Ti, Zr, Mo and Sc.

As many as 37 compositions of alloys of system Al-Zn-Mg-Cu, additionally alloyed by Sc, Zr. TM and REM, were produced during fulfillment of the project using the WA-N method (Table 3.1).

Table 3.1.

The composition of alloys of system Al-Zn-Mg-Cu
alloyed in addition by Sc, Zr, TM and REM produced by method WA-N

##	Alloy mark	Chemical composition , wt. %	##	Alloy mark	Chemical composition (by charge)
1	012	Al -9.5Zn-3.0Mg-1.2Cu	19	51	Al-9.5Zn-3Mg-1.2Cu-0.15Zr-0.3Sc-0.2Ni-0.3Mn (pH=4)
2	022	Al -9.5Zn-3.0Mg-1.2Cu + 0.2Zr	20	52	(Al-9.5Zn-3Mg-1.2Cu-0.15Zr-0.3Sc-0.15Y-0.3Mn (pH=4)
3	032	Al -9.5Zn-3.0Mg-1.2Cu + 0.2Zr + 0.3Sc	21	53	(Al-9.5Zn-3Mg-1.2Cu-0.15Zr-0.3Sc-0.15Y-0.3Mn (pH=3)
5	102	Al -9.5Zn-3.0Mg-1.2Cu-0.5Zr	22	57	Al-9.5Zn-3Mg-1.2Cu-0.15Zr-0.3Sc-0.2Ti-0.3Mn
4	112	Al - 9.5Zn-3.0Mg-1.2Cu-0.5Zr - 0.5Cr	23	63	Al-9.5Zn-3Mg-1.2Cu –0.15Zr-0.3Sc-0.2Pr
5	122	Al -9.5Zn-3.0Mg-1.2Cu-0.5Zr- 0.5Cr– 0.5Sc	24	64	Al-9.5Zn-3.0Mg-1.2Cu–0.15Zr-0.3Sc-0.2Nd
6	132-1	Al -9.5Zn-3.0Mg-1.2Cu-0.5Zr- 0.5Sc	25	65	Al-9.5Zn-3.0Mg-1.2Cu–0.15Zr-0.3Sc-0.2Nb
7	132-2	Al - 9.5Zn-3.0Mg-1.2Cu-0.5Zr- 0.5Sc	26	66	Al-9.5Zn-3.0Mg-1.2Cu–0.15Zr-0.3Sc-0.2V
8	132-3	Al -9.5Zn-3.0Mg-1.2Cu-0.5Zr- 0.5Sc	27	67	Al-9.5Zn-3.0Mg-1.2Cu–0.15Zr-0.3Sc-0.2Re
9	142	Al -9.5Zn-3.0Mg-1.2Cu-0.5Zr- 0.5Mn	28	68	Al-12Zn-3.0Mg-2Cu –0.3Zr-0.3Sc-0.5Mn
10	152	Al-9.5Zn-3.0Mg-1.2Cu-0.5Zr–0.5Sc–0.5Mn	29	75	Al-12Zn-3.0Mg-2Cu
11	161	Al-12.0Zn–3Mg–1.2Cu–0.5Zr–0.5Sc–0.5Mn	30	87	Al-9.0Zn-3Mg-1.2Cu-0.3Fe
12	162	Al-12.0Zn–3Mg–1.2Cu–0.5Zr–0.5Sc–0.5Mn	31	88	Al-9.0Zn-3Mg-1.2Cu-0.6Fe
13	43	Al-9.3Zn-2.9Mg-1.2Cu	32	89	Al-9.0Zn-3Mg-1.2Cu-1.0Fe
14	44	Al-9.5Zn-3Mg-1.2Cu-0.15Zr-0.3Sc	33	130	Al-9Zn-3Mg-1.2Cu - 0.3Si
15	45	Al-9.5Zn-3Mg-1.2Cu-0.15Zr-0.3Sc-0.25Hf	34	131	Al-9Zn-3Mg-1.2Cu - 0.6Si
16	47	Al-9.5Zn-3Mg-1.2Cu-0.15Zr-0.3Sc-0.2Ce	35	132	Al-9Zn-3Mg-1.2Cu – 1.0Si
17	49	Al-9.5Zn-3Mg-1.2Cu-0.15Zr-0.3Sc–0.2Ti (pH=4)	36	133	Al-9Zn-3Mg-1.2Cu – 1.0Si – 1.0Fe
18	50	Al-9.5Zn-3Mg-1.2Cu-0.15Zr-0.3Sc-0.2Ni (pH=3)	37	134	Al-9Zn-3Mg-1.2Cu - 1.3Fe

Consolidation of powders had been carried out applying the methods of vacuum forging of powder billets with following extrusion (HDVR) and method of sintering of powders in a special capsule in vacuum (CD) with the subsequent extrusion of ingots on a rod. The rods have been made from powders of two fractions with size of powder particles (0-63) and (63-100) micron respectively. The composition, structure and properties of powders and their semi-products had been studied

It was shown that to obtain a required plasticity of powder rods requires, while producing melt, to employ ceramic or graphite crucible with alundum coating.

We proved a practically identical level of mechanical properties of the alloys compacted by vacuum forging (HDVR) and by the method including the stage of preliminary degassing of a powder in hermetic capsules with subsequent extrusion (CD).

It is found that the extrusion at the temperature 350-400 ^{0}C is an optimum technique of powders compaction. Powders must be pressed at room temperature in geometric capsules (from alloy Al-Mg) with degassing at 350 - 400 ^{o}C. The graphite lubricant is used in extrusion process.

Powders of high-strength alloys of Al–Zn–Mg–Cu system of various compositions produced by WA–N technique for manufacturing compacts in their external appearance are characteristic by a developed relief and are very similar (Fig.3.2).

The complex form of particles reliably provides the good compressibility of powder. Compressibility of powders of high-strength alloys of Al–Zn–Mg–Cu system of various compositions produced with WA–N method is much higher than for the powders produced with other methods (gas atomization)

Powder morphology was studied also on a Superprobe 737 device (Fig. 3.2). It is shown that grain size in particles of WA–N powder achieves 2 μm in fraction of 0–63 μm and 5 μm in fractions 63–100 and 100–160 μm.) There is found no influence of Sc on the grain size in powders.

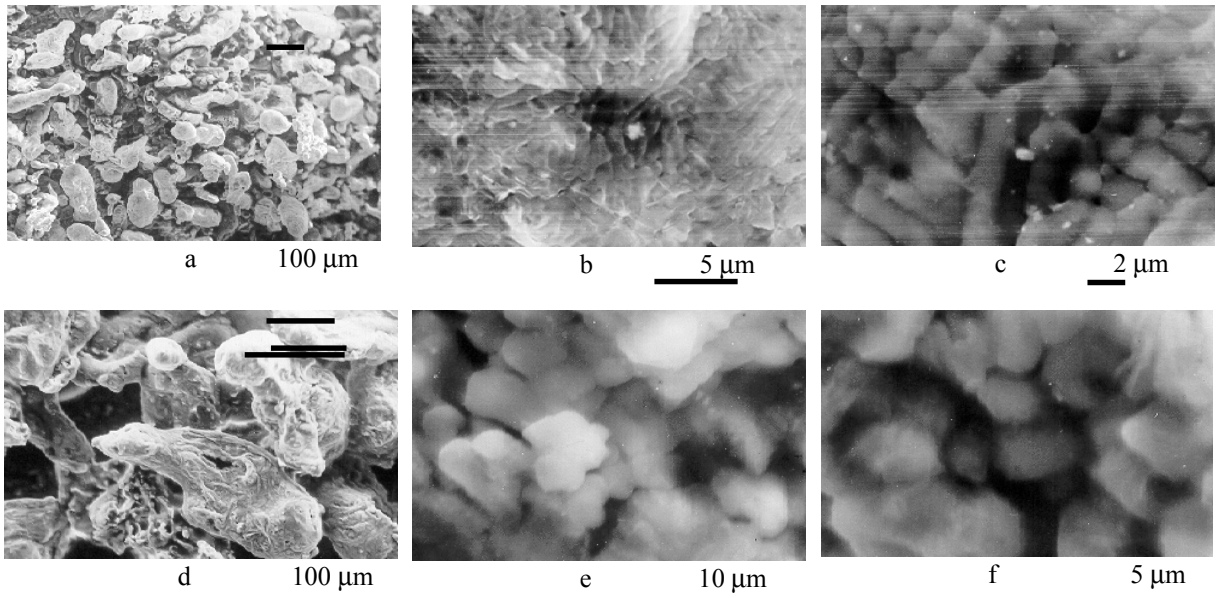

Figure 3.2. Surface morphology of particles of powders from
the alloy Al – 9.5Zn – 3.0Mg – 1.2Cu – 0.5Zr (a-e): a, b, c – fraction –63-0 μm;
d, e – fraction –160+100 μm and of the alloy Al–12.0Zn–3.0Mg–1.2Cu–0.5Zr–0.5Mn–0.5Sc
(f) fraction –100+63 μm.

We elaborated the technology of production of a melt, its sputtering by high-pressure water, and the subsequent compacting of powders. We established that the distribution of doping elements including transition metals (TM) and rare earth metals (REM) was practically uniform in powder grains, contrary to the alloys produced by casting.

The investigation has revealed primary $Al_3(Sc_{1-x}Zr_x)$ particles inside of grains that could be crystallization centers, but their size was much smaller than in ingots of cast alloys.

The primary $Al_3(Sc_{1-x}Zr_x)$ particles have not been found in the researched high-strength alloy if the content of scandium was less than 0.5 %, which is connected with high cooling velocity of solution with the used WA-N method. Small grain is formed in this case mainly due to high crystallization rate.

Assuming the possibility of increase in concentration of alloying elements in PM alloys, the following have been chosen as base alloys: Al-9.5Zn-3.0Mg-1.2Cu and Al-12.0Zn-3.0Mg-2.0Cu.

Metallographic examination of the structure of extruded rods after T6 treatment from powder alloys, including the baseline one (Al-9.5Zn-3.0Mg-1.2Cu), has not revealed any recrystallized grains that testifies to a high value of the temperature of recrystallization beginning in alloys under investigation.

For semi-products from all compositions of this system powder alloy the temperature of recrystallization beginning appeared to be higher than 465 ^{0}C that permits to carry out the T6 thermal treatment with obtaining high level of mechanical properties.

The analysis has shown that the contents of oxygen in WA-N powders of Al-Zn-Mg-Cu alloys is about 0.05% wt. It was found that powder particles of investigated high alloyed alloys Al-Zn-Mg-Cu-TM (REM) are covered with thin film of Al and Mg oxides of island-like character. Due to these oxides a recrystallization after T6 treatment does not occur in Al-9Zn-3Mg-1.2Cu rods that keeps their strength at a rather high level (YS = 649 MPa, UTS = 707 MPa). In alloys of this composition produced by casting technique (see Task 1) a comparable level of mechanical properties can be achieved only by additional alloying by Sc in combination with Zr. This conclusion seems to be significant, taking into account high cost of Sc.

Additional alloying of this basic alloy with scandium, zirconium and other transition and/or rare-earth metals provides an extra increase of strength characteristics up to YS = 670–730 MPa, UTS = 730-770 MPa, with satisfactory plasticity.

Whereas in the rods of the baseline alloy with increased content of Zn (12 wt. %) and Cu (2 wt.%) after T6 treatment a recrystallized structure is formed. Alloying this alloy with 0.15 wt. % Zr, 0.3 wt. % Sc and to 0.2 wt. % Mn reliably prevents from recrystallization after hardening treatment T6.

It is found that the optimum heat treatment of powder rods of high strength alloys coincides with optimum heat treatment for rods obtained by casting (T6 conditions: quenchening after 1 hour holding at 465 ^{0}C followed by aging at 120 ^{0}C, 24 hours).

The very small secondary particles of η′-phase and $Al_3(Sc_{1-x}Zr_x)$ that make a main contribution to hardening were revealed by TEM investigation in the rods from PM alloys as well as in alloy obtained by casting (Fig.3.3).

a b

Figure 3.3. Secondary particles in the PM rod of Al-Zn-Mg-Cu-Zr-Sc alloy after T6 treatment: a – dark-field image in reflection (001) of $Al_3(Sc,Zr)$; b – dark field image of η′ particles in a part of the ring in the electron diffraction pattern

Comparative analysis of the stress strain curves of the rods made from powder and cast high strength alloys shows that for both rod types the curves possess two-stage character with almost the same stress of transition from the first to the second stage of deformation. However, strain hardening is much higher in powder rods (probably, due to higher oxide content) and that is why fracture mechanism in these rods essentially differs from fracture mode of the alloys having approximately the same composition but obtained by casting. There is no pore coalescence fracture mechanism in powder-processed alloys, and fracture occurs by dimple mechanism on interfaces of deformation cells (Fig.3.4). Macroscopic fracture surface is oriented normally to the load direction. As a rule, small impurity particles with the composition noticeably different from the alloys composition act as fracture sources.

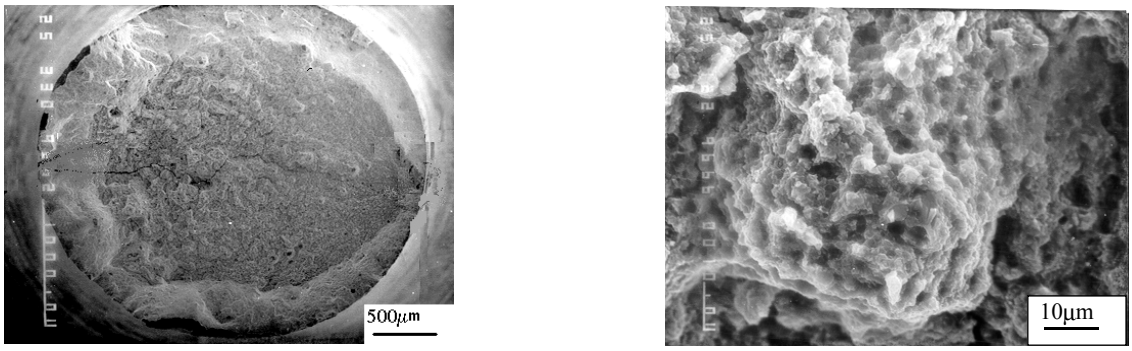

a b

Figure 3.4. Fracture surface in tensile test of rod samples in T6 condition, alloy Al-12Zn-3.0Mg-1.2Cu

Mechanical properties of the developed alloys of system Al-Zn-Mg-Cu for fraction (0-63)μm are submitted in Table 3.2.

It is seen from Tab 3.2 that alloying baseline alloy Al-9.5Zn-3.0Mg-1.2Cu with 0.15 wt. % Zr and 0.3 wt. % Sc has led to an increase of strength (YS ≈ 680 MPa, UTS ≈ 750 MPa) without loosing plasticity (EL ≈ 6.8 %).

It is shown that an additional alloying of the alloy Al-9.5Zn-3Mg-1.2Cu-0.15Zr-0.3Sc with 0.25 wt. % Hf or with 0.2 wt. % V as well increase rod plasticity El to 8.2 % and 9.4 %, respectively.

It is established a positive influence on the mechanical properties of the alloy Al-9.5Zn-3Mg-1.2Cu-0.15Zr-0.3Sc of alloying with Y+Mn (YS ≈ 713-727 MPa, UTS ≈ 754-770 MPa, EL ≈ 3.7-7 %), Nb (YS ≈ 704-713 MPa, UTS ≈ 746-776 MPa, EL ≈ 3.7-5 %), Re (YS ≈ 728-745 MPa, UTS ≈ 771-775 MPa, EL ≈ 4.2-6.9 %).

It is established a positive influence on the mechanical properties of the alloy Al-12Zn-3Mg-2.0Cu of alloying with Sc, Zr, Mn (YS ≈ 778 MPa, UTS ≈ 826 MPa, EL ≈ 4.64 % - for fraction 0-63 μm and (YS ≈ 803 MPa, UTS ≈ 843 MPa, EL ≈ 3.53 % - for fraction 63-100 μm).

Table 3.2.

The mechanical property of rods ∅ 6 mm in condition T6

Alloy mark	Content of alloying elements by charge, wt.%	HV, MPa	YS, MPa	UTS, MPa	EL, %
Alloys of system Al-9.5Zn-3.0Mg-1.2Cu					
431	Al-9.5Zn-3.0Mg –1.2Cu	2060	649	707	6.4
102	431 + 0.15Zr	2100	689	732	1,9
441	431 + 0.15Zr+0.3Sc	2160	678	751	6.8
441= Al – 9.5Zn – 3.0Mg – 1.2Cu – 0.15Zr - 0.3Sc + (TM)					
451	441+0.25Hf	2160	659	734	8.2
471	441+0.2Ce	2060	678	723	3.9
491	441+0.2Ti	2190	686	745	7.0
501	441+0.2Ni	2060	645	714	7,3
631	441+0.2Pr	2220	685	755	2.3
641	441+0.2Nd	2130	701	756	6.3
661	441+0.2V	2060	698	746	9.4
671	441+0.2Re	2060	728	771	6.9
511	441+ 0.2Ni+0.3Mn	2060	686	757	7
521	441+ 0.15Y+0.3Mn	2060	727	770	7
571	441+0.2Ti+0.3Mn	2120	702	752	4.1
Alloys of system Al-12.0Zn-3.0Mg-2.0Cu					
751	Al-12.0Zn-3.0Mg-2.0Cu	2270	732	765	1.6
681	751+0.3Zr+0.3Sc+0.5Mn	2320	778	826	4.64

It is shown that the increase of iron content to 1 wt. % in powder alloys leads to improving the mechanical properties (YS ≈ 680-690 MPa, UTS ≈ 740 MPa, EL ≈ 6-9 %) as distinct from cast alloys, where such content of iron significantly lowers the ductility of semi-finished products (Fig.3.5)

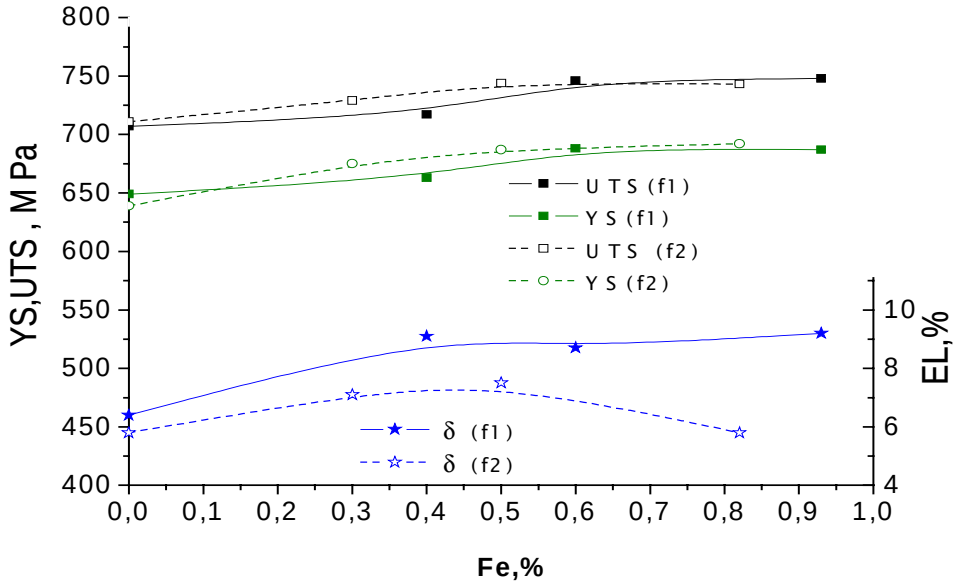

Figure 3.5. Influence of Fe content on mechanical properties of T6 rods from alloys Al-9Zn-3Mg-1.2Cu-xFe

The joint doping with Fe and Si (1 % Fe and 1 % Si) have led to YS = 530 MPa, UTS = 600 MPa at plasticity EL = 9-10 % (Fig.3.6). These values of strength and plasticity are intermediate between the results derived for the alloys doped only with Fe or Si.

It was established that the distribution of alloying elements in extruded rods produced by PM is essentially more uniform then for cast alloys (Fig 3.7).

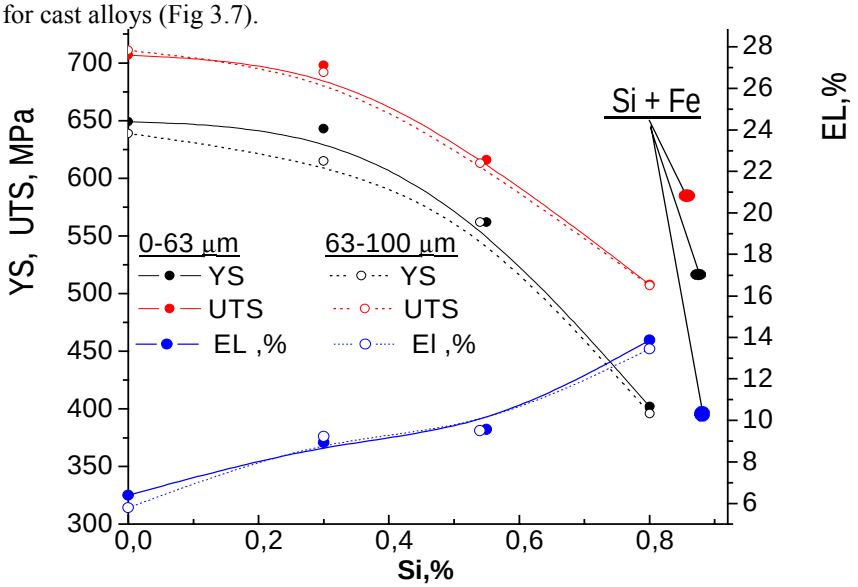

Figure 3.6. The influence of Si concentration as well as additional (Si+Fe) on the mechanical properties of rod ∅ 6 mm (µ = 17.4) in T6 conditions of Al - 9Zn - 3Mg - 1.2Cu alloys (PM). The points corresponding to alloy 133 (additions of 1 % Fe and 1 % Si) are given as well

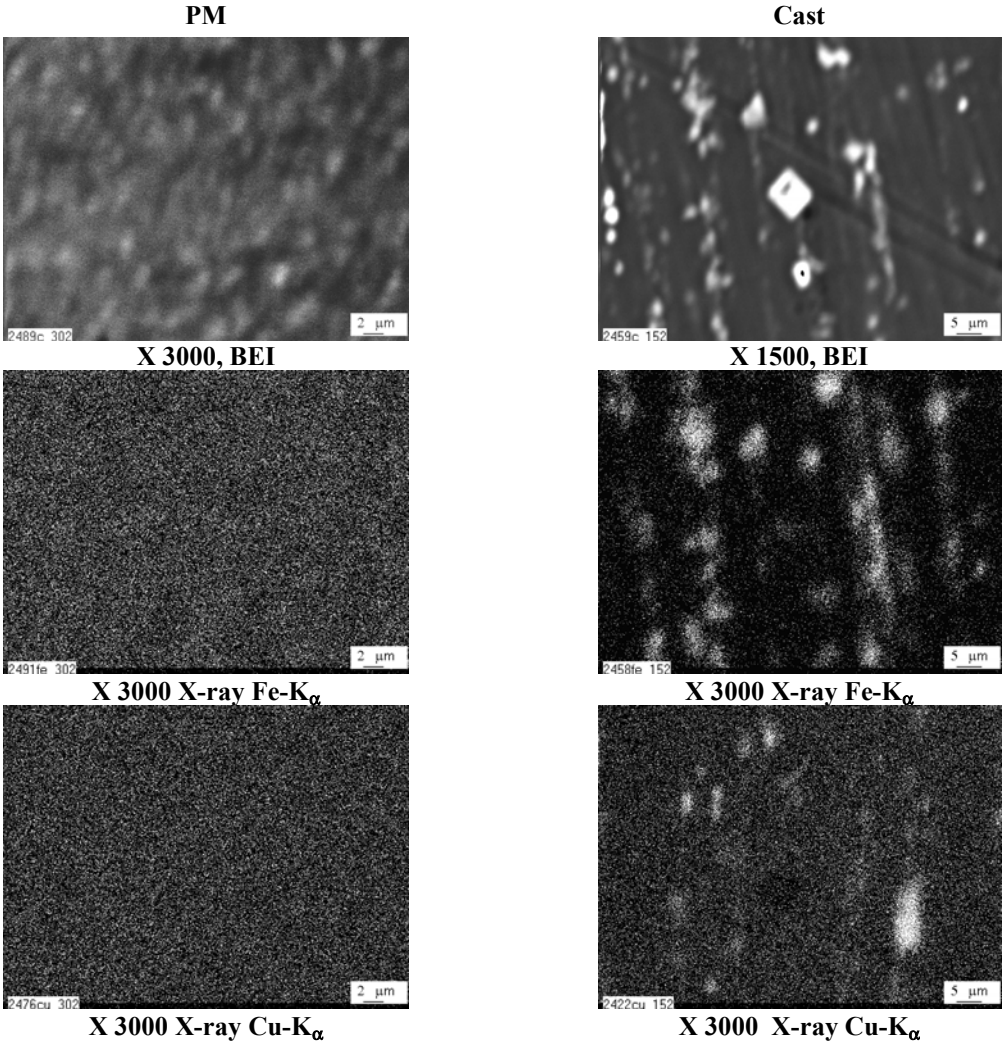

Figure 3.7. Distribution of Fe and Cu in extruded rods of the alloy Al-Zn-Mg-Cu, produced by PM and casting technique in T6 condition

CONCLUSION

1. Powder metallurgy opens the possibilities of additional alloying of aluminum alloys of Al–Zn–Mg–Cu system by the way of crystallization with high cooling rates.
   The executed modernization of the unit for WA–N process of producing water atomized powders provides the rate of melt cooling while crystallization up 10^6 K/s, the index S:L to 1:50, the possibility of a variation of the water hydrogen index (pH) from 1.0 to 7.0, and of water temperature from 2 to 10 ^{0}C with simultaneous providing of its predetermined pressure.
   Granulometric composition of water-atomized powders is in a complicated dependence on a large amount of factors. The main factors determining the atomization process are melt viscosity, water pressure, its specific consumption, diameter of the gravitation stream of the melt while contact with it of streams of high-pressure water, construction of the atomizing device and the atomizing chamber.

2. Surface oxidation during water atomization of Al-based alloy powders is strongly affected by the decrease in cooling rate with increasing powder size. The average thickness of the surface oxides increases with increased particle size and is estimated to be of approximately 5 and 7-8 nm for powder size fractions (0-63) μm and (63-100) μm, respectively.
   The oxide formed on the surface of WA powders is non-uniform in thickness: rather coarse surface oxide islands coexist with surface areas covered by a thin (<1.8 nm) oxide layer.
   The surface oxide film consists of Al and Mg oxides. A rather strong Mg segregation is observed on the surface. There exists a correlation in surface concentrations of Mg and O: the higher is oxygen concentration, the more intensive Mg peak is observed on the surface of individual particles. Zn does not appear in the surface oxide so that some surface depletion is observed for this element.
   Segregated impurities, such as S, C and Ca, are mainly accumulated on the top of the surface.

3. The intensity of hydrogen emission is used to characterize the oxidation process of aluminum alloy powders in water. The powder-water interaction rate strongly depends upon the value of water hydrogen index pH. At room temperature and pH = 3.0 the gas emission is practically absent for the first 2 h of the interaction of Al-Zn-Mg-Cu powders with water. An increase of pH from 3.0 to 4.0 doubles the gas emission intensity. The increase of the pH value to 6.0 leads to an abrupt change of the powder oxidation process under similar conditions and reaction time. A prolonged interaction of powders with the room temperature water at pH=4.0 does not cause any pronounced changes in the powder microstructure, while the interaction with the water at pH=6.0 leads the surface oxidation and formation of external oxyhydrate crystals grown on the particle surface.

4. PM technique with using WA-N powders makes possible to obtain a high level of mechanical properties in wrought semi-products of Al-Zn-Mg-Cu alloys with additional alloying with TM and REM (UTS = 750-820 MPa, δ = 1-7 %) that is comparable with the properties of these alloys produced in this project by casting technique (see Task 1 in the Report T03).

5. PM technique permits to obtain a high level of mechanical properties of T6 semi-products (UTS = 700 MPa, EL = 6 %) without using expensive Sc and with a considerable content of Fe (~ 0.3 wt. %).

6. Alloying the baseline alloy Al-9.5Zn-3Mg-1.2Cu with Sc and Zr leads to some growth of strength characteristics of T6 treated PM semi-products, but the effectiveness of alloying with Sc in PM Al-Zn-Mg-Cu alloys is lower than in cast alloys.

7. Two methods for powder consolidation were elaborated: CD – sintering of powders in aluminum capsule in vacuum with following extrusion and HDVC – vacuum forging of powder billets with following extrusion. These two methods have shown a practically equal level of mechanical properties.

8. For the first time powders of Al alloys based on the Al-Fe-Cr system with additional alloying by Ti, Zr, Mo have been produced by the technique of high-pressure water atomization. The results of the structure and mechanical properties investigation for these alloys are given in the report of Task 6.

9. It is established that consolidated powder alloys of Al-Zn-Mg-Cu system manufactured with using a ceramic crucible for melting have a high level of mechanical properties. The extruded rod of the baseline alloy Al-9.5Zn-3Mg-1.9Cu in T6 condition had the following characteristics: YS = 640-650 MPa, UTS = 700-710 MPa, EL = 5.8-6.4 %.
   Alloying the baseline alloy Al-9.5Zn-3Mg-1.9Cu with 0.15 wt. % Zr and 0.3 wt. % Sc has led to an increase of strength (YS ≈ 680 MPa, UTS ≈ 750 MPa) without loosing plasticity ($\delta \approx$ 5.7-6.8 %).
   It is shown that an additional alloying of the alloy Al-9.5Zn-3Mg-1.9Cu-0.15Zr-0.3Sc with 0.25 wt. % Hf and with 0.2 wt. % V as well increase rod plasticity EL to 8.2 % and 9.4 %, respectively.

It is established a positive influence on the mechanical properties of the alloy Al-9.5Zn-3Mg-1.9Cu-0.15Zr-0.3Sc of alloying with Y+Mn (YS = 713-727 MPa, UTS = 754-770 MPa, EL = 3.7-7 %), Nb (YS = 704-713 MPa, UTS = 746-776 MPa, EL= 3.7-5 %), Re (YS = 728-745 MPa, UTS = 771-775 MPa, EL = 4.2-6.9 %).
The baseline alloy with increased content of Zn (12 wt. %) and Cu (2 wt. %) produced with using a ceramic crucible is shown to have a high level of mechanical properties: YS = 732-761 MPa, UTS = 765-793 MPa, EL = 1.6-2.9 %. Additional alloying this alloy with 0.15 wt. % Zr, 0.3 wt. % Sc and to 0.2 wt. % Mn exerts a beneficial influence on the strength and ductility of this alloy (YS = 778-803 MPa, UTS = 826-843 MPa, EL = 3.5-4.6 %).

10. It is established that the distribution of alloying elements in powder particles of Al-Zn-Mg-Cu alloys under investigation is uniform within the resolution of our SEM apparatus, though the investigation in COMPO condition revealed in coarser particles a thin net of intergranular layers enriched with heavier elements.

11. It is shown that extruded rods of alloys containing about 9.5 wt. % Zn: the baseline alloy Al-9.5Zn-3Mg-1.9Cu and alloys additionally alloyed with Sc, Zr, Mn, Y, Hf etc. had a non-recrystallized structure in T6 condition, whereas in the rods of the baseline alloy with increased content of Zn (12 wt. %) and Cu (2 wt.%) after T6 treatment a recrystallized structure is formed. Alloying this alloy with 0.15 wt. % Zr, 0.3 wt. % Sc and to 0.2 wt. % Mn reliably prevents from recrystallization after hardening treatment T6.

12. The comparison of obtained results with the results for alloys produced by casting (see the Report T04, Task 1) shows the following:
    - Strength characteristics of semi-finished products of PM alloys from water-atomized powders are comparable with strength characteristics of ones from cast alloys;
    - The ductility of semi-finished products from PM alloys from water-atomized powders is somewhat lower than of ones from cast alloys. The PM technique have an advantage for Al-Zn-Mg-Cu alloys (at least for Zn content of 9.5 wt. %) that does not contain Sc: PM alloys without Sc do not recrystallize after T6 treatment and have a high level of mechanical properties that is not much lower than for the same alloys alloyed with Sc and Zr.
    - Semi-finished products of PM alloys Al-Zn-Mg-Cu as distinct from alloys produced by casting do not lower the level of mechanical properties, when they contain to 1 wt. % Fe. It opens the perspective for using not very pure as well as recycled aluminum.

13. It is established that the level of mechanical properties of T6 rods from PM alloy Al-9Zn-3Mg-1.2Cu (in wt. %) with iron admixtures is higher compared to the properties of the baseline alloy without iron (YS = 640 MPa, UTS = 700 MPa, EL = 6 %). Fe admixtures have increased the rod strength (YS = 660-690 MPa, UTS = 710-750 MPa at Fe content of about 1 wt. %) with preserving the plasticity on the level of EL = 6-9 %. The increase of strength characteristics compared to T6 rods of the cast alloy of the same composition (YS = 547 MPa, UTS = 641 MPa, EL = 13.3 %) was of about 23 % for $\sigma_{0.2}$ and of about 14 % for UTS due to the non-recrystallied structure of PM rods.
    It is shown that adding Si to the baseline alloy does not change mechanical properties of T6 PM rods when Si content is to 0.3 %, whereas at larger content of Si rod strength begins to lower with a growth of the plasticity. Thus, introducing into the baseline PM alloy to 1 wt. % Si has led to the following strength indices: YS = 400 MPa, UTS = 500 MPa, and the plasticity has grown to EL = 14 %. With the help of SEM investigation it was shown that such change of tensile properties is connected with the formation of rather coarse Mg_2Si particles, and this fact lowers the amount of the main hardening η'-phase.
    The PM high-strength alloy that contents Si and Fe additions together (each of them to 1 wt. %) had also a sufficient level of mechanical properties (YS = 531 MPa, UTS = 602 MPa) with preserving a satisfactory plasticity to EL = 9-10 %.
    Thus, it is shown that using the powder process WA-N permits to use recycled aluminum with a significant content of Fe and Si for producing high-strength aluminum alloys.

References

1. Non-ferrous metal powders. Handbook (in Russian), ed. S.S. Naboychenko, Metullurgiya, Moscow, 1997, pp. 541.
2. Neikov O.D., Kalinhin V.G., Vasilieva G.I.et al. Russian Federation Patent # 2078427, Information Bulletin No. 12, 1997.

Task 2. Producing high-quality semi-products from new high-strength Al alloys and investigation of their weldability

2.1. Introduction

High alloyed alloys of Al-Zn-Mg-Cu system are used as structural material due to their high strength. However, alloys of this alloying system still have a substantial drawback of a high hot cracking susceptibility in fusion welding and low level of strength and ductility values of the joints. Therefore, development of the compositions of readily weldable alloys with higher values of strength and ductility was an important final stage of the project.

The work consisted in investigation of the structure and physico-mechanical properties of welded joints, made using different filler wires, as well as determination of optimal modes of thermomechanical treatment of welded joints.

2.2. Technical approach

In keeping with the current standards on testing the base metal and welded joints data were obtained on the alloy susceptibility to hot cracking in welding, microstructural features and level of mechanical properties of the base metal and welded joints, depending on the content of scandium and other microadditives of transition metals. Hot cracking susceptibility and other mechanical properties of the joints were determined in welding samples without fillers and using various filler wires, including those of an alloy, containing scandium and zirconium. Generalization of investigation results was performed, and recommendations were proposed on the technology of manufacturing wrought semi-finished products of scandium-bearing alloys and their welding by fusion processes.

2.3. Technical progress

Determination of the properties of welded joints in experimental alloys and generalization of the derived experimental results

2.3.1. Determination of the structure and physico-mechanical properties of welded joints, made using different filler wires and mode of thermomechanical processing of welded joints

Studied alloys of Al-Zn-Mg-Cu system belong to the group of wrought heat-hardenable materials, which are difficult to weld for the reason of their higher susceptibility to hot cracking in welds. In argon-arc welding the joints have a low level of strength and ductility values [1, 2].

At this stage of work performance additional melting of the alloys was conducted, which contained the main alloying element of Zn, Mg, Cu in the sum of up to 14.3 % and microadditives of Zr, Nb, Ce, Hf (Table 2.1). Technology of melt preparation ensured improvement of metallurgical heredity of the semi-finished products in terms of metal purity, its density, structural and chemical homogeneity. Melting was conducted in an induction furnace, in order to improve melt homogeneity. Zn addition and dissolution were performed in the subsurface layer of the melt. Degassing, refining, and soaking were conducted in a separate mixer. Filtration was performed with ceramic filters directly before filling a water-cooled mould. Thermodeformational modes were optimized and 5 batches of sheets were manufactured, including two batches of basic alloy L6.1, and three test alloys L9, L10, L11, which contained 0.3% Sc and additives of other elements. Optimal modes (report T05, Table 2.1) of argon-arc and electron beam welding of the sheets of test alloys with scandium and without it were experimentally selected and samples of sound welded joints were made.

Data on mechanical properties of sheet semi-finished products after heat treatment by mode T6 are given in Table 2.2. Mechanical properties of welded joints are shown in Table 2.3.3. Welded joints of alloys L6.1, L9, L10, L11 were tested after welding, after artificial ageing and after heat treatment for maximum strength by T6 mode. The Tables give the average values of testing 3 to 5 samples.

Table 2.1.

Composition of experimental alloys

Alloy		Chemical element, %									
		Zn	**Mg**	**Cu**	**Mn**	**Zr**	**Sc**	**Nb**	**Ce**	**V**	**Hf**
L6	**plan**	8.5	2.6	2.3	0.25	0.2	-	-	-	-	-
	fact	8.4-8.8	2.5-2.7	2.4-2.6	0.2-0.26	0.16-0.18	-	-	-	-	-
L6.1	**plan**	9.0	3.0	2.3	0.30	0.15	-	-	-	-	-
	fact	9.0	3.1-3.2	2.5-2.6	0.28-0.30	0.11-0.17	-	-	-	-	-
L7	**plan**	8.5	2.6	2.3	0.25	0.2	0.3	-	-	-	-
	fact	8.6-8.9	2.6-2.8	2.1-2.4	0.19-0.25	0.15-0.18	0.27-0.31	-	-	-	-
L8	**plan**	8.5	2.6	2.3	0.25	0.2	0.3	0.3	0.2	0.1	-
	fact	8.3-8.9	2.6-2.9	2.3-2.6	0.21-0.26	0.16-0.19	0.29-0.32	0.16-0.26	0.16-0.18	0.06	-
L9	**plan**	9.0	3.0	2.3	0.30	0.15	0.30	0.15	-	-	-
	fact	9.0-9.1	3.3	2.6-2.65	0.29-0.32	0.14-0.19	0.31-0.32	0.07-0.13	-	-	-
L10	**plan**	9.0	3.0	2.3	0.30	0.15	0.30	-	0.2	-	-
	fact	8.4-10.8	2.8-3.3	1.8-2.0	0.29-0.35	0.11	0.3	-	0.33	-	-
L11	**plan**	9.0	3.0	2.3	0.30	-	0.30	-	-	-	0.25
	fact	9.0-9.3	3.2-3.3	2.6-2.7	0.28-0.29	-	0.35	-	-	-	0.10-0.12

Table 2.2.

Mechanical properties of sheet semi-finished products of experimental alloys $\delta = 3$ mm after heat treatment by T6 mode

Alloy	UTS, MPa	YS, MPa	δ, %
L6	622.0	552.0	8.2
L6.1	647.8	540.4	9.0
L7	682.0	645.0	5.1
L8	671.0	625.0	6.0
L9	701.2	644.4	5.6
L10	642.6	600.5	5.0
L11	723.5	678.3	6.8

Table 2.3.

Mechanical properties of welded joints of experimental alloys of Al-Zn-Mg-Cu system

Base metal	Filler wire	After welding					After welding and artificial ageing				After heat treatment by T6 mode			
		$\sigma_{T\,r}$, MPa	$YS_{w.m}$, MPa	$YS_{w.m}$, MPa	$YS'_{w.m}$, MPa	α, deg	YS_r, MPa	$YS_{w.m}$, MPa	$YS_{w.m}$, MPa	$YS'_{w.m}$, MPa	YS_r, MPa	$YS_{w.m}$, MPa	$YS_{w.m}$, MPa	$YS'_{w.m}$, MPa
L6	Al-6%Mg	343.3	-	356.6	404.4		-	-	-	-	607.4	-	567.9	635.7
	Al-6%Mg-0.5%Sc	348.4	-	367.1	400.3		-	-	-	-	614.0	-	581.9	659.6
L6.1	Al-6%Mg	367.0	254.0	377.4	376.3	22	432.0	342.3	428.7	453.8	597.4	501.1	547.7	603.3
	Al-6%Mg-0.5%Sc	361.5	247.2	393.0	376.1	20	421.3	338.4	395.7	455.0	617.2	504.6	564.6	642.2
L7	Al-6%Mg-0.5%Sc	433.9	-	365.2	410.5		-	-	-	-	676.3	-	599.1	692.7
L8	Al-6%Mg-0.5%Sc	415.5	-	380.6	406.0		-	-	-	-	648.7	-	621.0	642.1
L9	Al-6%Mg-0.5%Sc	438.7	327.6	392.9	400.2	12	444.8	377.9	448.4	475.3	652.7	573.2	619.5	673.7
L10	Al-6%Mg-0.5%Sc	463.0	342.9	416.2	408.2	31	454.7	339.0	427.6	369.3	631.0	522.2	561.9	620.0
L11	Al-6%Mg-0.5%Sc	424.2	325.0	445.4	424.0	12	466.6	327.5	425.3	474.4	647.2	562.3	605.7	677.6

Note: YS_r - strength of samples with reinforcement on the weld face side;
$YS_{w.m}$ - yield limit of weld metal;
$YS_{w.m}$ - strength of weld metal on samples without reinforcement;
$YS'_{w.m}$ - strength of weld metal on samples with a narrowing in the weld zone;
α, deg – angle of bend

Mechanical testing of base metal of alloys L6.1 without scandium and L9 and L11 with scandium showed that at heat treatment by T6 mode their average strength index is 647, 701 and 723 MPa, respectively, with preservation of ductility on the level of 9, 5.6 and 6.8 %. Positive effect of scandium additives in terms of improvement of ultimate strength is 10 – 12 %. Maximum strength after heat treatment by T6 mode was achieved in L11 alloy with scandium and hafnium. It is equal to about 680 - 728 MPa. Compared to basic alloy L6.1, strength increase was equal to 33 to 80 MPa. Ductility of these alloys is 8 - 9 and 5 – 7 %, respectively, i.e. it is noticeably decreased with increase of strength values. The mechanical properties of extruded strip of alloys L6.1 and L9 are given in Table 2.4.

Table 2.4.

Mechanical properties of extruded strip (10 mm thickness) of experimental alloys and after heat treatment by T6 mode

Alloy	YS, MPa	UTS, MPa	δ, %
L6.1	654.4	644.9	4.9
L9	714.8	664.3	7.7

In nonconsumable electrode argon-arc welding of sheets of scandium-bearing alloys the strength of the joints, which have a thickening in the weld zone and which fail in the base metal, is equal to 420 - 460 MPa. Increase of the strength of welded joints of scandium-containing sheets was 20-28 %, compared to basic alloy (350 - 360 MPa). Strength of welded joints after additional artificial ageing is 420 - 430 MPa for the base alloy and 440 - 466 MPa for scandium-bearing alloys. Full heat treatment by T6 mode allows raising the strength level of the joints of the alloy without scandium to 600 - 620 MPa, and for scandium-bearing alloys to 631 - 676 MPa. Strength coefficient of welded joints with a thickening in the weld zone is 1.0 for the basic alloy and 0.9 for scandium-bearing alloys, relative to the strength of the sheets.

Metallographic investigations of sheets of alloys of Al-Zn-Mg-Cu (±Sc) system and their welded joints showed that scandium presence in the alloys slows down the recrystallization processes at process heating of the base metal, and in the welded joints it leads to refinement of weld metal structure and less softening of the metal in the HAZ due to narrowing of the recrystallization zones, incomplete annealing and overageing of the base metal.

In welding of basic alloys L6, L6.1 with filler without scandium the welds usually form a dendritic structure. The maximum size of the dendrites is equal to 110 μm. Use of a scandium-containing filler leads to formation of a mixed dendritic-subdendritic structure of weld metal with dendrite dimensions of 60 - 80 μm. At scandium content of 0.20 - 0.24 % in the weld metal, a partially subdendritic structure (up to 30 %) can form. In scandium-bearing alloys (L7, L8, L9, L10, L11) the welds contain 0.32 - 0.35 % scandium, and the fraction of subdendritic structure is greater than 50 %. Subdentrite size is 8 to 10 μm, and that of the dendrites is up to 50 μm. Use of Al-6%Mg-0.5%Sc filler leads to a change of eutectic shape in the welds from continuous layers to discrete precipitates along the boundaries of dendrites and subdendrites.

In the HAZ in the region adjacent to the weld, base metal grain recrystallization occurs and increase of their initial dimensions in alloy L6 from 60 - 80 to 100 - 150 μm in the rolling plane, or from 20 - 30 to 40 - 50 μm along the height is observed. In scandium-containing alloys the dimensions of recrystallized grains are not greater than 15 - 20 μm. Width of the region of recrystallized grains in alloy L6 is 1.5 - 2.0 mm, and in alloys L7, L8, L9, L10, L11 it is from 0.3 to 0.5 mm. In this zone partial melting of the precipitates of low-melting structural components may occur along the boundaries of base metal grains. Location of intergranular partially-melted layers depends on the shape, dimensions and orientation of base metal grains. In alloy L6 the partially melted intergranular eutectic layers are observed in a region up to 1.5 mm wide, and in scandium-bearing alloys at up to 0.5 mm from the fusion line (Fig. 2.1).

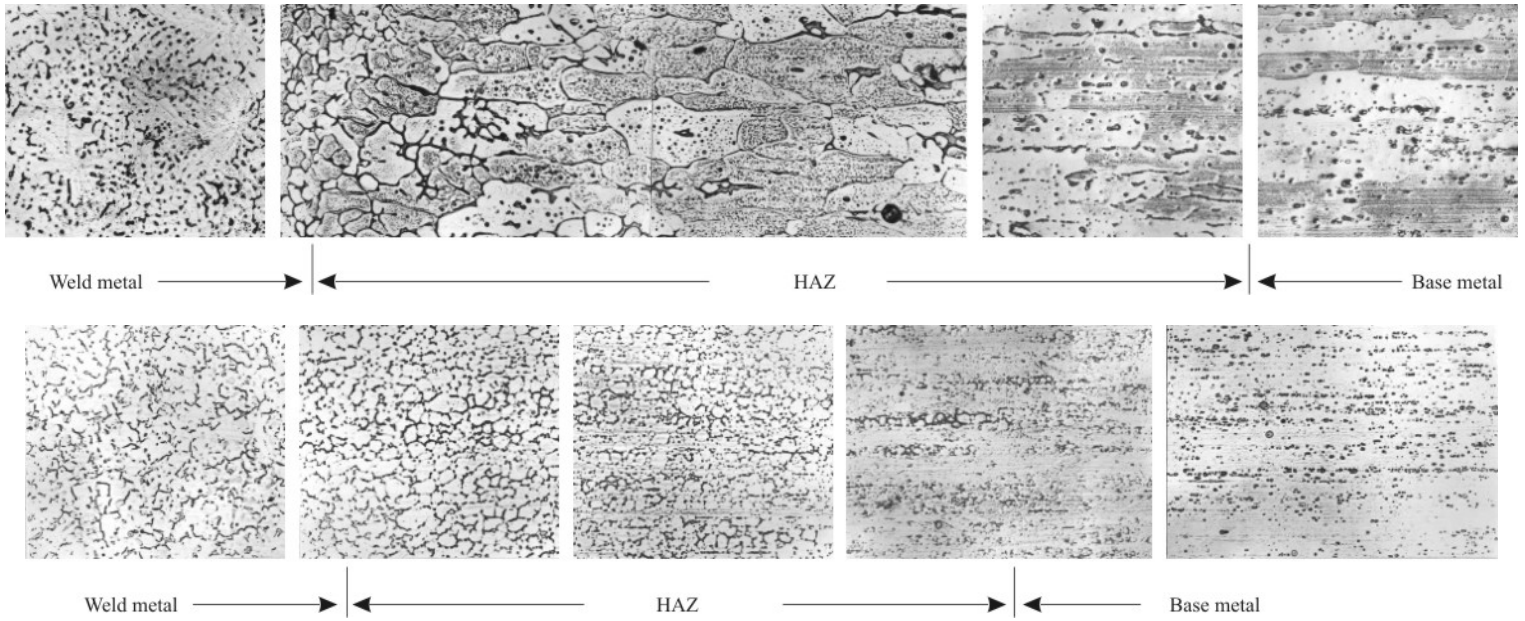

Figure 2.1. Microstructure of welded joints of TIG alloys:
a - L6 (Al-6%Mg filler);
b - L11 (Al-6%Mg-0.5%Sc filler), x320, reduced 2 times

A characteristic phenomenon for all the studied alloys is their softening in the HAZ. The extent of the entire softening zone (weld + HAZ) is within 35 - 50 mm (Fig. 2.2). Hardness level of the base metal near the line of fusion with the weld (location of prevailing fracture of welded joint samples) after welding is equal to 100-104 HRB, and for scandium-bearing alloys it is up to 104 - 107 HRB. Hardness in the annealing zone of welded joints on alloy L6 drops to 94 - 95 HRB, and in alloys with scandium it is up to 102 - 104 HRB. In welding of alloy L6 with a filler without scandium weld hardness is 93 - 95 HRB and in welding of scandium-bearing alloys with the appropriate filler it is 98 - 102 HRB.

At subsequent artificial ageing the hardness of all the HAZ regions increases, and the HAZ is shortened in alloy L6 to 28 - 30 mm, and to 25 - 28 mm in scandium-bearing alloys. Near the fusion line in the quenching zone, the hardness of alloy L6 rises to 110 -112 HRB, and in scandium-bearing alloys to 111-113 HRB. Hardness of welds in welded joints of alloy L6 rises to 103-104 HRB, and in scandium-bearing alloys up to 112-113 HRB.

Heat treatment by mode T6 leads to complete restoration of base metal hardness in the HAZ of welded joints on alloy L6 and scandium-bearing alloys, weld hardness in this case being somewhat lower at 110-112 HRB for alloy L6 and 112-114 HRB for scandium-bearing alloys.

Metallographic analysis showed that repeated heat treatment reduces the structural inhomogeneity of weld metal, fusion zone and HAZ (Fig. 2.3).

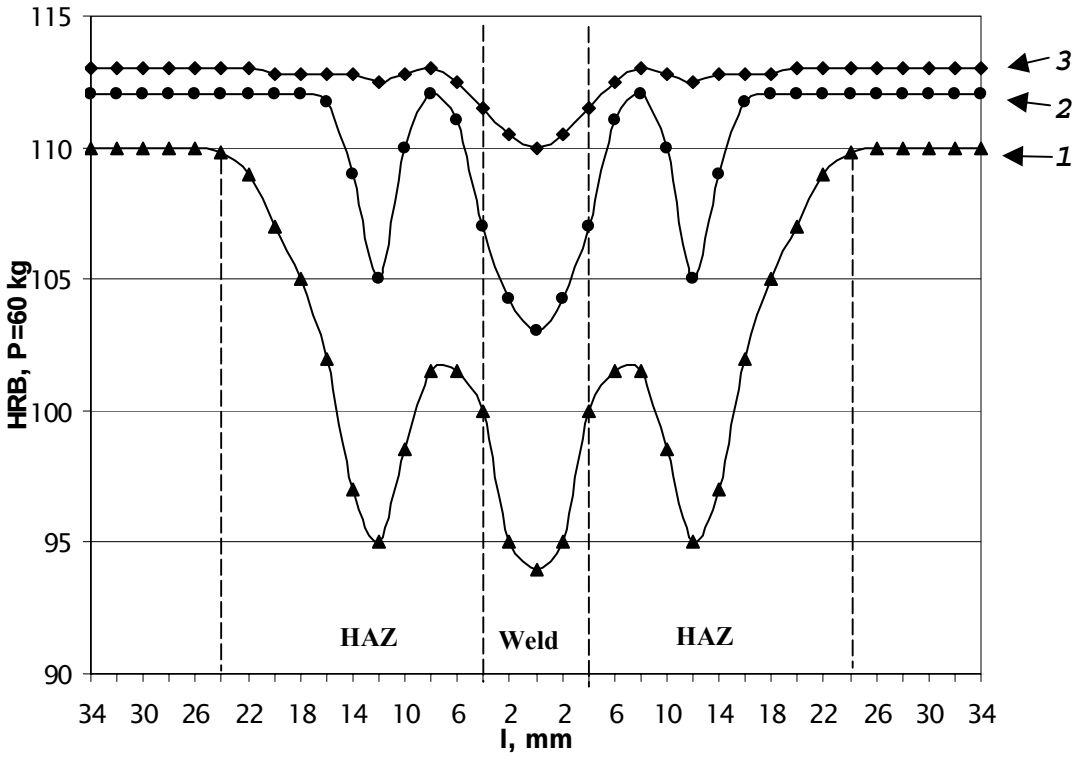

a

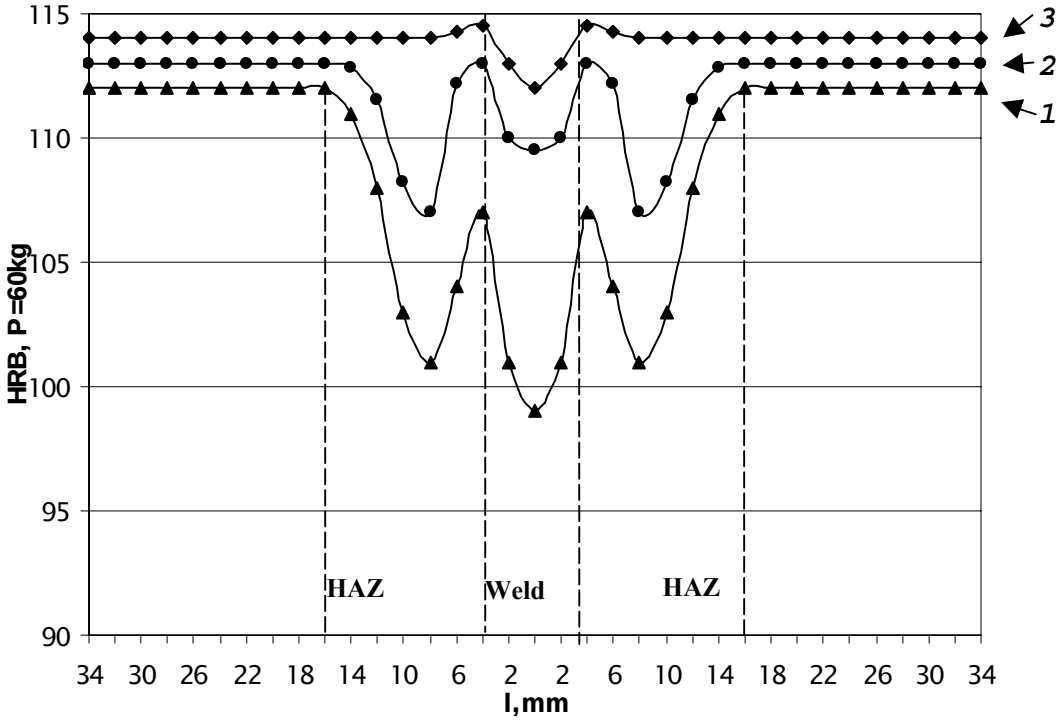

b

Figure 2.2. Influence of heat treatment on hardness variation in welded joints in AAW of alloys L6, Al-6%Mg filler (a), and L11, Al-6%Mg-0.5%SC filler (b):

1 - directly after welding;
2 - after welding + artificial ageing (120 C, 24 h);
3 - after welding + heat-hardening by T6 mode

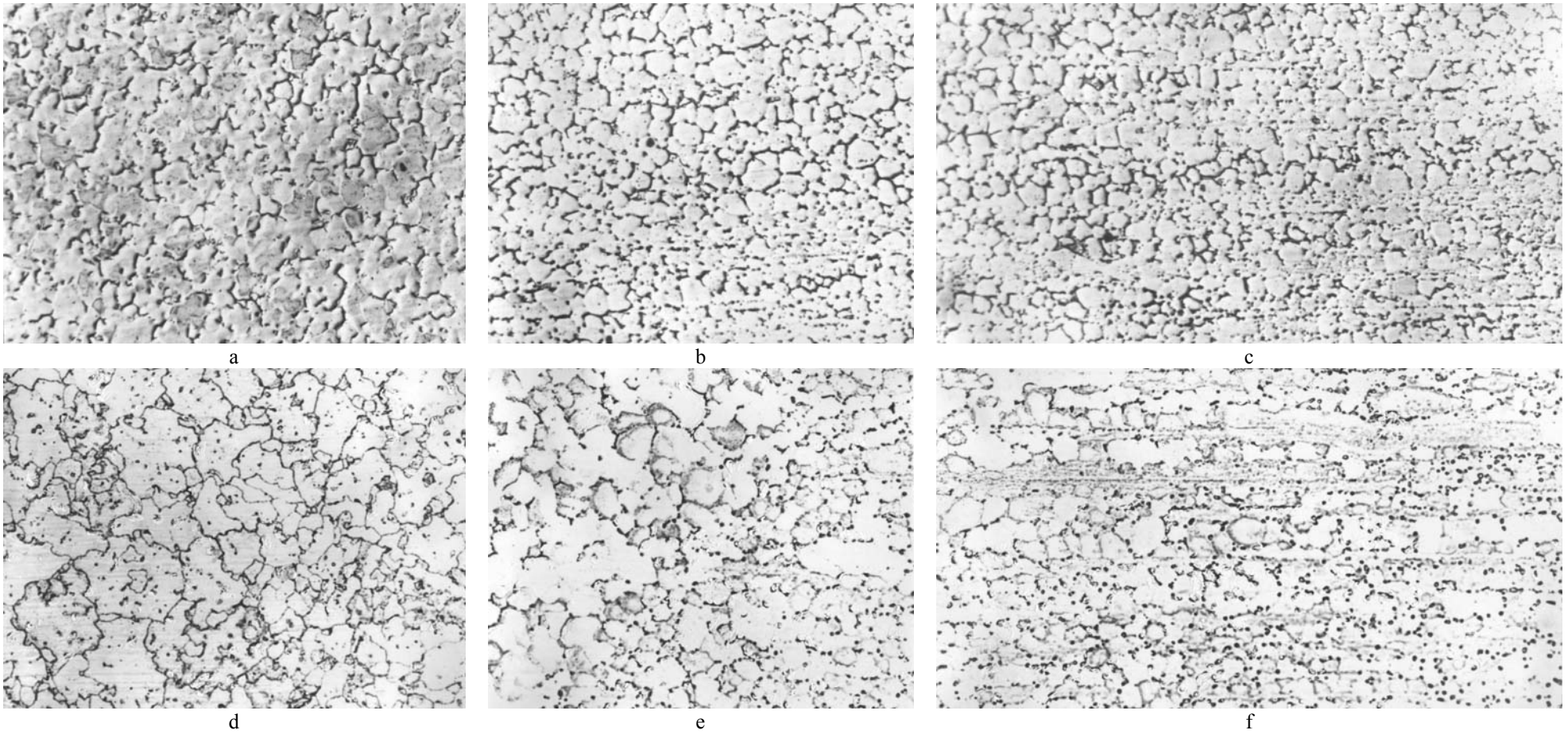

Figure 2.3.3. Microstructure of welded joints at AD3 of alloy L9 after welding (a - c) and after heat treatment by T6 mode
a, d - weld; b, e - fusion zone; c, f - heat-affected zone. X320.

Evaluation of hot cracking susceptibility

This index of weldability for the studied alloys was determined on Houldcroft technological sample, (A %). In welding samples of basic alloy without scandium and without a filler it is equal to 49 - 50% (Table 2.5), and for scandium-bearing alloys it is much lower, being 30.5 - 44.6 %.

Table 2.4.

Susceptibility of experimental alloys to hot cracking in welding without a filler

Base metal	Index of weld metal hot shortness (A, %)
L6.1	44.4 49.4 49.4 57.7
	50.2
L9	28.5 39,0 39.2 40.8 48.0
	39.1
L10	20.3 22.2 25.0 33.3 40.7
	30.5
L11	40.7 41.6 44.3 44.4 48.9
	44.6

In this case hot cracks propagate in the weld central part (Fig. 2.4). Method of X-ray spectral analysis revealed that depleting of solid solution grains of such elements as Zn, Mg and Cu and formation of eutectic layers on the grain boundaries are observed in the HAZ near the fusion line. Unlike Zn and Mg, copper has the highest susceptibility to leaving the solid solution. Compared to base metal, its concentration in the solid solution near the fusion line decreases two times. Scandium concentration in the base metal solid solution remains unchanged, when coming closer to the weld (Table 2.6, Fig. 2.5). Non-uniformity of alloying elements distribution in the weld metal is more pronounced (Fig. 2.6).

In welding samples of basic alloy, using fillers without scandium the cracks formed in the weld central zone, similar to the first case. Index A = 50.8 %. Scandium presence only in the filler (0.5 %) did not have any significant influence on the nature of weld cracking or hot cracking susceptibility index (49.2 %), as its amount after dilution in the weld pool (0.2 %) was insufficient for a significant refinement of weld structure.

Welded joints of test alloys with scandium and other microadditives in arc welding using a filler with 0.5 % Sc, did not have cracks in the weld central part, but cracking was observed along the line of weld fusion with the base metal (Table 2.7). In this case the index of cracking susceptibility was from 24 to 32 %. Lower values of this index (24 %) are found in the alloy, containing Hf microadditive in addition to scandium (Fig. 2.7 c). In electron beam welding of butt joints with a filler hot cracking was not observed either in the welds, or in the zone of their fusion with the base metal.

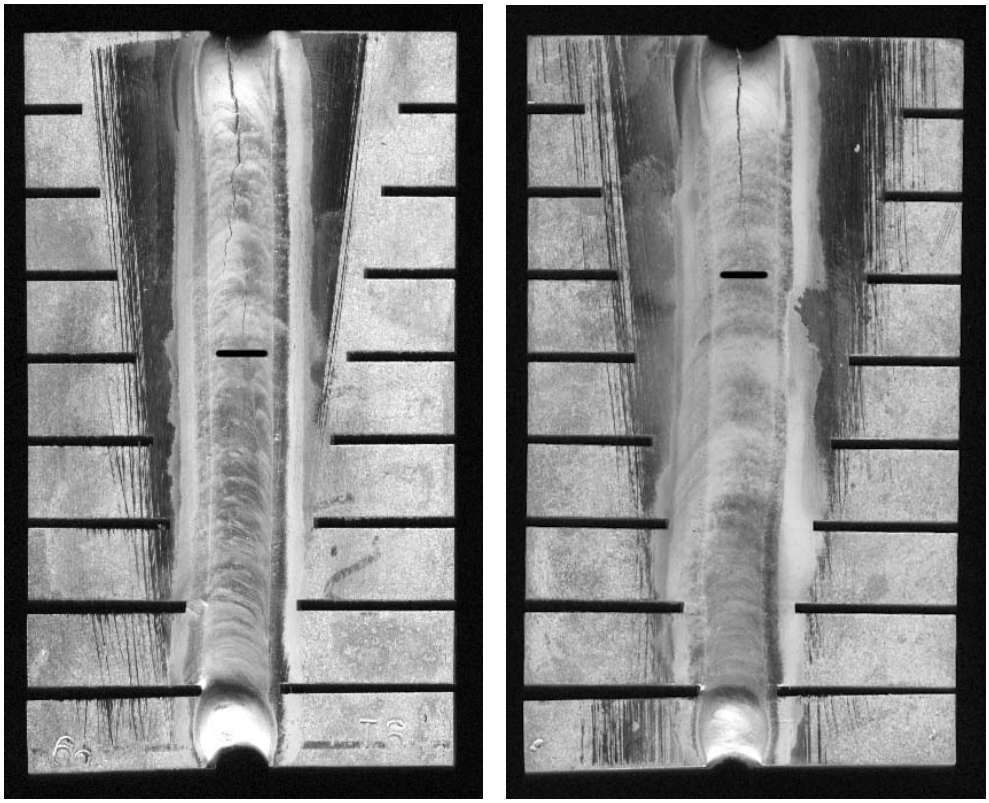

a b

Figure 2.4. Nature of cracking in the welds on Houldcroft samples in arc welding of test alloys L6.1 (a) and L11 (b) without a filler. X1

Table 2.6.

Element content in phase components in different zones of welded joints, made in AAW of alloys L6 and L7 without using filler wire

Element	Alloy	Base metal				Heat-affected zone at 60 μm distance from the fusion line			Heat-affected zone at 10 μm distance from the fusion line		Weld		
		Solid solution	Light-grey phase	Dark-grey phase	Intermetallic	Solid solution	Globular eutectic precipitates	Eutectic precipitates elongated along the grain boundaries	Solid solution	Eutectic along grain boundaries	Solid solution	Dense eutectic	Loose eutectic
Zn	L6	8.3-8.5	20.3-21.0	-	-	8.2-8.3	-	27.7	-	-	7.4-7.6	18.0-21.0	-
	L7	8.0-8.1	12.3-13.6	11.4-12.2	5.0-5.1	7.9-8.1	25.5-26.8	15.5-18.2	7.2-7.7	21.4-21.5	6.1	18.6-18.9	21.5-23.4
Mg	L6	2.1-2.3	11.7	-	-	2.2-2.3	-	12.0-12.5	-	-	1.8-2.0	6.4-7.5	-
	L7	2.3-2.4	3.8-4.6	3.0-3.6	0.1-0.2	2.3-2.4	11.7-12.0	4.6-5.3	1.8-1.88	7.6-9.2	1.16	6.0-6.4	8.5-9.0
Cu	L6	1.9-2.0	18.0-18.7	-	-	2.0-2.1	-	16.0	-	-	0.8-1.0	10.0-12.1	-
	L7	1.98-2.1	4.0-5.6	4.1-4.9	0.3-0.5	1.98-2.1	17.9-18.2	7.8-21.3	0.97-0.98	11.9-13.5	0.58	8.7-10.2	12.2-13.0
Sc	L6	-	-	-	-	-	-	-	-	-	-	-	-
	L7	0.14-0.16	0.05	6.1-7.7	18.0-19.0	0.14-0.15	0.02-0.04	3.1-8.4	0.16	0.05-0.04	0.2	0.18-0.19	0.11
Fe	L6	0.015	0	-	-	0.01	-	0.02	-	-	-	-	-
	L7	0.01	0.02	0.01	0.01	0.01	0.01	0	0.01	0.02-0.05	0	0.01	0
Si	L6	0.3	0.43	-	-	0.2	-	0.2	-	-	0.2	0.3-0.34	-
	L7	0.26-0.28	0.23	0.23	0.2	0.26-0.28	0.3-0.28	0.29	0.28	0.28	0.3	-	0.3

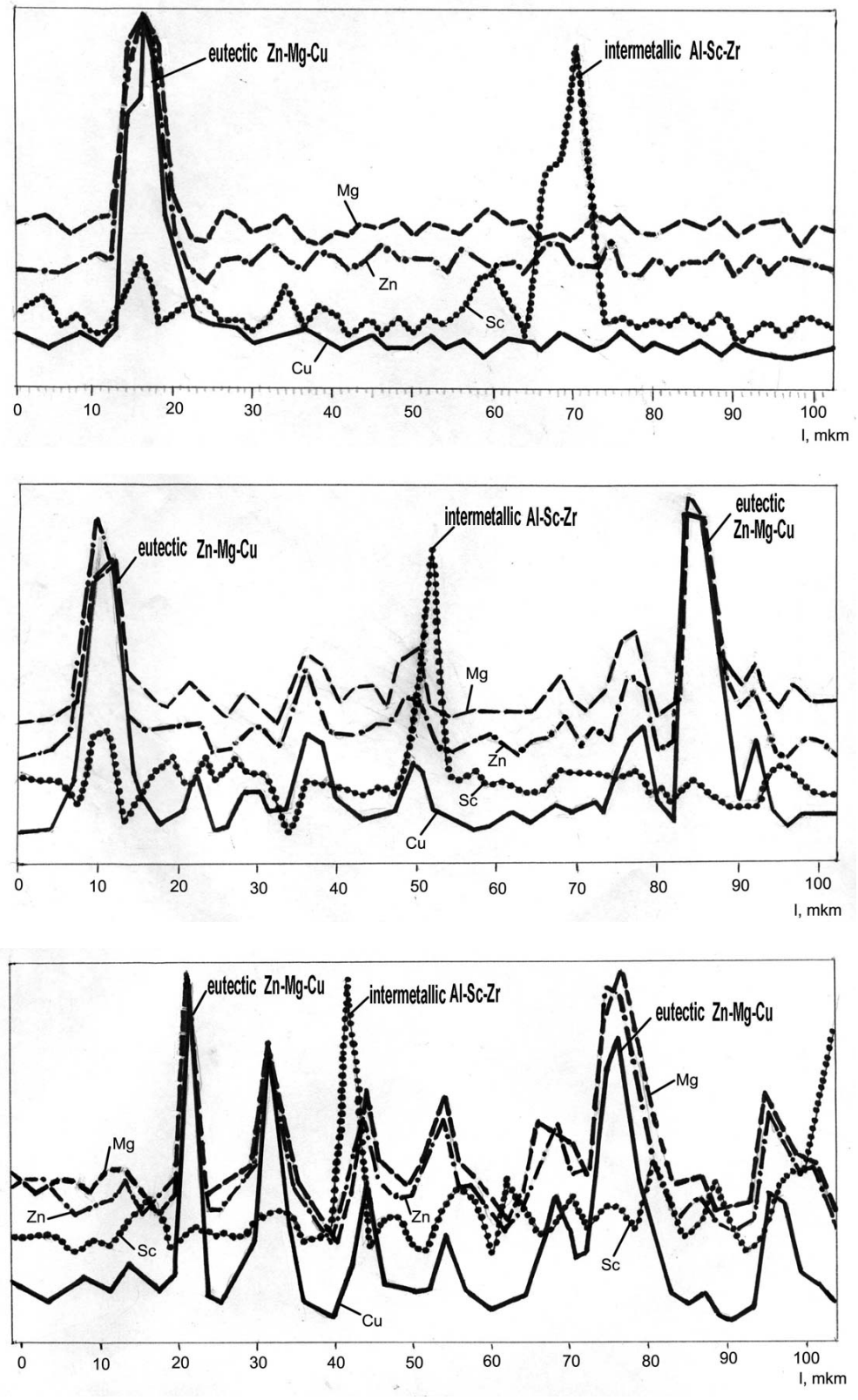

Figure 2.5. Distribution of alloying elements in different heat-affected zones of welding for alloy L7:
a - in the initial condition;
b - in the HAZ at 60 μm distance from the fusion line;
c - in the HAZ at 10 μm distance from the fusion line

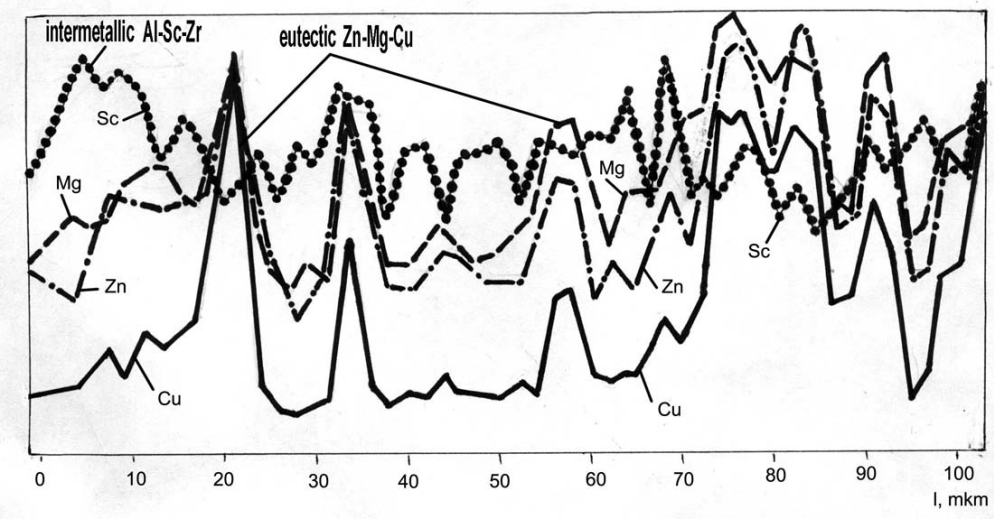

Figure 2.6. Distribution of alloying elements in the weld metal in welding of alloy L7 without a filler

Table 2.7.

Hot cracking susceptibility in TIG of test alloys, using filler wires

Alloy	Filler	Index of metal hot shortness in the HAZ (A, %)
L6.1	Al-6%Mg-0.2%Zr	48.1 50.8 50.8 53.6
		50.8
	Al-6%Mg-0.2%Zr-0.5%Sc	37.9 50.8 52.7 55.4
		49.2
L9	Al-6%Mg-0.2%Zr-0.5%Sc	26.8 32.2 34.2 36.0
		32.3
L10	Al-6%Mg-0.2%Zr-0.5%Sc	16.6 21.3 37.0 38.8
		28.4
L11	Al-6%Mg-0.2%Zr-0.5%Sc	15.7 26.8 26.8 27.2
		24.1

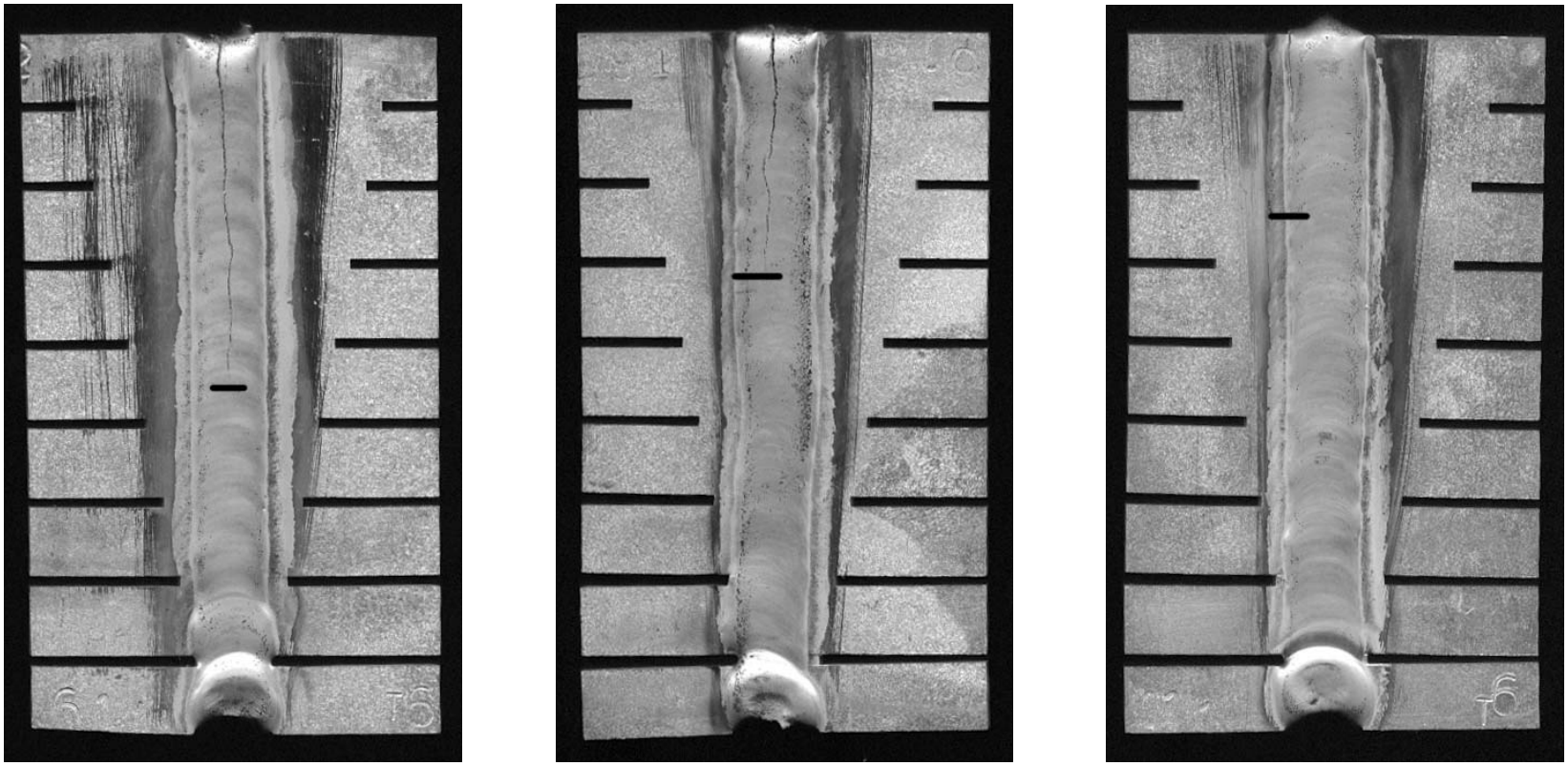

a b c

Figure 2.7. Nature of cracking of welds on Houldcroft samples in arc welding of the following test alloys, using fillers:
a - L6.1, Al-6%Mg filler;
b - L6.1, Al-6%Mg-0.5%Sc filler;
c - L11, Al6%Mg-0.5%Sc filler, crack along the fusion line. X1

Physical simulation of structural transformations in the alloys at process heating

In order to forecast the level of properties of wrought heat-hardenable alloys after abrupt process heating, in particular, in welding, structural transformations were studied and constitutional diagrams of microhardness of alloys L6 and L7 were plotted, depending on temperature-time conditions of heating. Change of microhardness of the alloys in T6 condition was recorded after isothermal heating at 200, 300, 350, 450, 550 and 600 ^{o}C for 5 - 3600 s (Fig. 2.8). After that samples 3 mm thick were immersed into a bath of tin melt, which was preheated to the required temperature. Monitoring the rate of through-thickness heating of the samples showed, that on the sample surface the specified temperature is reached in 2 s, and the sample is completely heated in 3 s. After isothermal soaking in a tin melt the samples were cooled in air, or under other conditions. Microhardness measurement was conducted in the solid solution grains 0.5 - 1.0 h after sample heating, as well as after their additional artificial ageing at 120 C for 24 h. Degree of strengthening (or microhardness) of the alloys at ageing depends on concentration of the solid solution, which formed as a result of heating and cooling of samples after isothermal soaking at the appropriate temperature. This circumstance allows evaluation of the nature and degree of structural transformations, occurring at heating, as well as the possibility of further strengthening of the welded joint metal.

Microstructure of the studied alloys in T6 condition is characterized by the presence of elongated, oriented along the direction of deformation grains of α-solid solution of the main components in aluminium, as well as $\eta(MgZn_2)$, $T(Al_2Mg_3Zn_3)$, $S(Al_2CuMg)$ and $Al_3(Sc, Zr)$ phases in L7 alloy. Dispersed precipitates of intermetallic phases strengthen the solid solution at heat treatment. Magnesium and zinc are mostly responsible for strengthening at ageing. Copper increases the strength of the alloys in the quenched state, but has little influence on the ageing effect, as it practically completely remains in the solid solution and forms a small amount of phase S. Additional strengthening of alloy L7 at Sc addition is determined by the following factors: structural strengthening as a result of formation of a fine subdendritic structure of the ingots and welds and preservation of non-recrystallized structure of the semi-finished products due to precipitation of primary scandium intermetallics from the melt and dispersion strengthening as a result of formation of secondary particles of $Al_3(Sc, Zr)$ during artificial ageing at temperature close to 350 C [1, 3].

Microhardness of alloy L6 in T6 condition is equal to 2370 MPa, and that of alloy L7 - 2445 MPa. At temperatures of 200, 300 and 350 ^{o}C, i.e. at overageing and annealing temperatures a gradual lowering of microhardness of both the alloys is found with longer isothermal soaking. The process of microhardness lowering becomes more intensive at temperature rise. At 350 ^{o}C and soaking for more than 180 s microhardness drop in both the alloys becomes slower, and at soaking for 1800 and 3600 s the microhardness of alloys L6 and L7 is somewhat increased, compared to heating to 300 ^{o}C. Maximum softening of both the alloys is found at 300 ^{o}C and soaking for 3600 s due to further decomposition of the solid solution of the main alloy components. Microhardness level in this case is 850 MPa for alloy L6 and 960 MPa for alloy L7.

Heating at 450 ^{o}C at soaking of up to 30 s first leads to an abrupt lowering of microhardness to 1300 MPa in alloy L6 and to 1385 MPa in alloy L7. Extension of the heating time to 3600 s results in a slight increase of microhardness of both the alloys due to dissolution of intermetallic phases in the matrix. At temperatures of 550 and 600 ^{o}C lowering of microhardness of alloys L6 and L7 proceeds more intensively, which is also accompanied by processes of a more complete dissolution of phases in the solid solution.

Subsequent artificial ageing allows determining more precisely, which processes (precipitation or dissolution of the strengthening phases, decomposition or formation of a new solid solution) are responsible for the level of alloy microhardness. For instance, after heating at 200 ^{o}C for 5 to 1800 s and subsequent artificial ageing microhardness increase in both the alloys is small, being 20 - 40 MPa (low-temperature recovery). Microstructure shows a larger amount of secondary precipitates along the body and boundaries of grains (Fig. 2.9). In this case, microhardness of both the alloys remains to be lower than the initial microhardness, which suggests that the process of coagulation of the strengthening particles started at 200 ^{o}C. At soaking for 3600 s and artificial ageing, microhardness of alloy L7 dropped from 2130 to 1810 MPa, and that of alloy L6 from 1820 to 1630 MPa, which is indicative of coagulation of the strengthening phases due to longer time of isothermal soaking. The same nature of microhardness lowering (at higher indices) is found in alloys L6 and L7 after heating up to 180 ^{o}C and subsequent artificial ageing.

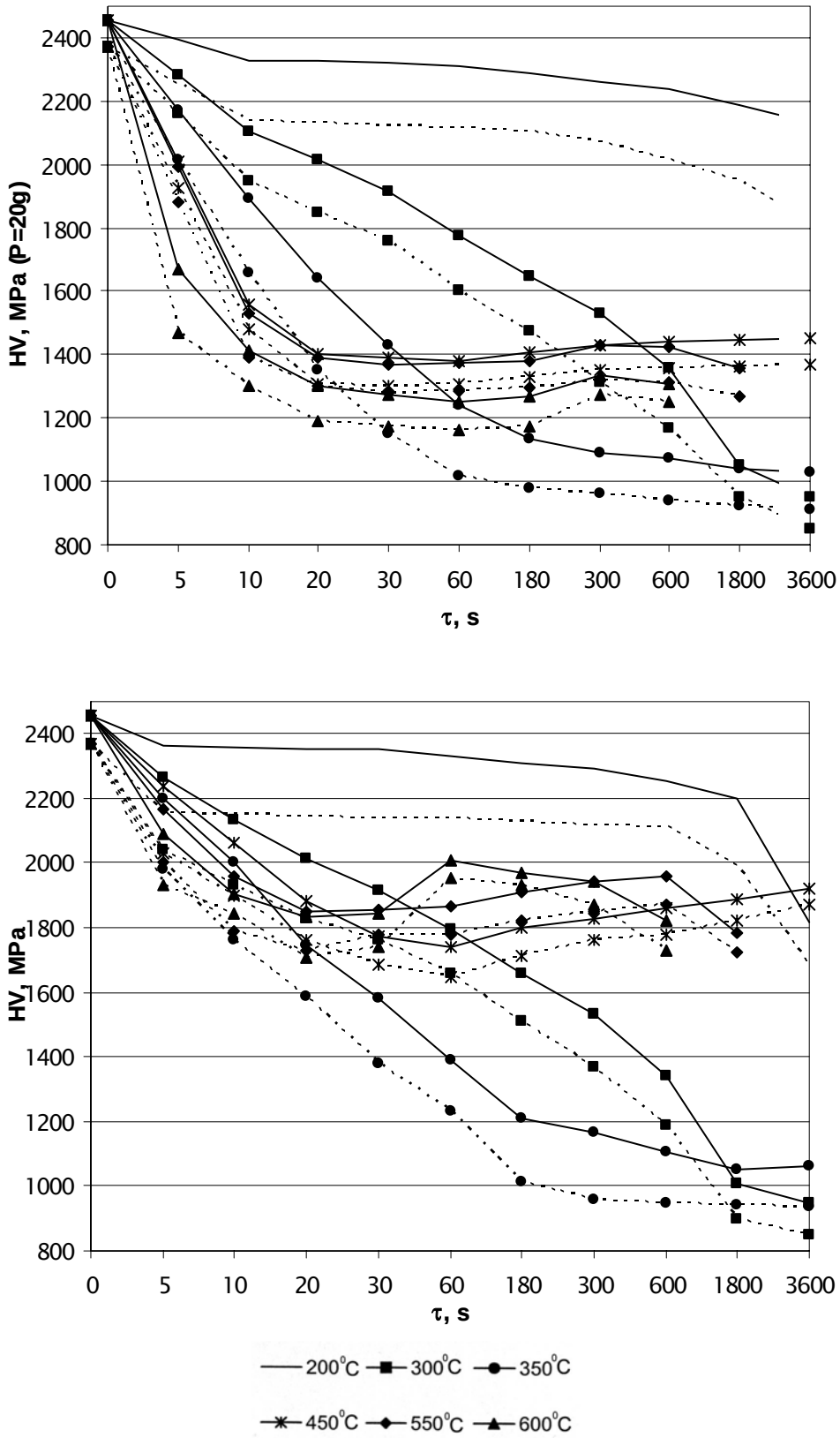

Note: continuous line is alloy L7; dashed line is alloy L6

Figure 2.8. Change of microhardness of alloys L6 and L7 (in T6 condition), depending on the temperature-time conditions of heating:

a - directly after heating;

b - after additional artificial ageing (120 °C, 24 h)

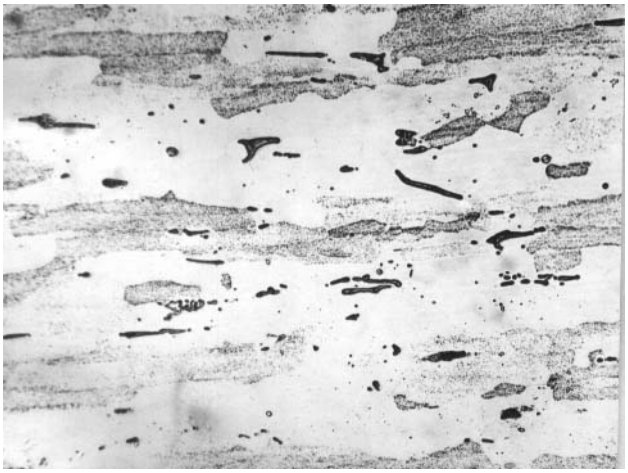

Alloy L6, in T6 condition

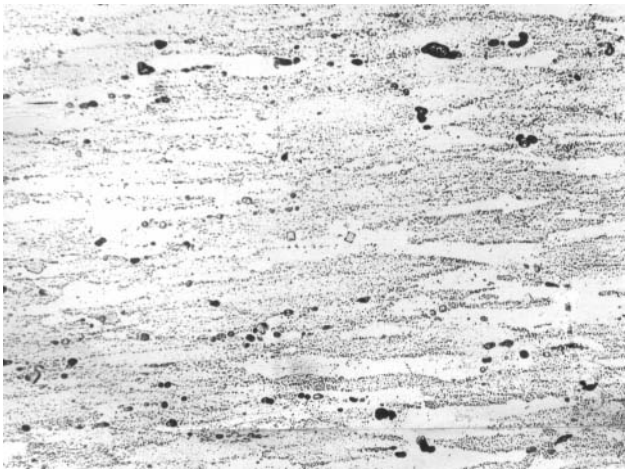

Alloy L7, in T6 condition

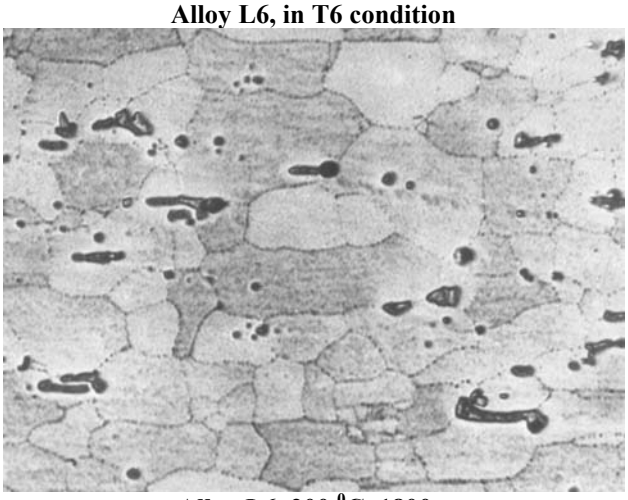

Alloy L6, 200 ^{0}C, 1800 s

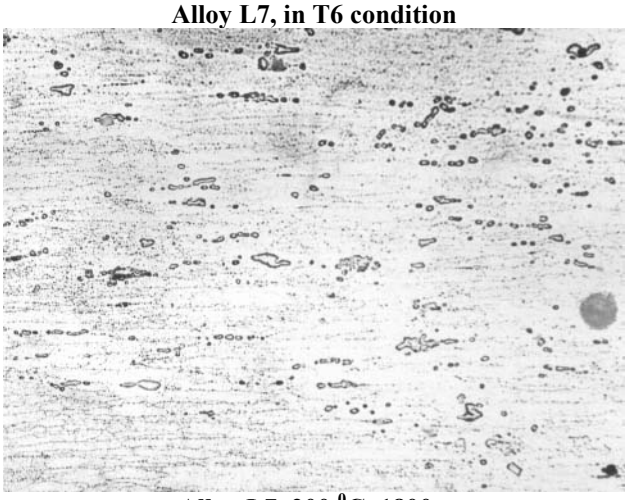

Alloy L7, 200 ^{0}C, 1800 s

Alloy L6, 200 ^{0}C, 3600 s

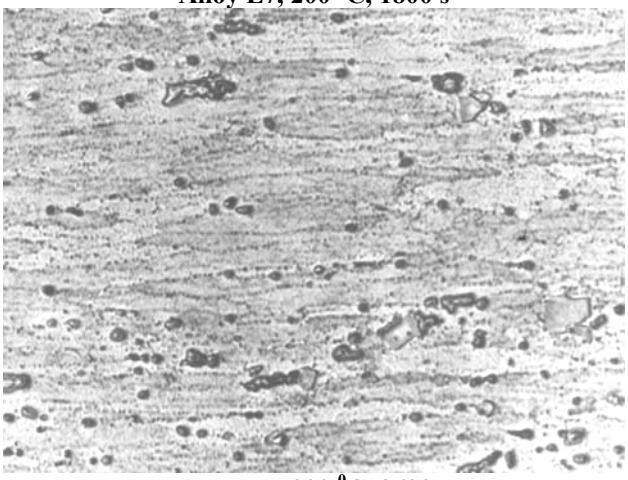

Alloy L7, 200 ^{0}C, 3600 s

Figure 2.9. Change of alloy microstructure
under different temperature-time conditions of heating (T6 initial condition). X500

After artificial ageing of samples, heated for a long time to 300 ^{o}C, the minimum level of microhardness of both the alloys remained unchanged. It shows that at this temperature the main process, determining the structure and properties of the studied alloys, is coagulation of the strengthening particles (Fig. 2.10). Microhardness of samples heated up to 350 ^{o}C for 1800 - 3600 s, is noticeably higher after artificial ageing than similar indices of the samples, heated up to 300 ^{o}C. This is indicative of the fact that the process of coagulation of the strengthening particles started changing into that of their dissolution. Artificial ageing of samples heated up to 450 ^{o}C showed that the maximum microhardness was achieved at soaking for 3600 s.

It is equal to 1920 MPa for alloy L7 and 1860 MPa for alloy L6, which is much lower than the initial microhardness for both the alloys. It is understandable that the rate of cooling of the alloys at quenching in air is insufficient and leads to partial decomposition of their solid solution already at cooling. Initial level of microhardness of samples heated up to 450 ^{o}C was achieved at their quenching in water and further artificial ageing (Fig. 2.11).

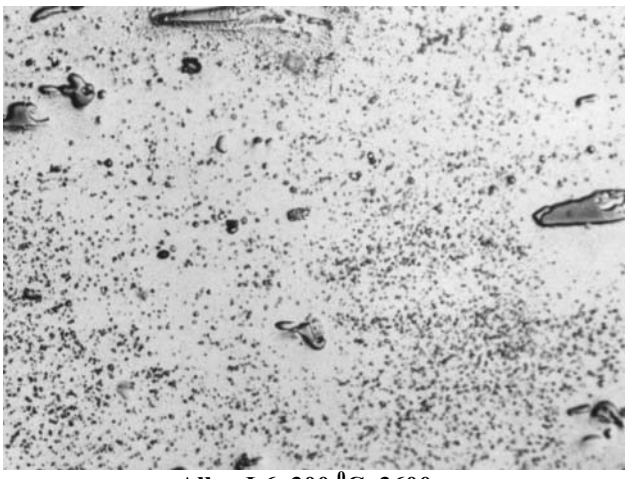

Alloy L6, 300 ^{0}C, 3600 s

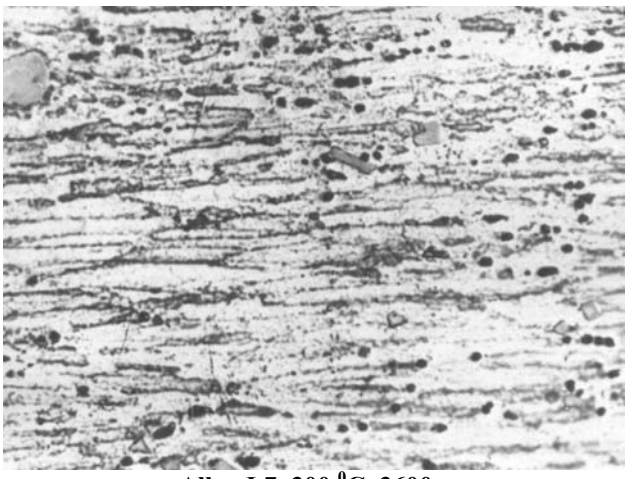

Alloy L7, 300 ^{0}C, 3600 s

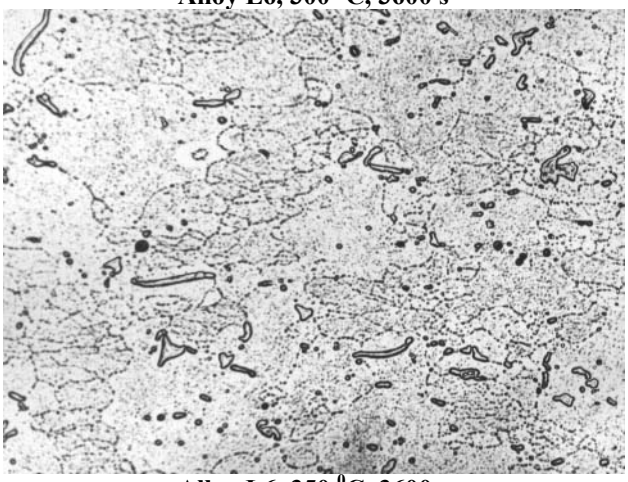

Alloy L6, 350 ^{0}C, 3600 s

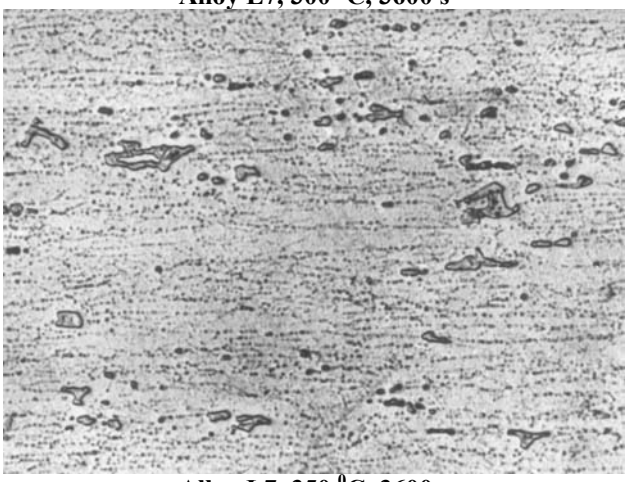

Alloy L7, 350 ^{0}C, 3600 s

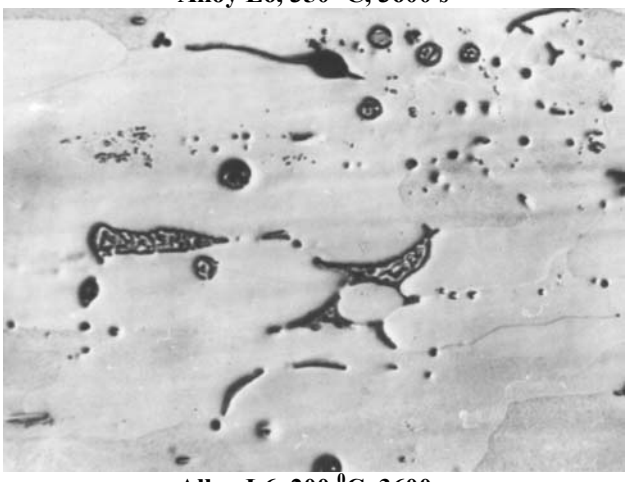

Alloy L6, 200 ^{0}C, 3600 s

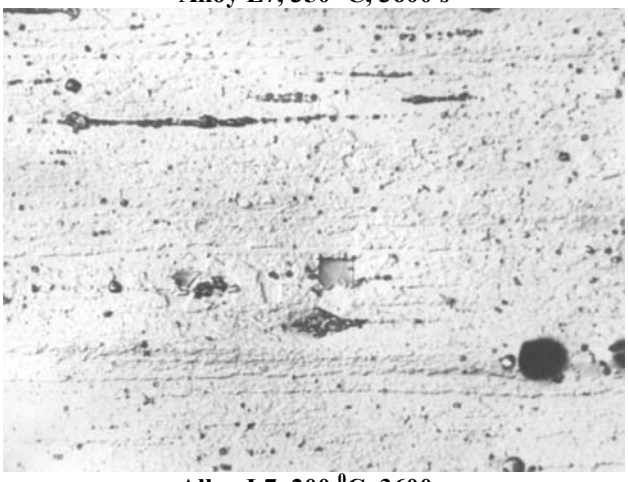

Alloy L7, 200 ^{0}C, 3600 s

Figure 2.10. Change of alloy microstructure
under different temperature-time conditions of heating (T6 initial condition). X500

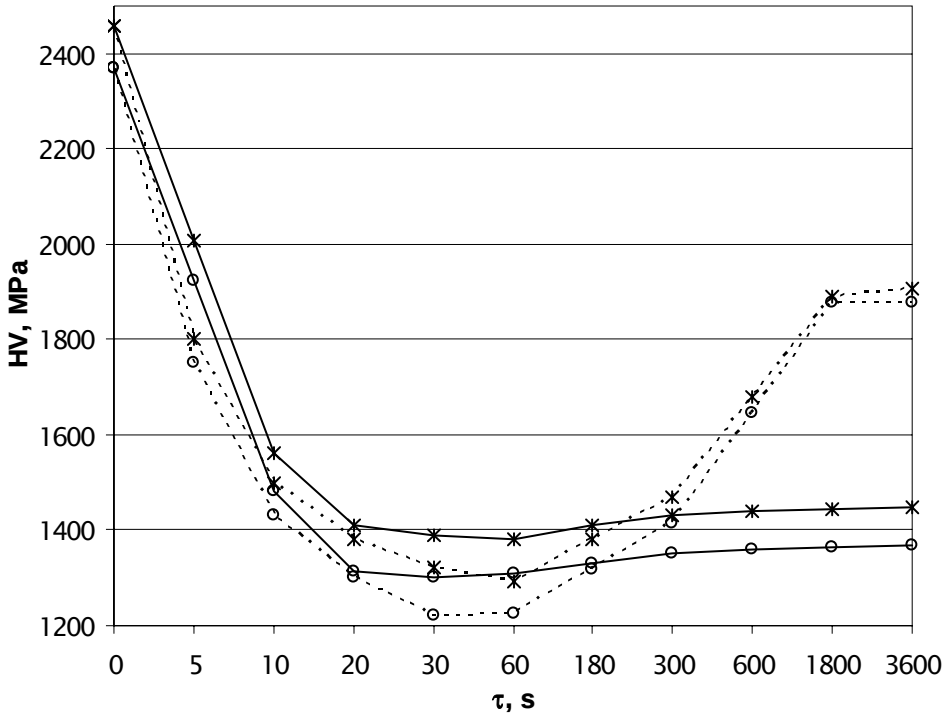

a

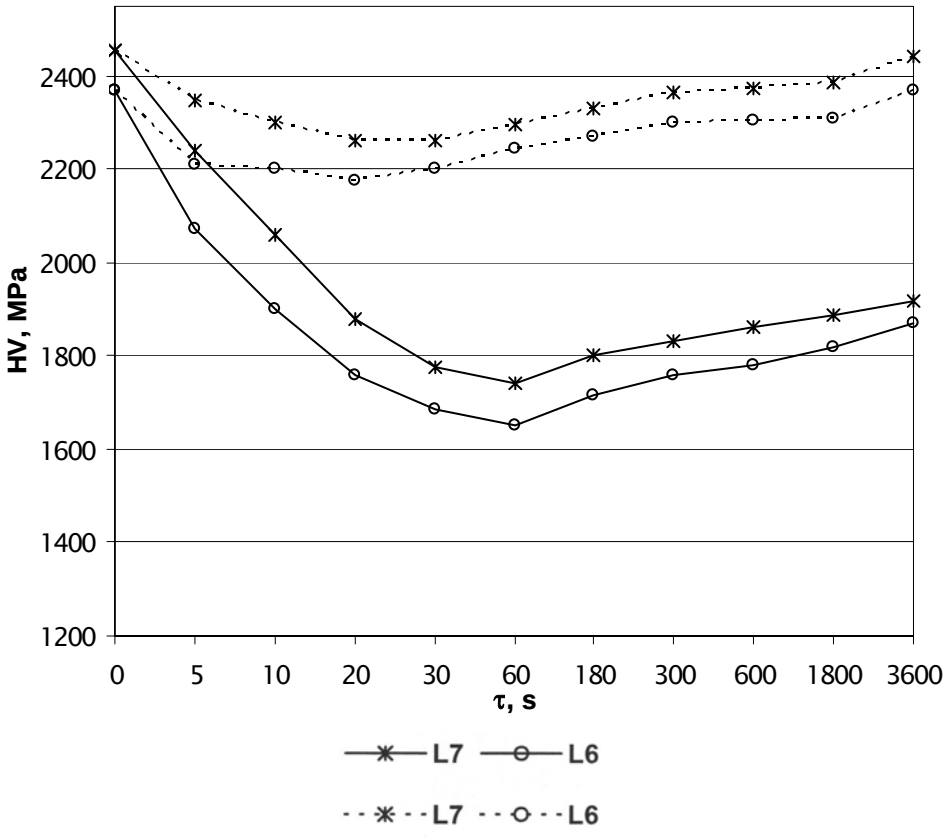

b

Note: Continuous line - alloys quenched in air; Dashed line - alloys quenched in water

Figure 2.11. Change of microhardness of alloys L6 and L7 directly after quenching (a) and after artificial ageing at 120 C for 24 hours (b)

Microstructural studies showed that at quenching from 470 ^{o}C and soaking for 3600 s, the initial stage of partial melting proceeds in the vicinity of the intermetallic inclusions in alloys L6 and L7 (Fig. 2.11). Microhardness of samples quenched in water and artificially aged is here equal to 2442 MPa for alloy L7 and 2378 MPa for alloy L6. At temperature rise up to 480 ^{o}C and quenching in water, microhardness of artificially aged samples was 2464 MPa for alloy L7 and 2340 MPa for alloy L6. Partial melting of the precipitates along the grain boundaries was more pronounced in this case. At temperature lowering to 440 ^{o}C and quenching in water, microhardness of both the alloys was somewhat lower and equal to 2348 MPa for alloy L7 and 2258 MPa for alloy L6. This is indicative of the fact that temperatures of 450 to 460 ^{o}C are the most optimum for quenching of the studied alloys.

Investigation of the structure of samples heated up to 550 - 600 ^{o}C indicated that at increase of isothermal soaking in alloys L6 and L7 the entire range of structural transformations proceeds to a certain extent, namely recovery, annealing and quenching. The solid solution maintains its artificial ageing ability and has quite high values of microhardness, but now an irreversible process of partial melting of eutectic phase precipitates along the boundaries of solid solution grains begins. At 550 ^{o}C temperature partial melting is observed already at soaking for 15 - 20 s, and at 600 ^{o}C it starts at 5 s (Fig. 2.12).

Obtained results of investigation of the influence of heating and cooling conditions on the structure and hardness of test alloy samples are indicative of the possibility of simulation of the physical processes and structural transformations in the alloys, which proceed under different temperature-time conditions of heating, related to heat treatment and welding of the alloys. As regards the studied alloys the following processes should be noted:

- low-temperature recovery, which is due to dissolution of individual fine particles (180 - 200 ^{o}C);
- further decomposition of the solid solution with partial coagulation of the strengthening phases (200 - 350 ^{o}C);
- high-temperature recovery to the hardened condition due to dissolution of the strengthening phases, i.e. solid solution formation (400 - 550 ^{o}C).

All these structural transformations result in the change of hardness, which is exactly what characterizes the processes of strengthening and softening of the base metal and HAZ of welded joints.

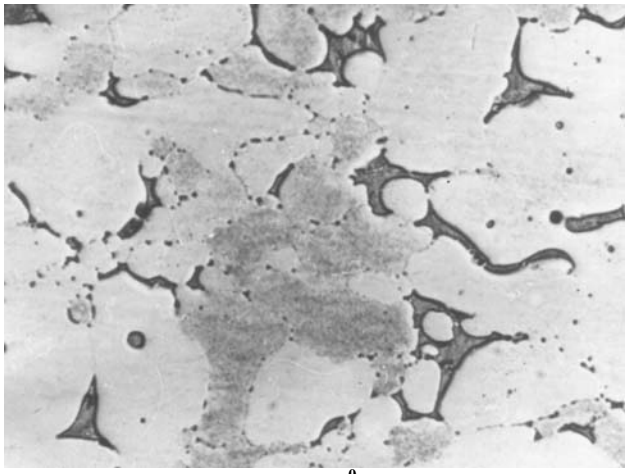

Alloy L6, 550^{0}C, 20 s

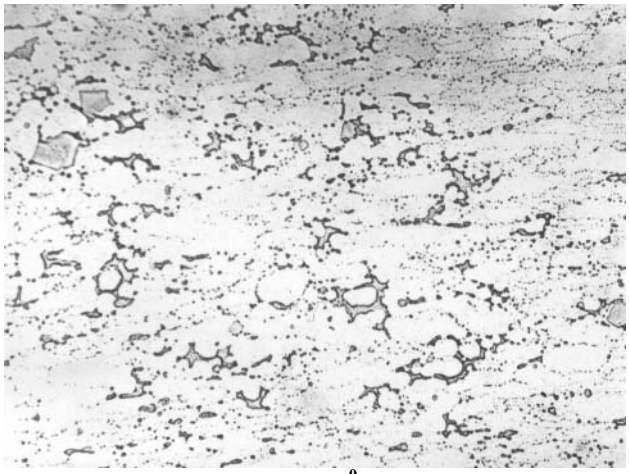

Alloy L7, 550^{0}C, 20 s

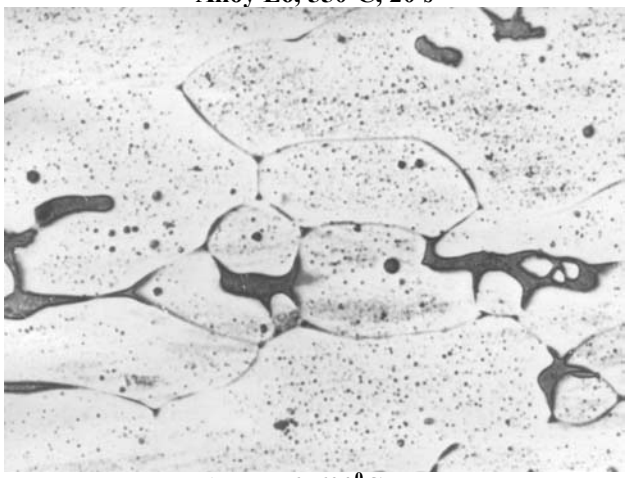

Alloy L6, 600^{0}C, 5 s

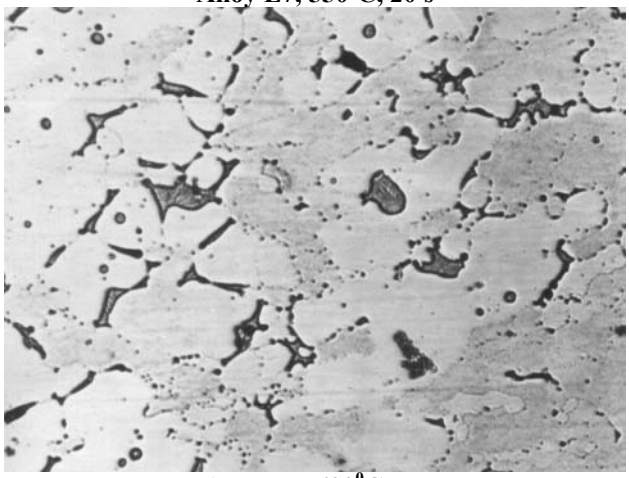

Alloy L7, 600^{0}C, 5 s

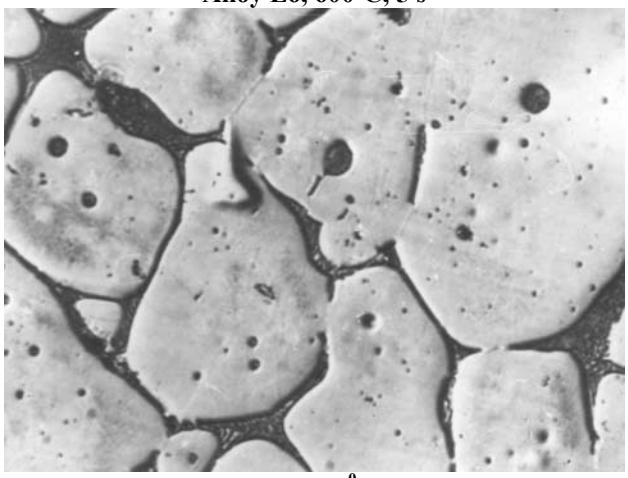

Alloy L6, 600^{0}C, 60 s

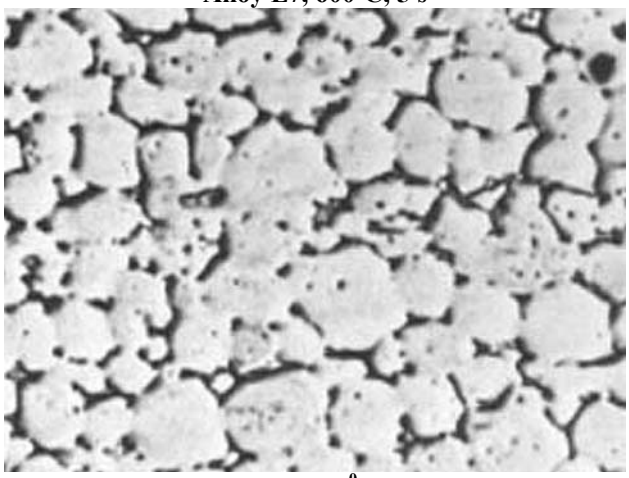

Alloy L7, 600^{0}C, 60 s

Figure 2.12. Change of alloy microstructure under different temperature-time conditions of heating (T6 initial condition). X500.

2.3.2. Generalization of the obtained results of investigations and preparation of scientific-technical report

Analysis of the diagrams of phase composition, published data and results of investigations conducted jointly with IPM allowed determination of the composition of test alloys, which contain Sc, Zr, Nb, Ce, Hf, V. Alloys of the respective composition were produced simultaneously for fillers used in welding of the test alloys.

Sound ingots of 62 and 150 mm diameter were produced using modern technologies of casting and refining of liquid metal and successive rapid solidification. Their chemical and structural inhomogeneity after heat treatment by different modes was studied, and optimum conditions of cast metal homogenizing were determined. A positive effect of scandium microalloying to refine the crystalline structure of the ingots, increase their hardness and strength by 10 – 15 % and preserve the ductility on the level of 5 – 6 % was confirmed.

A highly effective technology was suggested and tried out for manufacturing sheet semi-finished products from ingots of 150 mm diameter by hot pressing of slabs of 10x100 mm cross-section and subsequent hot and cold rolling into 3 mm sheets. This technology was used to make 7 batches of sheets, including two batches of base alloy L6, L6.1 and five experimental alloys L7, L8, L9, L10, L11, which contained 0.3 % Sc and additives of other elements, namely Zr, Nb, Ce, Hf, V.

Method of physical simulation of thermal processes and structural transformations, which proceed in alloys at heating (homogenizing, hot deformation, welding heat, heat treatment) was used to plot the diagrams of dependence of metal microhardness on temperature-time conditions of heating in the temperature range of 200 - 600 ^{o}C and soaking from 5 s up to 1 h. Obtained results confirm the positive influence of Sc on the structure and properties of sheet semi-finished products in different conditions after process heating in manufacturing of the semi-finished products and their welding. Analysis of the diagrams allows evaluation of the degree of decomposition or recovery of the solid solution under different conditions of heating and cooling. This permitted optimization of the modes of alloy heat treatment (homogenizing, quenching, annealing, artificial ageing) and forecasting the level of metal properties in different sections of the welded joint.

Modes of heat and thermomechanical treatment were determined to improve a set of physico-mechanical properties of the sheets of scandium-bearing alloys. Heating conditions were optimized, based on analysis of the thermal effect related to structural transformations. It is suggested to perform heat treatment to maximum strength by the following mode: quenching from 450 - 460 ^{o}C into water + artificial ageing at 120 ^{o}C, soaking for 24 h (T6). At heat treatment by such a mode the maximum strength of sheets of the scandium-bearing alloy is 700 -720 MPa, whereas the base alloy strength is 620 - 640 MPa. Developed modes of thermomechanical treatment in manufacturing of the semi-finished products increase the density of crystalline lattice defects. Crystalline lattice defects introduced by cold plastic deformation change the kinetics of decomposition of oversaturated solid solution, and largely influence the amount and nature of distribution of the decomposition products in the alloy matrix. Selection of an optimum level of deformation and sequence of operations with regard to artificial ageing allows increasing the material strength with satisfactory ductility. At thermomechanical treatment of alloy L7 by the mode of quenching + artificial ageing + cold deformation to 14 % (T9) the maximum level of strength and yield point reaches 730 and 700 MPa, while the ductility level is 5 %. Use of different modes of thermomechanical treatment for welded joints to improve their physico-mechanical properties can be the subject of further investigations.

Optimum modes of fusion welding of sheets of test alloys with scandium and without it were selected experimentally, and samples of sound welded joints were produced.

Metallographic investigations of Al-Zn-Mg-Cu alloy sheets and their welded joints showed that scandium presence in the alloys slows down the recrystallization processes at process heating of the base metal, and in the welded joints it leads to refinement of the crystalline structure of weld metal and less softening of the metal in the HAZ. The width of the zone of base metal recrystallization near the weld is also reduced. Strength of the joints in nonconsumable electrode argon-arc welding of the sheets of scandium-bearing alloys is 420 - 460 MPa. Increase of strength of welded joints on scandium-bearing sheets is 22 – 28 %, compared to basic alloy (340 - 360 MPa). In electron beam welding the weld metal strength in the welded joints rises by 10 – 15 %.

Studying the hot cracking susceptibility in welding of sheets of basic alloy without scandium showed that this index, determined on Houldcroft technological sample (A %) is 49 – 50 % in welding without a filler, and in alloys with scandium it is much lower at 30.5 - 44.6%. When fillers are used, the hot cracking susceptibility index is 48 – 50 % for alloys without scandium, and 24 – 32 % for scandium-bearing alloys. Cracks form mostly in the zone of weld fusion with the base metal. In electron beam welding with a filler of all the test butt joints of such a type, no cracking was observed either in the weld metal, or in the zone of weld fusion with the base metal.

As a result of performance of Project Agreement new alloys of Al-Zn-Mg-Cu (±Sc) system with the sum of the main alloying elements (Zn, Mg, Cu) of up to 14.3 % and microalloyed with Zr, Nb, Ce, Hf were studied. Strength level of the alloys with new microalloying after heat treatment by T6 mode is equal to 700 - 720 MPa at ductility of 5 %. Investigation of weldability of the new alloys showed that they can be included into the group of commercially weldable materials. A conclusion was made on the rationality of applying the developed alloys and technologies of their welding for manufacture of products in the most diverse industrial sectors, primarily in aerospace engineering and transportation. The main advantage is the fact that structure weight can be reduced by 8 – 12 %, which, in its turn, provides a considerable saving of energy resources.

CONCLUSION

1. Optimized technologies of casting, hot and cold deformation were used to make batches of sheets 3 mm thick of alloys L6.1, L9, L10, L11. Optimal modes of fusion welding were established, and samples of sound welded joints were produced. Structure and physico-mechanical properties were determined for the base metal and welded joints made with Al-6%Mg and Al-6%Mg-0.5%Sc filler wires.
2. A positive influence of additives of scandium, zirconium and other transition metals on the physico-mechanical properties and the weldability of Al-Zn-Mg-Cu alloys was established. The anticipated strength level of extruded semi-finished products (800 MPa) and sheets (700 - 720 MPa) has been achieved. Strength coefficient of welded joints without heat treatment is 0.55 for alloys without scandium and 0.63 for alloys with scandium, and after heat treatment by T6 mode it is 0.9-0.97 for scandium-bearing alloys and 1.0 for alloys without scandium.
3. The achieved level of hot brittleness factor of 50 % for alloys without scandium and of 24-32 % for scandium-bearing alloys indicates that the studied alloys can be used for commercial production of critical welded structures under the condition of selection of optimum welding consumables, processes and modes of welding.
4. Methods of physical simulation of the processes proceeding in the alloys as a result of structural transformations while heating (homogenizing, hot deformation, welding heat, heat treatment) were used to plot diagrams of the dependence of metal microhardness on the temperature-time conditions of heating. The results obtained confirm a positive influence of Sc on the structure and properties of sheet semi-finished products in different conditions after process heating during semi-finished product manufacture and welding. Analysis of the diagrams allows to compare the degree of decomposition or recovery of the solid solution under different conditions of heating and cooling. This permitted optimizing the modes of alloy heat treatment and predicting the level of metal properties in different sections of the welded joint.

References

1. Commercial aluminium alloys: Ref. Book / Alieva S.G., Altman N.B., Ambartsumyan S.M. et al. - M.: Metallurgia, 1984, 528 p.
2. Sukhoverkhov A.A., Fetisov G.P., Viskov A.S. Influence of the welding process on the mechanical properties of the HAZ in alloy 01963. // Svarochnoje proizdovstvo, 1976, #10, p.28- 30.
3. Elagin V.I. Alloying of wrought aluminium alloys with transition metals. - M.: Metallurgia, 1975, 248 p.

Task 1. Elaboration of high-strength wrought Al alloys produced by casting

The present investigation was devoted to increasing the strength characteristics of the most strength aluminum alloys of the 7XXX type (Al-Zn-Mg-Cu).

The idea of the investigation is to use "the scandium effect" of increasing mechanical properties of aluminum alloys and to increase the concentration of the main alloying element Zn in the presence of Sc.

The results obtained under this project to define regularities of formation of mechanical properties of deformed semi-products of high strength alloys Al-Zn-Mg-Cu-TM (REM) (obtained by casting), to optimize chemical compositions and technology to produce semiproducts with the best mechanical properties were summarized.

As many as 61 compositions of alloys of system Al-Zn-Mg-Cu, additionally alloyed by Sc, Zr. TM and REM, were produced during fulfillment of the project using the cast method (Table 1.1 – 1.4).

The appropriate technology was developed, and the extrusion of ingots to rods 6 mm in diameter was carried out. There was executed the investigation of the influence of alloying on the structure and mechanical properties of ingots and rods as well as on fracture character of rods after T6 treatment (quenching and aging). There are revealed the compositions of alloys, in which ingots have a uniform structure of small equiaxial grains.

Table 1.1.

Alloys of Al – Zn – Mg – Cu system produced in graphite crucibles

Alloy #	Alloy mark	Chemical composition, wt.%	Grain size, μm	HV, (cast) MPa	Metallographic description
1	3-83	Al-11Zn-3.3Mg-1.2Cu	1000	1322	Dendritic structure
2	3-84	Al-9.0Zn-3.1Mg-1.2Cu-0.2Zr	600-900	1348	Dendritic structure
3	3-85	Al-10.8Zn-3.5Mg-1.2Cu-0.15Zr-0.39Sc	15-25	1485	Grain structure, uniform equiaxial grains
4	L10	Al-10.3Zn-2.85Mg-1.19Cu-0.15Zr	300	1355	Dendritic structure
5	L11	Al-10.0Zn-2.8Mg-1.1Cu-O.11Zr-0.25Cr	100	1333	Fine uniform dendritic structure
6	L12	Al-10.0Zn-3.1Mg-l.lCu-0.16Zr-0.285Cr-0.45Sc	21	1355	Grain structure, uniform equiaxial grains
7	L13	Al-10.2Zn-2.9Mg-1.35Cu-0.15Zr-0.43Sc	32	1423	Grain structure, uniform equiaxial grains
8	L14	Al-10.2Zn-2.7Mg-1.15Cu-0.16Zr-0.50Mn	85	1347	Dendritic structure
9	L15	Al-10.35Zn-2.7Mg-1.29Cu-0.15Zr-0.39Mn-0.49Sc	26	1319	Grain structure, uniform, equiaxial grains
10	L16	Al-12.0Zn-3.3Mg-1.2Cu-0.13Zr-0.38Mn-0.49Sc	14-17	1497	Grain structure, uniform, equiaxial fine grains
11		Al-9.0Zn-3.0Mg-2.6Cu-0.lCr-0.2Ce-0.2Nb-0.1V-0.2Zr-0.2Sc	17-20	1431	Grains structure, homogeneous, equilibrium fine grains
12		Al-8.0Zn-2.3Mg-2.0Cu-0.1Mn-0.2Zr-0.4Sc-0.1Cr	17-20	1400	Grains structure, homogeneous, equilibrium fine grains
13		Al-10.0Zn-3.5Mg-3.0Cu-0.2Zr-0.3Sc	20-26	1463	Grain structure, uniform equiaxial fine grains
13a		Al-9.6Zn-3.8Mg-3.2Cu-0.2Zr-0.38Sc	15-40	1400	Grain structure, uniform equiaxial fine grains
14		Al-8.5Zn-2.6Mg-2.3Cu-0.4Mn-0.2Zr-0.3Sc	30	1362	Grain structure, uniform equiaxial fine grains
15		Al-8.5Zn-2.6Mg-1.9Cu-0.4Mn-0.2Zr	50-150	1319	Dendritic structure
16	UM-27	Al-5Zn-3Mg-1.2Cu-0.15Zr (analogue to L10) ($T_{melting}$ = 790 ^{0}C)	100-120	1022	Grain structure, non-uniform non-equiaxial grains
17	UM-28	Al-5Zn-3Mg-1.2Cu-0.15Zr-0.3Cr-0.3Sc (analogue L12) ($T_{melting}$ = 830 ^{0}C)	20	1008	Grain structure, uniform equiaxial fine grains
18	UM-29	Al-5Zn-3Mg-1.2Cu-0.15Zr-0.3Sc (analogue to L13) ($T_{melting}$ = 815 ^{0}C)	42	890	Grain structure, non-uniform
19	UM-30	Al-5Zn-3Mg-1.2Cu-0.15Zr-0.3Mn-0.3Sc (analogue to L15) ($T_{melting}$ = 800 ^{0}C)	44	940	Grain structure, non-uniform

Table 1.2.

Alloys of Al – Zn – Mg – Cu system manufactured in ceramic crucible

Alloy #	Alloy mark	Content of alloying elements by charge, wt. %	Size of cast grain, μm	HV (as cast) MPa	Metallographic description
20	UM-22	Al-9Zn-3Mg-2.3Cu		1450	Dendritic structure
21	UM-7	Al-9Zn-3Mg-2.3Cu-0.3Mn	30-40	1333	Dendritic structure
22	UM-7.1	Al-9.3Zn-2.3Mg-2.6Cu-0.33Mn-0.68Si	30-40	1333	Dendritic structure
23	UM-7.2	Al-8.6Zn-2.0Mg-3.0Cu-0.35Mn blow free	40-45		Dendritic structure
24	UM-7.8	Al-8.6Zn-2.0Mg-3.0Cu-0.35Mn	40-50	1431	Dendritic structure
25	UM-8.1	Al-9.16Zn-2.7Mg-2.4Cu-0.30Mn-0.16Zr blow free	40-50	1415	Dendritic structure
26	UM-8.2	Al-8.08Zn-2.6Mg-2.0Cu-0.23Mn-0.07Zr	40-50	1415	Dendritic structure
27	UM-9	Al-9.6Zn-2.4Mg-2.36Cu-0.22Mn-0.17Zr-0.095Ti	25-30	1340	Grain structure, non-uniform, non equiaxial
28	UM-10	Al-9.2Zn-2.4Mg-2.17Cu-0.26Mn-0.19Zr-0.41Sc	20-30	1312	Grain structure, uniform, equiaxial fine grains
29	UM-11	Al-9.42Zn-2.3Mg-2.37Cu-0.29Mn-0.15Zr-0.35Sc-0.11Re	40-50	1320	Grain structure, non uniform
30	UM-12	Al-9.7Zn-2.8Mg-2.51Cu-0.24Mn-0.078Zr-0.39Sc-0.2Hf	30-35	1312	Grain structure, non-uniform
31	UM-13	Al-9.27Zn-3.0Mg-2.4Cu-0.27Mn-0.09Zr-0.39Sc-0.12Ti	30	1250	Grain structure, non-uniform
32	UM-14	Al-9.16Zn-3.1Mg-2.32Cu-0.28Mn-0.15Zr-0.37Sc-0.22V	25-30	1312	Grain structure, non-uniform
33	UM-15	Al-9Zn-2.75Mg-2.3Cu-0.3Mn-0.14Zr-0.35Sc-0.22Ni	25-30	1326	Grain structure, non-uniform
34	UM-16	l-9.2Zn-2.9Mg-2.36Cu-0.25Mn-0.12Zr-0.36Sc-0.05Nb	25-30	1330	Grain structure, non-uniform
35	UM-17	Al-9.14Zn-2.6Mg-2.37Cu-0.3Mn-0.12Zr-0.29Sc-0.19Ce	25-30	1355	Grain structure
36	UM-18	Al-9.18Zn-3.3Mg-2.4Cu-0.3Mn-0.16Zr-0.4Sc-0.22Cr	20-25	1340	Grain structure
37	UM-19	Al-9.2Zn-2.4Mg-2.17Cu-0.26Mn-0.19Zr-0.41Sc-0.14Y	15-20	1369	Grain structure, uniform
38	UM-20	Al-9.9Zn-3.2Mg-2.5Cu-0.28Mn-0.14Zr-0.32Sc-0.175Pr	20-25	1280	Grain structure, uniform
39	UM-21	Al-9Zn-3.25Mg-2.3Cu-0.31Mn-0.09Zr-0.35Sc-0.23Nd	15-25	1304	Grain structure, non-uniform
40	UM-23	Al-10.6Zn-2.9Mg-2.6Cu-0.27Mn-0.15Zr-0.12Ti	25-30	1304	Grain structure, non-uniform

Table 1.3.

The alloys, that were melted with additional purification of a melt upon the use of ceramic crucibles and filters and with additional purification of a melt by its blowing with argon

Alloy #	Alloy mark	Content of alloying elements by charge, wt. %	HV, MPa
41	UM22.2	Al - 9.9Zn - 2.9Mg - 2.6Cu	1463
42	UM10.2	Al -7.8Zn - 2.0Mg - 2. 37Cu - 0. 26Mn - 0. 15Zr -0.34Sc	1355
43	UM12.2	Al - 9.1Zn - 3.5Mg - 2.5Cu - 0.22Mn - 0.14Zr - 0.37Sc - 0.15Hf	1333
44	UM15.2	Al - 8.0Zn - 3.0Mg - 2.3Cu - 0.25Mn - 0.12Zr - 0.3Sc - 0.18Ni	
45	UM16.2	Al - 8.9Zn - 3.25Mg - 2. 35Cu - 0.26Mn - 0.12Zr - 0.36Sc - 0.054Nb	1430
46	UM17.2	Al - 9.0Zn - 3.0Mg - 2. 37Cu - 0. 25Mn - 0.2Zr - 0.32Sc - 0.2Ce	1284
47	UM35	Al - 9Zn - 3Mg - 2.3Cu - 0.3Mn - 0.25Hf - 0.3Sc	1400
48	UM36	Al - 9Zn - 3Mg - 2.3Cu - 0. 3Mn - 0.25Hf - 0.15Zr	1219
49	UM37	Al - 6Zn - 2.3Mg - 1.7Cu - 0. 4Mn - 0.18Cr (B95)	1050
50	UM26.2	Al - 12.2Zn - 3.6Mg - 1.18Cu - 0.15Zr- 0.24Sc - 0.4 Mn	1700
51	UM-8.2	Al – 9.64Zn - 3.1Mg – 2.54Cu -0.23Mn 0.12Zr	1415

We have produced a number of alloys of the systems Al - Zn - Mg - Cu and Al - Zn - Mg - Cu - Mn – Zr - Sc Icadditionally doped with Fe (Table 1.4).

Table 1.4.

The alloys of the systems Al – Zn – Mg – Cu and Al – Zn – Mg – Cu – Mn additionally doped with Fe

#	Marking of alloy	Chemical composition, wt. %
		Al - 9Zn - 3Mg - 2.3Cu + (x)Fe
52	UM22	Al - 9.6Zn - 2.6Mg - 2.6Cu
53	UM44	Al - 9.4Zn - 3.1Mg - 2.34Cu - 0.11Fe
54	UM45	Al - 9.3Zn - 3Mg - 2.32Cu - 0.14Fe
55	UM51	Al - 9.7Zn - 3.3Mg - 2.5Cu - 0.33Fe
56	UM52	Al - 9.66Zn - 3.5Mg - 2.5Cu - 0.62Fe
57	UM46	Al - 9.25Zn - 3Mg - 2.26Cu - 0.78Fe
58	UM53	Al - 9.8Zn - 4Mg - 2.6Cu - 1.0Fe
		Al - 9Zn - 3Mg - 2.3Cu + 0.3Mn - 0.15Zr - 0.3Sc - (x)Fe
52	UM10	Al - 9.2Zn - 2.4Mg - 2.17Cu - 0.26Mn - 0,19Zr - 0,41Sc
59	UM47	Al - 9.25Zn - 3Mg - 2.35Cu - 0.36Mn - 0.17Zr - 0.35Sc - 0.33Fe
60	UM48	Al - 9.4Zn - 3.15.Mg - 2.6Cu - 0.3Mn - 0.12Zr - 0.37Sc - 0.64Fe
61	UM49	Al - 9.45Zn - 3.2Mg - 2.6Cu - 0.15Mn - 0.14Zr - 0.42Sc - 1.0Fe

Alloying the alloy Al-9Zn-3Mg-2.3Cu-0.3Mn-0.15Zr by Sc has led to the formation of a fine-grained structure in ingots produced by both techniques (graphite and ceramic crucibles).

A positive influence of small additives of Sc, Zr on cast structure in an Al – Zn – Mg – Cu alloy has been shown (Fig.1.1).

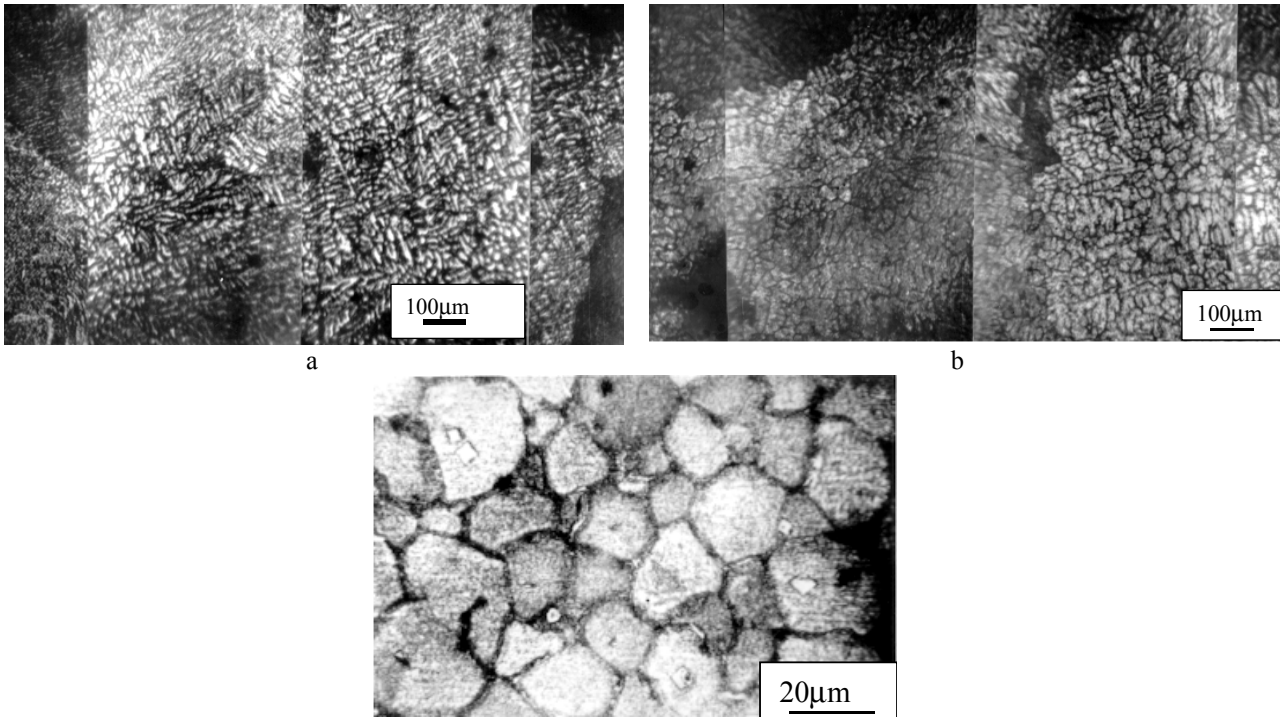

a b

Figure 1.1. Microstructure of ingots of Al–9.5Zn–3Mg–1.2Cu– (Zr, Sc) alloys, longitudinal section:
a – alloy 1 (baseline – Al–9.5Zn–3Mg–1.2Cu); b – alloy 2 (baseline + Zr); c – alloy 3 (baseline + Zr + Sc)

With optimum alloying while crystallization of ingots equiaxial and uniform grain structure is formed, grain size in ingots decreases from 1000 μm (with out Sc) to 14-17 μm (with optimum alloying by Sc).

It was shown that alloying of alloys with small amount of scandium (0.3 mass. %) together with zirconium causes a preservation of not-recrystallized structure in rod after T6 treatment (Fig 1.2). The presence of this structure accompanied by the appearance of ensemble of coherent nanosized particles of intermetallic $Al_3(Sc_{1-x}Zr_x)$ (Fig.1.2) is a reason for additional strengthening of studied alloys along with strengthening by dispersion particles of η′ phase $Mg_4Zn_{13}Al_2$, which are quite usual for the above said system (Fig.1.3).

It was found out that in the investigated alloyed alloys the particles of $Al_3(Sc_{1-x}Zr_x)$ intermetallic are stable, and those particles remain disperse and coherent with Al matrix after T6 treatment (including heating to 460 ^{0}C).

Thus, the temperature of recrystallization beginning in extruded rods:

T_{rb} = 350 ^{0}C for the baseline alloy Al – Zn – Mg – Cu;

T_{rb} = 400 ^{0}C for the alloy Al – Zn – Mg – Cu alloyed by Zr;

T_{rb} > 560 ^{0}C for the alloy Al – Zn – Mg – Cu alloyed by Zr + Sc.

Thanks to that, alloys containing Sc can be subjected to the T6 thermal treatment without any sign of recrystallization.

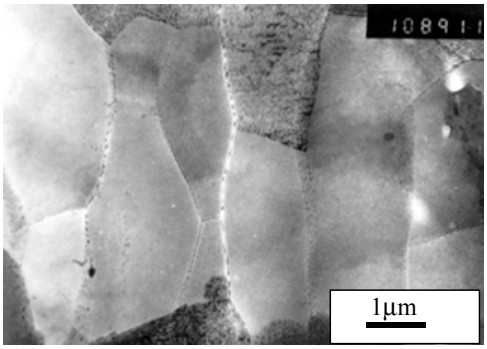

Figure 1.2. Cellular structure of thin foils from rods of alloy Al-Zn-Mg-Zr-Sc after extrusion and T6 treatment, transmission electron microscopy

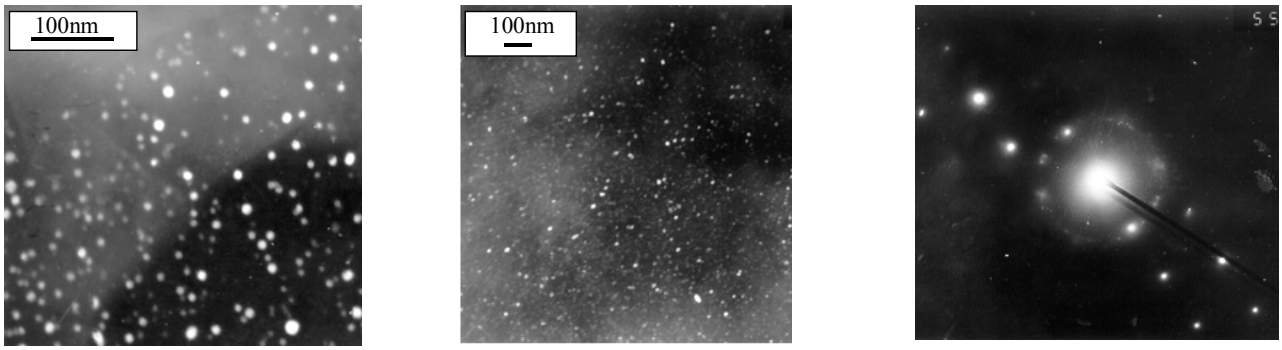

a b c

Figure 1.3. Two ensembles of the secondary particles in rods of the alloy of system Al – Zn – Mg – Cu – Sc – Zr after T6 treatment: a – dark field photo in the reflection (001) of Al_3Sc; b – dark field photo in a part of rings of η′-phase; c – electron diffraction pattern from the area

Parameters of substructure (the size of cells, the size of particles) of this alloys depend on their composition and thermal treatment (Tab.1.5).

Table 1.5.

Structural parameters of rods from alloys of Al – Zn – Mg – Cu system additionally alloyed with TM, REM and Sc

Chemical composition of alloys, wt.%	**Zn, % wt.**	**Cells size after T6, μm**	**Size of η′-phase in rods after T6**	**Size of $Al_3(Sc_{1-x}Zr_x)$ in rods after T6**
Al-10Zn-2.8Mg-1.2Cu	10	1.8	8.2 (Zr)	-
Al-10Zn-2.8Mg-1.2Cu-0.46Sc	10	1.3	9.6 (Zr, Sc)	5.7
Al-10Zn-2.8Mg-1.2Cu-0.25Cr	10	1.0	2.9 (Zr, Cr)	-
Al-10Zn-2.8Mg-1.3Cu-0.25Cr-0.46Sc	10	1.3	3.5 (Zr, Cr, Sc)	11.8
Al-10Zn-2.8Mg-1.0Cu-0.50Mn	10	1.7	6.2 (Zr, Mn)	-
Al-10Zn-2.7Mg-1.3Cu-0.5Sc-0.3Mn	10	1.6	12.5 (Zr, Mn, Sc)	6.6
Al-12Zn-3.2Mg-1.25Cu-0.5Sc-0.37Mn	10	1.5	6.6 (Zr, Mn, Sc)	8.5
Al-5Zn-3Mg-1.2Cu-0.15Zr	5	1.9	2.2	13.5 (Al_3Zr)
Al-5Zn-3Mg-1.2Cu-0.15Zr	5	1.0		12.0
Al-5Zn-3Mg-1.2Cu-0.15Zr -0.3Sc	5	1.5	3.17	11.2
Al-5Zn-3Mg-1.2Cu-0.15Zr–0.3Mn-0.3Sc	5	2.0		

It is established that an increase of Zn content lowered the size of $Al_3(Sc_{1-x}Zr_x)$ particles and increased the size of η′-phase particles that precipitate during T6 treatment. An additional alloying with chromium preserved a small size of η′-phase particles and an increased size of the secondary $Al_3(Sc_{1-x}Zr_x)$ particles. The size of dislocation cells in the rods after T6 treatment was practically independent on Zn content. On the base of the analysis of the obtained results it is proposed a principal scheme that generalizes the influence of alloying elements on the size of disperse particles (Fig.1.4).

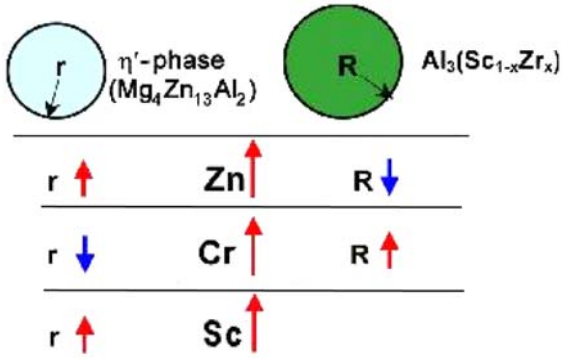

Figure 1.4. Scheme of effect of Zn, Cr, and Sc content on size of disperse precipitations in high-strength Al alloys

On the base of analyzing the dependence of YS on the size of disperse particles it is given a principal explanation of such effect of alloying with Sc in combination with other TM and REM on the mechanical properties when an increase of strength and plasticity of wrought semi-finished products after T6 treatment are achieved simultaneously (Fig. 1.5). Sc increases the size of η′-particles. In this case, the size of η′-particles, 2r, can exceed the critical size d_{cr}, which leads to the transition from the mechanism of cutting of the particles by dislocations to the mechanism of detour according to the Orowan model. Under such a transition, the plasticity of an alloy grows. At the same time, strength can decrease. However, under alloying with Sc, the second ensemble of dispersed particles of $Al_3(Sc_{1-x}Zr_x)$, is formed that compensates the loss of strength. Thus, the alloying with Sc can, in principle, lead to the simultaneous increase in strength and plasticity.

The character of the distribution of alloying elements (main as well as additionally introduced while project performance) in structural components of cast alloy and rod ∅ 6 mm in T6 is studied by SEM technique.

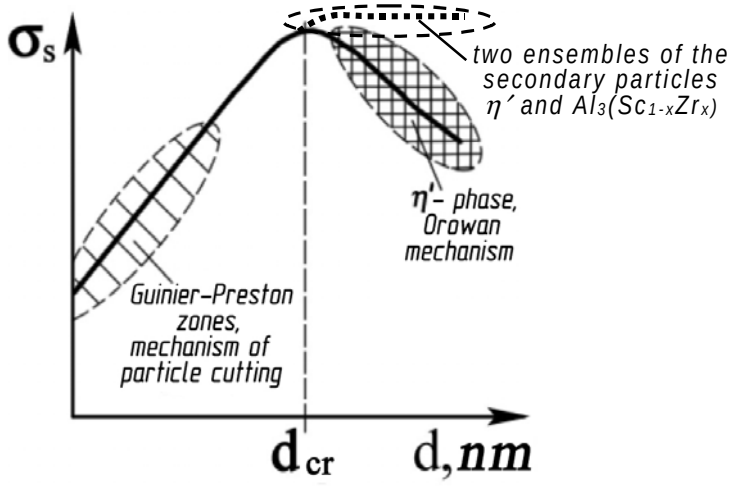

Figure 1.5. Scheme of the dependence of the yield stress σ_s on the average size of second phase particles in Al – Zn – Mg alloys

It is shown that after the solid solution treatment Zn entirely leaves grain boundaries and becomes uniformly distributed in the solid solution in the grain body, Mg in the most part is dissolved in the solid solution too, but somewhere it is left in boundaries in separate areas. Mn and Cu after quenching are also dissolved in the solid solution. Separate congestions were observed in the same places in grain boundaries where accumulations of signals from Cu atoms took place that corresponds to the formation of $Al_{20}Cu_2Mn_3$ phase. Primary $Al_3(Sc_{1-x}Zr_x)$ intermetallics remain after quenching in grain body. Alloying the baseline alloy with REM and TM did not change the regularities of the distribution of the main alloying elements. It was shown that It was shown that Hf and Ti introduced in amount of up to 0.2 wt.% are partially dissolved in the initial intermetallics $Al_3(Sc_{1-x}Zr_x)$. In the alloy A1-Zn-Mg-Cu additionally alloyed with only Mn and Zr, Ti is uniformly distributed in grains body and does not enter to intermetallics.

The results on investigation of the distribution of alloying elements in ingots of alloys # 20-40 (Tab.1.2) produced with using ceramic crucible are summarized in Table 6.

It was shown that the purity in oxide inclusions and carbon may be essentially increased by using ceramic crucibles (instead of graphite ones), melt filtration and blowing by argon.

A rod sample from the alloy Al-9Zn-3Mg-2.3Cu manufactured in the graphite crucible in the air was completely recrystallized and failed during tensile test without signs of macroplastic deformation, the fracture being mainly intercrystalline. A rod sample of the same alloy produced in the ceramic crucible with blowing the melt by argon and pouring through a ceramic filter was also completely recrystallized, but showed a high ductility $\delta = 20$ % and high level of strength properties: YS = 530 MPa, UTS = 619 MPa.

By this way it was found that the employment of ceramic crucibles and filtration of the melt through ceramic filters in process of production of ingots increase the plasticity of T6 semi-products due to purification of ingots from oxide inclusions that allows to increase the content of Cu in the alloy to 2.3 mass %.

Alloying with Sc and Zr does makes the alloys significantly less sensitive to the technology of melting. So the alloy close in composition to Al-9.2Zn-2.4Mg-2.17Cu-0.26Mn-0.19Zr-0.41Sc (#28), which was executed in graphite crucible had mechanical properties YS = 705 MPa, UTS = 753 MPa, $\delta = 10$ %.

By using the baseline alloy Al - 9Zn - 3Mg - 2.3Cu doped with Zr and Sc, we have repeatedly melted the alloys with Hf, Ni, Nb, and Ce in ceramic crucibles with the use of ceramic filters and the blowing of a melt with argon. These alloys after deformation and thermal treatment in condition T6 have a high level of mechanical properties. The results derived in the present project concerning the influence of the complex alloying with TM and REM on mechanical properties of high-strength aluminum alloy UM22 summarized in Tab.1.7. For comparison alloy #2, melted in the graphite crucible is given in the Tab.1.7 as well.

Table 1.6.

Distribution of elements in structural components of ingot of alloys Al - 9Zn - 3Mg - 2Cu + (Sc, REM, TM)

Alloy	Element	Element's place in cast structure of alloy			
		In grain boundaries	In grain uniformly from grain to grain	In grain non-uniformly from grain to grain	Included to intermetallic particles
#20	Zn	+ (in a form of eutectic)	+	-	-
#20	Mg	+ (in a form of eutectic)	+	-	-
#20	Cu	+ (in a form of eutectic)	+	-	-
#23	+Mn	+ (in a form of Al_6Mn)	+	-	Al_6Mn
#25	+ Mn+Zr	-	+	-	$Al_3(Sc_{1-x}Zr_x)$
#28	+ Mn+Zr + Sc	-	+	-	$Al_3(Sc_{1-x}Zr_x)$
#28 + element	+Hf	-	+	-	$Al_3(Sc_{1-(x+y)}Zr_xHf_y)$
#28 + element	+V	-	-	+	-
#28 + element	+Ni	-	-	+	$Al_4(CuMnNi)$
#28 + element	+Nb	-	+	-	-
#28 + element	+Ce	+	+	-	$Al_{24}Ce_2Cu_3Mn$
#28 + element	+Cr	-	+	-	-
#28 + element	+Ti	-	-	+	$Al_3(Sc_{1-(x+y)}Zr_xTi_y)$
UM8 + Ti	+Ti	-	-	+	-

This table yields that the alloying of the baseline alloy UM22 with Mn and Zr induces the small increase in strength parameters. The alloying with Sc leads to the essential growth of strength properties. The additional alloying of alloy UM10 (UM22 + Mn + Zr + Sc) with TM and REM leads to the additional improvement of mechanical properties. The best results are attained on the additional alloying of UM10 with Hf, Ce, Ni, and Nb.

It is shown that the melting in a ceramic crucible with the use of a filter and the purification of a melt with blowing by argon allows one to get, with good reproducibility, high-strength aluminum alloys with Sc and Zr and with high content of Zn (~ 12 %). These alloys have a high level of mechanical properties (YS = 797 MPa; UTS = 839 MPa, EL = 7.2 %).

Plastic deformation while tension of samples made from highly-alloyed alloys under investigation in T6 condition goes through two stages (Figs. 1.9 and 1.10). In the first stage of deformation ($E \le 1\%$) an extremely high strain hardening is observed – the strain hardening coefficient $\frac{d\sigma}{dE} \ge 5$ GPa, that is a consequence of a strong resistance of the system of disperse particles to dislocation movement. In the second stage of deformation (from E ~ 1 % up to fracture) the strain hardening dramatically falls and is coming to $\frac{d\sigma}{dE} \approx \sigma \approx 0.7$ GPa, *i.e.* the

Considere criterion takes place for a considerable part of the stress-strain curve, that stipulates a possibility of deformation localization in a few slip planes located at 45 ^{0} to sample axis. A reduction of strain hardening in the second stage can be explained by cutting of disperse particles by dislocations and / or their pushing out of planes of localized shear. A considerable duration of the stage 2 is obviously stipulated by a delay of crack front on second phase particles.

Table 1.7.

The influence of alloying elements on the mechanical properties of Al - 9Zn - 3Mg - 2.3Cu alloy in T6 condition

Alloy	Alloying elements	Mechanical property of rods ∅ 6 mm in T6 conditional			HV, MPa
		YS, MPa	UTS, MPa	EL,%	
Alloy #2 (Al-9Zn-3Mg-1.2Cu) melted in the graphite crucible	-	-	554	0	1920
#20: Bazeline alloy Al-9Zn-3Mg-2.3Cu	-	530	619	20.4	2070
#23 = #20 + Mn	+Mn	548	636	17	2070
#25 = #23+Zr	+Zr	545	621	13.8	2050
#28 = #25 + Sc	+ Sc	696	789	12.3	2160
#28 + TM and RE metals					
	+V	717	767	7.3	2090
	+Ni	735	807	10.2	2150
	+Nb	722	824	11.4	2130
	+Ce	744	809	10.0	2150
	+Cr	725	804	10.2	2150
	+Hf	700	810	14.1	2090
	+Ti	718	779	10.3	2210
	+Fe	741	802	9.3	2170
#50 ≈ UM10 (12 %Zn !)	+Zn	797	839	7.2	2280
#25 + Ti	+Ti	654	707	7.2	2130

Analyzing stress strain curves we found that due to a very low strain hardening of T6 rods at the second stage of deformation the rods fail under the mechanism of pores coalescence in shear planes.

Analysis of strain hardening revealed a different nature of influence of additional alloying elements on parameters of both stages of deformation due to their different behavior in alloy. Thus, according SEM investigations and micro X-ray analysis, hafnium is included in intermetallics $Al_3(Sc_{1-x}Zr_x)$ and in that way effects on particles of this intermetallic, as well as dramatically increases parameters of the first stage of deformation and a bit decreases parameters of the second stage that brought the highest plasticity (δ = 14.1 %) in alloy Al-8.7Zn-2.8Mg-2.5Cu-0.24Mn-0.08Zr-0.39Sc-0.21Hf at rather high strength characteristics (YS = 700 MPa, UTS = 810 MPa). And from the other side, the elements like Nb and Ce are not included in intermetallic $Al_3(Sc_{1-x}Zr_x)$, can effect on strengthening particles of η'-phase. These elements increase parameters of the first stage of plastic deformation but not that much than Hf does, and a bit accelerate strengthening of the second stage but along with that elevate value of the yield stress and as a result rods plasticity a bit falls and strength characteristics can be increased (for rods with Nb YS = 722 MPa, UTS = 824 MPa, δ = 9.6 %).

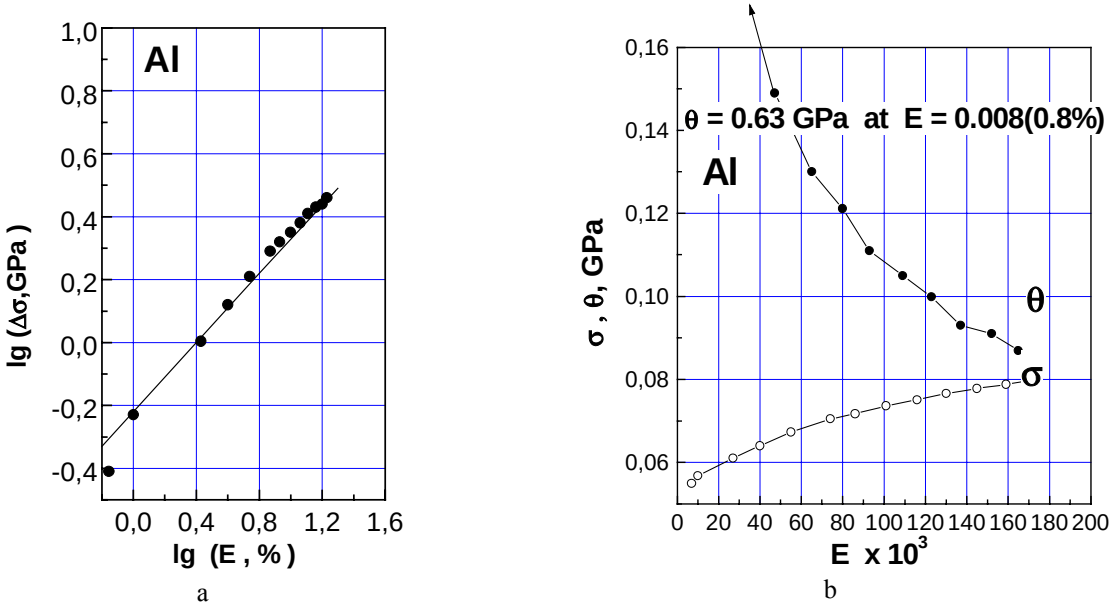

a b

Figure 1.6. Dependence of hardening $\Delta\sigma$ (a) and true stress σ and strain hardening coefficient $\frac{d\sigma}{dE}$ (b) on the strain in a sample of unalloyed aluminum

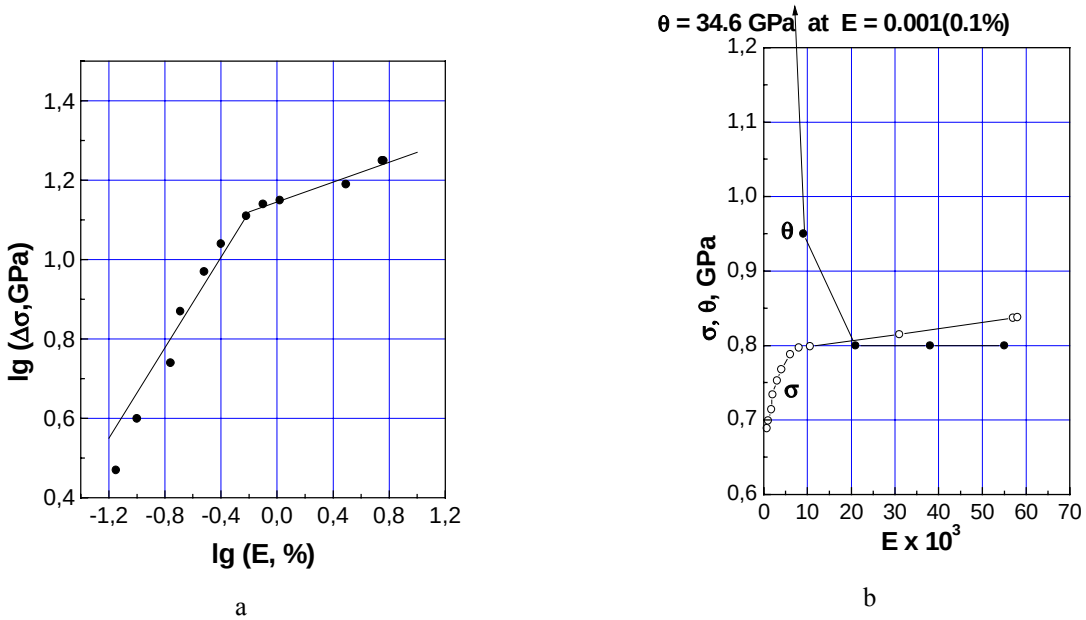

a b

Figure 1.7. Two stage deformation of alloy Al–10.3Zn–2.85Mg–1.19Cu–0.15Zr in T6 condition; a -hardening $\Delta\sigma$ as a function of deformation; b -true stress σ and strain hardening coefficient θ

As a result of optimization of chemical composition, production technology and thermal treatment of extruded semi-products of highly alloyed high strength aluminum alloys we arrived the following strength characteristics YS = 700 - 740 MPa, UTS = 770 - 820 MPa and plasticity δ = 9 – 14 % at a room temperature.

These alloys are referred to the class of industrial welded (see Task 2).

The efforts of project customer showed that these alloys can be employed at cryogenic temperatures where they have a record strength and a rather good plasticity. In over-aged conditions an increase in elongation to a value as high as 8.5 % at the values of YS = 805 MPa and UTS = 835 MPa at cryogenic temperature was observed (Al-12Zn-3Mg-1.2Cu-0.38Mn-0.13Zr-0.49Sc).

The effect of various modes of thermomechanical treatment (TMT) on the level of rod mechanical properties is investigated. It is shown that for working at ambient temperature the optimal mechanical properties of high-alloyed Al-Zn-Mg-Cu alloys additionally alloyed with Sc, Zr, TM and / or REM are achieved by using the T6 mode of TMT.

It was studied the influence of the alloying of the baseline alloy with admixture of Fe up to 1 wt. %

We have shown that the introduction of up to 1.0 % Fe in the baseline alloy leads to the insignificant increase in strength characteristics (YS increases from 530 to 572 MPa) and to the decrease in plasticity from 20.4 % to 13.3 % (Fig 1.8).

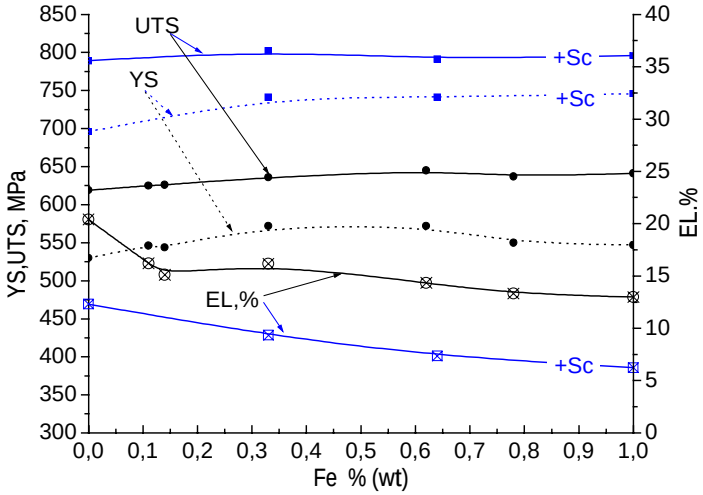

Figure 1.8. The influence of iron concentration on the mechanical properties of rods ∅ 6 mm (μ =17.7) Al-Zn-Mg-Cu alloys in T6 conditions. Alloys obtained by casting (compare with PM method in task 3 of this report)
alloy 1: Al - 9Zn - 3Mg – 2.3Cu + (x)Fe;
alloy 2: Al - 9Zn - 3Mg – 2.3Cu - 0.3Mn - 0.15Zr - 0.3Sc + (x)Fe

Such a variation in mechanical properties was caused by the formation of Fe-containing intermetallics. We have demonstrated that the presence of Fe in the baseline alloy decelerates the process of recrystallization.

The additional alloying of the high-strength aluminum alloy containing Sc and Zr with Fe up to 1% led to the increase in strength characteristics (YS increased from 696 to 746 MPa) and to the decrease in plasticity from 12 to 6 % (Fig. 1.8).

Thus, additional alloying with scandium of aluminum alloys with increased content of iron (to 1 wt. %) permits to manufacture alloys with high level of strength and satisfactory ductility of wrought semi-finished products. This opens the possibility of using recycled aluminum with high iron content for producing high-strength Al alloys.

CONCLUSIONS

1. Optimal composition of the high-alloyed baseline Al-Zn-Mg-Cu alloy for further alloying with various transition and rare-earth metal additives has been theoretically grounded and experimentally proved, the alloy has been melted and investigated. High-alloyed Al-Zn-Mg-Cu alloys with additional alloying by Zr, Sc, Mn, Cr, V, Nb, Re, Ti, Hf, Y, Nd and Ce as well as optimal techniques of their thermal treatment allowing to obtain a high level of mechanical properties close to ones planned in this project were offered.

2. A positive influence of small additives of Sc, Zr, Mn, Cr, Ni, Hf, Nb and Ce into an Al-Zn-Mg-Cu alloy on metal structure was shown.
With optimum alloying an equiaxial and uniform grain structure is formed in ingots while crystallization, grain size in ingots decreases from 1000 μm in unalloyed ingot to 14-17 μm in alloyed ingots.
The availability of Sc (in combination with Zr) in the alloy considerably elevates the temperature of recrystallization beginning thanks to a high thermal stability of the precipitates of $Al_3(Sc_{1-x}Zr_x)$ intermetallic.
Thus, the temperature of recrystallization beginning in extruded rods:
T_{rb} = 350 ^{0}C for the baseline alloy Al-Zn-Mg-Cu;
T_{rb} = 400 ^{0}C for the alloy Al-Zn-Mg-Cu alloyed by Zr;
T_{rb} > 560 ^{0}C for the alloy Al-Zn-Mg-Cu alloyed by Zr + Sc.
Thanks to that, alloys containing Sc can be subjected to the T6 thermal treatment without any sign of recrystallization. It was found out that in the high-alloyed alloys under investigation the particles of $Al_3(Sc_{1-x}Zr_x)$ intermetallic are more stable than in low-alloyed alloys, and those particles remain disperse and coherent with Al matrix after T6 thermal treatment including heating to 460 ^{0}C.

3. The main advantage of high-alloyed alloys containing Sc appears in welding process, where of importance is a fine grain of cast metal and elevated temperature of recrystallization beginning in the heat-affected zone close to the weld (see Task 2 in this report). Just alloying by Sc (along with other microadditives) has allowed a considerable increase of the total content of alloying elements in the alloy (up to about 17 wt. %), preserving a satisfactory weldability together with a high level of mechanical properties.

4. Plastic deformation while tension of rod samples of highly-alloyed alloys under investigation in T6 condition goes through two stages. In the first stage of deformation (E ≤ 1 %) an extremely high strain hardening is

observed: the strain hardening coefficient $\frac{d\sigma}{dE} \geq 5$ GPa that is a consequence of a strong resistance of the system of disperse particles to dislocation movement. In the second stage of deformation (from E ~ 1 % up to fracture) the strain hardening dramatically falls and is coming to $\frac{d\sigma}{dE} \approx \sigma \approx 0.7$ GPa, *i.e.* the Considere criterion takes place for a considerable part of the stress-strain curve that stipulates a possibility of deformation localization in a few slip planes located at 45^0 to sample axis. A reduction of strain hardening in the second stage can be explained by cutting of disperse particles by dislocations and/or their pushing out of planes of localized shear. A considerable duration of the stage 2 is obviously stipulated by a delay of the crack front on second phase particles.

5. It was shown that the purity in oxide inclusions and carbon can be essentially increased by using ceramic crucibles (instead of graphite ones) as well as melt filtration and blowing by argon. Under these conditions of melting, extrusion and T6 treatment even the baseline alloy Al-9Zn-3Mg-2.3Cu had a high level of mechanical properties: YS = 530 MPa, UTS = 619 MPa, and EL =20.4 %. Additional alloying of the baseline alloy by TM and REM essentially increased mechanical properties of the alloys (YS = 630-744 MPa, UTS = 770-824 MPa, and EL = 9-14 %). Optimum compositions of high-strength alloys are developed. Alloys with additions of Hf, Ni, Nb, Ce produced by the developed technology have the highest complex of mechanical characteristics (YS = 700-744 MPa, UTS = 807-824 MPa, EL = 9.6-14 %).

6. It is established that an increase of Zn content lowered the size of $Al_3(Sc_{1-x}Zr_x)$ particles and increased the size of η'-phase particles that precipitate during T6 treatment. An additional alloying with chromium preserved a small size of η'-phase particles and an increased size of $Al_3(Sc_{1-x}Zr_x)$ particles. Alloying by Sc somewhat increased the size of η'-phase particles. The size of dislocation cells in the rods after T6 treatment was practically independent on Zn content. Analysis was carried out for the dependence of the size of disperse particles of the η'-phase and secondary $Al_3(Sc_{1-x}Zr_x)$ intermetallics that are formed during extrusion and thermal treatment on the kind of alloying (alloying elements and their concentration). On the base of the analysis of the obtained results it is proposed a principal scheme that generalizes the influence of alloying elements on the size of disperse particles. On the base of analyzing the dependence of YS on the size of disperse particles it is given a principal explanation of such effect of alloying with Sc in combination with other TM and REM on the mechanical properties when an increase of strength and plasticity of wrought semi-finished products after T6 treatment are achieved simultaneously.

7. The character of the distribution of alloying elements (main as well as additionally introduced while project performance) in structural components of cast alloys is studied by SEM technique. It is shown that after the solid solution treatment Zn entirely leaves grain boundaries and becomes uniformly distributed in the solid solution in the grain body, Mg in the most part is dissolved in the solid solution too, but somewhere is left in boundaries in separate areas. Mn and Cu after quenching are also dissolved in the solid solution. Separate congestions of Mn were observed in the same places in grain boundaries where accumulations of signals from Cu atoms took place that corresponds to the formation of the $Al_{20}Cu_2Mn_3$ intermetallic. Primary $Al_3(Sc_{1-x}Zr_x)$ intermetallics remained after quenching in grain body.

8. Alloying the baseline alloy with REM and TM did not change the regularities of the distribution of the main alloying elements. It was shown that Hf and Ti additionally introduced into the baseline Al-Zn-Mg-Cu-Mn-Sc-Zr alloy in the amount of up to 0.2 wt. % are partially dissolved in primary $Al_3(Sc_{1-x}Zr_x)$ intermetallics. In the alloy A1-Zn-Mg-Cu additionally alloyed with only Mn and Zr, Ti is uniformly distributed in grains body and does not enter to intermetallics.

9. By using the baseline alloy Al - 9Zn - 3Mg - 2.3Cu doped with Zr and Sc, we have repeatedly melted the alloys with Hf, Ni, Nb, and Ce in ceramic crucibles with the use of ceramic filters and the blowing of a melt with argon. These alloys after deformation and thermal treatment in condition T6 have a high level of mechanical properties:

   alloy with Hf and Sc: YS = 728 MPa, UTS = 797 MPa, EL = 11 %;
   alloy with Nb and Sc: YS = 747 MPa, UTS = 796 MPa, EL = 11 %;
   alloy with Ce and Sc: YS = 751 MPa, UTS = 803 MPa, EL = 10.3 %;
   alloy with Ni and Sc: YS = 739 MPa, UTS = 801 MPa, EL = 10.6 %.

10. It is shown that melting in a ceramic crucible with the use of a filter and purification of the melt with blowing by argon allows to get, with good reproducibility, high-strength aluminum alloys alloyed with Sc and Zr that have as high content of Zn as 12 wt. %. These alloys had a high level of mechanical properties (YS = 797 MPa; UTS = 839 MPa, EL = 7.2 %).

11. The influence of alloying the baseline alloy with an admixture of Fe up to 1 wt. % was studied (melting and crystallization of the high-strength aluminum alloys were carried out by the technology developed during the project execution). It is shown that the introduction of up to 1.0 % Fe in the baseline alloy leads to an insignificant increase in strength characteristics (YS increased from 530 to 572 MPa) and to a decrease in plasticity from 20.4 % to 13.3 %. Such a variation in mechanical properties was caused by the formation of Fe-containing intermetallics. We have demonstrated that the presence of Fe in the baseline alloy decelerates the process of recrystallization. The additional alloying of the high-strength aluminum alloy containing Sc and Zr with Fe up to 1 % led to the increase in strength characteristics (YS increased from 696 to 746 MPa) and to the decrease in plasticity from 12 to 6 %.
    Thus, additional alloying with scandium of aluminum alloys with increased content of iron (to 1 wt. %) permits to manufacture alloys with high level of strength and satisfactory ductility of wrought semi-finished products. This opens the possibility of using recycled aluminum with high iron content for producing high-strength Al alloys.

6.2. Alloys reinforced with nanosize quasicrystalline particles

6.2.1. Introduction

Works for the investigation of elevated temperature aluminum alloys with quasicrystalline phases and with micro- and nanocrystalline structure in Task 6 of the project were planned as searching works because at the beginning of works we had a low experience in studying such alloys. Project authors have started this work after the execution of a large amount of investigations of the structure and mechanical behavior of Al-Cu-Fe quasicrystals [9]. Our task in project was to obtain the strength of semi-finished products at 300 °C of not lower than 300 MPa and their ductility at ambient temperature of not lower than 5 %.

The known ways for creation of elevated temperature Al alloys are the retardation of diffusion processes in them and their reinforcing with disperse intermetallic particles that are stable at elevated temperatures of working. Both of these ways are realized by alloying Al with refractory transition metals [5]. But the equilibrium solubility of these metals in Al is very low, and the only way of its increase is using rapid solidification (RS) for alloy manufacture. RS provides also the formation of very fine nanosize reinforcing intermetallics, either in the RS process or by the precipitation from the supersaturated solid solution [6]. The highest solidification rates can be realized by the techniques of melt spinning (producing thin ribbons) and melt atomization (producing RS powders). Bulk semi-finished products of elevated temperature Al alloys are manufactured by the techniques of powder metallurgy. The handbook [6] presents several PM alloys of this class based on Al-Fe system. For alloy Al-10.5Fe-2.5V (in wt. %) that is the strongest of them the tensile characteristics at a temperature of 316 °C of the extruded rod are: YS = 206 MPa, UTS = 240 MPa, El = 6.9 %.

For last ten years this class was supplemented mainly by a group of Japanese scientists headed by Prof. A. Inoue [1] with a new class of aluminum alloys reinforced by nanosize quasicrystalline particles. Peculiarities of deformation processes in quasicrystals and interface boundaries quasicrystal–Al matrix as well as very low diffusion rate in a complicated quasicrystalline lattice promised to achieve higher level of elevated temperature strength combined with a sufficient ductility. Thus, the PM rod from argon-atomized powder of (0-26 μm) size fraction of alloy $Al_{93}Fe_3Cr_2Ti_2$ that is the strongest in this group had a strength of 360 MPa, which is USA Air Force goal [1], but its room temperature ductility was not higher than 2 %, whereas the demand of USA Air Force is not lower than 5 %. The rod strength after holding the samples at 300 °C for 1000 h remained practically unchanged [7]. Japanese scientists have published several patents about heat-resistant aluminum-base alloys, in which more than 200 compositions of high-strength elevated temperature aluminum alloys with quasicrystalline reinforcing phase are described [8-14]. In accordance to the review [1], powder alloys reinforced with quasicrystalline phase were produced in Japan in a closed system filled by argon, without showing the material to open air in all processes from melt atomization to powder consolidation by hot extrusion. Some French scientists studied PM rods of Al-Fe-Cr alloys with quasicrystalline component produced with using centrifugal atomization of the melt [15].

The Al-Fe-Cr system is very promising for producing RS alloys of high quality for the fact that Fe enters into interaction with Al of eutectic type, whereas the interaction of Cr with Al is peritectic [16]. A combined alloying of such type permits to obtain a uniform distribution of alloying elements because for a peritectic interaction the maximal saturation occurs in the dendrite center, and for a eutectic interaction it takes place in the dendrite periphery. This enables to obtain a uniform distribution of small intermetallic precipitates. The experience of WILS (Moscow) in working with this system using the granular technology for alloy manufacture has shown a stabilizing action for these alloys of additional alloying with Mo, Ce, Zr. In particular, good strength characteristics were obtained for Al-Fe-Cr-Zr-Mo alloys, but for their manufacture a solidification rate of about 10^6 K/s was recommended [17].

In our laboratory we had the following possibilities for producing RS alloys:

- Melt spinning with flat casting on a rapidly rotating polished copper roll-cooler through a slit quartz nozzle, a cooling rate of about 10^6 K/s;
- Melt atomization by high-pressure water (WA-N process, see this report, Task 3), a cooling rate of 10^4-10^6 K/s depending on powder particle size;
- Plasma atomization (centrifugal atomization of the rotating electrode in the form of preliminary cast alloy ingot of 50 mm in diameter by plasma arc, the plasma forming gas being a mixture of He and Ar in proportion of 9:1). Using a water-cooled copper screen-crystallizer permitted to achieve cooling rates to 10^6 K/s.

Works in all of these directions were started simultaneously: works with melt spun ribbons – in frames of Task 6, and works with water-atomized and plasma-atomized powders – in frames of Task 3. Later all works for studying elevated temperature aluminum alloys were concentrated in Task 6, and here they are discussed together.

6.2.2. Works with melt spinning

These works were carried out to study structure and properties of ribbons produced under conditions developed in the IPMS for aluminum alloys in order to determine optimum chemical compositions of alloys and some regularities in the influence of structure on mechanical properties. On the base of works [1, 7-14]

6 compositions of ribbons and powder alloys with the best elevated temperature characteristics were chosen (Table 6.3). In addition the influence on ribbon structure and properties of additional alloying of these alloys with 0.2 at. % Sc was studied, the corresponding alloys being designated as 1a-6a. Such alloying appeared to be very useful in various Al alloys [2] and was not investigated earlier for RS alloys with quasicrystalline component.

Table 6.3.

Literary data about mechanical properties of alloys chosen for the investigation of ribbons

Alloy #	Chemical composition, at. %	Mechanical properties				State	Powder size fraction, μm	Refe-rence
		T_{test}, °C	σ_f*, MPa	HV, MPa	Ductility			
1	$Al_{92}Mn_6Ce_2$	20	1320		Ductile in bending	Ribbon	-	[1]
2	$Al_{94.5}Cr_3Ce_1Co_{1.5}$	20	1340		Ductile in bending	Ribbon	-	[1]
3	$Al_{94}Cr_3Y_1Co_1Ti_1$	20 300	990 345	2950	El = 16 %	PM rod		[11]
4	$Al_{95}Mo_2Ce_{0.5}Co_{1.5}Zr_1$	20 300	970 310	3100	El = 17 %	PM rod		[11]
5	$Al_{93}Cr_5Co_2$	20	1240		Ductile in bending	Ribbon	-	[11]
6	$Al_{93}Fe_3Cr_2Ti_2$	20 20 200 300 300	660 540 460 360 330		El = 4.5 % El = 5.6 % El = 1.5 %	PM rod PM rod PM rod PM rod PM rod	(0-26) (0-125) (0-26) (0-26) (0-125)	[1, 7, 18]

*) σ_f is fracture stress

We succeeded to obtain the ribbon structure of one of the strongest alloy #1 in the form of uniformly distributed quasicrystalline particles of 50-100 nm in size (Fig. 6.15, a, b) that is quite similar to the structure given by A. Inoue [1] only when we reproduced the manufacture conditions used by Japanese scientists (using silica nozzles with round aperture of 0.2-0.5 mm that gave ribbon thickness t ≈ 20 μm and width b ≈ 1 mm).

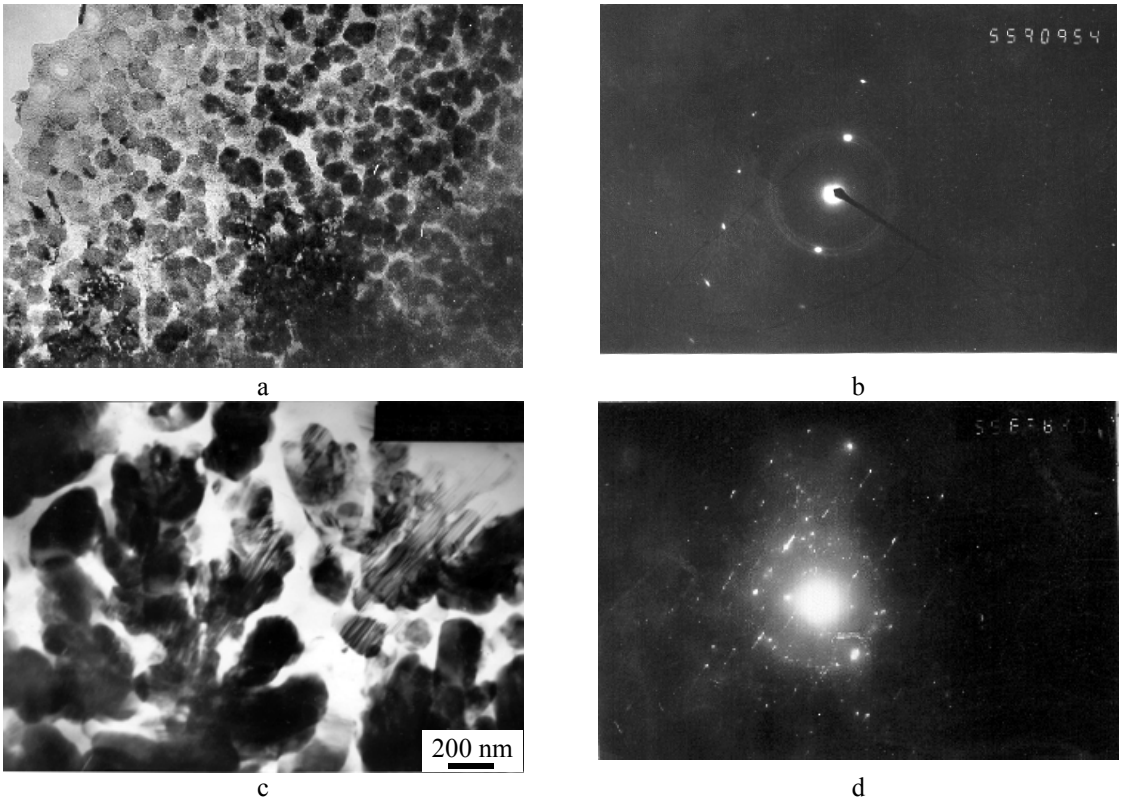

a b c d

Figure 6.15. Fine structure of Al-Mn-Ce-(Sc) ribbons, TEM investigation:
a – ribbon $Al_{92}Mn_6Ce_2$, t = 20 μm (alloy #1); b – ribbon $Al_{91.8}Mn_6Ce_2Sc_{0.2}$, t = 60 μm (alloy #1a)

Two fine rings in the electron diffraction pattern (EDP) in Fig. 6.15, b are reflections 15/23 and 18/29 of an icosahedral quasicrystal in Cahn indices N/M [3]. The appearance of strong reflections with odd values of N in accordance to the work [4] means an increase of the degree of ordering in the quasicrystal lattice, which is expressed in the fact that the reciprocal 6-dimensional lattice of the quasicrystalline phase at least in its large part becomes face-centered, and it is characteristic for alloying quasicrystals with rare-earth metals (REM) and Y.

Under conditions used in the IPMS ribbons had typical values of t = 35-70 μm and b = 10-12 mm. In such ribbons of alloy #1 and #1a the precipitates were rather non-uniform in size that achieved about 400 nm, in some particles there were seen stripes in images (Fig. 6.15, c) and striations in electron diffraction patterns (Fig. 6.15, d) characteristic for decagonal quasicrystals [19,20], and this made these ribbons very brittle. Thus, the structure and properties of Al-Mn-Ce ribbons appeared to be extremely sensitive to manufacture conditions, and further works with this composition were stopped.

The most fine and uniformly distributed reinforcing quasicrystalline particles were obtained under conditions used in the IPMS in ribbons of alloys $Al_{93}Fe_3Cr_2Ti_2$ and $Al_{92.8}Fe_3Cr_2Ti_2Sc_{0.2}$ (Figs 6.16, 6.18).

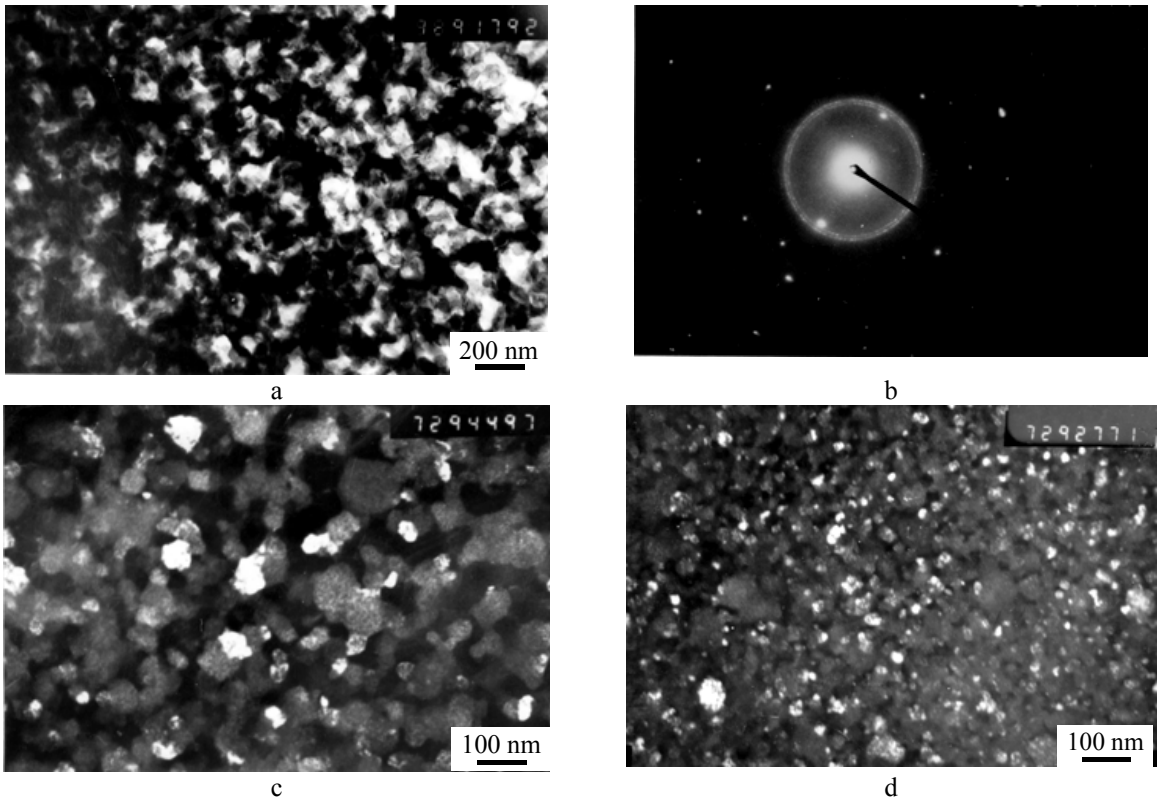

Figure 6.16. Fine structure of ribbons of alloy #6 ($Al_{93}Fe_3Cr_2Ti_2$) with t = 40 μm, TEM investigation:
a – bright field image; b – EDP of the area (a); c, d – dark field images with using a part of rings 18/24 and 20/32 from the quasicrystalline phase in the EDP (b) in various areas of the TEM sample

The size of quasicrystalline particles in ribbons of alloy #6 was not quite uniform and could fluctuate in different areas of thin foils in the limits of 10-100 nm (Fig. 6.16, c-d). It is interesting to note that α-Al grains in ribbons were more than of 1-2 μm in size because α-Al reflections in EDP are of a point character as in single crystals (Figs 6.15, b, 6.16, b). The EDP of the ribbon shown in Fig. 6.16 contains ring reflections of a normal icosahedral lattice with even values of N, the rings 18/29, 20/32, and 52/84 being the brightest. The same reflections were detected in the X-ray diffraction pattern together with strong reflections of α-Al (Fig. 6.17, a).

Alloying with scandium (alloy #6a) did not change the size of the overwhelming majority of particles in the ribbon (Fig. 6.18, a, c). Just for this ribbon we first obtained the EDP of an individual particle at the foil edge (a bright particle in the middle of the upper part of Fig. 6.18, c) with 5-fold symmetry (Fig. 6.18, d). Quite seldom rather coarse particles happen, in which a specific contrast characteristic for TEM images of quasicrystalline particles is well seen (Fig. 6.18, e). EDX analysis of the foil edge has shown that Sc enters both into quasicrystalline particles and α-Al in practically the same proportion. The presence of such a small amount of Sc as about 0.2 at. % caused appreciable changes in ribbon diffraction patterns that are expressed in the appearance of the reflection 14/21 of the quasicrystalline lattice in the EDP (Fig. 6.18, b) and in the XRDP (Fig. 6.17, b) as well. The reflections from the quasicrystalline phase with odd N were not detected, though the appearance of an additional reflection of the main lattice may mean some increase in lattice ordering under the influence of Sc like the case of alloying with Ce [4]. It

effected ribbon hardness rather weakly, but lowered its ductility. Thus, the unalloyed ribbon of alloy #6 of about 40 μm in thickness failed in bending at a plastic strain in outer layer $\varepsilon_p \approx 3$ %, and ribbon of alloy #6a of the same thickness failed at $\varepsilon_p \approx 1.3$ %.

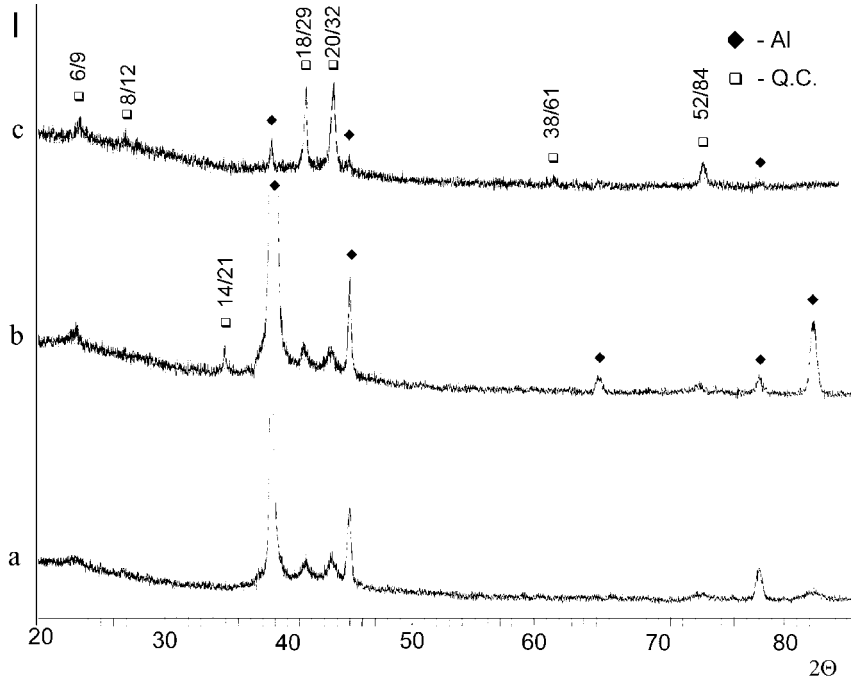

Figure 6.17. Fragments of X-ray diffraction patterns of melt-spun ribbons $Al_{93}Fe_3Cr_2Ti_2$ (a), $Al_{92.8}Fe_3Cr_2Ti_2Sc_{0.2}$ (b), $Al_{84.2}Fe_7Cr_{6.3}Ti_{2.5}$ (c)

After the results of EDX analysis of the quasicrystalline phase in the ribbon $Al_{93}Fe_3Cr_2Ti_2$ carried out in works [7, 18] we have manufactured a ribbon of a model alloy #7 ($Al_{84.2}Fe_7Cr_{6.3}Ti_{2.5}$) that consisted almost completely of the icosahedral phase (Fig. 6.17, c) in the form of large (of several micrometers) particles (Fig. 6.19).

Analysis of X-ray line broadening of the quasicrystalline (QC) phase in the model alloy #7 and in the alloy #6 with nanosize quasicrystalline particles embedded in the α-Al matrix has shown that the nanosize phase has much higher phonon and phason components of lattice distortions, the difference being especially large for phonon component. The analysis has also shown that the average value of non-uniform distortions in α-Al matrix $\Delta a/a = 3.4 \cdot 10^{-3}$, which is on the level of this quantity for cold rolled metals [21]. Evidently, this fact makes a contribution to a low ductility of ribbons under investigation.

Experiments in annealing Al-Fe-Cr-Ti ribbons for 1 h at temperatures to 550 °C have shown that very small changes in ribbon X-ray diffraction patterns indicative of the appearance of crystalline intermetallics occurred after annealing at 400 °C, and after annealing at 450 °C these changes were quite apparent. The drop of hardness in ribbons from alloys reinforced with fine quasicrystalline particles was appreciably more rapid than in the model quasicrystalline ribbon #7 (Fig. 6.20). It can be explained by the fact that in ribbons with QC precipitates a phase transformation at high temperatures is accompanied by particles coagulation.

These results point out that in order to keep the quasicrystalline phase in these RS alloys the operations of their thermomechanical treatment shall be carried out at temperatures not higher than 400 °C.

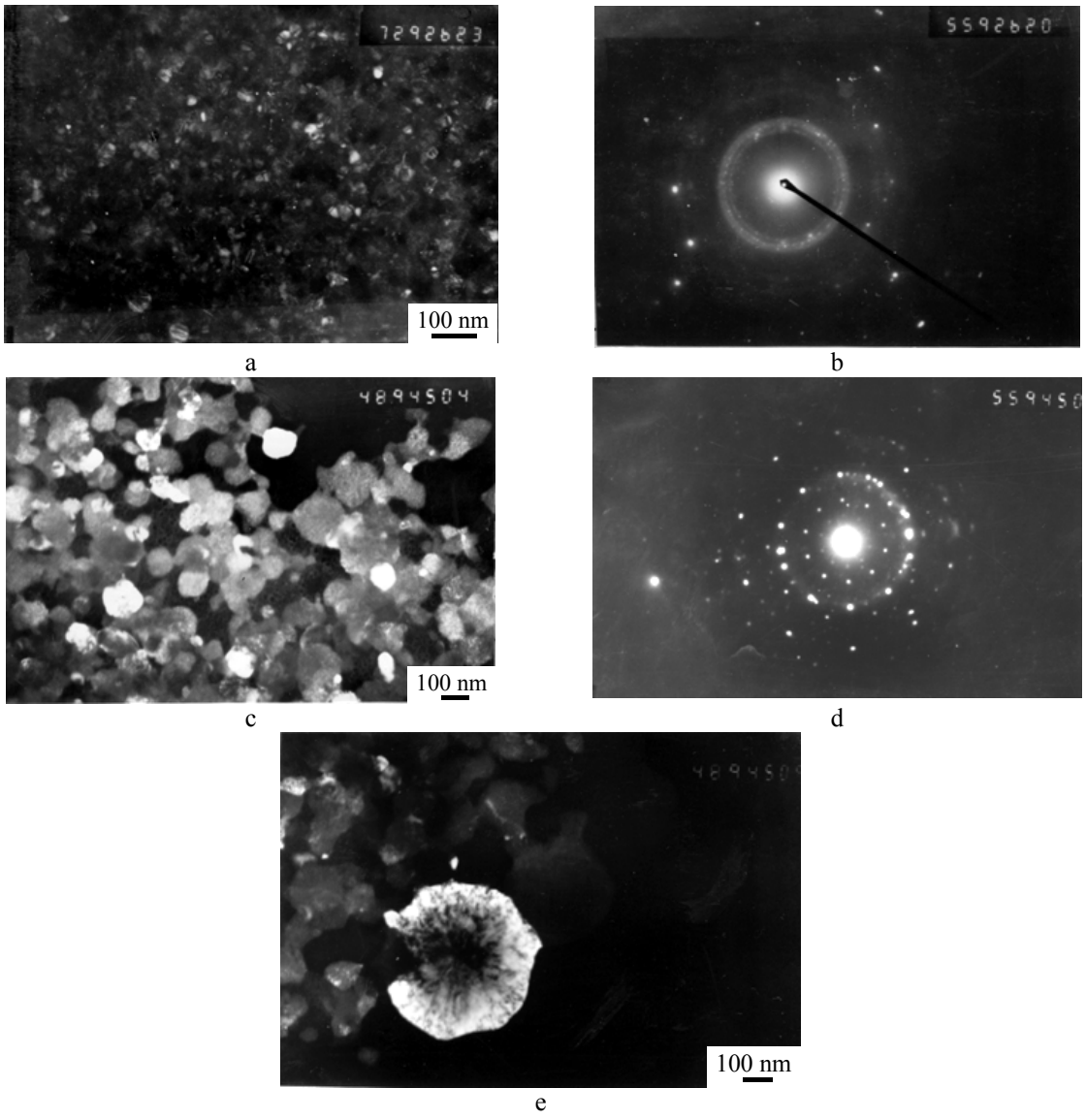

Figure 6.18. Fine structure of ribbons of alloy #6a ($Al_{93}Fe_3Cr_2Ti_2Sc_{0.2}$) with t = 40 μm, TEM investigation:
a, c, e – dark field images with using a part of rings in the EDP in various areas of the TEM sample;
b – EDP of the area (a); d – EDP of a bright particle in the middle of the upper part in the area (c)

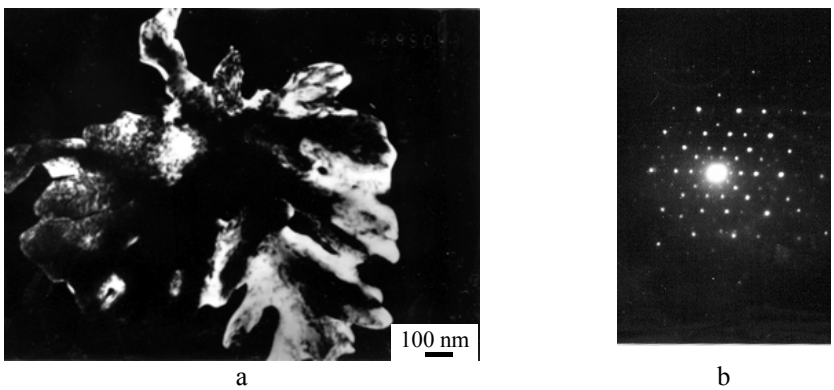

Figure 6.19. A quasicrystalline particle in the ribbon of alloy #7 ($Al_{84.2}Fe_7Cr_{6.3}Ti_{2.5}$), TEM dark field image (a) with using a (4/6 0/0 0/0) reflection in the EDP (b)

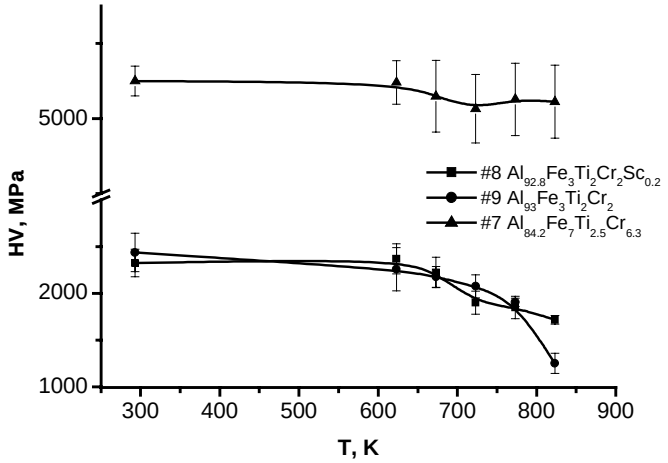

Figure 6.20. Changing of microhardness of AlFeCrTi(Sc) ribbons after annealing for 1h at various temperatures

Among ribbons of other selected alloys (Table 6.3) only the ribbons of alloy #5 ($Al_{93}Cr_5Co_2$) and alloy #5a ($Al_{92.8}Cr_5Co_2Sc_{0.2}$) that contain neither REM elements nor Y had a phase composition of α-Al + QC phase, but average sizes of QC particles in them were more than twice larger than in ribbons of alloy #6 ($Al_{93}Fe_3Cr_2Ti_2$), and ribbon hardness was appreciably lower. In all ribbons of alloys containing Ce or Y QC particles existed together with crystalline intermetallics that was registered by X-ray as well by TEM investigation. This fact cardinally changes the type of contrast in TEM images of particles (Fig. 6.21, a) as well as the appearance of the EDP (Fig. 6.21, b). Alloying with Sc always aggravated this tendency.

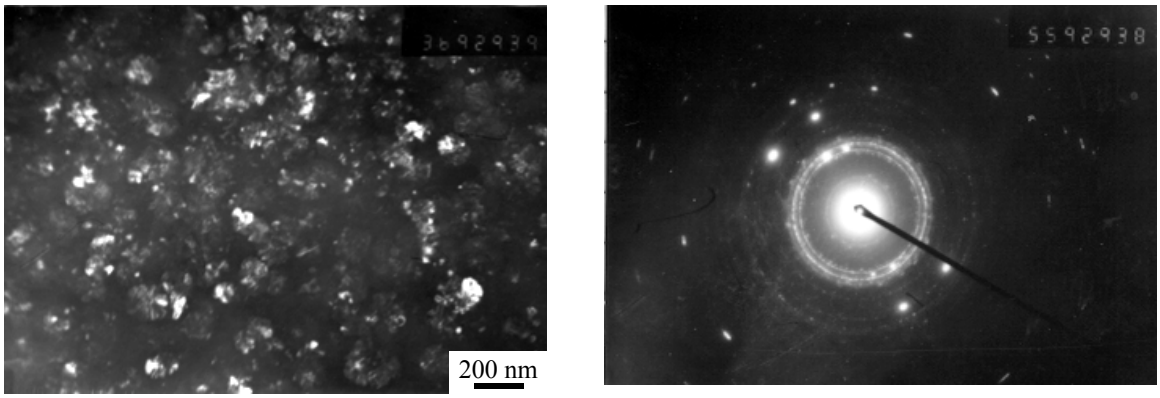

a b

Figure 6.21. Microstructure of ribbon of alloy #3 ($Al_{94}Cr_3Y_1Co_1Ti_1$), TEM investigation: a – dark-field image with using a part of intense ring in the EDP (b)

Inoue and Kimura have shown [22] that for a large amount of Al-V-, Al-Fe-, Al-Ti-, Al-Cr-based alloys with QC particles of a size larger than 40 nm a linear growth of the yield stress $\sigma_{0.2}$ with $d_s^{-1/2}$ of Hall-Petch type takes place, d_s being the space between QC particles (which evidently determines the length of the sliding path). At constant volume part of the QC phase the value of d_s drops with decreasing particle size. As a first approximation, assume that the volume part f of reinforcing particles in all our ribbons is equal. An exact definition of the value of f is under our conditions quite impossible because (i) we cannot define the exact value of foil thickness in TEM investigation; (ii) particle TEM images screen each other because their size is about 10 times smaller than the foil thickness; (iii) we have no correct standards for X-ray phase analysis. The estimation of the maximum possible content of the QC phase in the ribbon of alloy #6 ($Al_{93}Fe_3Cr_2Ti_2$) from the compositions of the QC phase ($Al_{84.6}Fe_7Cr_6Ti_{2.4}$) and of α-Al ($Al_{97.5}Fe_{1.1}Cr_{0.9}Ti_{0.5}$) determined by EDX analysis [18] gave the value f = 0.35. A simple consideration shows that at a constant value of f the quantity d_s is proportional to the average particle size d, so a linear dependence of the type $\sigma_{0.2} = \sigma_0 + K'd^{-1/2}$ shall take place. If to consider hardness HV to be proportional to the yield stress, we can try to check this dependence for our ribbons (Fig. 6.22).

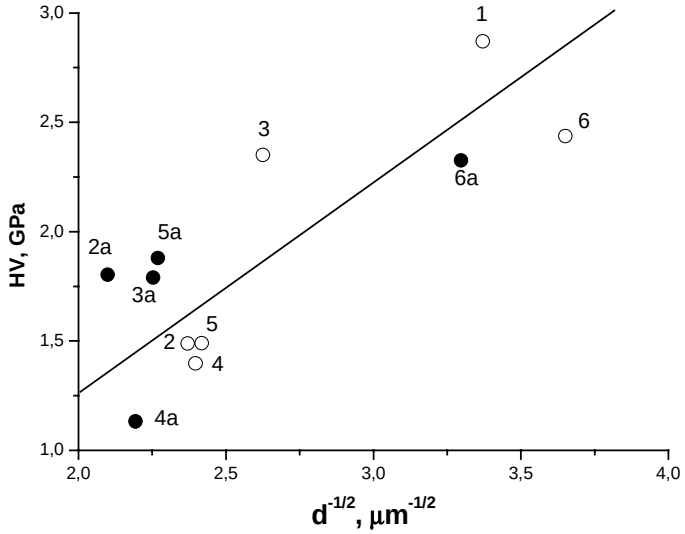

Figure 6.22. Correlation between ribbon hardness and reciprocal square root of the size of reinforcing particles

It is seen that a correlation of the supposed type really exists. The scatter of the experimental points may be caused first of all by an incorrectness of the assumption about the equality of f in all alloys under investigation. Thus, it is obvious that f shall be larger in alloys with a lower content of Al. Evidently, for this reason the point for alloy #1 lies above the correlation line, and the points for alloys #4 and #4a lie below it (see Table 6.3). This reason cannot explain a high hardness in the ribbon from alloy #3 that contains 94 at. % Al. This alloy appeared to be the most sensitive to details of the manufacture process and most non-uniform along the ribbon thickness, and there were ribbons of this alloy with a hardness of 1.97 GPa. At equal Al content f shall depend on the density of the precipitates that is determined by their structure and chemical composition. One more reason for the scatter is insufficient statistics in evaluation of the average particle size. A comparison of points with "a" and without it in Fig. 6.22 shows that the influence of Sc is as a rule expressed in increasing the particle size, but its effect on ribbon hardness is rather different in alloys of various chemical composition.

So, the results of ribbon investigation have led us to a conclusion that the best RS alloys under our conditions are Al-Fe-Cr-(Ti) alloys, and this system was selected for producing powder alloys with using water-atomized powders.

6.2.3. Works with PM alloys from water-atomized powders

Works with elevated temperature powder alloys based on Al-Fe-Cr system were started in frames of Task 3. The technique of water atomization of the melt for producing powders is known in the world to give good results for high-alloyed steels, and it is considered non-desirable for aluminum alloys because of their strong tendency to oxidation. The process of water atomization for producing Al alloy powders (WA-N process) with precautions to obtain a minimum oxidation was developed by a group of scientists in the IPMS headed by Dr O.D. Neikov. In frames of this project the process was adjusted to alloys of chemical composition under investigation with improvements that are described in details in this report for Task 3. In the same report there are also given the details of producing consolidated semi-finished products in the form of extruded rods. Here we shall discuss the results of the application of this technique for manufacture of elevated temperature Al-Fe-Cr alloys reinforced with quasicrystalline precipitates. Altogether we have manufactured and investigated alloys of 18 chemical compositions (Table 6.4).

The first three compositions (alloys #20, #21, #29) were selected basing on the results of investigations in VILS [17]. Compositions of alloys #30 and #31 correspond to the compositions of ribbons that were the best under our manufacture conditions, the composition of alloy #30 being proposed in the work [1]. The rest of compositions are our variations according to the results of studying structure and mechanical properties of rod semi-finished products. In particular, the composition #32 was the result of improving alloy #20 by lowering the content of (Fe+Cr) and addition of Ti and Mo. Rod tensile testing was carried out in air at temperatures of 20, 190 and 300 °C after holding the sample at testing temperature for 15 min. The results of testing are presented in Tables 6.5 – 6.7. Values of mechanical properties represent averages of 2 or 3 sample tests.

Table 6.4.

Chemical composition of Al powder alloys manufactured by water atomization technique

Alloy #	Content of element	
	wt. %	at. %
20	Al–10Fe–1.3Cr–1.3Zr–1.3Mo	$Al_{93.2}Fe_{5.25}Cr_{0.75}Zr_{0.4}Mo_{0.4}$
21	Al–1.5Fe–8Cr	$Al_{94.9}Fe_{0.75}Cr_{4.35}$
29	Al–9.5Fe–3.5Cr–3.3Ti	$Al_{91}Fe_5Cr_2Ti_2$
30	Al–5.8Fe–3.6Cr–3.3Ti	$Al_{93}Fe_3Cr_2Ti_2$
31	Al–5.8Fe–3.6Cr–3.3Ti–0.25Sc	$Al_{92.8}Fe_3Cr_2Ti_2Sc_{0.2}$
32	Al–5Fe–5Cr–2Ti–1.3Zr–2.5Mo	$Al_{92}Fe_{2.7}Cr_{2.85}Ti_{1.25}Zr_{0.4}Mo_{0.8}$
40	Al–5Fe–5Cr	$Al_{94.7}Fe_{2.6}Cr_{2.7}$
77	Al–5Fe–5Cr–2Ti	$Al_{93.4}Fe_{2.6}Cr_{2.8}Ti_{1.2}$
78	Al–5Fe–5Cr–1Ti–1Zr	$Al_{93.7}Fe_{2.6}Cr_{2.8}Ti_{0.6}Zr_{0.3}$
39	Al–5Fe–5Cr–2Ti–1.3Zr	$Al_{93}Fe_{2.6}Cr_{2.8}Ti_{1.2}Zr_{0.4}$
82	Al–4Cr–4Fe	$Al_{95.8}Fe_2Cr_{2.2}$
83	Al–4Fe–4Cr–2Ti	$Al_{94.7}Fe_2Cr_{2.1}Ti_{1.2}$
135	Al–5.86Fe–5.45Cr	$Al_{94}Fe_3Cr_3$
136	Al–4.88Fe–6.37Cr	$Al_{94}Fe_{2.5}Cr_{3.5}$
137	Al–6.88Fe–4.65Cr	$Al_{94}Fe_{3.5}Cr_{2.5}$
138	Al–4.89Fe–4.55Cr–1.68Ti	$Al_{94}Fe_{2.5}Cr_{2.5}Ti_1$
139	Al–4.82Fe–4.49Cr–3.15Zr	$Al_{94}Fe_{2.5}Cr_{2.5}Zr_1$
140	Al–4.86Fe–4.52Cr–0.83Ti–1.59Zr	$Al_{94}Fe_{2.5}Cr_{2.5}Ti_{0.5}Zr_{0.5}$

For manufacture of rods powder size fractions of (0-63) μm (fraction 1) and (63-100) μm (fraction 2) were used as a rule. The conditions of producing powders and rods were continuously improved during project work (see this report for Task 3). At the beginning of the work powder billets of 25 mm in diameter cold pressed to about 30 % porosity were subjected to hot vacuum degassing treatment and further to vacuum forging at 400-450 °C (hot dynamic vacuum consolidation: HDVC process developed in the IPMS). Forged billets were extruded to rods of 6 and 9 mm in diameter (extrusion ratio λ of 17 and 7.7, respectively). Later separate compacts were extruded after vacuum degassing in hermetic capsules without forging (CD technique), and it was shown that the tensile properties of rods extruded by both techniques were very close. Beginning from the alloy #82 we executed the extrusion by the CD technique.

As for other alloys based on the Al-Fe system [6], we had difficulties in extrusion processes for high elevated temperature strength of our alloys, and the extrusion of alloys that contain about 93 at. % Al with λ=17 was possible only when using the forging temperature of 450 °C and the extrusion temperatures of 500-540 °C, and for alloys #29 and #32 that contain 91 and 92 at. % Al, respectively, we should to elevate the extrusion temperature to 560 °C (Table 6.5). In order to lower the temperature of plastic working to 400 °C we should decrease λ to 7.7, and even after this the extrusion was possible when heating the die to 500 °C (Table 6.5). Using a graphite lubricant GRA-51 permitted to produce rods of 7 mm in diameter (λ = 12.8) with lowering the extrusion temperature (both of the billet and the die) to 350 °C for alloys #82 and #83 (Table 6.6) and to 400 °C for alloys #135-140 (Table 6.7).

For comparison we manufactured powder of the alloy #21 by argon atomization technique (alloy #21a in Table 6.5), which allowed to carry out billet extrusion with λ=17 at 400 °C. We tested also the structure and properties of this alloy produced in the form of a melt-spun ribbon of about 50 μm in thickness. The consolidation of this ribbon into a rod of 6 mm in diameter (λ=17) at 400 °C was possible with heating the die to 520 °C (alloy #21r in Table 6.5). The consolidation of the ribbon of alloy #30 (rod #30r) that had a higher strength and a lower ductility required a preliminary crushing of the ribbon in a ball mill.

Evidently, rod mechanical properties are to be discussed in connection with their structure. In WA powders of alloys #20 and #21 the reinforcing particles had only a form of crystalline intermetallics that was shown by X-ray diffraction analysis. SEM investigation of cold-pressed billets from these powders with X-ray spectral microanalysis permitted to reveal some characteristic features. The first of them that appeared to be a common feature for all WA powders is a rather strong non-uniformity in the size of reinforcing precipitates in various powder particles with its much better uniformity inside of powder particles (Fig. 6.23). It is to be a consequence of various cooling rates while solidification of particles of different size, still a rather large difference of precipitate size in particles of close dimensions takes place. It means that particles with coarser precipitates were cooled in the periphery of the high-pressure water stream like particles of powder with an amorphous constituent (see Section 6.2.1.2 in T06).

Table 6.5.

Mechanical properties of PM rods of Al-Fe-Cr alloys depending on manufacture conditions and testing temperature

Alloy #	Fraction	$T_{forging}$, °C	$T_{extrusion}$, °C	λ	T_{test} = 20 °C			T_{test} = 190 °C			T_{test} = 300 °C		
					YS, MPa	UTS, MPa	δ, %	YS, MPa	UTS MPa	δ, %	YS, MPa	UTS MPa	δ, %
20	1	450	500	17	477	521	0.9	370	417	1.5	260	287	1.1
	2	450	500	17	449	492	0.4	381	391	0.3	280	313	1.8
21	1	450	500	17	402	483	4.5	332	364	4.3	236	261	4.7
	2	450	500	17	380	463	4.3	306	344	3.0	229	253	3.6
	3	450	500	17	384	456	4.3	318	348	4.3	213	243	4.1
	4	450	500	17	365	435	3.1	308	341	3.2	200	233	5.5
21a[1)]	1	400	400	17	415	475	9.6	304	331	10.1	187	226	12.6
	2	400	400	17	336	419	7.6	273	304	11.1	178	205	14.0
21r[2)]	-	400	400b+ 520d	7.7	367	424	5.3	264	296	9.1	172	220	1.9
29	1	450	560	17	471	513	0.8	379	437	0.4	278	312	2.2
30	1	450	540	17	472	534	3.3	366	419	4.1	212	231	0.9
	2	450	540	17	438	499	4.5	3414	382	5.1	247	272	5.3
	1	450	400b+ 520d	7.7	538	574	1.0	11	450	1.7	255	294	2.5
30r[2)]	-	400	400b+ 520d	7.7	-	449	0	486	512	0.46	321	360	1.67
31	1	450	540	17	492	546	2.0	405	439	2.0			
	2	450	540	17	445	499	1.8	369	411	5.1	258	290	4.2
	1	450	400b+ 520d	7.7	520	567	0.7	400	434	0.6	271	315	2.9
32	1	450	560	17	-	494	0	-	421	0.2	312	329	0.5
40	1	450	500	17	340	392	14.3	293	325	7.3	209	234	8.7
	1	400	400b+ 500d	7.7	398	459	10.6	328	359	7.4	221	247	3.1
77	1	400	400b+ 500d	7.7	469	561	5.1	366	426	1.5	269	313	2.7
	2	-	400b+ 500d	7.7	476	531	1.5	369	416	1.7	271	295	3.7
78	1	400	400b+ 500d	7.7	-	536	0.07	438	458	0.3	313	343	1.5
	2	400	400b+ 500d	7.7	-	539	0.17	413	445	0.7	297	328	1.5
	2	-	420	7.7	618	649	0.6	419	448	0.2	274	303	1.9
39	2	450	520	17	519	531	0.4	409	444	1.2	236	265	0.7
	1	400	400b+ 500d	7.7	-	627	0.1	427	450	0.3			

[1)] PM rod from argon-atomized powder;
[2)] rod from melt-spun ribbon extruded after cold pressing;
400b + 500d means that while extrusion the billet and the die were heated to 400 °C and 500 °C, respectively

This non-uniformity is preserved in extruded rods. E.g., in the rod of alloy #21 of the finest powder fraction used of (0-63) μm extruded at 500 °C TEM investigation has revealed precipitates from 50 nm to 500 nm in size (Fig. 6.24, a), and often rather large congestions of them of 1-2 μm in size occurred (Fig. 6.24, b). However, a tendency to increasing the average precipitate size in rods from coarser powder fractions alloy #21 for 4 size fractions is quite obvious that explains lowering their strength characteristics with coarsening the powder size fraction shown with the example of alloy #21 in Table 6.5. TEM investigation revealed also in these rods a very small size of α-Al grains of about 0.5-1.5 μm that appeared to be a common feature of all Al-Fe-Cr PM rods under investigation, and it shall make an appreciable contribution to rod strength. This grain size did not change after a high-temperature annealing for about 100 h (Fig. 6.24, c).

Table 6.6.

Effect of extrusion temperature on the tensile properties of rods from alloys #82 ($Al_{95.8}Fe_2Cr_{2.2}$) and #83 ($Al_{94.7}Fe_2Cr_{2.1}Ti_{1.2}$)

Alloy #	Chemical composition, at. %	λ	Size fraction, μm	20 °C			190 °C			300 °C		
				YS, MPa	UTS, MPa	EL, %	YS, MPa	UTS, MPa	EL, %	YS, MPa	UTS, MPa	EL, %
Extrusion at 350 °C												
82	$Al_{95.8}Fe_2Cr_{2.2}$	12.8	(0-63)	426	469	10.4	339	380	5.8	228	272	4.5
82	$Al_{95.8}Fe_2Cr_{2.2}$		(63-100)	409	449	10.5						
83	$Al_{94.7}Fe_2Cr_{2.1}Ti_{1.2}$		(0-63)	509	555	7.9	409	446	4.5	308	326	3.3
83	$Al_{94.7}Fe_2Cr_{2.1}Ti_{1.2}$		(63-100)	498	535	8.7	381	415	5.3	272	296	2.2
Extrusion at 400 °C												
82	$Al_{95.8}Fe_2Cr_{2.2}$	7.7	(0-63)	342	393	12.4	274	290	7.7	189	206	8.0
82	$Al_{95.8}Fe_2Cr_{2.2}$		(63-100)	335	386	12.7	263	290	5.3	192	209	7.1
83	$Al_{94.7}Fe_2Cr_{2.1}Ti_{1.2}$		(0-63)	444	496	10.9	342	382	8.1	235	271	4.3
83	$Al_{94.7}Fe_2Cr_{2.1}Ti_{1.2}$		(63-100)	443	490	9.3	337	369	5.5	256	272	6.7

Table 6.7.

Tensile properties of rods of elevated temperature $Al_{94}Fe_xCr_yTi_zZr_{6-x-y-z}$ alloys (λ = 12.8, T_{extr} = 400 °C)

Alloy #	Chemical composition, at. %	20 °C			190 °C			300 °C		
		YS, MPa	UTS, MPa	EL, %	YS, MPa	UTS, MPa	EL, %	YS, MPa	UTS, MPa	EL, %
Size fraction (0-63) μm										
135	$Al_{94}Fe_3Cr_3$	446	496	9.8	366	397	4.7	250	280	4.7
136	$Al_{94}Fe_{2.5}Cr_{3.5}$	426	484	8.7	354	385	5.6	244	271	5.4
137	$Al_{94}Fe_{3.5}Cr_{2.5}$	421	473	12.0	347	382	5.7	245	270	5.8
138	$Al_{94}Fe_{2.5}Cr_{2.5}Ti_1$	470	534	8.0	398	430	7.0	286	312	5.4
139	$Al_{94}Fe_{2.5}Cr_{2.5}Zr_1$	584	615	5.1	427	456	4.8	265	302	3.2
140	$Al_{94}Fe_{2.5}Cr_{2.5}Ti_{0.5}Zr_{0.5}$	588	620	5.4	436	465	3.9	307	332	3.0
Size fraction (63-100) μm										
135	$Al_{94}Fe_3Cr_3$	411	466	6.6	337	369	4.8	230	258	3.7
136	$Al_{94}Fe_{2.5}Cr_{3.5}$	413	466	6.5	334	368	4.7	230	255	3.9
137	$Al_{94}Fe_{3.5}Cr_{2.5}$	365	423	9.0	308	341	6.2	218	242	6.6
138	$Al_{94}Fe_{2.5}Cr_{2.5}Ti_1$	453	504	8.0	367	402	7.0	267	293	6.3
140	$Al_{94}Fe_{2.5}Cr_{2.5}Ti_{0.5}Zr_{0.5}$	562	580	6.1	412	434	3.4	253	273	4.3

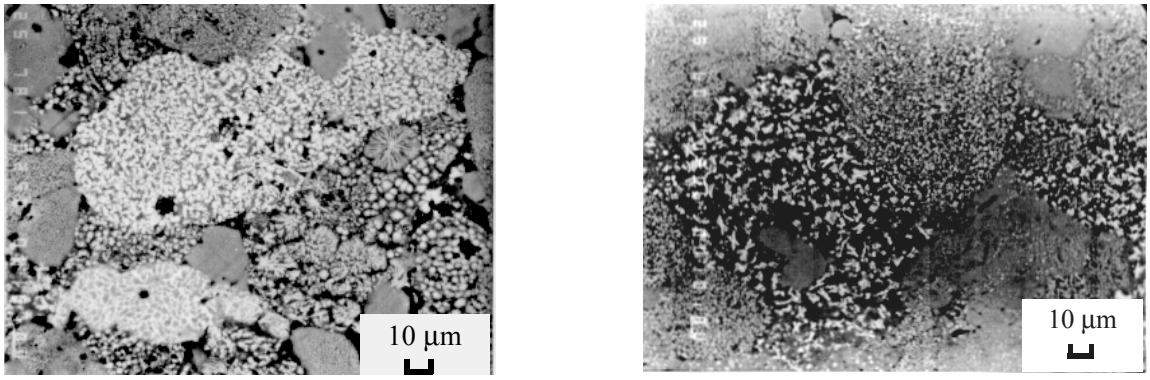

a b

Figure 6.23. SEM images (BEI mode) of cross sections of WA powders, size fraction of (63-100) μm: a – alloy #21 ($Al_{94.9}Fe_{0.75}Cr_{4.35}$), b – alloy #30 ($Al_{93}Fe_3Cr_2Ti_2$)

The structure of the rod #21a from gas-atomized (GA) powder was similar to the structure of the rod #21 (Fig. 6.24, d), but the lowest precipitate size was some higher (about 140 mm), and the structure non-uniformity was stronger. The analysis of the total oxygen content carried out by burning technique has shown the content of oxygen in the WA powder (alloy #21) to be of about 0.1 wt. %, whereas in the GA powder (alloy #21a) it was of about 0.05 wt. % that depicts the existence of more oxides on the rod #21. Maybe, for these two reasons the strength of the rod #21a was lower than the strength of the rod #21 in spite of a lower extrusion temperature (Table 6.5), and its ductility was appreciably higher (Table 6.5). A large difference in strengthening PM rods from WA-N and GA powders in tensile test is clearly seen from the stress-strain curves in coordinates true stress σ_t – true plastic deformation e_p (Fig. 6.25): strengthening of the rod from GA powder is noticeably weaker.

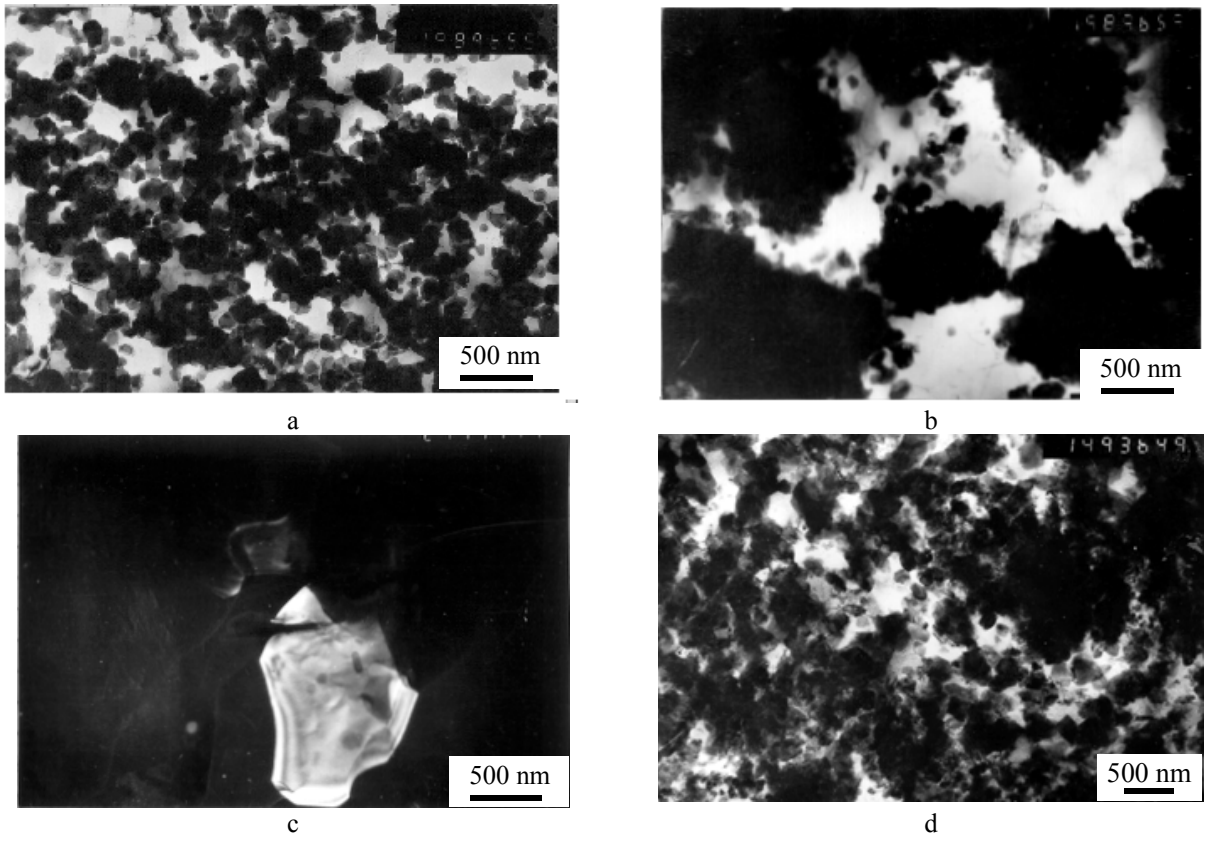

Figure 6.24. Structure of extruded rods from water-atomized (a-c) and argon-atomized (d) powders with crystalline intermetallics, TEM investigation: a, b – alloy #21 ($Al_{94.9}Fe_{0.75}Cr_{4.35}$), as-extruded;
c – alloy #20 ($Al_{93.2}Fe_{5.25}Cr_{0.75}Zr_{0.4}Mo_{0.4}$), annealed at 500 °C for 99 h; d – alloy #21a ($Al_{94.9}Fe_{0.75}Cr_{4.35}$), as-extruded

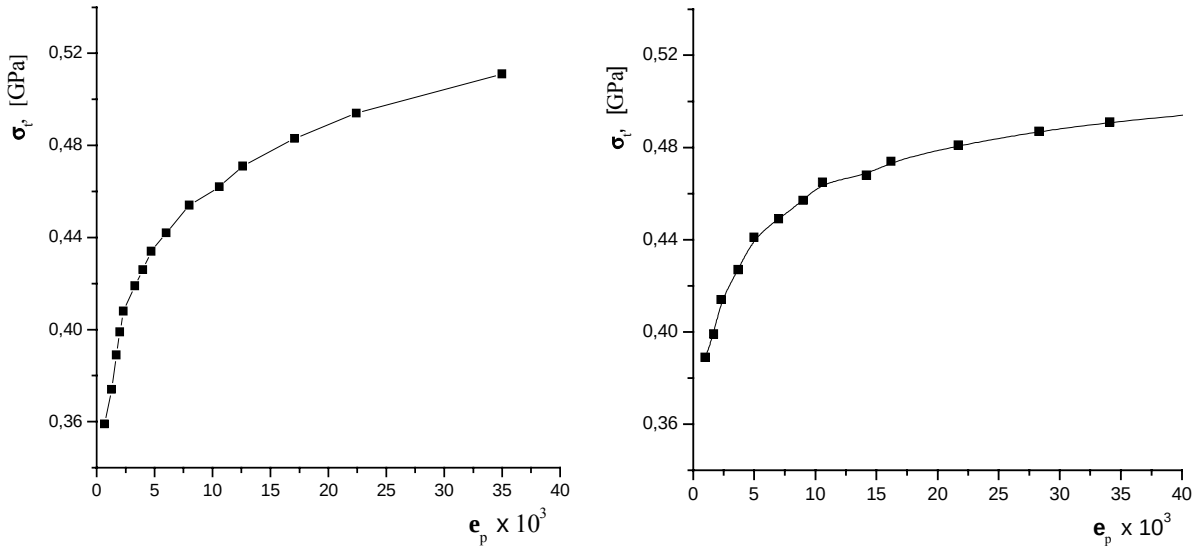

Figure 6.25. True stress – true plastic strain curves of tensile test of PM rods of alloy $Al_{94.9}Fe_{0.75}Cr_{4.35}$: a – rod from WA powder (alloy #21); b – rod from GA powder (alloy #21a)

Quasicrystalline particles in alloy $Al_{94.9}Fe_{0.75}Cr_{4.35}$ were obtained only by melt spinning (alloy #21r), but their size was rather large (of 300-500 nm), the quasicrystalline structure was not preserved after extrusion, and the mechanical properties of samples from the consolidated ribbon were not better than of PM samples (Table 6.5).

In WA powders of all other compositions quasicrystalline precipitates were formed alone or in combination with crystalline intermetallics, e.g. $Al_{23}Ti_9$ in the case of alloys #29-32 (Fig. 6.26).

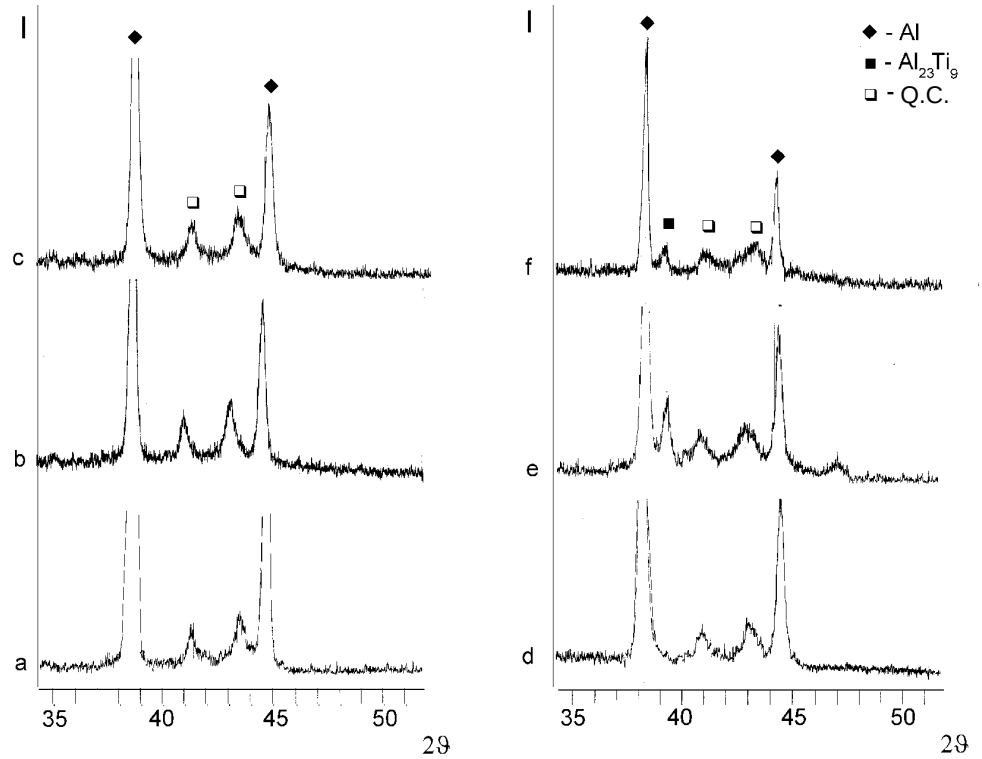

Figure 6.26. Fragments of XRD patterns of WA powders of (0-63) μm size fraction: a – alloy #40 ($Al_{94.7}Fe_{2.6}Cr_{2.7}$); b – alloy #78 ($Al_{93.7}Fe_{2.6}Cr_{2.8}Ti_{0.6}Zr_{0.3}$); c – alloy #77 ($Al_{93.4}Fe_{2.6}Cr_{2.8}Ti_{1.2}$); d – alloy #39 ($Al_{93}Fe_{2.6}Cr_{2.8}Ti_{1.2}Zr_{0.4}$); e – alloy #32 ($Al_{92}Fe_{2.7}Cr_{2.85}Ti_{1.25}Zr_{0.4}Mo_{0.8}$); f – alloy #29 ($Al_{91}Fe_5Cr_2Ti_2$)

Studying powders containing crystalline intermetallics permitted to establish an interesting feature of the formation of intermetallics composition: SEM with X-ray microanalysis has shown that in RS powders crystalline

intermetallics of Al-Cr-Fe or Al-Cr-Ti-Zr-Mo compositions were formed, Fe was never found in combination with Ti, Zr, or Mo. At the same time quasicrystalline precipitates contained Fe, Cr, Ti, and Zr.

In extruded rods the amount of crystalline intermetallics increased, a part of the quasicrystalline phase was kept in rods of alloys #30 and #31 only after extrusion with the billet temperature as low as 400 °C. It appreciably increased rod strength characteristics, but rod ductility remained lower than 5 % (Table 6.5). Rods of all compositions extruded at temperature higher than 400 °C contained no quasicrystalline phase. Especially high elevated temperature strength (UTS = 360 MPa at 300 °C) was observed in rods #30r from consolidated ribbon that had a uniform distribution of very fine crystalline intermetallics, but their ductility at room temperature was zero.

In 1963 Gurland at al. [23] have proposed an analytical model for the formation of the plastic elongation ε while tensile fracture of plastic metals with a volume concentration of rigid particles f. The model is based on the formation of elliptical pores elongated along the tensile axis formed by cracks in inclusions and has led to a conclusion that ε is a function of only f and does not depend on particle size (Fig. 6.27).

Some variations of the model gave curves presented in Fig. 6.27 as dotted lines, but all of them lead to the conclusion that alloys with f higher than 20-25 % shall have a very low ductility, and experimental pints confirm this conclusion rather well. Evidently, the value of f in the RS alloy is immediately connected with the total amount of alloying elements that follows from the content of Al (in at. %). To the point, this consideration shows that a lower ductility of PM rods from the WA powder of alloy #21 compared to rods of the same alloy from the GA powder (Table 6.5) is connected mainly with the presence of oxides rather than with a difference in average size of precipitates.

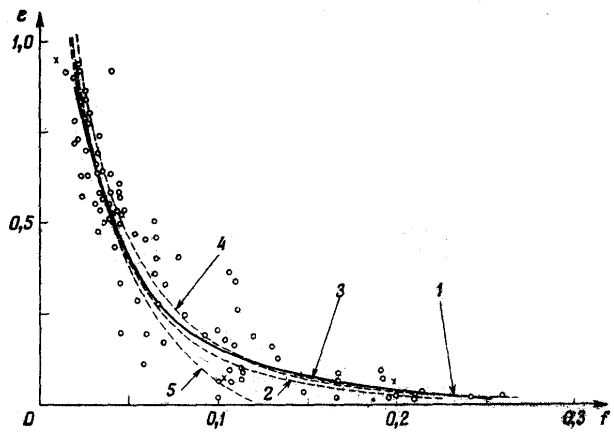

Figure 6.27. Dependence of the elongation to fracture ε on the volume part of the rigid reinforcing phase in two-phase alloys according to Gurland formula (full line) and experimental points [23]

Therefore, in the next stage in order to increase rod ductility alloys with increased Al content were studied (alloys #40, #77-78, #82-83, #135-140, see Table 6.4). Choosing the alloy composition we tried to keep the atomic concentrations of Fe and Cr nearly equal in order to equalize an opposite influence of these elements on the state diagram of Al alloys (see Section 6.3.2.1 in T06). Indeed, for alloys under investigation a distinct correlation between rod ductility and Al content, namely a growth of ductility with lowering the content of Al, takes place (Fig. 6.28).

Together with this, Fig. 6.28 shows a drop of strength characteristics with the growth of Al content, because with lowering f the average interparticle distance d_s increases (see Section 6.3.2.2 in T06). In order to equalize, to a first approximation, the precipitate size in the rods being compared, the data for Fig. 6.28 were taken for the temperature of rod extrusion of 400 °C. Fig. 6.28 is also very informative for demonstrating the effect of additional alloying of Al-Cr-Fe alloys with Ti and Zr with the preservation of the Al content (compare alloys #40 and #83, alloys #135 and #138-140). A comparison shows that such additional alloying increases the strength characteristics with maintaining the room temperature ductility not less than of 5 %. Small (by 0.5 at. %) variations of Cr and Fe concentrations did not make any improvements to rod mechanical properties, slightly decreasing the strength and elevating the ductility (compare alloys #135-137 in Fig. 6.28), and the composition with their equal concentrations was considered to be optimal.

In powders of alloys #40, 77, 78, 135-138 only quasicrystalline precipitates were formed (Figs 6.26, 6.29), in powders of alloys #139 and #140 some crystalline intermetallics were present in addition (Fig. 6.30, a, e). As noted above, a rather strong difference of the size of quasicrystalline precipitates in various powder particles was observed (Fig. 6.29, a). SEM images of coarser precipitates like Fig 6.29, b may evidently serve for the most reliable evaluation of the precipitates volume part f that in powders of alloys #135-138 appeared to be of 20-30 %, of 25 % on

average. In the work [15] for the PM alloy of the composition corresponding to our alloy #135 manufactured from a centrifugally atomized powder the volume part of the QC phase was determined as 24 %.

In PM rods of these alloys extruded at 400 °C most of the quasicrystalline phase was preserved, but as a rule a small amount of crystalline intermetallics emerged (Figs 6.31, 6.32). These intermetallics may appear both as precipitates from the supersaturated solid solution and as a consequence of a phase transformation of the quasicrystalline phase. X-ray investigation has shown that the emerging of crystalline intermetallics in extrusion process proceeds much quicker than in process of annealing at the same temperature (Fig. 6.33).

Quasicrystalline particles neither deform nor fail in extrusion process, they are only redistributed according to the deformation of former powder particles (Fig. 6.34). The strength of rods with quasicrystalline particles produced from powders of the finest size fraction of (0-63) μm was as rule higher compared to rods from the coarser fraction of (63-100) μm (Tables 6.5 - 6.7), evidently, due to a smaller average size of quasicrystalline precipitates.

The quasicrystalline phase appeared to be the most stable in the rods of alloys #135-138 (see Fig. 6.31, a-d), in the rods of alloys #139-140 the amount of accompanying crystalline intermetallics was appreciably higher than in the rods of alloys #135-138 (Fig. 6.31, e-f). The strength of the rod from the centrifugally atomized powder of the composition corresponding to alloy #135 [15] was remarkably lower than of the rod from WA powder, and it can be explained by a lower solidification rate compared to the WA-N process.

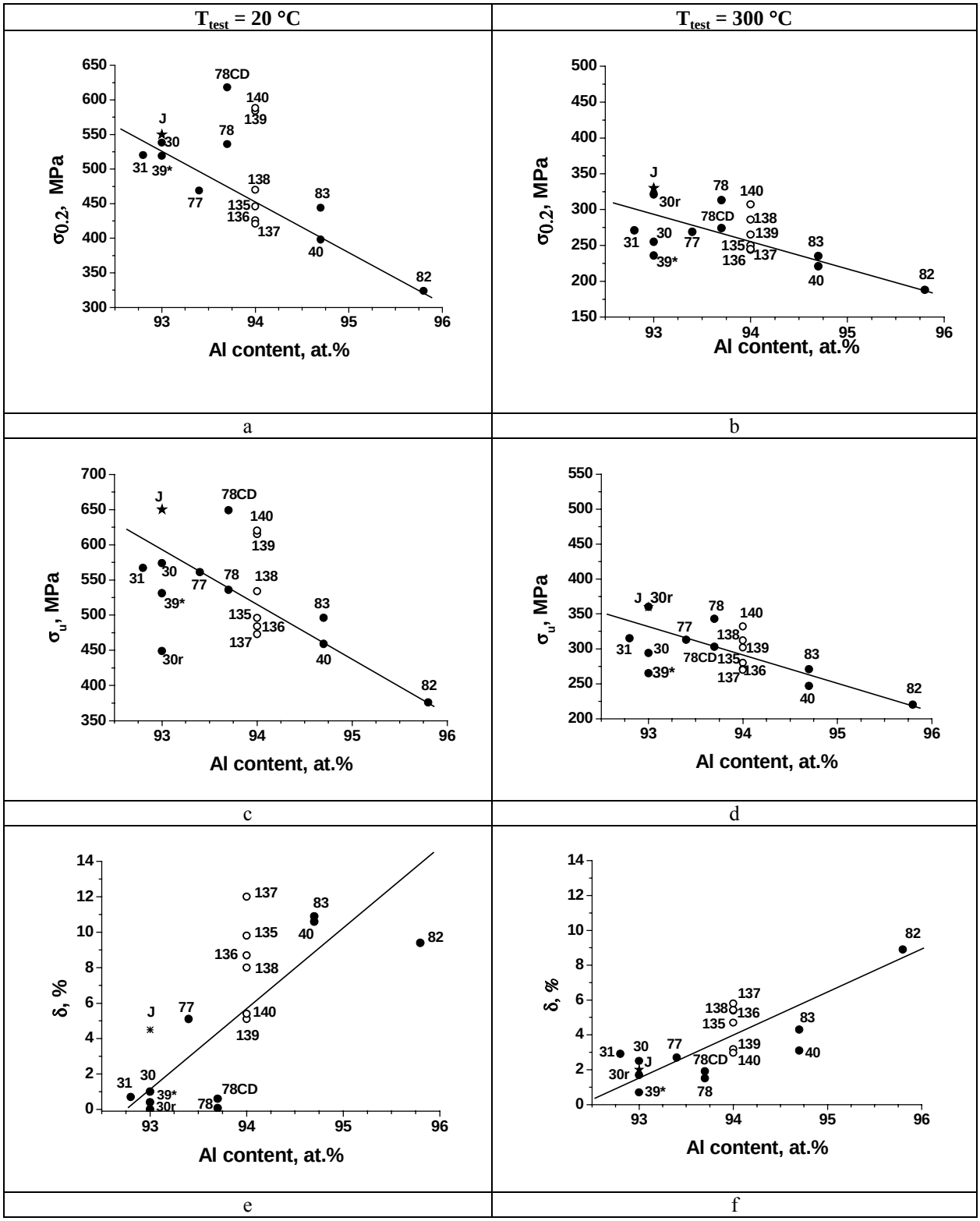

Figure 6.28. Correlation between tensile properties of rods from powder fraction of (0-63) μm extruded at 400 °C: proof stress $\sigma_{0.2}$ (a, b), ultimate tensile strength σ_U (c, d), and residual elongation δ (e, f), and Al content in the alloy for two testing temperatures: room temperature (a, c, e) and 300 °C (b, d, f).
For alloy compositions corresponding to the numbers see Table 6.4; "J" is the best PM alloy $Al_{93}Fe_3Cr_2Ti_2$ in works of Japanese scientists [1]

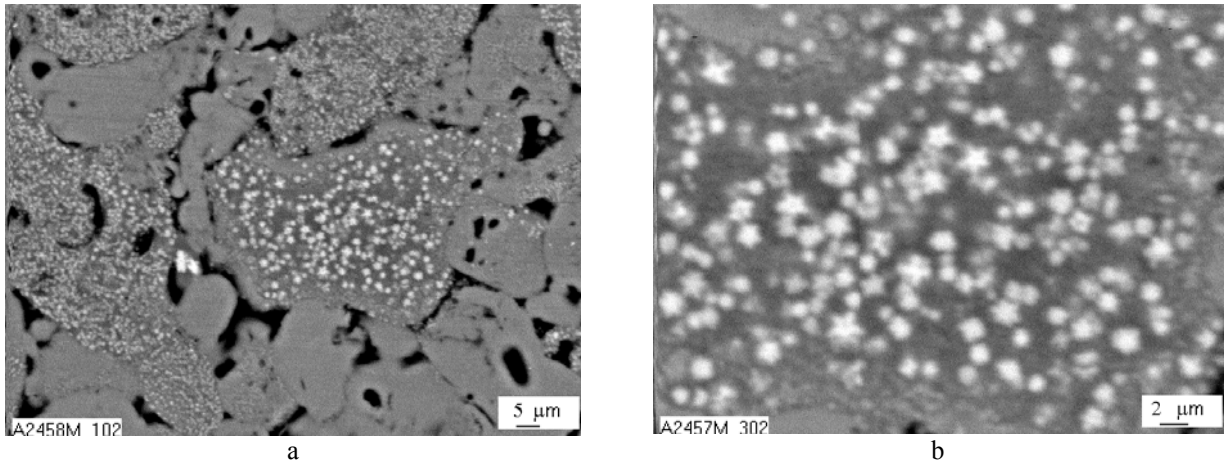

a b

Figure 6.29. Quasicrystalline precipitates in cross section of powder particles of alloy #135 ($AL_{94}Fe_3Cr_3$), SEM images in back-scattered electrons (BEI)

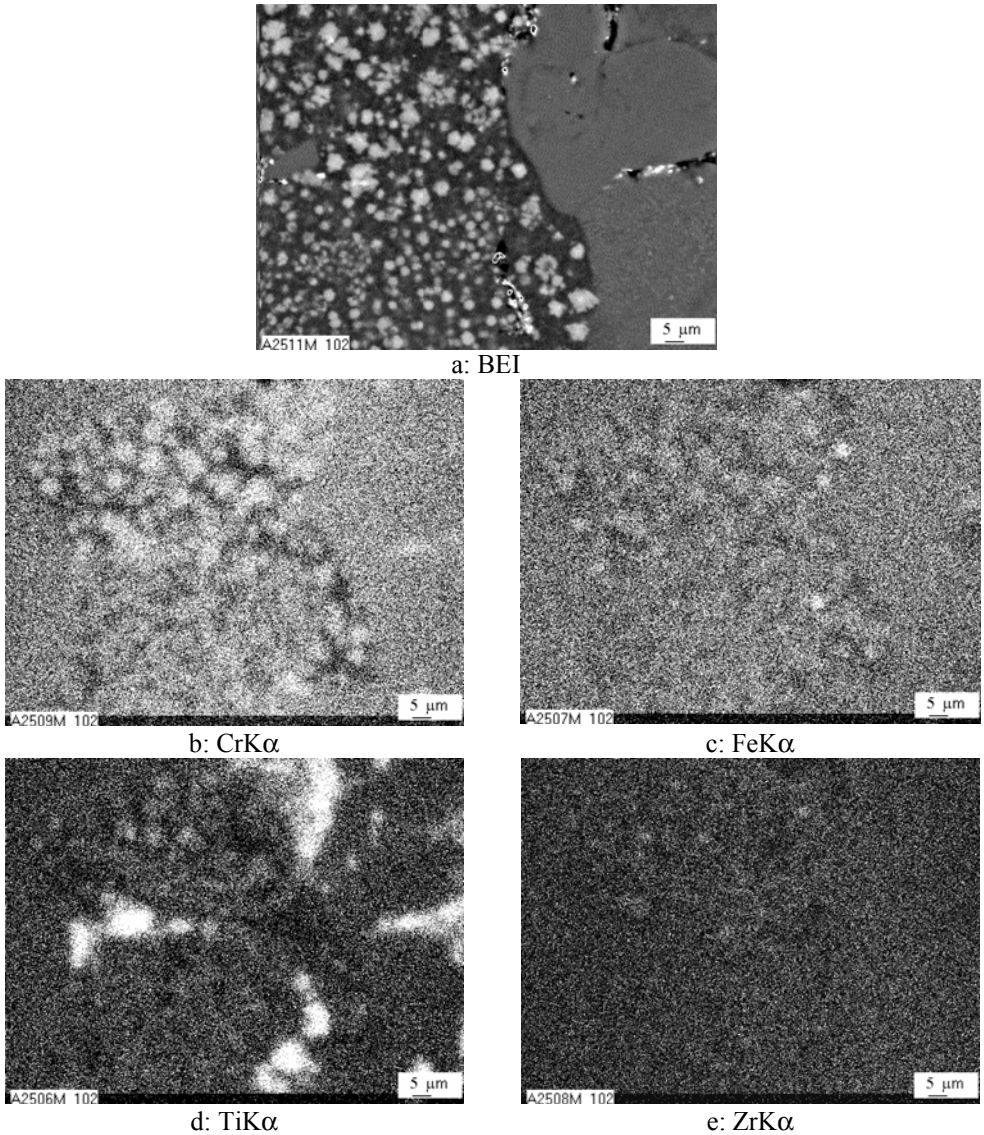

a: BEI

b: CrKα c: FeKα

d: TiKα e: ZrKα

Figure 6.30. SEM images of a particle with coarse QC precipitates in powder of alloy #140 ($Al_{94}Fe_{2.5}Cr_{2.5}Ti_{0.5}Zr_{0.5}$) in BEI mode and in characteristic X-ray emanations of alloying elements

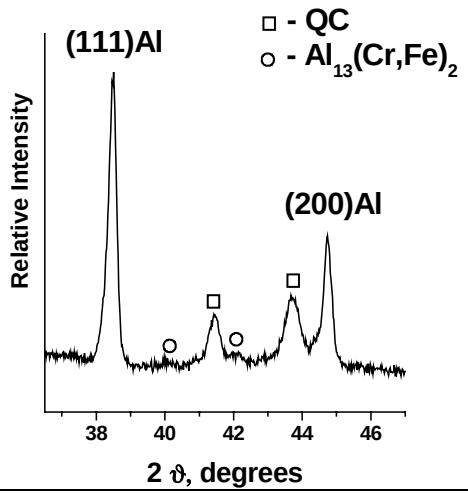

a: alloy #135, $Al_{94}Fe_3Cr_3$

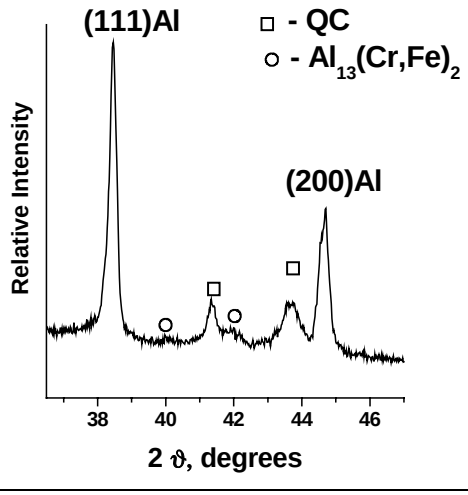

b: alloy #136, $Al_{94}Fe_{2.5}Cr_{3.5.}$

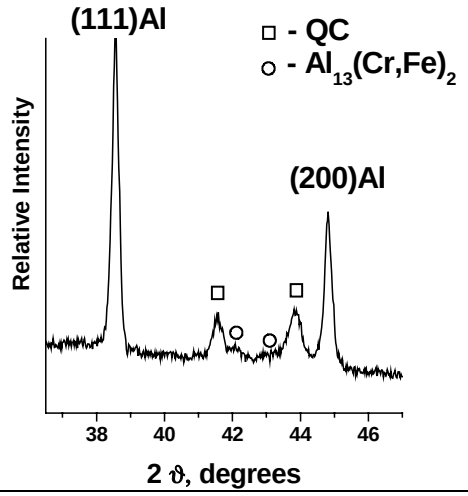

c: alloy # 137, $Al_{94}Fe_{3.5}Cr_{2.5}$

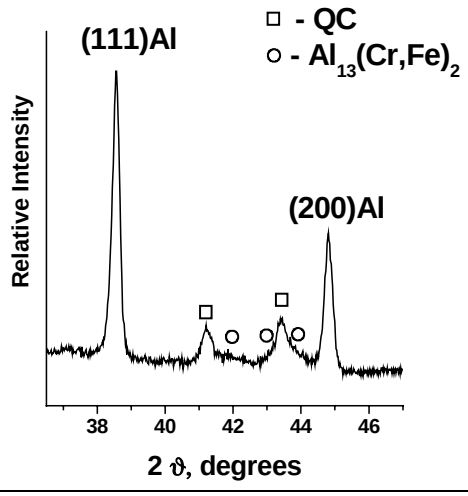

d: alloy #138, $Al_{94}Fe_{2.5}Cr_{2.5}Ti_1$

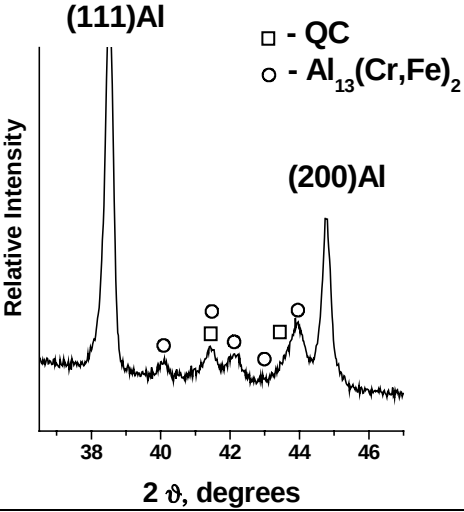

e: alloy #139, $Al_{94}Fe_{2.5}Cr_{2.5}Zr_1$

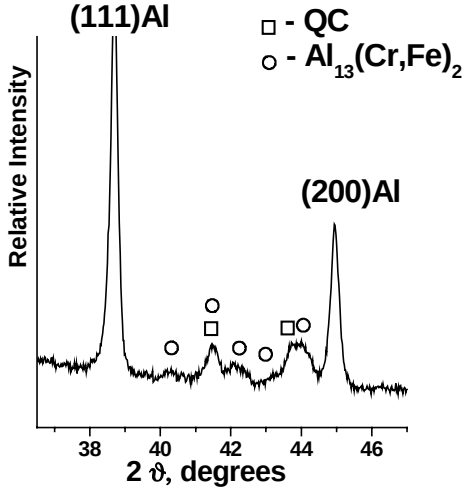

f: alloy #140, $Al_{94}Fe_{2.5}Cr_{2.5}Ti_{0.5}Zr_{0.5}$

Figure 6.31. Fragments of X-ray diffraction patterns of extruded rods (400 °C, λ=12.8) from alloys #135-140, powder size fraction (0-63) μm

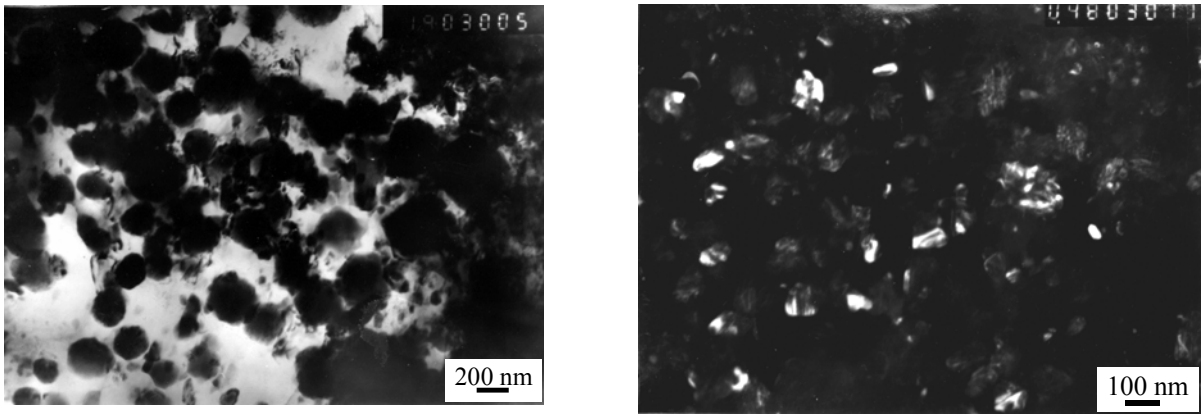

a b

Figure 6.32. Reinforcing precipitates in PM rods extruded at 400 °C, TEM investigation: a – quasicrystalline particles in alloy #137 ($Al_{94}Fe_{3.5}Cr_{2.5}$), bright field image; b – intermetallic particles in alloy #138, dark field image

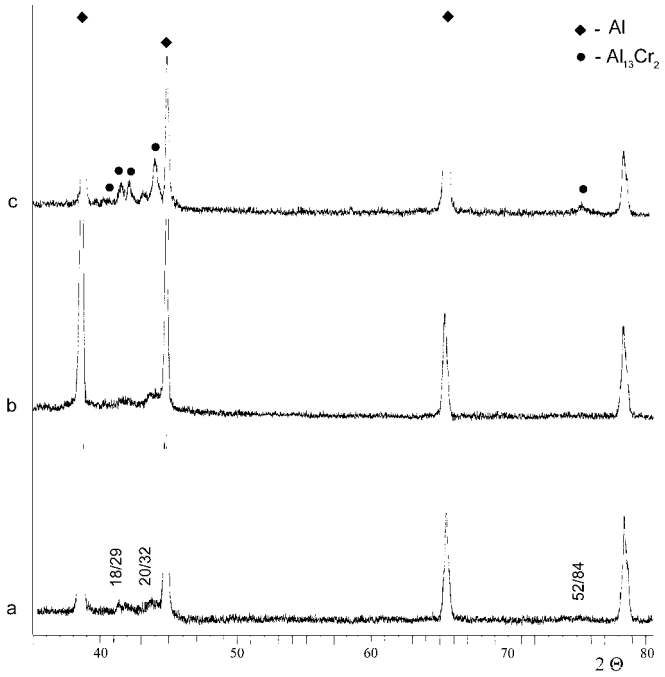

Figure 6.33. Fragments of XRD patterns from PM alloy #82 ($Al_{95.8}Fe_2Cr_{2.2}$), size fraction of (0-63) μm: a – as-atomized powder, b – powder annealed at 400 °C for 1 h, c – rod extruded at 400 °C after forging at 400 °C

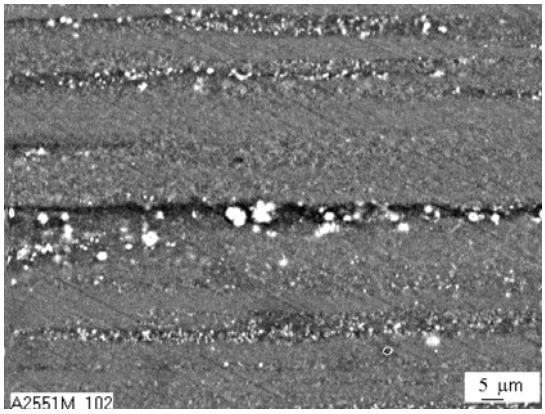

Figure 6.34. Quasicrystalline particles in the rod of alloy #82 ($Al_{95.8}Fe_2Cr_{2.2}$) extruded at 350 °C with λ=12.8 from powder fraction of (0-63) μm, SEM image in BEI mode

A comparison of the ductility of the rods reinforced with quasicrystalline particles manufactured from WA powders (Table 6.7) with the predictions of Gurland's model (Fig. 6.27) shows that the room temperature ductility of rods #135-138, especially ones manufactured with using the finest powder fraction, is remarkably higher (of 8-12 %) than one predicted by Gurland's model for f ≈ 25 % (lower than 4 %). This fact demonstrates one of the main advantages of using quasicrystalline reinforcing in Al alloys that corresponds to the concept of facilitating the plastic deformation of Al alloys reinforced with quasicrystalline particles (QC) by sinking dislocations to the interface boundaries QC–α-Al [1]. A predominant accumulation of dislocations in regions around QC particles in a tensed rod sample was confirmed with using the weak-beam technique of TEM investigation (Fig. 6.35) like for the model alloy $Al_{94}Cr_1Mn_3Cu_2$ in work [24].

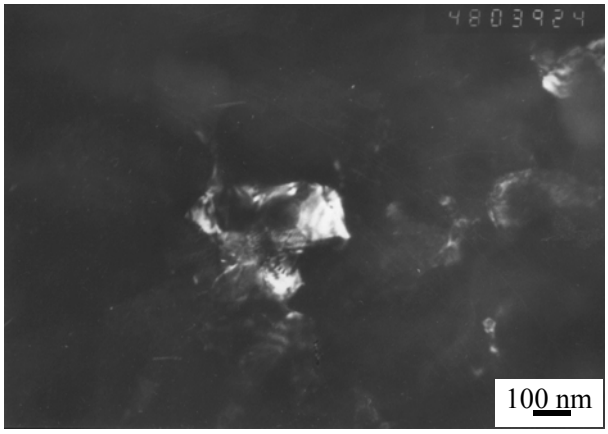

Figure 6.35. Dark field images of dislocations inside of α-Al grains in the tensed rod sample of alloy #135 ($Al_{94}Fe_3Cr_3$) with using the weak beam technique

With the participation of project authors a local plasticity of Al-Cu-Fe quasicrystal that arises in process of nanoindentation was studied [25, 26]. This local plasticity in a macroscopically brittle material was explained in connection with deformation phason defects and a possibility of a phase transformation quasicrystal-crystal in deformation process. Probably, the situation at the head of a dislocation pile-up in the α-Al matrix hindered by a disperse quasicrystalline particle can also be regarded as a local plastic deformation of the quasicrystal, and in this place a phase transformation may occur instead of the microcrack formation, as in Gurland's model.

The plasticity of alloys under investigation that contained a large amount of the QC phase (Tables 6.6, 6.7) as well as of analogical alloys in works of Japanese scientists [1, 24] remarkably (more than 2 times) lowered with increasing the testing temperature from 20 to 300 °C, and the reason for this drop was never explained. We suppose that the explanation is in the increased rate of pores formation by merging of dislocations due to increased dislocation mobility.

Fracture of rods reinforced with QC particles at all testing temperatures was of a cup-and-cone type with large flat bottom, as in the model alloy [24]. Fracture surface was of a dimple character (Fig. 6.36, a), some microcracks occurred only rarely. Large magnification revealed very narrow edges of dimples, their size being of 0.5-2 μm. An exception was the rod of alloy #139 with Zr that contained mainly crystalline intermetallics: in its fracture surface there were signs of brittle fracture (Fig. 6.36, b).

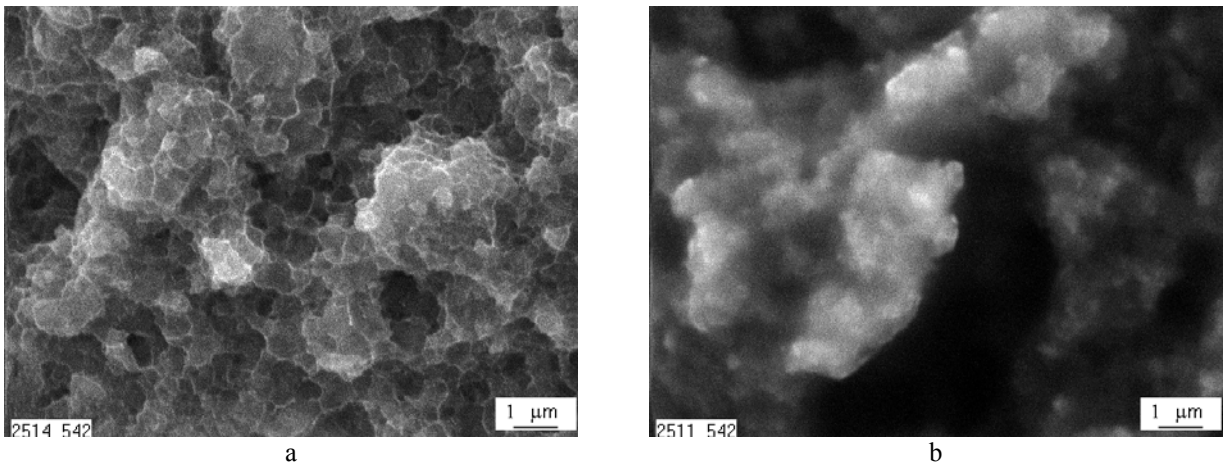

a b

Figure 6.36. Fracture surface of tensile samples of rods tested at 20 °C: a – alloy #135; b – alloy #139

An increase of rod strength characteristics with lowering the extrusion temperature from 400 °C to 350 °C observed for rods #82 and #83 (Table 6.6) was explained by the formation in them while extrusion in addition to quasicrystals of the finest (of 10-30 nm in size) particles of crystalline intermetallics.

The rods of the developed PM elevated temperature Al alloys have an elevated Young modulus, E. *E.g.*, the rods of alloys #135-140 have E = 84.8-89.6 GPa (Table 6.8) compared to E = 68.5 GPa for unalloyed Al.

Hence, as a result of project work it was shown that with using water-atomized powders of (0-63) μm size fraction PM rod semi-finished products with a strength at 300 °C of 310-330 MPa and the plasticity of 5.4-8 % at room temperature can be produced on the base of Al-Fe-Cr-Ti and Al-Fe-Cr-Ti-Zr alloys. An experiment with the separation from the WA powder of the finest size fraction of (0-25) μm for alloy $Al_{94}Fe_{2.5}Cr_{2.5}Ti_1$ has shown (see Section 6.3.1.2.1 in T06) a possibility to increase rod strength characteristics by about 5 %, but this increase is accompanied by some lowering of the ductility, evidently, due to an increase of the contribution of oxides.

Table 6.8.

Young modulus of rods produced from powder size fraction (0-63) μm by extrusion at 400 °C

Alloy #	Chemical composition	Young modulus, GPa
135	$Al_{94}Fe_3Cr_3$	87.5
136	$Al_{94}Fe_{2.5}Cr_{3.5}$	86.9
137	$Al_{94}Fe_{3.5}Cr_{2.5}$	84.8
138	$Al_{94}Fe_{2.5}Cr_{2.5}Ti_1$	89.6
139	$Al_{94}Fe_{2.5}Cr_{2.5}Zr_1$	88.0
140	$Al_{94}Fe_{2.5}Cr_{2.5}Ti_{0.5}Zr_{0.5}$	86.0

6.2.4. Works with plasma atomization and centrifugal atomization

Producing powders by centrifugal atomization of a rotating electrode by plasma arc (PA) technique was successfully used in our works for high-speed steels [27] and titanium alloys [28] and was tested for the manufacture of elevated temperature Al-Fe-Cr alloys [29]. In frames of the project we continued to develop this technique for elevated temperature Al alloys. The work consisted of three stages:

- Development of the technology for producing homogeneous ingots of Al–Fe–Cr alloys;
- Development of the technology for producing powders of Al–Fe–Cr alloys by the PA technique;
- Investigation of alloys produced by electrode atomization.

In process of work it was established that the PA technique was not efficient for producing powders of alloys on the base of heterogeneous systems like Al–Fe–Cr. For the fact that the atomized electrode consists of fusible Al matrix and refractory Al intermetallics as well as for high thermal conductivity of Al while electrode atomization, a phase separation of powders into aluminum and intermetallic powders occured in atomization process. As a result, it was impossible to obtain from such powders a homogeneous material with high level of properties.

Therefore for further works to produce PM compact materials of Al-Fe-Cr alloys the technique of centrifugal atomization of the melt was used, and the equipment for this process was designed and manufactured. Using a new scheme of melt atomization permitted a significant increase of atomized material homogeneity in comparison with the former technique of plasma atomization of a rotating electrode. It is connected first of all with the fact that instead of the high-temperature plasma source for heating the face plane of the billet (to about 2000 ^oC) that facilitated a non-uniform melting (of relatively fusible components in the first place) the technique of induction heating was used. This technique allowed to hold the total volume of the melt for a certain time that facilitated a significant increase of melt uniformity as well as to control structure and properties of flakes on the account of various overheatings and holdings of the liquid metal. The problems of the influence of overheating and duration of the holding of the liquid melt on the structure of flakes was studied in details.

In addition to a significant increase of flake homogeneity, the above technique allowed a substantial increase of flake solidification rate. Thus, in the case of plasma atomization the rate of flake solidification was in the limits of $10^4 \div 10^5$ $^oC/s$. With using the new atomization scheme we succeeded in a significant increase of the solidification rate. We consider the maximum allowable cooling rate for elevated temperature alloys under investigation to be of 10^6 ^oC /s. The increase of the cooling rate to 10^6 $^oC/s$ due to refining the process of melt centrifugal atomization allowed to manufacture the flakes of Al-8Fe-3.4Cr (wt. %) alloy with a pseudo-eutectic structure. This structure consists of α-Al solid solution and uniformly distributed quasicrystalline (QC) particles of not more than 5-20 nm in size (Fig. 6.37). Fine rings in EDP (Fig. 6.37, b) are formed by very fine QC particles shown in Fig. 6.37, c.

A partial replacement of chromium by zirconium in alloy Al-8Fe-2Cr-1.5Zr gave rise to changing the crystallization mechanism of rapidly cooled flakes to dendritic/cellular (Fig. 6.38). The structure of such alloy is characterized by a high inhomogeneity and a smaller dispersivity. The qusicrystalline (QC) phase is observed along boundaries of cells. A size of single QC particles was of about 500 nm.

The technique of high temperature X-ray „in situ" investigation allowed the following issues to be established:

- kinetics of the phase transformation from QC phase to metastable Al_6Fe phase;
- temperature range of existing the metastable Al_6Fe phase is 380-550 ^oC;
- thermal expansion coefficient (TEC) of the metastable Al_6Fe phase was first determined, and it was shown that the TEC of the Al_6Fe phase at T = 400 ^oC is close to that of aluminum matrix;
- the formation of Al_6Fe intermetallics occurs with the participation of two initial phase constituents: α-Al and QC phase.

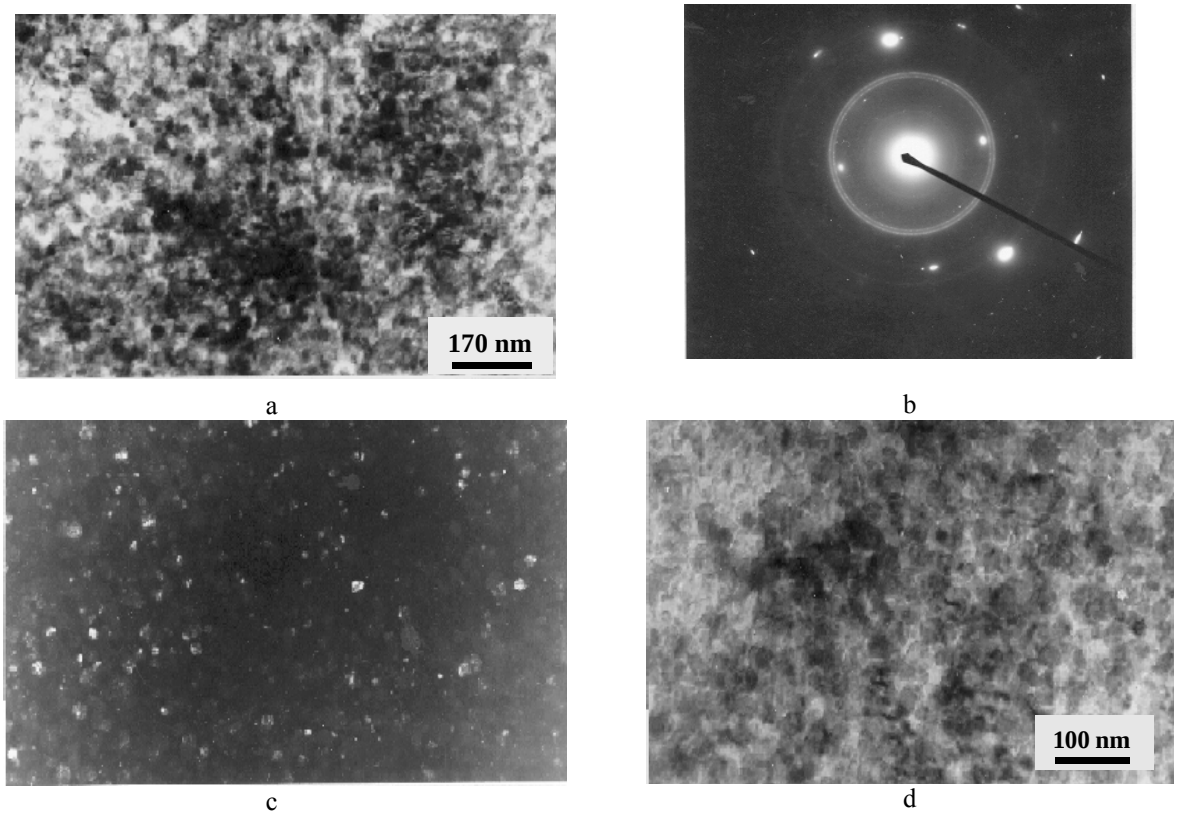

Figure 6.37. Structure of flakes from alloy #14 (Al-8Fe-3.4Cr, wt. %), TEM investigation:
a – bright field image; b – EDP formed by area (a); c - dark field image with using a part of intense rings in the EDP;
d – dark field image formed by a point reflection of α-Al

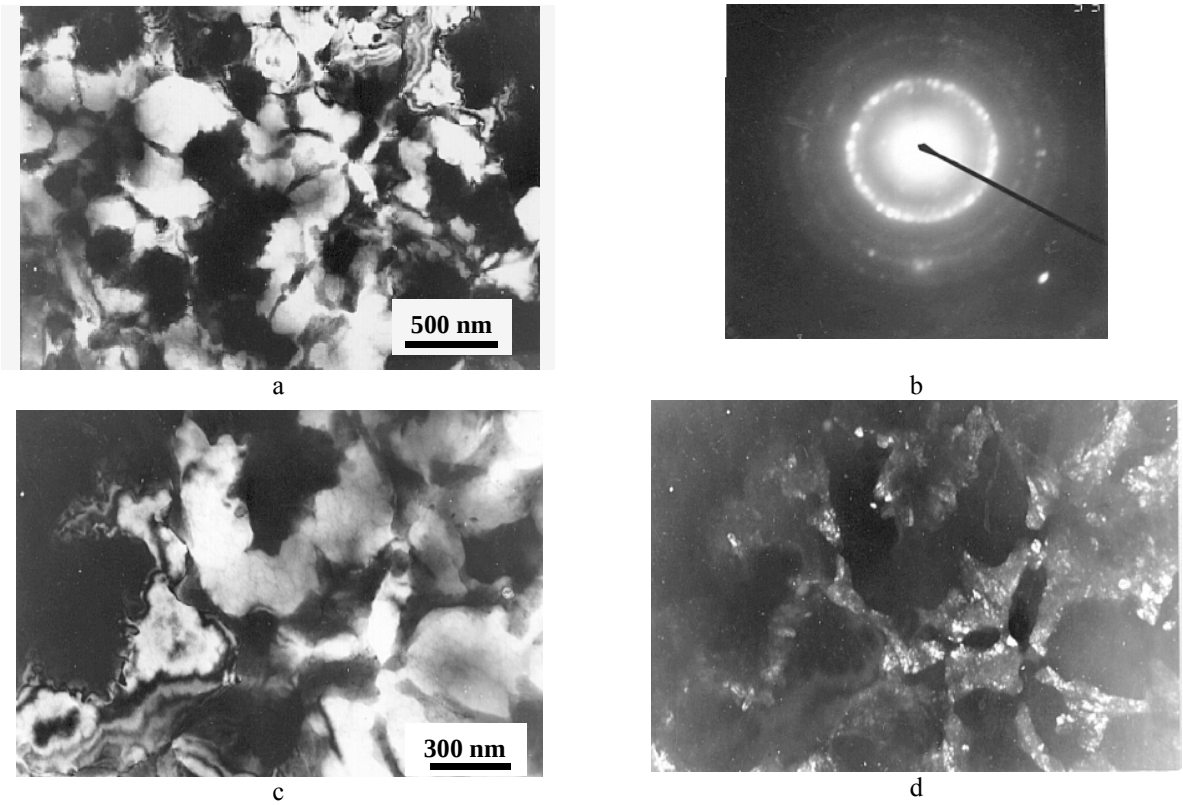

a b c d

Figure 6.38. Structure of flakes from alloy #13 (Al-8Fe-2Cr-1.5Zr), TEM investigation:
a, c – bright field images; d-dark field image of the area (c) with using a part of the intense rings in the EDP (b)

In order to preserve rapidly solidified metastable phases in the compact material, hot plastic deformation of Al-Fe-Cr flakes to produce extruded rods was carried out at a temperature of about 400 ^{0}C with using a short-term heating. The investigation of these rods of Al-9.1Fe-3.8Cr and Al-8Fe-3.4Cr has shown that these alloys are promising for producing elevated temperature Al alloys with using the technologies of manufacturing rapidly solidified powders. But the ductility of rods from flakes was low (see Table 6.9), and a study of structure and fracture surfaces of tensile samples showed that these rods had fragmented structures. Therefore, a sufficient diffusion interaction of separate flakes in extrusion process was absent that resulted in the impossibility to produce high quality material under compacting processing used. It is possible that new progressive kinds of deformation instead of extrusion will allow to produce a compact material of improved properties at 350 ^{o}C. Advantages of centrifugally atomized flakes compared to WA powders are a higher oxidic cleanness of the material as well as a smaller variation in size of disperse quasicrystalline and intermetallic precipitates in the α-Al matrix.

Table 6.9.

Tensile properties of rod samples from centrifugally atomized flakes of the alloy $Al_{94}Fe_{4.1}Cr_{1.9}$

Mode of extrusion	Testing temperature, ^{o}C	YS, MPa	UTS, MPa	El, %
#1 (with capsule evacuation)	20	431	461	1.07
	300	206	215	0.17
№2 (without capsule evacuation)	20	444	485	0.9
	300	201	234	3.0

CONCLUSIONS

Task 6 has been devoted to the investigation of non-equilibrium states in aluminum alloys manufactured by rapid solidification (RS) techniques, and of the possibility to obtain high-strength and elevated temperature materials by this way. The following problems were studied:

1. Melt-spun ribbons of aluminum alloys with amorphous structure:

1.1 In the IPMS of NAS of Ukraine the equipment and the technique for manufacturing melt-spun ribbons of amorphous alloys on Al base was developed. Ribbons of more than 20 compositions: Al-Sc (7 alloys), Al-Ce-Sc (6 alloys), Al-Ni-Ce-Sc (7 alloys), Al-Ni-Ce-Fe (1 alloy) were manufactured and investigated by the techniques of TEM, X-ray diffraction analysis, DSC, and measuring microhardness. Aluminum alloys with high Sc concentrations (up to 15 at. %) were first produced by RS technique.

1.2 It is shown that in rapidly solidified Al-Sc alloys no amorphous phase is formed, as distinct from other Al-RE alloys (RE is rare-earth metal or Y). It is supposed to be caused by a smaller atomic radius of Sc. In the melt-spun ribbon of Al-14.9 at. % Sc alloy the formation of an icosahedral quasicrystalline phase in the form of nanosize (60-140 nm) precipitates was first revealed. It is shown that this phase is not stable at room temperature and transforms into a crystalline intermetallic phase in 90 days.

1.3 It is shown that in the Al-Ce-Sc system a formation of a composite that consists of an amorphous matrix with embedded nanosize (5-10 nm) α-Al particles and has a high hardness HV = 3.5 GPa is possible ($Al_{91}Ce_6Sc_3$ alloy). At the same time the substitution of a small (of 1 at. %) amount of Sc for Ce increases the thermal stability of the amorphous state. It is found that in the ribbon of $Al_{91}Ce_4Sc_5$ alloy the structure of a very fine nanostructural α-Al + Al_4Ce + Al_3Sc eutectic was formed that ensured ribbon hardness of almost the same level (3.4 GPa).

1.4 It is established that in $Al_{85}Ni_{10}Ce_{5-x}Sc_x$ ribbons of about 35 μm in thickness at all values of x an amorphous structure with a high hardness to 4 GPa and a low density $\rho \approx 3$ g/cm^3 is formed. It is supposed to be connected with the fact that in the case of Al-Ni-Sc alloy scandium plays a role of rather an early transition metal than of a rare-earth metal. A special X-ray investigation has shown that in these ribbons a phase separation takes place with the formation of areas to 10 nm in size with two types of short order that correspond to presumable contents of Al or Ni. At the same time in the $Al_{85}Ni_{10}Sc_5$ ribbon of about 50 μm in thickness the structure of amorphous matrix reinforced with nanosize α-Al particles has formed.

2. Rapidly solidified amorphous powders of Al-based alloys:

2.1 For the first time a possibility of producing amorphous powders of Al-based alloys ($Al_{85}Ni_{10}Ce_5$ and $Al_{87}Ni_9Ce_3Fe_1$ at. %) with a high (larger than 50 %) content of the amorphous phase by water atomization technique was shown. The development technique of water atomization of the melt for Al alloys developed in the IPMS (the WA-N process) is described in details in this Report for Task 3. The details of the WA-N process were adapted to alloys with an amorphous component. Works for consolidation of these powders are started. Taking into account a searching character of works in Task 6, the line of investigation "Amorphous powders of Al alloys and their consolidation" deserves a separate attention as a technique for producing bulk amorphous and/or nanostructural materials with a high level of mechanical properties. This line can be a basis of a special project.

3. Melt-spun ribbons of elevated temperature aluminum alloys containing a quasicrystalline phase

3.1 The development of elevated temperature Al alloys reinforced with quasicrystalline particles was started by manufacture and investigation of melt spun ribbons of 6 compositions selected on the base of articles and patents of Japanese scientists. The base for this development was formed by former investigations of project authors of mechanical behavior of Al-Cu-Fe icosahedral quasicrystal by means of modern indentation techniques.

3.2 Ribbons of 25-70 μm in thickness and of about 10 mm in width were manufactured in the installation for producing amorphous aluminum alloys, and manufacture conditions were optimized. 6 ribbons of the selected compositions alloyed with 0.2 at. % Sc were studied in addition.

3.3 Studying ribbon structure has shown that the structure of Al-Mn-Ce ribbon is extremely sensitive to details of the manufacture process. Reinforcing by particles of an icosahedral quasicrystalline phase was obtained in alloys $Al_{93}Fe_3Cr_2Ti_2$ and $Al_{93}Cr_5Co_2$, but in the second of them the particle size was too large to provide a high hardness. The rest of alloys contained Ce or Y, and quasicrystalline particles in them co-existed with crystalline intermetallics that also did not provide a good combination af ribbon strength and ductility. Alloying these compositions with Sc increased the amount of crystalline intermetallics. Thus, as a result of these investigations the composition of $Al_{93}Fe_3Cr_2Ti_2$ with the best structure and mechanical properties was

chosen for detailed studying. A model ribbon $Al_{84.2}Fe_7Cr_{6.3}Ti_{2.5}$ that consisted almost completely of large (of several micrometers) icosahedral particles was manufacture for this study too. Studying Al-Fe-Cr-Ti ribbons has shown that the ribbons $Al_{93}Fe_3Cr_2Ti_2$ contained uniformly distributed quasicrystalline particles of 10-100 nm in size and a hardness of about 2.4 GPa, and the hardness of the model quasicrystalline ribbon was of about 5.3 GPa. Experiments of ribbon annealing have shown a high thermal stability of their structure and strength to temperatures of 350-400 °C.

3.4 This study has a consequence that the temperature of the thermomechanical treatment of this material has not to exceed 400 °C.

3.5 Alloying the ribbon $Al_{93}Fe_3Cr_2Ti_2$ with Sc has shown that Sc enters into both the quasicrystalline phase and the α-Al matrix, and its entering into the quasicrystalline phase increases the degree of atomic ordering in it that is expressed in a redistribution of intensities of X-ray and electron diffraction peaks.

3.6 It is shown the existence to a first approximation of a linear dependence of ribbon hardness on the quantity $d_s^{-1/2}$ where d_s is the average interparticle distance.

4. Elevated temperature PM aluminum alloys reinforced with nanosize quasicrystalline particles

4.1 The idea of this direction was to produce RS powders by the technique of water atomization of the melt elaborated for Al alloys in the IPMS (WA-N process, see this report for Task 3) and to consolidate them by a severe plastic deformation without sintering. The water-atomization technique was applied for manufacture of Al alloys reinforced with quasicrystalline particles for the first time. Al-Fe-Cr alloys additionally alloyed with Ti, Zr, and Mo were chosen for this purpose on the base of investigating the melt-spoon ribbons (see above), investigations of PM alloys produced by granular technology carried out earlier, and the concept about quasicrystal plasticity while local loading developed by project authors. This work was executed in frames of both Task 3 and Task 6.

4.2 PM alloys of the compositions $Al_{93}Fe_3Cr_2Ti_2$ and $Al_{92.8}Fe_3Cr_2Ti_2Sc_{0.2}$ corresponding to the best ribbons were studied for the beginning, and the rest of alloys under investigation had the compositions varied for achieving the best combination of structure and mechanical properties. Altogether 18 Al-Fe-Cr alloys with additions of Ti, Zr, Mo were manufactured and studied.

4.3 Studying rods of these alloys permitted to establish some regularities common for all Al-Fe-Cr alloys under investigation:

- the size of reinforcing precipitates was rather uniform inside of individual powders particles and differed rather strongly in various powder particles, obviously, due to various solidification rates that, as in the case of powders with an amorphous component, depend on the size of a powder particle and on its place in the water stream as well;
- rods manufactured from coarser size fraction of powder have lower strength characteristics due to a larger average size of reinforcing precipitates;
- strain hardening in rods from water-atomized (WA) powders is higher than in rods from gas-atomized (GA) powders due to the influence of fine oxides formed in a small amount in the WA-N process (*e.g.*, for alloy $Al_{94.9}Fe_{0.75}Cr_{4.35}$ the content of oxygen was of about 0.1 and 0.05 wt. % in the WA powder and the GA powder, respectively).

4.4 X-ray investigation has shown that in WA powders of all other compositions quasicrystalline precipitates were formed alone or in combination with crystalline intermetallics, e.g. $Al_{23}Ti_9$ type. SEM with X-ray microanalysis has established that crystalline intermetallics were of Al-Cr-Fe or Al-Cr-Ti-Zr-Mo compositions, and Fe was never found in crystalline precipitates in combination with Ti, Zr, or Mo. At the same time quasicrystalline precipitates contained Fe, Cr, Ti, and Zr.

4.5 It is shown that in extrusion process the quasicrystalline precipitates neither deform nor fail, in the rod they are redistributed in accordance to the deformation of former powder particles. In PM rods from powders containing quasicrystalline precipitates extruded at 400 and 350 °C in addition to quasicrystals some amount of crystalline intermetallics is formed as a consequence of a decomposition of the supersaturated α-Al matrix as well as of a phase transformation of the smallest quasicrystalline particles. These processes while extrusion proceed much faster than in process of annealing at the extrusion temperature. It is supposed that a phase transformation, in accordance to former investigation by project authors of microindentation of Al-Cu-Fe quasicrystal, can be stipulated by a dislocation pile-up in the α-Al matrix before a quasicrystalline particle.

4.6 To a first approximation, a linear correlation between tensile properties (YS, UTS, and EL) of Al-Fe-Cr rods and the content of Al in them was established that depicts their connection with the total amount of the reinforcing phase. On the base of these correlation we came to a conclusion that the optimum Al content in elevated temperature Al-Fe-Cr alloys is of 94 at. %. Powders and rods from 6 alloys of the group $Al_{94}Fe_xCr_yTi_zZr_{6-x-y-z}$ were produced and investigated. The quasicrystalline phase in extruded rods of these alloys was of the highest stability. Rod mechanical properties confirmed the advantage for our manufacture conditions of alloys containing 94 at. % Al over alloys with lower Al concentration (93 at. %) used in works of

Japanese scientists. PM rods of these alloys had an optimum combination of strength and ductility characteristics. With the examples of alloys with 94 at. % Al and 94.7 at. % Al it was established that a partial substitution of Cr and Fe for Ti and Zr permits to obtain an additional increase in strength properties. The best combination of tensile properties for rods from powder fraction of (0-63) μm was obtained in two alloys:

alloy $Al_{94}Fe_{2.5}Cr_{2.5}Ti_1$: YS = 286 MPa, UTS = 312 MPa, EL = 5.4 % at 300 °C, EL = 8.0 % at 20 °C;

alloy $Al_{94}Fe_{2.5}Cr_{2.5}Ti_{0.5}Zr_{0.5}$: YS = 307 MPa, UTS = 332 MPa, EL = 3.0 % at 300 °C, EL = 5.4 % at 20 °C.

A combination of the results of X-ray and TEM investigations shows that the most probable reason of this effect is the contribution of very fine crystalline intermetallics precipitated in addition to quasicrystalline particles. For the same reason lowering the extrusion temperature of the (0-63) μm powder of alloy $Al_{94.7}Fe_2Cr_{2.1}Ti_{1.2}$ from 400 °C to 350 °C was effective. For this case YS = 308 MPa, UTS = 326 MPa, EL = 3.3 % at 300 °C, EL = 7.9 % at 20 °C.

4.7 The evaluation of the amount of the quasicrystalline phase in $Al_{94}Fe_xCr_yTi_zZr_{6-x-y-z}$ powders from SEM images in BEI mode has shown that the volume part of this phase is of the order of 20-35 %. The fact that the ductility of rods under investigation (of 8-12 %) is much higher than one from the known data of Gurland for the ductility (lower than 4 %) of composites with the same amount of the crystalline reinforcing phase confirms the concept about special properties of interface boundaries between small quasicrystalline particles and α-Al matrix that can be sinks for dislocations moving in the matrix.

4.8 The fractographic investigation of rod tensile samples has shown that their fracture surfaces had a dimple character with the dimple size of about 1-3 μm except the rod $Al_{94}Fe_{2.5}Cr_{2.5}Zr_1$ that had the lowest amount of the quasicrystalline phase in its structure.

4.9 Studying structure and hardness of rod samples of alloys $Al_{94}Fe_xCr_yTi_zZr_{6-x-y-z}$ after a prolonged (for 600 h) annealing at 300 °C has shown that rod hardness changed rather weakly, but a transformation of the quasicrystalline phase to crystalline intermetallics developed, especially in alloys that contain no Zr. A special investigation is necessary to determine a change in rod tensile properties, ductility in particular, after a prolonged annealing at 300 °C as well as studying the stability of rod structure and mechanical properties after annealing at somewhat lower temperatures.

4.10 It was shown that among rods of alloys with 94 at. % Al Young modulus changed from 84.8 to 89.6 GPa, being the largest in the alloy $Al_{94}Fe_{2.5}Cr_{2.5}Ti_1$. As the Young modulus of composites is formed to a first approximation by additive principle, this result evidences the existence in the rod of this alloy of larger amount of phases with increased Young modulus that are crystalline intermetallics. A correlation between the values of rods Young modulus and yield proof stress $\sigma_{0.2}$ is observed that can be also explained as a variable contribution of small intermetallic particles. Young modulus of the rod $Al_{94.7}Fe_2Cr_{2.1}Ti_{1.2}$ extruded at 350 °C was a little lower: of 83.3 GPa that depicts the smaller amount of reinforcing phases in it due to higher content of Al. Evidently, in this case a high level of rod strength is caused by a small size of reinforcing particles.

4.11 In process of work it was established that the technique of plasma atomization of a rotating electrode that allows to manufacture powders of increased purity is not efficient for producing powders of alloys on the base of heterogeneous systems like Al–Fe–Cr. For the fact that the atomized electrode consists of fusible Al matrix and refractory Al intermetallics as well as for high thermal conductivity of Al a phase separation of powders into aluminum and intermetallic powders occurs in atomization process. As a result, it was impossible to obtain from such powders a homogeneous material with high level of properties. Therefore for further works to produce high-purity PM compact materials of Al-Fe-Cr alloys the technique of centrifugal atomization of the melt was used, and the equipment for this process was designed and manufactured. Alloys Al-9.1Fe-3.8Cr, Al-8Fe-3.4Cr, Al-8Fe-2Cr-1.5Zr (in wt. %) were selected for the investigation. Flakes-ribbons of 40-100 μm in thickness were produced with solidification rates to 10^6 K/s in a pure argon medium. The formation of quasicrystalline particles of 20-200 nm in size in these flakes was shown. Flakes of alloy Al-8Fe-3.4Cr ($Al_{94}Fe_{4.1}Cr_{1.9}$ in at. %) were selected for producing a bulk semi-finished product by extrusion at 400-410 °C. It was shown that a large amount of crystalline intermetallics of Al_6Fe and $Al_{13}Fe_4$ types, and tensile samples had a low ductility (0.2-3.0 %) both at 20 and 300 °C. Evidently, the reason for this was an insufficient interaction of separate flakes while consolidation that caused a pronounced lamination along their boundaries. It is possible that new progressive kinds of deformation instead of extrusion will allow to produce a compact material of improved properties at 350 °C. Advantages of centrifugally atomized flakes compared to WA powders are a higher oxidic cleanness of the material as well as a smaller variation in size of disperse quasicrystalline and intermetallic precipitates in the α-Al matrix.

4.12 Thus, using the technique of water atomization of the melt for producing powders and consolidation of powders by severe plastic deformation (extrusion in evacuated capsules) without sintering for producing rods permits to obtain semi-finished products of Al-Fe-Cr-Ti alloys with a tensile strength at 300 °C on the level higher than 300 MPa together with the residual elongation at ambient temperature of about 8 %. These results are of a great scientific and practical value, and it is important to develop this direction in frames of a special STCU project “Advanced nanostructural aluminum alloys reinforced with quasicrystalline particles”.

References

1. Inoue A. Amorphous, nanoquasicrystalline and nanocrystalline alloys in Al-based systems // Progress in Mater. Sci. - 1998. – **43**. – P. 365-520.
2. Milman Yu.V., Lotsko D.V., Sirko O.I. 'Sc effect' of improving mechanical properties in aluminum alloys // Mater. Sci. Forum. – 2000. – **331-337**. – P. 1107-1112.
3. Cahn J.W., Schechtman D., Gratias D. Indexing of icosahedral quasiperiodic crystals // J. Mater. Res. – 1986. – **1**, No.1. – p.13-26.
4. Manaila R., Popescu R., Jianu A., Constantin M., Devenui A. Icosahedral nanophases in the Al-Mn-Ce system // Mater.Res.v.15, No.1, 2000, p.56-62.
5. Фридляндер И.Н. Конструкционные деформируемые алюминиевые сплавы. – Москва: Металлургия, 1979. – 208 с.
6. Aluminum and Aluminum alloys, ASM Speciality Handbook / J.R.Davis (ed.). - ASM International, 1993. – 784 p.
7. Inoue A., Kimura H.M., Development of high-strength aluminum-based alloys by synthesis of new multicomponent quasicrystals // *Quasicrystals,* compiled by J.-M. Dubois, P.A. Thiel, A.-P. Tsai and K. Urban, Materials Research Society, Warrendale, PA, 1999. - **553**. - P. 495-506.
8. Masumoto T., Inoue A., Odera K., Ogushi M. High strength, heat resistant aluminum-based alloys, Patent US 5368658, Nov. 29, 1994, 6 p.
9. Kita K. Aluminum-based alloy with high strength and heat resistance containing quasicrystals, Patent US5419789, May 30, 1995, 7 p.
10. Miura H., Imahashi K., Michioka H., Yamada Y., Kusui J., Tanaka A. Heat resistant aluminum alloy powder, heat resistant aluminum alloy and heat wear resistant aluminum alloy-base composite material, Patent US5464463, Nov. 7, 1995, 13 p.
11. Masumoto T., Inoue A., Kimura H., Shinodara Y., Kita K. High strength aluminum-base alloy, Patent US5593515, Jan. 14, 1997, 6 p.
12. Imahashi K., Miura H., Yamada Y., Michioka H., Kusui J., Tanaka A. High heat resisting and high abrasion resisting aluminum alloy, Patent US5614036, March 25, 1997, 16 p.
13. Buchler E., Kita K. High-strength and high-ductility aluminum-base alloy, Patent US5900210, May 4, 1999, 3 p.
14. Masumoto T., Inoue A., Horio Y. High strength and high rigidity aluminum-base alloy, Patent US6017403, Jan. 25, 2000, 5 p.
15. A. Ziani A., G. Michot G. Rapidly solidified Al-Cr-Fe alloys for elevated-temperature applications: mechanical properties and thermal stability (Part 2) // Intern. J. of Non-Equilibrium Processing. – 1997. – **10**. – P. 59-82.
16. Mondolfo L.F. Aluminum Alloys: Structure and Properties, Butter Worths, London-Boston, 1976, 639 p.
17. Добаткин В.И., Елагин В.И. Гранулируемые алюминиевые сплавы. - Москва: Металлургия, 1981. – 175 с.
18. Kimura H.M., Sasamori K., Inoue A. Al-Fe-based bulk quasicrystalline alloys with high elevated temperature strength // J. Mater. Res.- 2000. – **15**, No. 12. – p. 2737-2744.
19. S.Takeuchi S., K.Kimura K. Structure of Al_4Mn decagonal phase as a Penrose-type lattice // J. Phys. Soc. Jap. – 1987. – **56**, No. 3. – p. 982-988.
20. Pérez-Campos R., Pérez-Ramirez J.G., Gómez A., Herrera R., José-Yacamán M. On the structure of the quasicrystalline T-phase in $Al_{84}Mn_{14}$ alloy // Scripta Metal. – 1986. – **20**. – p. 401-405.
21. Trefilov V.I., Milman Yu.V., Ivashchenko R.K. et al. Structure, texture and mechanical properties of wrought molybdenum alloy. – Kiev: Naukova Dumka, 1983. – 230 p.
22. Inoue A., Kimura H. High-strength aluminum alloys containing nanoquasicrystalline particles // Mater. Sci. & Eng. – 2000. – **A286. –** P. 1-10.
23. Gurland J., Parih N.M., Microsructural aspects of failure of two-phase alloys // Fracture, an Advanced Treatise, ed. by H. Liebowitz,, New York and London: Academic Press, 1972, Vol. 7: Fracture of Nonmetals and Composites, P. 472-512.
24. F. Haas F., K. Saitoh K., D. Nakazato D., A. Inoue A., The behavior of quasicrystal reinforced extruded Al alloys under tensile loading at room and elevated temperatures // Mater. Sci. Forum. – 2000. – **343-346**. – P. 761-766.
25. Dub S.N., Milman Yu.V., Lotsko D.V., Belous A.N. The anomalous behavior of Al-Cu-Fe quasicrystal during nanoindentation // J. Mater. Sci. Letters. – 2001. – **20**. – P. 1043-1045.
26. Dub S., Novikov N., Milman Yu. The transition from elastic to plastic behaviour in an Al-Cu-Fe quasicrystal studied by cyclic nanoindentation // Phil. Mag. A. – 2002. – **82**, No. 10. – P. 2161-2172.
27. Golub S.Ya., Katrus O.A., Kulak L.D., Kuzmenko N.N. Structural state of rapidly quenched deformed powders of high-speed steels // Poroshkovaya Metallurgia. – 1990. – No. 12. – P. 6-10.

28. Golub S.Ya., Kotko A.V., Kuzmenko N.N., Kulak L.D., Firstov S.A., Khajenko B.V. Forming in titanium alloys during quenching from the liquid state // Fizika Metallov I Metallovedenie. – 1992. – No. 6. – P. 94-102.
29. Kulak L.D., Kuzmenko N.N., Golub S.Ya., Litvinenko Yu.M. Manufacture and properties of an elevated temperature granular alloy of Al-Fe-Cr system // Proc. of the III All-Union Conf. "Granule metallurgy-91", Moscow, 1991, P. 91-94.

MAIN CONCLUSIONS

Task 1. Elaboration of high-strength wrought Al alloys produced by casting

- The purpose of the Task 1 was to improve mechanical properties with the increase of strength and the preservation of a good ductility of the strongest aluminum alloys of Al-Zn-Mg-Cu system using additional alloying by Sc in combination with other transition or rare-earth metals (TM or REM).
- As many as 61 compositions of Al-Zn-Mg-Cu alloys additionally alloyed by Sc, Zr, TM and REM were produced during project execution using the cast method.
- Wrought semi-finished products from the obtained ingots were manufactured in the form of extruded rods of 6 mm in diameter, the appropriate technology being developed.
- Influence of alloying elements on the phase composition, the structure and the mechanisms of deformation and fracture was investigated.
- A possibility of a simultaneous increase of strength and plasticity of T6 rods of Al-Zn-Mg-Cu and Al-Zn-Mg alloys by alloying with Sc has been shown and explained.
- It was found that the employment of ceramic crucibles and filtration of the melt through ceramic filters in process of ingot production increase the plasticity of T6 semi-products due to purification of ingots from oxide inclusions.
- It was shown that alloying of high-strength Al-Zn-Mg-Cu alloys with scandium permits to increase the concentration of the main alloying element Zn to 9-12 wt. % and the content of Cu to 2.3 wt. %, and alloys with **a record level of strength YS = 700-740 MPa, UTS = 770-820 MPa with a rather good plasticity of 9-14 % in T6 semi-products** can be produced.
- A positive influence of Zr, Hf, Nb, Ce and Ni additions on the mechanical properties of these alloys has been shown. The results of investigations stated above have been used by the customer of the project for drawing up of the USA patent application ”High strength aluminum alloy composition”. **These compositions of alloys may be used in industry, and the Institute for Problems of Materials Science (Ukraine) can give the scientific support for the production of these alloys.**

Task 2. Producing high-quality semi-products from new high-strength Al alloys and investigation of their weldability

- Technology for producing sheet semi-finished products from ingots of Sc-containing alloy (developed in the framework of Task 1) is elaborated. Ingots of 150 mm in diameter were melted and hot pressed to slabs having the section of 10x100 mm and then hot and cold rolled into sheets of 3 mm in thickness. Evaluation of hot cracking susceptibility in welds of sheet semi-finished products shows that for the baseline alloy (without Sc) this value determined from Houldcroft technological sample (A %) in welds with special fillers is equal to 48-50 % and for new scandium-bearing alloys this value is much better: A = 24-32 %. Strength of the joints in non-consumable-electrode argon-arc welds of sheets of scandium-bearing alloys is of 420-460 MPa. Increase of strength of welded joints of sheets of scandium-bearing alloys is of 20-28 % compared to the baseline alloy (350-360 MPa). In electron beam welding the strength of the weld metal in welded joints rises by 10-15 %.
- Investigation of the weldability of new alloys showed that **they may be considered in the category of commercially weldable materials.** A conclusion was made on the rationality of applying the developed alloys and their welding technologies for product manufacturing in the most diverse industrial sectors, primaryly in aerospace engineering and transportation. The main advantage of their application is the fact that the structure weight can be reduced by 8-12 %, which will ensure significant saving of power resources.

Task 3. Elaboration of high-strength and elevated temperature Al alloys produced by PM methods

- The first developed method for powder production by high pressure water atomization (WA-N process) along with the elaborated powder consolidation technique enabled to produce semi-products of high strength **PM alloys having a record level of mechanical properties that approaches to the properties of the best alloys produced by casting** (see Task 1). In addition, T6 treated rods of **alloys**

not containing expensive alloying elements like Sc, Hf etc. possess the strength properties much higher than rods of the same alloys produced by casting.

- It was found that particles of WA-N powders of Al-Zn-Mg-Cu-TM (REM) alloys are covered with a thin film of Al and Mg oxides of island-like character. The total oxygen content in these powders appeared to be as low as 0.05 wt. % that confirms a possibility to produce high-quality Al-Zn-Mg-Cu alloys by water-atomization technique.
- The ductility of semi-finished products of PM alloys from water-atomized powders is somewhat lower than of ones from cast alloys. The PM technique has an advantage for Al-Zn-Mg-Cu alloys (at least for Zn content of 9.5 wt. %) that does not contain Sc: wrought semi-products of PM alloys without Sc do not recrystallize after T6 treatment and have a high level of mechanical properties that is not much lower than for the same cast alloys alloyed with Sc and Zr.
- It was shown that an increased concentration of Fe (to 1 wt. %) and Si (to 0.5 wt. %) in PM alloys did not affect a high level of mechanical properties. It enables **to use the recycled aluminum, which may contain a rather high amount of Si and Fe**, for production of these alloys.

Task 4. Development of the physical fundamentals for creation of Al elevated temperature eutectic cast alloys with optimum combination of strength and ductility characteristics on the base of intermetallic phases

- As a result of the researches carried out in the ternary Al-Ti-Cr system a large compositional region has been established, in which a univariant eutectic transformation $L \leftrightarrow L1_2+\beta$ is realized. In cooling of eutectic ($L1_2+\beta$) alloys, the intermetallic compounds $AlCr_2$ or TiAlCr can precipitate from the β-solid solution as a result of the phase transformations in the solid state. The position of the boundary (ss′) between the compositions of alloys with the formation of $AlCr_2$ or TiAlCr intermetallics was determined, at which a change of precipitating phases occurs. It was found that the two-phase ($L1_2+\beta$) structure is partially preserved near this line. The periodic structure of eutectic ($L1_2+\beta$) alloys is formed by alternate lamellae and/or fibers of two phases: $L1_2$ and β.
- In compression tests cast alloys containing two cubic phases $L1_2$ and β are characterized by a significant deformation before fracture, exceeding that of single-phase $L1_2$ alloys. **On the basis of the ($L1_2+\beta$) eutectic the light-weight, high-modulus cast alloys with a unique complex of properties were elaborated.** For hypoeutectic alloy (at. %): 55Al-22Ti-23Cr (wt. %: 39.75Al-28.217Ti-32.033Cr) formed by this phases the next properties were obtained:
  - hardness **HV = 2660 MPa**;
  - compressive fracture strength σ_f **= 1666 MPa**;
  - bending fracture strength σ_f= 605 MPa;
  - compressive yield strength σ_y **= 598 MPa**;
  - deformation before fracture in compression ε **= 22 %**;
  - stable level of mechanical properties **up to 750 °C**;
  - elasticity modulus **E = 183 GPa**;
  - density ρ **= 3.9 g/cm^3**.

  A significant content of Cr in alloys predetermines the enhanced corrosion resistance at high temperatures, the availability of the eutectic leads to a good creep resistance, and a small temperature interval of melting (about 10 °C) stipulates good casting properties.
- Complex alloyed eutectic ($L1_2+\beta$) alloys containing V, Mn, Re, Nb, Zr, B were elaborated. These alloys were characterized by extremely high and stable strength properties up to 750 °C: compressive yield strength in the temperature interval of 20-750 °C was of 650-800 MPa, and of 145 MPa at 1000 °C (0.8 T_{melt}).

  The continuation of these investigations in frames of special project will be very perspective.

Task 5. Investigation of structure and mechanical properties of high-strength Al based composites

- Technology for production of particle reinforced composites based on heat resistant Al alloys was elaborated. In elaboration process the conditions of powder mixing, the optimum reinforcement size, forging and extrusion temperatures were determined.
- Effect of the matrix to reinforcement particle size ratio on the structure and the mechanical properties of the composites was studied. The model was elaborated, which describes well the decrease of the material Young's modulus due to the reinforcement clustering. It was found that a linear dependence exists between the tensile property change and the damage parameter $D = 1 - \frac{E}{E_0}$, where E is Young's modulus of the clustered composite and E_0 is Young's modulus of the composite without reinforcement clusters.
- It was shown that the effect of the reinforcement clusters on the relative change of material properties does not depend on the matrix alloy ductility. The plasticity was found to be a characteristic the most sensitive to the reinforcement clustering, and the yield stress was the least sensitive one.
- **Composites based on the matrix of a heat resistant Al alloy reinforced by quasicrystalline particles (elaborated in frames of Tasks 3 and 6) and reinforced additionally with SiC particles were first manufactured**, and their mechanical properties at room and elevated temperatures were studied. The highest mechanical properties were realized in Al-4Cr-4Fe-2Ti (wt. %) matrix alloy composites. The composite Al-Cr-Fe-Ti + 10 % SiC was found to have a high strength at 300 ^{0}C (UTS = 293 MPa) combined with a satisfactory elongation to fracture at room temperature (2 %), increased Young's modulus (E = 106 GPa), increased wear resistance and decreased friction force. The composite Al-Cr-Fe-Ti + 5 % SiC also had good mechanical characteristics. It had approximately the same strength at 300 ^{0}C (287 MPa), but higher room-temperature ductility (4.4 %) and Young's modulus of 100 GPa. Thus, elevated temperature mechanical properties of the elaborated composites are essentially higher in comparison with the properties of Al-alloy based composites known from the literature.

Task 6. Investigation of structure, phase transitions and mechanical properties of high-strength rapidly solidificated Al alloys with amorphous and quasicrystalline phases and with micro- and nanocrystalline structure

Task 6 has been devoted to the investigation of non-equilibrium states in aluminum alloys manufactured by rapid solidification (RS) techniques, and of the possibility to obtain high-strength and elevated temperature materials by this way. The following results were obtained:

- Melt spun ribbons of aluminum alloys with amorphous structure were produced and studied.
  - It was first shown that in RS aluminum alloys with a high concentration of Sc an icosahedral quasicrystalline phase in the form of nanosize (60-140 nm) particles is formed.
  - It was first shown that in the **Al-Ce-Sc system** a formation of **a composite that consists of an amorphous matrix with embedded nanosize (5-10 nm) α-Al particles** and has a high hardness HV = 3.5 GPa is possible.
  - It is established that in $Al_{85}Ni_{10}Ce_{5-x}Sc_x$ ribbons of about 35 μm in thickness at all values of x an amorphous structure with a high hardness to 4 GPa and a low density $\rho \approx 3$ g/cm^3 is formed. It is supposed to be connected with the fact that in the case of Al-Ni-Sc alloy scandium plays a role of rather an early transition metal than of a rare-earth metal.
- **Rapidly solidified powders with a high content of amorphous phase** of Al-based alloys ($Al_{85}Ni_{10}Ce_5$ and $Al_{87}Ni_9Ce_3Fe_1$) **were first produced by water atomization technique**. The first experiments for consolidation of these powders by severe plastic deformation were carried out. Taking into account a searching character of works in Task 6, the line of investigation "Amorphous powders of Al alloys and their consolidation" deserves a separate attention as a technique for producing bulk amorphous and/or nanostructural materials with a high level of mechanical properties. This line can be a basis of a special project.

- Melt spun ribbons of aluminum alloys alloyed with transition and rare-earth metals containing nanosize quasicrystalline particles were produced and investigated. Ribbons of Al-Fe-Cr alloys additionally alloyed with Ti had the best structure and mechanical properties. These compositions were used to produce RS powders (see lower). Alloying the ribbon $Al_{93}Fe_3Cr_2Ti_2$ with Sc has shown that Sc enters into both the quasicrystalline phase and the α-Al matrix, and its entering into the quasicrystalline phase increases the degree of atomic ordering in it that is expressed in a redistribution of intensities of X-ray and electron diffraction peaks. It is shown the existence to a first approximation of a linear dependence of ribbon hardness on the quantity $d_s^{-1/2}$ where d_s is the average interparticle distance.

- **Elevated temperature PM aluminum alloys reinforced with nanosize quasicrystalline particles were produced and studied.** The idea of this direction was to produce RS powders by the technique of water atomization of the melt elaborated for Al alloys in the IPMS (WA-N process, see this report for Task 3) and to consolidate them by a severe plastic deformation without sintering. The water-atomization technique was applied for manufacture of Al alloys reinforced with quasicrystalline particles for the first time. Al-Fe-Cr alloys additionally alloyed with Ti, Zr, and Mo were chosen for this purpose on the base of investigating the melt-spoon ribbons (see above), investigations of PM alloys produced by granular technology carried out earlier, and the concept about quasicrystal plasticity while local loading developed by project authors.

  The elevated temperature aluminum alloys obtained had a nanostructural Al matrix and were reinforced by nanosize (50-100 nm) quasicrystalline particles and nanosize crystalline intermetallics. **The best compositions of Al-Fe-Cr-Ti and Al-Fe-Cr-Ti-Zr had tensile strength at 300 °C on the level of 300 MPa and higher together with the residual elongation at ambient temperature of about 8 % and Young modulus close to 89 GPa.** The produced alloys had a good thermal stability of strength properties at 300 °C.

  Taking into account these results, **it is expedient to develop this direction in frames of a special STCU project** "Advanced nanostructural aluminum alloys reinforced with quasicrystalline particles".

Publications in scientific journals:

1. Yu.V.Milman, D.B.Miracle, S.I.Chugunova, I.V.Voskoboinik, N.P.Korzhova, T.N.Legkaya & Yu.N.Podrezov. Mechanical behaviour of Al_3Ti intermetallic and $L1_2$ phase on its base. *Intermetallics* No.9, 2001, p. 839-845.
2. O.N.Senkov, D.B.Miracle, Yu.V.Milman, J.M.Scott, D.V.Lotsko, A.I.Sirko. Low Temperature Mechanical Properties of Scandium-Modified Al-Zn-Mg-Cu Alloys. *Materials Science Forum*, 2002, vol. 396-402, p. 1127-1132.
3. Yu.V.Milman, D.V.Lotsko, A.I.Sirko, O.N.Senkov, D.B.Miracle. Microstructure and Mechanical Properties of Cast and Wrought Al-Zn-Mg-Cu Alloys Modified with Zr and Sc. *Materials Science Forum*, 2002, vol. 396-402, p. 723-728.
4. Yu.V.Milman, D.V.Lotsko, O.D.Neikov, A.I.Sirko, N.A.Yefimov, A.N.Bilous, D.B.Miracle, O.N.Senkov. Processing, Structure and Mechanical Behavior of Rapidly Solidified Aluminum Alloys Containing Quasicrystalline Particles. *Materials Science Forum*, 2002, vol. 396-402, p. 723-728.
5. O.M.Barabash, Yu.V.Milman, N.P.Korzhova, T.N.Legkaya, Yu.N.Podrezov. Design of new cast aluminium materials using properties of monovariant eutectic transformation $L \Leftrightarrow \alpha\text{-Al} + Mg_2Si$. *Materials Science Forum*, 2002, vol. 396-402, p. 729-734.
6. O.D.Neikov, A.I.Sirko, A.V.Sameljuk, G.E.Thompson, N.P.Zakharova, N.A.Yefimov. Properties of Rapidly Solidified Powder Alloys of the Al-Zn-Mg System. *Materials Science Forum*, 2002, vol. 396-402, p. 1223-1228.
7. M.V.Karpets, Yu.V.Milman, O.M.Barabash, N.P.Korzhova, O.N.Senkov, D.B.Miracle, T.N.Legkaya, I.V.Voskoboinik. The influence of Zr alloying on the structure and properties of Al_3Ti. *Intermetallics*, vol. 11, 2003, p.241-249.
8. Yu.V.Milman. The review paper "The influence of the scandium on the structure, mechanical properties and resistance to corrosion of the aluminum alloys" in the book devoted to *the Jubilee of Professor Paton, president of the National Academy of Sciences of Ukraine: Advanced Materials and Technologies*, Kyiv: Editorial House "Akademperiodyka", 2003, vol. 1, p. 335-360 (in Russian).
9. M.V.Karpets, Yu.V.Milman, O.M.Barabash, N.P.Korzhova, O.N.Senkov, D.B.Miracle, T.N.Legkaya, I.V.Voskoboinik. The influence of Zr alloying on the structure and properties of Al_3Ti. *Intermetallics*. vol. 11, 2003, p. 241-249.
10. Yu.V.Milman. Structure and mechanical properties of materials in the temperature ranges of cold, warm and hot deformation. *Materials Science Forum.* vol. 426-432, 2003, p. 4399-4404.
11. A.N.Slipenyuk, Yu.V.Milman, S.N.Dub, H.A.Makarenko. Peculiarities of the mechanical behavior of metallic glasses investigated by indentation technique. *Materials Science Forum.* vol. 426-432, 2003, p. 4513-4518.

Publications in Proceedings of conferences:

1. O.D.Neikov. Water Atomized Powder Technologies for Advanced Aluminum Alloy Production. Published in Proceedings *2000 Powder Metallurgy World Congress. Kyoto International Conference Hall, Japan (November 12-16, 2000)* p. 464-466.
2. O.D.Neikov, A.I.Sirko, N.P.Zakharova, G.I.Vasilieva. High-Strength Rapidly Solidified Aluminium Powder Alloys. Published in Proceedings *2000 Powder Metallurgy World Congress. Kyoto International Conference Hall, Japan (November 12-16, 2000)* p. 1089-1091.
3. O.D.Neikov, Yu.V.Milman, D.B.Miracle, D.V.Lotsko, A.I.Sirko, N.A.Yefimov. Effect of Sc Alloying Additions on Structure and Mechanical Properties of PM and Cast High-Strength Al alloys of same composition. Published in Proceedings *EURO PM2001, Acropolis Convention Centre, Nice, France (October 22-24, 2001)* v. 2, p. 219-224.
4. O.D.Neikov, Yu.V.Milman, D.B.Miracle, D.V.Lotsko, A.I.Sirko, N.P.Zakharova. Effect of Powder Size on Mechanical Properties of Elevated Temperature Aluminium Alloys produced by Water Atomization. Published in Proceedings *EURO PM2001, Acropolis Convention Centre, Nice, France (October 22-24, 2001)* v. 2, p. 225-230.
5. Yu.V.Milman. Quasicrystals. Structure and Peculiarities of Mechanical Behaviour. Thesis are published in Proceedings *XXXVII International Seminar "Actual Problems of Strength", Kiev, Ukraine (July 3-5, 2001)* p. 95-96.
6. D.V.Lotsko, Yu.V.Milman, O.D.Neikov, A.I.Sirko, N.A.Yefimov, N.P.Zakharova, A.V.Laptev, V.S.Voropayev, N.I.Danylenko. Influence of alloying by scandium and zirconium on the structure and mechanical properties of cast and powder Al-Zn-Mg-Cu alloys. Thesis are published in Proceedings *XXXVII International Seminar "Actual Problems of Strength", Kiev, Ukraine (July 3-5, 2001)* p. 303-304.
7. Yu.V.Milman, D.V.Lotsko, D.Miracle, N.A.Yefimov, A.N.Bilous, V.V.Kuprin, N.I.Danilenko, A.V.Sameljuk. Structure and mechanical properties of the rapidly solidificated aluminum alloys, hardened by nanosize quasicrystalline particles. Published in Proceedings *The conference "Deficiencies of structure and strength of crystal", Chernogolovka, Russia (June 4-7 2002)*, p. 61.
8. Yu.V.Milman, D.B.Miracle, S.I.Chugunova, I.V.Voskoboinik, V.Z.Voynash, N.P.Korzhova, T.N.Legkaya, Yu.N.Podrezov. The plasticity of intermetallic Al_3Ti and $L1_2$ phase on its base. Published in Proceedings *The conference "Deficiencies of structure and strength of crystal", Chernogolovka, Russia (June 4-7 2002)*, p. 154.

9. O.M.Barabash, D.B.Miracle, Yu.V.Milman, N.P.Korzhova, T.N.Legkaya, I.V.Voskoboinik. Structure and Properties of Eutectic Alloys of the Ternary System Al-Ti-Cr Based on $Al_2Ti_{1-x}Cr_x$, in Bulletin of the American Physical, Society Published in Proceedings *March Meeting 2002, Indianapolis, USA*, vol. 47, No.1, part 1, p. 274-275.
10. O.D.Neikov, D.V.Lotsko, N.A.Yefimov, A.I.Sirko, A.V.Sameljuk, Yu.V.Milman, D.B.Miracle. Rapidly Solidified P/M Al Alloys of Elevated Temperature Produced by Water Atomization. Published in Proceedings *2002 World Congress on Powder Metallurgy & Particulate Materials, Orlando, USA (June 16-21, 2002),* p. 7-14–7-26.
11. Y.N.Podrezov, O.M.Barabash, Y.V.Milman, N.P.Korzhova, T.N.Legkaya, N.M.Mordovets, I.V.Voskoboinik. New rigid materials with high elevated-temperature strength based on intermetallic aluminum phases. Published in Proceedings *The conference "Materials and Coatings for Extreme Performances: Investigations, Applications, Ecologically Safe Technologies for Their Production and Utilization", Crimea, Ukraine (September 16-20, 2002)*, p. 394-395.
12. D.B.Miracle, S.Firstov, Yu.Milman. Metallic aerospace materials with exceptional structural efficiency. Published in Proceedings *International Conference "Science for Materials in the Frontier of Centuries: Advantages and Challenges". Kyiv, Ukraine (November 4-8, 2002)*, p. 12-13.
13. Yu.V.Milman. High-strength aluminum-based alloys. Published in Proceedings *International Conference "Science for Materials in the Frontier of Centuries: Advantages and Challenges". Kyiv, Ukraine (November 4-8, 2002)*, p. 15-16.
14. M.V.Karpets, Y.V.Milman, D.B.Miracle, O.M.Barabash, N.P.Korzhova, T.N.Lagkaya, I.V.Voskoboinik, O.N.Senkov. Investigation of phase transformations in the $Al_3(Ti_{1-x}Zr_x)$ intermetallic by in situ X-ray diffraction method. Published in Proceedings *International Conference "Science for Materials in the Frontier of Centuries: Advantages and Challenges". Kyiv, Ukraine (November 4-8, 2002)*, p. 188-189.
15. R.V.Patsyna, V.S.Voropaev, V.A.Goncharuk, M.I.Danylenko, N.P.Zakharova, D.V.Lotsko, Yu.V.Milman, A.V.Sameljuk, O.I.Sirko. Influence of melting conditions and of alloying with transition and rare-earth metals on structure and properties of high-strength aluminum alloys. Published in Proceedings *International Conference "Science for Materials in the Frontier of Centuries: Advantages and Challenges". Kyiv, Ukraine (November 4-8, 2002)*, p. 245-246.
16. D.V.Lotsko, Yu.V.Milman, D.B.Miracle, O.I.Sirko, M.O.Yefimov, A.M.Bilous, M.I.Danylenko, O.D.Neikov, V.S.Voropayev. High-strength aluminum-based alloys hardened by quasicrystalline nanoparticles. Published in Proceedings *International Conference "Science for Materials in the Frontier of Centuries: Advantages and Challenges". Kyiv, Ukraine (November 4-8, 2002)*, p. 371-372.
17. O.D.Neikov, Yu.V.Milman, A.I.Sirko, D.V.Lotsko, N.P.Zakharova, M.I.Danylenko, A.V.Laptev, R.V.Patsyna, V.G.Tokhtuev, V.S.Voropaev, A.V.Samelyuk. High-strength rapidly solidified P/M aluminum alloys. Published in Proceedings *International Conference "Science for Materials in the Frontier of Centuries: Advantages and Challenges". Kyiv, Ukraine (November 4-8, 2002)*, p. 377-378.
18. O.M.Barabash, Y.V.Milman, D.B.Miracle, M.V.Karpets, N.P.Korzhova, T.N.Legkaya, N.M.Mordovets, Y.N.Podrezov, I.V.Voskoboinik, V.Z.Voynash. New eutectic materials of the ternary system Al-Ti-Cr based on the intermetallic $Al_3Ti_{1-x}Cr_x$. Published in Proceedings *International Conference "Science for Materials in the Frontier of Centuries: Advantages and Challenges". Kyiv, Ukraine (November 4-8, 2002)*, p. 476-477.
19. D.V.Lotsko, Yu.V.Milman, R.K.Ivashchenko, O.I.Sirko, A.V.Sameljuk, G.F.Sarzhan. Deformation and fracture of high-strength alloys based on Al-Zn-Mg-Cu system. Published in Proceedings *International Conference "Science for Materials in the Frontier of Centuries: Advantages and Challenges". Kyiv, Ukraine (November 4-8, 2002)*, p. 527-528.
20. M.O.Yefimov, D.B.Miracle, Yu.V.Milman, D.V.Lotsko, A.N.Slipenyuk, V.V.Kuprin, M.I.Danylenko. Structure of rapidly solidified Al - 13 at. % Sc alloy. Published in Proceedings *International Conference "Science for Materials in the Frontier of Centuries: Advantages and Challenges". Kyiv, Ukraine (November 4-8, 2002), p. 533-534.*
21. D.V.Lotsko, Yu.V.Milman, M.O.Yefimov, N.M.Mordovets, O.P.Rachek, L.M.Trofimova. Effect of small additions of transition metals on the structure of Al-Zn-Mg-Zr-Sc alloys. Published in Proceedings *International Conference "Science for Materials in the Frontier of Centuries: Advantages and Challenges". Kyiv, Ukraine (November 4-8, 2002)*, p. 535-536.
22. Yu.V.Milman, O.Neikov, A.Sirko, G.Vasilieva, V.Voropayev, N.Zakharova, V.Panasenko, R.Patsina, N.Chaykina. Production of the rapidly solidificated aluminum alloys by out-of-furnace treatment of melt by the high-pressure water. Published in Proceedings *International Scientific and Technical Conference "The special metallurgy: yesterday, today, tomorrow" Kyiv, Ukraine (October 8-9, 2002)*, p. 331-336 (in Russian).
23. R.Patsina, N.Zakharova, A.Sirko, V.Voropayev, Yu.Milman, N.Krapivka, A.Sameljuk, V.Goncharuk, R.Ivashchenko The influence of the melting conditions on the structure and properties of the high-strength aluminum alloys. Published in Proceedings *International Scientific and Technical Conference "The special metallurgy: yesterday, today, tomorrow" Kyiv, Ukraine (October 8-9, 2002)*, p. 361-366 (in Russian).
24. Yu.V.Milman. High-strength aluminum alloys. Published in Proceedings *International Conference NATO Advanced Research Workshop "Metallic Materials with High Structural Efficiency" that took place in Kyiv, Ukraine, 7-13 September 2003.*

25. D.Lotsko. Quasicrystals in Al alloys. Published in Proceedings *International Conference NATO Advanced Research Workshop "Metallic Materials with High Structural Efficiency" that took place in Kyiv, Ukraine, 7-13 September 2003.*
26. M.V.Karpets, O.M.Barabash, Yu.V.Milman, N.P.Korzhova, T.N.Legkaya, I.V.Voskoboinik, V.Z.Voynash. An experimental in situ X-ray diffraction study of phase transformations in Al-Ti-Cr eutectic alloys with $L1_2$ intermetallic phase. Published in Proceedings *International Conference NATO Advanced Research Workshop "Metallic Materials with High Structural Efficiency" that took place in Kyiv, Ukraine, 7-13 September 2003.*
27. N.P.Korzhova, O.M.Barabash, Yu.V.Milman, D.Miracle, M.V.Karpets, T.N.Legkaya, N.M.Mordovets, Yu.N.Podrezov, I.V.Voskoboinik. Microstructure and mechanical behaviour of multicomponent eutectic Al-Ti-Cr alloys. Published in Proceedings *International Conference NATO Advanced Research Workshop "Metallic Materials with High Structural Efficiency" that took place in Kyiv, Ukraine, 7-13 September 2003.*
28. Y.N.Podrezov, O.M.Barabash, Yu.V.Milman, N.P.Korzhova, T.N.Legkaya, V.H.Mel'nik, D.G.Verbilo, I.V.Voskoboinik. Influence of temperature on mechanical properties of Al-Ti-Cr eutectic ($L1_2$+β) alloys. Published in Proceedings *International Conference NATO Advanced Research Workshop "Metallic Materials with High Structural Efficiency" that took place in Kyiv, Ukraine, 7-13 September 2003.*
29. Yu.Milman, D.Lotsko, A.Sirko, O.Neikov, N.Zakharova, A.Sameljuk, M.Danylenko, A.Koval, V,Voropaiev, A.Sharovski, O.Senkov, D.Miracle. Effect of Fe and Si on structure and mechanical properties of complex-alloyed al-Zn-Mg-Cu alloys produced by P/M and casting techniques. Published in Proceedings *International Conference NATO Advanced Research Workshop "Metallic Materials with High Structural Efficiency" that took place in Kyiv, Ukraine, 7-13 September 2003.*
30. A.Slipenjuk, D.Lotsko, Yu.Milman, V.Kuprin, N.Yefimov, N.Danylenko. Influence of Sc on the amorphization of Al alloys. Published in Proceedings *International Conference NATO Advanced Research Workshop "Metallic Materials with High Structural Efficiency" that took place in Kyiv, Ukraine, 7-13 September 2003.*

Basing on the results of the investigations obtained in Task 1 a USA patent application "High Strength Aluminum Alloy Composition" is prepared.

The following works are presented for printing:
1. A.Ya.Ishchenko "Increasing of weldability of alloys Al-Zn-Mg-Cu by Sc additions".
2. A.Slipenyuk, V.Kuprin, Yu.Milman, D.Miracle "The effect of the matrix to reinforcement particle size ratio on the structure and mechanical properties of AlCuMn/SiC_p MMCs processed by powder metallurgy route" to be published in the Journal of Materials Sciences and Engineering A.

Project manager

Yuly V.Milman
Professor, Dr.Sci.,
Head of Department of IPMS,
Corresponding Member of the
Ukrainian Academy of Science